PRIMARY PRODUCTIVITY OF WEST AFRICAN TROPICAL FORESTS



Huanyuan Zhang-Zheng

St Catherine's College & School of Geography and the Environment

University of Oxford

Supervised by:

Yadvinder Malhi (University of Oxford),

Imma Oliveras Menor (University of Oxford),

Iain Colin Prentice (Imperial College London)

Thesis submitted to the University of Oxford in fulfilment of the requirements for the degree of

Doctor of Philosophy

Hilary 2023

The thesis is dedicated to Mr Chuqiang Zhang and Mrs Lishan Zheng, for forever trusting me, and for funding the DPhil.

In memory of my dear Grandma Meixian Zhang-Lin



At the entrance to the most productive forests measured to date, Credit: Huanyuan Zhang-Zheng

PLAIN LANGUAGE SUMMARY

The natural energy on Earth is primarily harnessed through photosynthesis by plants and algae, with a significant portion taking place in tropical forests. The Gross Primary Productivity (GPP) of a forest measures the amount of photosynthate it produces. The field measurement of GPP, which requires extensive fieldwork, has been attempted at Amazonia forests and Southeast Asian forests, but no field measurements have been taken for African forests until now. The thesis presents the first field quantification of GPP in West African forests.

The study also delves into several aspects of GPP, including (1) how plants allocate photosynthate to their own metabolism (autotrophic respiration) versus building plant tissue (biomass production), which is later consumed by other organisms (heterotrophic respiration). (2) Considering that the main environmental variable in West Africa is aridity, how do plant photosynthetic strategies vary from wet to dry sites? (3) The first part of the thesis found that West African forests have higher GPP than Amazonia forests. The study also explores whether global vegetation models, used for climate change projections, can account for this pattern. If not, the thesis seeks to uncover the cause of the deficiency.

ABSTRACT

Carbon exchange with terrestrial ecosystems, especially in tropical forests, is considered a critical aspect of the carbon cycle. Tropical forests, the most productive ecosystem, account for 44% of the global forest biomass and approximately 43% of global gross primary productivity (GPP). However, multiple global-scale forest GPP studies have indicated that the largest uncertainty applies to tropical forests, especially in the West African region, likely due to the inherent complexity of the forests and the paucity of field measurements. Previous West African studies on net primary productivity (NPP) allocation, on satellite and model-based NPP, and on aboveground biomass response to drought events and decadal long-term drying trends all have suggested that West African forests could have very different carbon strategies from other tropical forests. However, the GPP of African forests has not been field quantified, and its associated physiology has not been explained. To address this, **my DPhil research objective was to understand West African forest GPP from three perspectives**: in situ quantified GPP and its allocation (Paper 1); photosynthesis strategy (which is the basis of GPP, Paper 2) and data-model discrepancy in GPP (Paper 3).

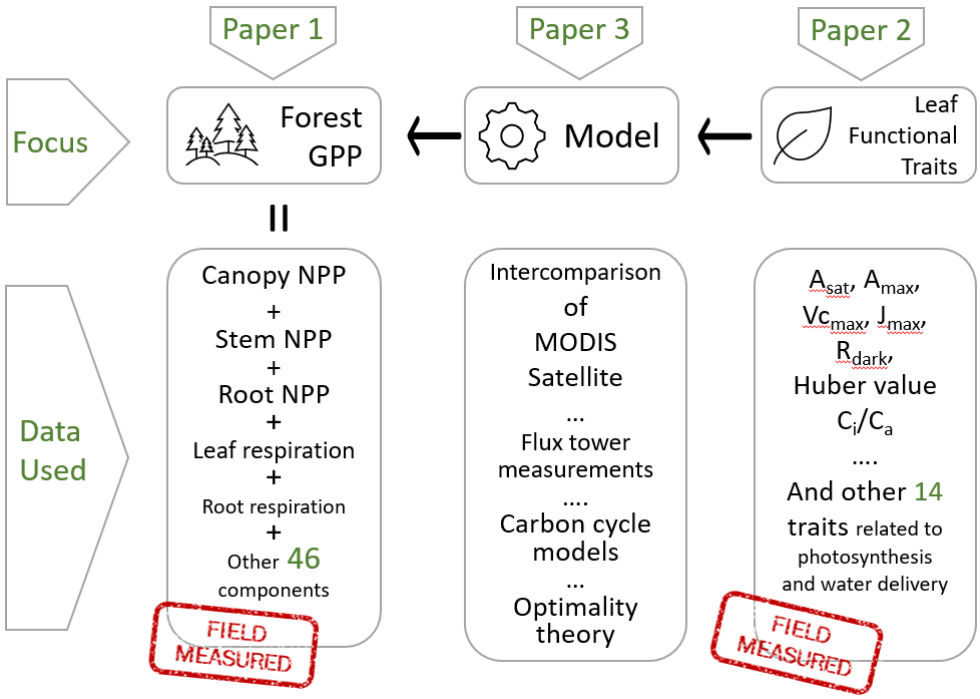
Leveraging an exhaustive dataset that collated 10 years of data collection efforts, **Paper 1** presents the first whole carbon budget of African forests along an aridity gradient in Ghana, West Africa. The paper covers the most productive intact forest measured to date. This highlights West African forests' differing productivity and carbon allocation patterns in contrast to Amazonia forests.

To understand the spatial pattern in photosynthesis (the basis of GPP), **Paper 2** applies optimality theory, which predicts GPP and photosynthetic traits from climate variables, to explain plant photosynthetic strategies along the aridity gradient in Ghana West Africa. The paper shows and explains why the net assimilation rate (photosynthesis)

per leaf area is higher in drier sites. The paper also explains that compared to wet sites, the higher transpiration demand in drier sites was met by fewer leaves, less stomatal conductance and more hydraulic efficiency.

Paper 3 analyses the common data-model discrepancy regarding the GPP of West African forests using both field GPP and trait measurements. The main causes include (1) the fraction of photosynthetically active radiation (fAPAR) being underestimated by satellite products due to cloudiness and (2) the photosynthetic capacity being underestimated. Photosynthetic capacity predicted by optimality theory can improve the estimation.

I conclude the thesis with a synthesis in Chapter 5. This thesis presents the first full carbon budget of African forests and shows how these forests diverge from previously studied sites in Amazonia and also diverge from model predictions and satellite estimates. The thesis also provides physiological insight into their distinct carbon assimilation strategy. Overall, the DPhil research highlights the uniqueness of a poorly studied but important biome – the West African tropical forests.



Graphical Abstract, See Abstract for explanation.

ACKNOWLEDGEMENTS

Words cannot express how grateful I am to my supervisors, Prof. Yadvinder Malhi, Prof. Imma Oliveras Menor, and Prof. I. Colin Prentice. Their influence has gone beyond academic development and has impacted my career choice, personal life, and beliefs. Their trust in my abilities has helped me overcome self-doubt and setbacks. Specifically,

I would not have a passion for the West African forest without Yadvinder.

I would not be a writer and continue my academic career without Imma.

I would not be in the field of carbon cycle and photosynthesis without Colin.

I would like to thank the main funders, Mr Chuqiang Zhang and Mrs Lishan Zheng. I am very grateful for the Tang Scholarship by China Oxford Scholarship Fund. and the Henfrey Scholarship by St Catherine's College (named after Mr Tony Henfrey). I would also like to thank the Environmental Change Institute, School of Geography and the Environment, and St Catherine's College for providing funding for my fieldwork and conference attendance.

A huge thank you to the many researchers, assistants, and staff at the Forest Research Institute of Ghana who have made incredible contributions to collecting most of the field data in the past decade. This research would not have been possible without our field collaborators, especially the help of Prof. Stephen Adu-Bredu, Dr Akwasi Duah-Gyamfi, Ms Theresa Peprah, and Mr Kelvin Anim-Adjei.

Kicking off a DPhil is often thought to be challenging, but I thoroughly enjoyed the first three months of my DPhil at Xishuangbanna Tropical Botanic Garden (XTBG). I gained an understanding of plant traits and R programming during the field course AFECX, and while I was a visiting scholar in 2020, I owe a particular debt of gratitude to Zexin Fan, Jingxin Liu, Peili Fu, Mohd Zeeshan, Richard Corlett, and Kyle Tomlinson for

their teachings and for hosting me. I am also thankful for the mindfulness writing course provided by Ana Pineda in 2022.

I would also like to thank many members, some of whom are now former members, of my supervisors' labs. I have had the privilege of attending three lab meetings and indulged in a wealth of knowledge and ideas exchanged. I am particularly grateful to Guillaume Delhaye, Sam Moore, Agne Gvozdevaite, Dong Ning, Han Wang, Jesús Aguirre-Gutiérrez, Benjamin Stocker, César Terrer, David Sandoval, Alexander Shenkin, Rodolfo Nobrega, Terhi Riutta, Cécile Girardin, Kathryn Brun-Jeffery, Manoela Machado, Jeppe Kristensen, Erika Berenguer and Cecilia Dahlsjö for exhibiting great patience in teaching me and providing me with advice, much of which has now become important pieces in this thesis.

I have been so lucky to be surrounded by many warm-hearted fellow doctoral students and friends, including Haisen Ding, Yunke Peng, Mengmeng Liu, Ruijie Ding, Xiongjie Deng, Mark Arcebal K. Naïve, Laura Picot, Tina Christmann, Carlota Segura Garcia, Acheampong Atta-Boateng, Eleanor Thompson, Jed Soleiman, Ty Loft, Kate Vogiatzis, Francisco Navarro Rosales, and Trisha Gopalakrishna. They lend me a selfless ear for my constant complaints and brought immense joy.

I am grateful for the wider tropical forest research community, being so kind, supportive and nurturing. Though receiving a rejection letter for my first paper was discouraging, I found solace in the spontaneous affirmation and valuable feedback provided by Prof. Christian Körner, who read my preprint on Biorxiv. My attendance at the ATBC2022 conference brought me the pleasure of meeting Dr Nathalie van Vliet, who graciously hosted me at her heavenly Airbnb on Isla de Providencia, and meeting my undergraduate tutor Dr Thomas Pugh who took me kayaking. Furthermore, I am deeply appreciative of researchers such as Jens Kattge, H.J. de (Hugo) Boer, and Maurizio Mencuccini, who helped me when I first reached out by email.

I moved house six times during my DPhil. COVID, energy crisis, and soaring living cost… I would not carry on without the support of the wonderful Chinese community in Oxford, especially Jiashun Huang, Tuoran Chen, Zhe Wang, Zun Chen, Yu Han, Zhichao Liu and Junqing Xie, and there are dozens more!

Because of COVID, I stayed with my family from March 2020 to July 2021 and travelled to many places in Western China. The COVID pandemic did impede my originally planned fieldwork, but I firmly believe, I got a better DPhil plan and a better idea of life.

Lastly, to my parent (Mr Chuqiang Zhang and Mrs Lishan Zheng), family and many dear friends on Nanao Island, Shantou, China.

Huanyuan Zhang,

14th April 2023, Wytham Wood Chalet, Oxford, UK



From left to right: Yadvinder Malhi, Adriane Esquivel-Muelbert, Erika Berenguer; Imma Oliveras Menor; Huanyuan Zhang; Jesus Aguirre Gutierrez; Acheampong Atta-boateng. We are at Yadvinder's house because Imma would soon move from Oxford to AMAP for her new professorship. Photo credit: Imma Oliveras Menor



On the way to the field sites! From left to right: Akwasi Duah-Gyamfi, Micheal Gati, Huanyuan Zhang-zheng, and Kelvin Anim-Adjei. Photo credit:Huanyuan



I am very honoured to be invited to the Master's lodge at St Catherine College for lunch with my Henfrey scholarship donor. From left to right: Kersti Borjars (Master of St Catherine's College), Huanyuan Zhang-Zheng, Tony Henfrey (Benefactor), Photo credit: Laura Stoker



From left to right: Yadvinder Malhi, Iain Colin Prentice, Huanyuan Zhang-Zheng,

Photo credit: Huanyuan

TABLE OF CONTENTS

PLAIN LANGUAGE SUMMARY ..... **II**

ABSTRACT ..... **III**

ACKNOWLEDGEMENTS ..... **V**

1 GENERAL INTRODUCTION **1**

1.1 THESIS RATIONALE 1

1.2 THESIS OUTLINE AND RESEARCH QUESTIONS 4

2 RESEARCH BACKGROUND **7**

2.1 GPP ASSESSMENT TECHNIQUES AND THEIR APPLICATION IN WEST AFRICAN FORESTS 7

2.2 THE UNIQUE AND IMPORTANT ROLE OF WEST AFRICAN FORESTS IN THE GLOBAL CARBON CYCLE 9

2.3 PHOTOSYNTHESIS EXPLAINED THROUGH OPTIMALITY THEORY 10

2.4 P-MODEL, AN OPTIMALITY THEORY-BASED MODEL 12

3 OVERVIEW OF METHODS **16**

3.1 STUDY SITE 16

3.2 SOURCES OF DATA 21

4 PAPER 1 ..... **23**

CONTRASTING CARBON BUDGET ALONG FOREST ARIDITY GRADIENTS IN AFRICA AND AMAZONIA **23**

4.1 PREFACE 24

4.2 ABSTRACT 27

4.3 INTRODUCTION 28

4.4 AMAZONIA AND WEST AFRICA COMPARISON REGARDING PRODUCTIVITY AND RESPIRATION 31

4.5 VARIATION ALONG THE ARIDITY GRADIENT AND VARIATION WITHIN THE SITE 32

4.6 CONTRASTING PATTERNS IN CARBON ALLOCATION 33

4.7 WHY WEST AFRICAN SEASONALLY DRY FOREST IS MORE PRODUCTIVE 34

4.8 FIGURES 37

4.9 METHODS 40
4.10 ACKNOWLEDGEMENTS 46
4.11 SUPPLEMENTARY TABLES 47
4.12 SUPPLEMENTARY 1 FIELD MEASUREMENTS AND PROCESSING PROCEDURE 47
4.13 SUPPLEMENTARY 2: CORRELATION BETWEEN NPP AND GPP 51
4.14 SUPPLEMENTARY 3 PLOTS INFORMATION 53
4.15 SUPPLEMENTARY 4 THOROUGH CARBON BUDGET QUANTIFICATION FOR WEST AFRICAN CARBON FLUXES 54
4.16 REFERENCES FOR PAPER 1 58

5 PAPER 2 66

PHOTOSYNTHETIC AND WATER TRANSPORT STRATEGIES OF PLANTS ALONG A TROPICAL FOREST ARIDITY GRADIENT: A TEST OF OPTIMALITY THEORY 66

5.1 PREFACE 67
5.2 SUMMARY 69
5.3 INTRODUCTION 71
5.4 OPTIMALITY THEORY REVIEW 73
5.5 MATERIALS AND METHODS 77
5.6 RESULTS 81
5.7 DISCUSSION 84
5.8 DATA AVAILABILITY 87
5.9 ACKNOWLEDGEMENTS 88
5.10 APPENDIX 1 FIELD SAMPLING PROTOCOL 92
5.11 APPENDIX 2 STUDY SITES, THE ARIDITY GRADIENT 93
5.12 APPENDIX 3 INFORMATION ASSOCIATED WITH LEAF ECONOMY 97
5.13 APPENDIX 4 REPORT ON HYPOTHESIS 15 97
5.14 APPENDIX 5 TRAIT EXTRAPOLATION AND VARIANCE PARTITIONING 102
5.15 APPENDIX 6 OTHER FIGURES 106
5.16 REFERENCES FOR PAPER 2 107

6 PAPER 3 113

WHY MODELS UNDERESTIMATE TROPICAL FOREST PRODUCTIVITY: A CASE STUDY IN WEST AFRICA 113

6.1 PREFACE 114
6.2 ABSTRACT 116
6.3 INTRODUCTION 117
6.4 METHODS 119
6.5 RESULT 128
6.6 DISCUSSION 133
6.7 SUPPLEMENTARY METHOD – MANUAL FOR REPRODUCING RESULTS 137
6.8 SUPPLEMENTARY FIGURES 148
6.9 REFERENCES FOR PAPER 3 152

7 GENERAL DISCUSSION 157
7.1 KEY FINDINGS AND IMPLICATIONS 157
7.2 GENERAL DISCUSSIONS AND LIMITATIONS 160
7.3 CONCLUDING REMARK 166
7.4 FUTURE RESEARCH DIRECTIONS: 167

8 REFERENCES FOR INTRODUCTION AND DISCUSSION 172

1 GENERAL INTRODUCTION

1.1 Thesis rationale

Paramount to the projection and mitigation of climate change is the reliability of the quantification and modelling of the global carbon cycle. Carbon exchange with terrestrial ecosystems, especially tropical forests, is considered a critical aspect of the carbon cycle. As the most productive terrestrial ecosystems (Grace *et al.*, 2001), tropical forests account for 44% of global forest biomass and approximately 43% of the global forest carbon uptake (Pan *et al.*, 2011; Liu *et al.*, 2015). Moreover, tropical terrestrial carbon fluxes dominate the year-to-year variations in atmospheric carbon stocks (Bousquet *et al.*, 2000; Friedlingstein *et al.*, 2019), and more specifically, the variation appears to be driven by variations in gross primary production (GPP) rather than in ecosystem respiration (Piao *et al.*, 2009; Zhao & Running, 2010; Jung *et al.*, 2011).

Nonetheless, our confidence in tropical forest primary productivity estimation is much lower than other components of the global carbon cycle (Menon *et al.*, 2007; Ciais *et al.*, 2014, p. 499; Pugh *et al.*, 2018). A key uncertainty resides in the estimation of forest primary productivity (Menon *et al.*, 2007). A large discrepancy among independent studies still exists regarding the spatial-temporal pattern of both tropical forest net primary productivity (NPP) (Cleveland *et al.*, 2015) and GPP (Jung *et al.*, 2011; Anav *et al.*, 2015; Yang *et al.*, 2022). Multiple global-scale forest GPP studies have reported the largest uncertainty for tropical forests (Bonan *et al.*, 2011; Frankenberg *et al.*, 2011; Badgley *et al.*, 2019). In fact, the large uncertainty seen in the current literature and divergence among independent estimates of tropical forest productivity is an inevitable consequence of the

relatively insufficient data for the tropics (Hickler *et al.*, 2008; Wood *et al.*, 2012; Babst *et al.*, 2021), the inherent complexity and diversity of tropical forest ecosystems (Malhi *et al.*, 2008; Gillman *et al.*, 2015), and tropical forest sensitivity to climate variability (Zhao *et al.*, 2005; Cox *et al.*, 2013).

The uncertainty in estimates of tropical forest productivity is particularly large in the West African region (Ardö, 2015). There are several techniques for assessing forest primary productivity and biomass, including data-driven machine learning (Jung *et al.*, 2019), remote sensing-based modelling (Zhao *et al.*, 2005), vegetation models (Friedlingstein *et al.*, 2020), flux towers (Pastorello *et al.*, 2020) and field measurements (Malhi *et al.*, 2021). However, the application of the above techniques in the West African region is very limited or challenging (see Research Background). Unlike primary productivity, measurements of forest carbon allocations, respiration and plant functional traits still require intensive field campaign, which have never been attempted in many African countries. Several previous studies concluded that the lack of African study sites was a common problem in the carbon-cycle research community (Schimel *et al.*, 2015; Xu & Shang, 2016). As an inevitable consequence of the paucity of field measurements, West African forests were often omitted or represented using parameters from other tropical forests in previous 'global' or 'pantropical' carbon cycle studies (for example, (Mahecha *et al.*, 2010; Collalti *et al.*, 2020; Cai & Prentice, 2020; Zuidema *et al.*, 2022)). However, West African forests should not be omitted because some pioneering studies (on NPP and biomass) have suggested that African forests' carbon cycle could be very different from that of the Amazonian forest, and African forests play a key role in global carbon cycling (see Research Background). To address this research gap, **my DPhil research aims to quantify and understand West African forest GPP** using thorough field measurements of carbon fluxes, plant traits and environmental variables.

The DPhil research thus begins with **Paper 1**, which presents forest-inventory-based GPP and a thorough forest carbon budget of 14 one-hectare plots in Ghana, West Africa, in comparison to Amazonia forests. Study sites were arranged along an aridity gradient[1] because (1) aridity is the key environmental variable in West Africa and (2) the predicted drier climate in most tropical regions could result in forest dieback and further accelerate global warming (Cox *et al.*, 2000; Corlett, 2016; Malhi *et al.*, 2018). Arranging study sites along a wet–dry gradient could provide a "natural laboratory" to understand forest adaptation to dry environments.

Paper 2 focuses on thorough field measurements of plant functional traits related to photosynthesis along the aridity gradient. Photosynthesis forms the basis for estimating gross primary productivity (GPP) in most dynamic global vegetation models (DGVMs). Optimality theory was recently developed to explain and predict GPP and photosynthetic traits from climate variables (see Research Background). However, the implication of the optimality theory along tropical aridity gradient has not been explained as previous studies focused more on elevation gradient (Peng *et al.*, 2020; Xu *et al.*, 2021). The 'pure' effect of aridity on photosynthesis still remains unclear because many previous studies on the trait-aridity relationship were confounded by temperature due to the covariation of temperature and aridity on a large spatial scale. The aim of **Paper 2** is to explain the photosynthetic strategies of the forests along the aridity gradient and to test the optimality theory. **Paper 2** also gains a physiological understanding of the spatial variation of GPP (presented in Paper 1).

In **Paper 1**, I also reveal that West African forest GPP has been underestimated in many global GPP products. Thus, the aim of **Paper 3 is to investigate the cause of GPP data-model discrepancy**. As models are designed based on current ecological theory

[1] The term 'Aridity' here incorporates many indices associated with atmospheric dryness and soil water availability (Paper 2 for details), without consideration of rooting depths and belowground water access due to the lack of relevant data.

(Franklin *et al.*, 2020), a large discrepancy signals a lack of physiological explanation for high productivity. Although **Paper 2** qualitatively explains photosynthetic strategies along the aridity gradient, it is not known whether the field measured photosynthetic traits are quantitatively consistent with in situ GPP. Therefore, along with the investigation into the GPP data-model discrepancy, **Paper 3** synthesises observed GPP (Paper 1) and plant traits (Paper 2) to explain that the high productivity is consistent with measured leaf photosynthetic traits and other forest properties.

The three papers touch on several facets of gross primary productivity of West African forests and there are a lot more investigations needed for a complete understanding of the forests carbon cycling. Moreover, the thesis has several limitations especially that all our study sites are in one country. The **Discussion** chapter of the thesis explains these limitations and draws overall conclusions and suggestions for future research.

1.2 Thesis outline and research questions

The aim of this thesis is to quantify and understand West African forest GPP using thorough field measurements of carbon fluxes, plant traits and environmental variables along an aridity gradient. This aim was addressed through three research articles:

1.2.1 Paper 1

Title: Contrasting carbon budget along forest aridity gradients in Africa and Amazonia

Research aim: to quantify the gross primary productivity and carbon allocation of 14 one-hectare plots in Ghana, West Africa, in comparison to forests in Amazonia.

Novelty: This study presents the first full analysis of GPP, NPP and their components for African tropical forests and savannas and compares these findings with those of

previously published analyses from Amazonia to explore how similar or ubiquitous these variables are and how they vary with aridity.

Hypotheses:

1. Is the higher NPP reported for the West African forests also reflected in higher GPP, or in higher CUE?

2. Is the relationship between productivity and aridity similar along the West African and Amazonian Forest gradients?

3. Do the studied Amazonian and West African forests share similar carbon flux partitioning patterns?

1.2.2 Paper 2

Title: Photosynthetic and water transport strategies of plants along a tropical forest aridity gradient: a test of optimality theory

Research aim: to explain the variation in photosynthesis-related traits along an aridity gradient with optimality theory.

Novelty: We propose an integrated theoretical framework to investigate the 'pure' effect of aridity on photosynthesis, which disentangles the effect of aridity on photosynthesis from that of temperature. We also expand the optimality theory to consider water delivery to leaves (see the introduction of the manuscript for more details on the theory).

Research questions:

1. Are there higher photosynthesis rates under drier environments, and if so, why do plants grown in drier climates adopt such a photosynthetic strategy?

2. How is a higher rate of photosynthesis supported by greater water transportation, given greater water stress in drier places?

There are 16 trait-specific hypotheses; please refer to Table 1 of the manuscript for more details.

1.2.3 Paper 3

Title: Why models underestimate tropical forest productivity: a case study in West Africa

Research aim: to investigate the cause of the GPP data-model discrepancy in the region, and to explain the high GPP using photosynthetic traits.

Novelty: Using study sites in Ghana, West Africa as an example, the study not only identifies key areas for model improvement but also provides an ecological explanation for the remarkably high GPP observed in the field.

Specific objectives:

1. Compare inventory-based GPP to multiple models and satellite-based products to quantify the data-model discrepancy.

2. Then, before the cause of data-model discrepancy could be examined, we investigate whether the high productivity was also reflected in leaf photosynthetic traits and other field measurements.

3. Finally, we investigated the data-model discrepancy in the West-African region by substituting model inputs (or parameters) with field measurements according to hypotheses explained in 6.4 (Paper 3).

2 RESEARCH BACKGROUND

2.1 GPP assessment techniques and their application in West African forests

There are multiple techniques for estimating GPP, NPP and other fluxes of carbon cycling, but their current application in the West African region is limited. In situ GPP, net ecosystem exchange (NEE) and ecosystem respiration (Reco) are usually reported by eddy covariance flux towers. The global flux tower network, despite having at least 200 towers with GPP measurements (Tramontana *et al.*, 2016), contains only one[2] tower situated in a West African forest, which reported three years of data (2011-2014) (Chiti *et al.*, 2010; Fattore *et al.*, 2014). Passive remote sensing techniques (e.g., MODIS and ERA5-Land) provide estimates of GPP and key parameters in modelling GPP, such as leaf area index (LAI) and fraction of active photosynthetic radiation (fAPAR), but not respiration. However, due to high cloudiness, passive remote sensing satellites obtain almost no information over West African forests during the rainy season, leaving a blind spot on the global map (Zhao *et al.*, 2005; Fensholt & Proud, 2012; Sudmanns *et al.*, 2020; Fuster *et al.*, 2020). Poor satellite visibility challenges the reliability of many satellite-based land carbon estimates and modelling for West African forests (e.g., see conclusion in (Yang *et al.*, 2022)). Carbon observation satellites (e.g., GOSAT and OCO) (Doughty *et al.*, 2022) could also indirectly provide information on GPP via atmospheric inversion modelling or

2 The flux tower is named Gh-ANK at our study site ANK. Across all the African regions, there are woody savanna sites (Mongu, Zambia) and mono-culture plantation sites (Kissoko & Hinda) (Merbold *et al.*, 2009; Longdoz *et al.*, 2010). There is a newly established African forest flux tower in the Congo basin, but it has not yet reported data (Babst et al., 2021).

solar-induced chlorophyll fluorescence (SIF) but are also limited by cloudiness. All the above require modelling and assumptions to estimate GPP.

Recently, the active remote sensing techniques (e.g., LiDAR and Synthetic-aperture radar (SAR)) that have been developed have contributed significantly to the mapping of forest aboveground biomass and canopy height (not carbon flux) (Goetz *et al.*, 2009; Abbas *et al.*, 2020), which are free of cloud obstruction (Patenaude *et al.*, 2005; Koch, 2010). Nonetheless, previous studies have been more dedicated to the Congo basin, South Africa and South America than to West Africa (see systematic reviews and references at (Timothy *et al.*, 2016; Abbas *et al.*, 2020; Gyamfi-Ampadu & Gebreslasie, 2021)). Moreover, a consensus has not been reached among the limited number of publications focusing on the region. A West African forest study (Sierra Leone) found that hyperspectral data (passive remote sensing) alone have limited predictive power of biomass, and combination with LiDAR could dramatically improve the estimate (Laurin *et al.*, 2014). On the other hand, a study in Burkina Faso found SAR a worse predictor than multispectral data (Forkuor *et al.*, 2020). There are now multiple maps of overall African forest biomass, but a large discrepancy is evident among studies (Bouvet *et al.*, 2018). More field data, including terrestrial LiDAR (TLS), drone-based study and forest census data (see below), are required to improve biomass mapping of the region.

The recruitment and mortality of the forest, autotrophic respiration (R_{auto}), carbon use efficiency (CUE) and partitioning of R_{auto} and NPP are only measurable via intensive fieldwork. ‘Census data’, which measures the tree stem diameter and height of each tree in a forest plot, provides high accuracy for forest demography, woody NPP and aboveground biomass (although the accuracy is subject to the accuracy of allometry equations). However, there are no West African forest plots in one of the global ‘census data’ networks, ForestsGEO (Anderson-Teixeira *et al.*, 2015). There are numerous West African plots on “forestplots.net”, but the number is relatively scarce compared to the number from

the Congo basin and other tropical regions (Blundo *et al.*, 2021). The Global Forest Carbon Database (ForC) incorporates both biomass and carbon flux measurements, but currently, only biomass has been reported from the West African region (Anderson-Teixeira *et al.*, 2016, 2021). In fact, the lack of study sites in West Africa is a common issue across many 'global' or 'pantropical' carbon cycle studies (such as (Parazoo *et al.*, 2014; Zhang *et al.*, 2015; Anderson-Teixeira *et al.*, 2016; Collalti *et al.*, 2020; Zuidema *et al.*, 2022) and plant trait studies (Kattge *et al.*, 2020), which are the source of carbon model parameters. Many previous studies concluded that the lack of African study sites was a common problem in the carbon-cycle research community (Schimel *et al.*, 2015; Xu & Shang, 2016).

The Global Ecosystems Monitoring network incorporates measurements from NPP, autotrophic respiration, and biomass allocation to plant functional traits (see reviews and references in (Malhi *et al.*, 2011, 2021)), data from which the foundation of this thesis is built.

2.2 The unique and important role of West African forests in the global carbon cycle

Due to the paucity of field measurements, West African tropical forests are inevitably often omitted or parameterised based on data collected from other tropical forest regions. However, it may be incorrect to assume that all tropical forest regions exhibit similar carbon dynamics and climate sensitivities. Some pioneering studies have suggested that African forest carbon cycles could be very different from those of other tropical forests. For example, African and Amazonian tropical forests have experienced very different biogeographic and climatic histories (Malhi *et al.*, 2013). A satellite-based study found that the trend of African NPP from 2000–2009 contrasted with that of the Amazon forest (Zhao & Running, 2010). Furthermore, a stable and positive carbon sink in stem biomass for African forests was reported to contrast with the declining trend in Amazonian forests,

owing to the different mortality rates following short-term drought events (Hubau *et al.*, 2020). Decadal long-term drought, however, was found to lead to an increase in biomass, along with an increase in deciduous species, in West Africa (Fauset *et al.*, 2012), but led to a decrease in biomass in tropical Australia (Bauman *et al.*, 2022). Bennett et al. (2021) suggested that African forests are more resistant to drought than other tropical forests, likely linked to the long history of greater climatic variation in the African tropics compared to Amazonia. The regional difference may be linked to a strong contrast in leaf functional traits. West African forests feature a large proportion of semideciduous species (5 months leaf lifespan compared to >12 months at Amazonia) (Moore *et al.*, 2018; Flack-Prain *et al.*, 2019). West African species grown in an arboretum (Tomlinson *et al.*, 2013) have higher photosynthesis (net assimilation rate, A_{net}) than other tropical species, which is also reflected in field measurements (Domingues *et al.*, 2010; Oliveras *et al.*, 2020) and in satellite-based (Liu *et al.*, 2023) and modelling studies (Dong *et al.*, 2022).

African forests play a key role in the global carbon cycle and should not be omitted. They dominate the variability in the tropical atmospheric CO_2 signal (Palmer *et al.*, 2019). These forests boast a high biomass stock in both lowland and mountainous regions (Cuni-Sanchez *et al.*, 2021), as well as in nonwoodland areas (Tucker *et al.*, 2023), and have higher net primary productivity than other tropical forests (Moore *et al.*, 2018; Morel *et al.*, 2019). Despite this, there has been no field quantification of the West African forests' GPP, autotrophic respiration, and their allocation, an investigation of which is the research aim of **Paper 1**.

2.3 Photosynthesis explained through optimality theory

Optimality theory is a theoretical framework that originated in linguistics, specifically phonology. It proposes that the sound patterns of a language reflect an optimal balance between conflicting constraints (Prince & Smolensky, 2004). Since its inception,

optimality theory has been applied to a wide range of fields, including economics and psychology. The framework is used to explain how organisms or systems optimise some function in response to competing pressures or constraints. In the context of plant photosynthesis, it has been proposed that plants optimise the net assimilation rate (A_{net}) (photosynthesis) by balancing three key constraints: light, water, and CO_2. The current version of 'optimality theory' comprises multiple principles (see thorough reviews by Franklin *et al.*, (2020); Harrison *et al.*, (2021)). As the most relevant to this thesis, the 'least-cost' hypothesis works on the balance between the cost of maintaining carbon fixation and water transport, which is used to calculate c_i/c_a (leaf internal to external CO_2 concentration) or g_s (stomatal conductance). The coordination hypothesis, used to calculate Rubisco carboxylation capacity (Vc_{max}) and electron-transport capacity (J_{max}), works on the balance between light-limited and RuBisCo-limited photosynthesis rates. Additionally, photosynthesis is constrained by hydraulics because water transported through the xylem must replenish water lost through stomata during CO_2 uptake (Brodribb, 2009). Tight coordination between hydraulic and photosynthetic traits has been shown and quantitatively modelled (Deans *et al.*, 2020; Xu *et al.*, 2021; Joshi *et al.*, 2022).

Some have even argued that optimality theory has universal applicability, leading to the development of optimality-based models for estimating global gross primary production (Wang *et al.*, 2017b). However, the implication of this theory on plant photosynthetic strategy along aridity gradients has not been summarised and tested. This knowledge gap undermines the application of optimality-based models in tropical regions, where aridity is a critical environmental factor.

Testing optimality theory-based predictions of plant photosynthesis strategies along tropical aridity gradients also contributes to the global challenge of incorporating the interactions between the carbon and water cycles (Rogers *et al.*, 2017; Canadell *et al.*, 2021). Such challenges become particularly pressing in the climate change era, as greater

atmospheric dryness (denoted by vapour pressure deficit, VPD) is predicted for most of the tropics (Neelin *et al.*, 2006), and a reduced tropical forest carbon sink due to future reduction in water availability has been categorised as 'high confidence' (Canadell *et al.*, 2021). Most current earth systems models predict a negative relationship between photosynthesis (A_{net} per leaf area) and VPD simply due to the closing of stomata without incorporating the dynamics of photosynthetic capacity (denoted by J_{max} and Vc_{max}) (Wang *et al.*, 2017a; Green *et al.*, 2020). However, previous studies have shown that plants grown in drier environments could have higher A_{net} and V_{cmax} (Wright *et al.*, 2005; Peng *et al.*, 2021). Such variation in photosynthetic capacity has not been incorporated in models (Rogers *et al.*, 2017) because the 'pure' effect of aridity on photosynthesis and plant adaptation to a drier climate remains unclear. The main challenge is that, on a large spatial scale, aridity is inevitably confounded with temperature, a stronger driver of photosynthesis than aridity (Smith *et al.*, 2019), and few studies have tried to disentangle them (Grossiord *et al.*, 2020). It has been hypothesised that in the long term, plants acclimate to dry environments by having fewer leaves, which reduces transpiration demand and maintains high photosynthetic capacity at the expense of a reduced foliage surface area (Joshi *et al.*, 2022). However, it has not been explained why, along a wet-dry aridity gradient, plants at dry sites acclimate to (not just maintain) high photosynthetic capacity and how these plants manage water transportation under great hydraulic demand (Mencuccini *et al.*, 2019). **Paper 2** addresses the above challenges by testing optimality theory along a tropical aridity gradient.

2.4 P-model, an optimality theory-based model

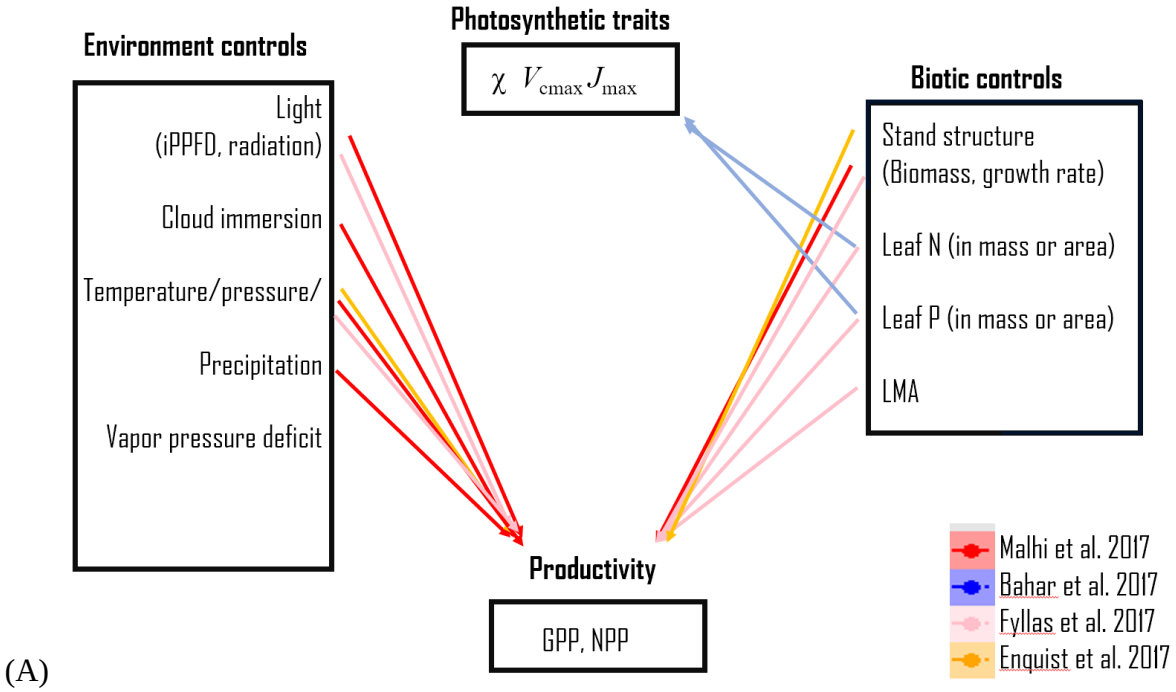
Field-measured photosynthetic traits were used to quantify the physical and physiological characteristics of plant photosynthesis. Photosynthetic traits are often used to estimate gross primary production (GPP) in plants. Several photosynthetic traits are closely

related to GPP, including (1) leaf internal to external CO_2 ratio (c_i/c_a) (or stomatal conductance, g_s), depending on overall stomatal openness and the number and size of stomata. (2) photosynthetic capacity (Vc_{max} and J_{max}) and (3) net assimilation rate (A_{net} and specifically, the light-saturated rate of photosynthesis, A_{sat} and the maximum rate of photosynthesis under light and CO_2 saturation, A_{max}). Leaf-level photosynthesis can be calculated using the above traits via the Farquhar-von Caemmerer-Berry (FvCB) photosynthesis model (Farquhar *et al.*, 1980). Leaf-level photosynthesis could then be scaled up to the canopy level, and thus to GPP (Figure 1b), by methods that vary in complexity, but all depend on the estimated leaf area index (LAI) or the fraction of absorbed photosynthetically active radiation (fAPAR), which determines the total light absorption of a forest. Optimality theory could not only be used to explain spatial and temporal variation in the above traits but also to quantitatively calculate the above traits (and GPP) using environmental variables. P-model has been designed for this purpose (Stocker *et al.*, 2020; Peng *et al.*, 2020). P-model does not calculate GPP from biotic control variables (e.g. Leaf nitrogen content) (see Figure 1b) mostly because global maps of these variables have substantially larger uncertainty than climate variables. Nonetheless, there are other methods for estimating GPP (Malhi *et al.*, 2015; Enquist *et al.*, 2017; Fyllas *et al.*, 2017; Bahar *et al.*, 2017) which are illustrated in Figure 1a. There is currently no consensus on how GPP should be calculated in a model.

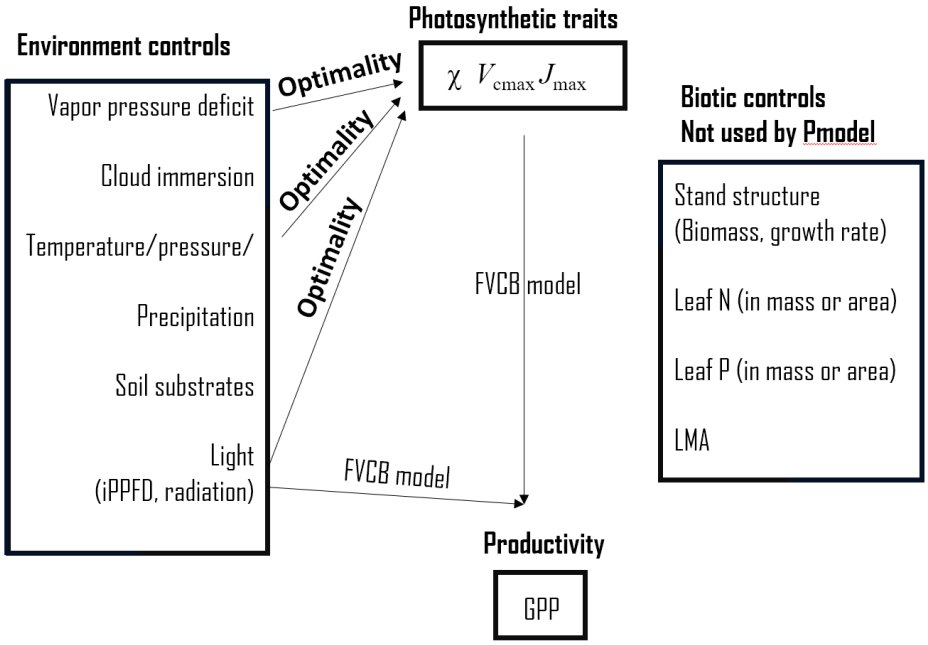
P-model has been demonstrated to be successful in explaining plant photosynthesis along elevation gradients (Peng *et al.*, 2020), in soil drought experiments (Joshi *et al.*, 2022), in seasonal variation (Jiang *et al.*, 2020), and in diurnal variation (Mengoli *et al.*, 2022).

The P-model differs from previous vegetation models by proposing a way to calculate c_i/c_a (Prentice *et al.*, 2014), Vc_{max} and J_{max} (Wang *et al.*, 2017b; Stocker *et al.*, 2020) from climate variables that account for the dynamics of these parameters. Nonetheless, other

GPP calculation methods exist, for example (also see reviews in (Rogers *et al.*, 2017)), (1) calculating Vc_{max} and J_{max} from leaf nitrogen and leaf phosphorus and (2) linking GPP or NPP directly with stand structure and other site or climate characteristics (Figure 1). Paper 3 thus compares GPP from multiple independent estimates to the observed GPP (in Paper 1). Paper 3 uses the P-model to reproduce the field-observed GPP of West African forests using field-measured photosynthetic traits and investigates the data-model discrepancy by varying inputs into P-model (e.g., field-measured photosynthesis capacity versus optimality-estimated photosynthesis capacity) and checking contaminant changes in GPP.



(A)



(B)

Figure 1 Productivity calculation approaches. P-model (B) estimates photosynthetic traits first from climate variables (Peng *et al.*, 2020). Then GPP is calculated from photosynthetic traits, light and fraction of absorbed photosynthetic active radiation (fAPAR). Before the development of the P-model, there have been other models or statistical analyses (A) in explaining GPP (Malhi *et al.*, 2015; Enquist *et al.*, 2017; Fyllas *et al.*, 2017; Bahar *et al.*, 2017) using environmental or biotic variables different to P-model. In most current carbon models, GPP was calculated using the FVCB photosynthesis model (Farquhar *et al.*, 1980), which takes climate variables, leaf internal to external CO_2 ratio (c_i/c_a), and photosynthesis capacity (V_{cmax} and J_{max}) as input. The P-model advance by using optimality theory to calculate c_i/c_a, V_{cmax} and J_{max} from climate variables, so that GPP can be calculated using climate variables only. There are more GPP estimation methods than the above-cited studies. The above citations are selected as they worked on the same study sites.

3 OVERVIEW OF METHODS

In this chapter, I begin by providing a detailed description of the three study sites, which are common to all three papers. Then, I highlight the main methodological advancements that go beyond the current literature.

3.1 Study site

The United Nations defines Western Africa as the area including 16 countries, from the coast to the north of Mauritania, Mali, and Niger and the east of Nigeria. West African forests feature a transition from the coast (high forests) to the desert (savanna). West African forests in this study refer to Uppthe er Guinea forest. The study Ghanian forests are located at the east end of Upper Guinea forests. Upper and Lower Guinea forests are separated by the Dahomey Gap (White, 1983; Luiselli & Fa, 2019) (Figure 2).

This thesis focuses on an aridity gradient established in Ghana, West Africa (Figure 2), that features a strong variation in aridity with only a 1.4 °C change in mean annual temperature (Paper 1 Figure 1). The gradient contains three wet (mean annual precipitation, MAP 2000 mm) evergreen forest one-hectare plots in the Ankasa national forest (ANK-01 to ANK-03) in the extreme southwest of Ghana, close to the Côte d'Ivoire border. Two hundred kilometres to the northeast, there are six semideciduous one-hectare forest plots (MAP 1500 mm) located within Bobiri Forest Reserve (BOB-01 to BOB-06), close to the second largest city in Ghana, Kumasi. An additional one hundred kilometres to the northeast, there are six one-hectare plots located within the Kogyae Strict Nature Reserve, which encompasses the dry forest (MAP 1200 mm) to a savanna transition zone

(KOG-02 to KOG-06). All these plots are part of the African Tropical Forest Observation Network (AfriTRON) and ForestPlots. Apart from precipitation, we also discuss many alternative metrics of 'aridity' along the gradient in Paper 2.

The sites were at least 100 km away from each other. Plots within the same site were approximately 1 km away from each other. Therefore, the three study sites were in different grid cells of a model (or satellite product), but plots belonging to the same site were in the same grid cell. Paper 1 and Paper 2 focus on the plot scale. Paper 3 (the modelling paper) focuses on the site scale. Several traits were sampled from 7 plots only. Therefore, there are 7 plots in paper 2 but 14 plots in paper 1.

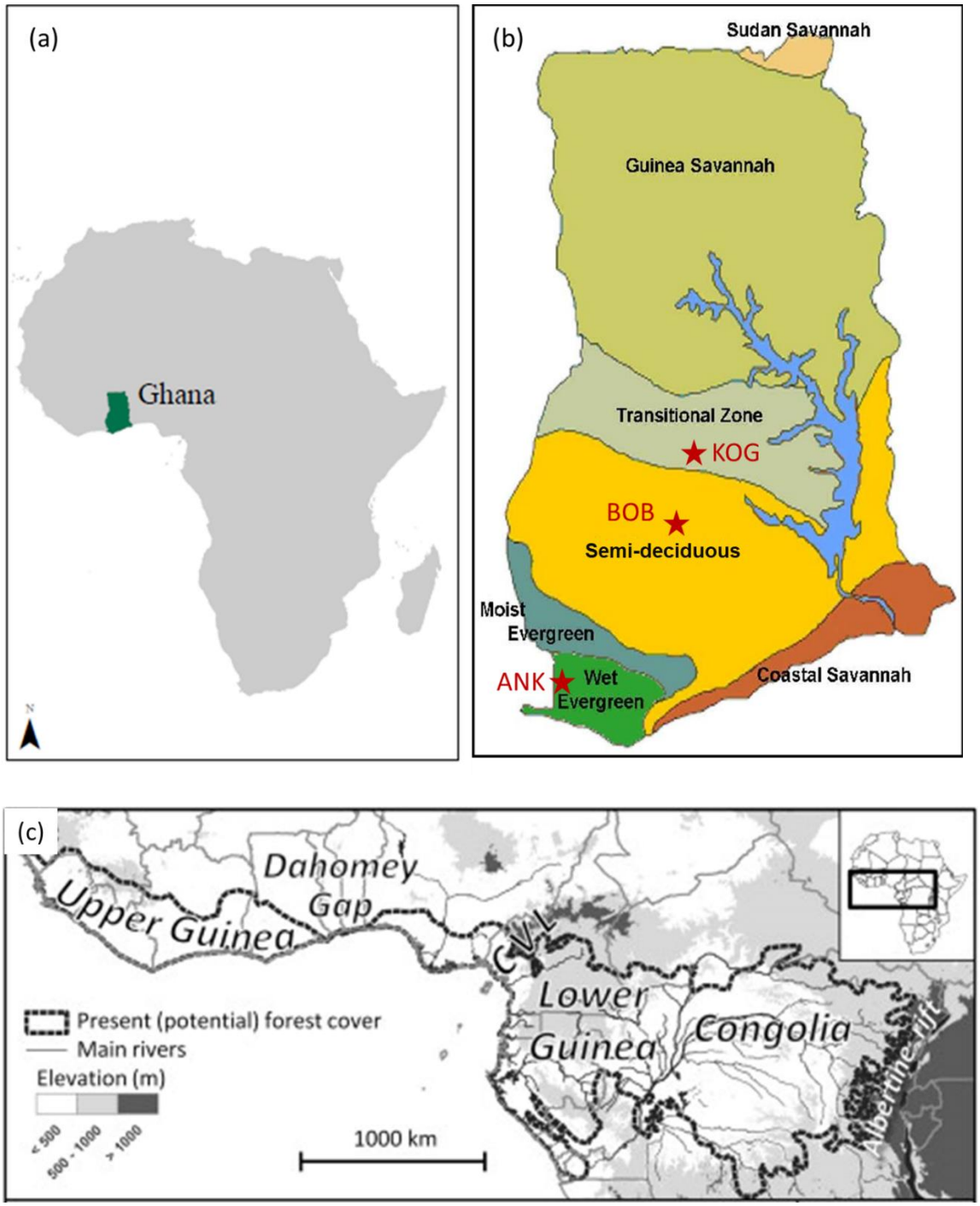


Figure 2 Map of the location of Ghana within the African continent (a); The study plots and forest types in Ghana (b) (Appiah *et al.*, 2014). Plot Ankasa (ANK) is classified as Wet evergreen forest. Plot Bobiri (BOB) is classified as semi-deciduous forest. Plot Kogaye (KOG) is classified as forest-savanna transition zone; The location of Upper and Lower Guinea forests in Africa (c) (Hardy *et al.*, 2013).

3.1.1 KOGYAE (dry, including KOG-02 to KOG-06)

The Kogyae Strict Wildlife Reserve (7.28464, -1.42414) is located near the Ejisu-Juaben District of the Ashanti Region, Ghana. The reserve covers 386 km^2 and was created in 1971. From KOG02 to KOG06, it spans from semideciduous forest to open grassland (forest-savanna transition). In the past, the forest was a continuous block that covered the whole reserve's centre and took up nearly one-third of its space. However, during the 1980s and the early 1990s, logging, farming, and bushfires all contributed to a significant loss of forest cover and the consequent fragmentation of the forest into isolated areas. The main wet season lasts from April through June with a secondary wet season from September to November, which in total delivers 1200-1300 mm average annual rainfall (See Figure S10 in paper 2 for seasonality for each site). The Voltarian system characterises Kogyae's geology, and exposed rocks are typically reddish-brown sandstone. The soil in the savanna and transition regions is Haplic Arenosols, with thin, sandy loam topsoil, while the forest sites have Haplic Nitosols, which are more acidic than the savanna soil (Domingues *et al.*, 2010; Oliveras *et al.*, 2020).

3.1.2 BOBIRI (middle, including BOB-01 to BOB-06)

The Bobiri Forest Reserve (6.68697, -1.34401) covers 54.65 km^2 and was established in 1931. It is largely covered with semideciduous and old-growth forest, which has a multilayered canopy structure, including an understorey layer composed of both shade-tolerant and shade-intolerant species, large coarse woody debris in all decay stages on the forest floor, and the presence of ferns. This site has six 1 ha plots (BOB-01 to BOB-06) with different levels of logging: BOB-01 is intact forest. BOB-02, 03 and 04 were last logged approximately 50 years ago (2-4 stems per hectare; BOB-05 and BOB-06 were last logged in 2012. The 10-yr annual rainfall ranges from 1210 to 1800 mm, with a dry season lasting from December to mid-March. The soils are Oxisoils, deeply weathered, and highly acidic (3.5–4.0 in pH).

3.1.3 ANKASA (wet, including ANK-01 to ANK-03)

The Ankasa National Forest (5.26313, -2.57924) was created in 1976 and has an area of 500 km^2. The reserve is mostly covered by tropical evergreen rainforest. The mean annual precipitation (MAP) is approximately 2,000 mm, mainly concentrated from March to mid-July and from September to November. A dry period extends from December to February. The relative humidity is high throughout the year; daily, it ranges from 90% at night to 75% in the early afternoon. The landscape is characterised by the presence of small, gentle hills with an average elevation of 90 m.a.s.l., such that rugged and deeply divided terrains characterise the forest, with ANK03 in the swampy valley and others on the drier hills. The deeply weathered soils are highly acidic, 3.5–4.0 in pH, and on a broad basis classified as Oxisols.



Figure 3 Photo of KOG02 (dry site), KOG05 (dry site), ANK03 (wet site), and BOB01 (mid site). All photos were taken in January 2022 by Huanyuan Zhang-Zheng.

3.2 Sources of data

All three papers within this thesis focus on the same sites as mentioned above. Paper 1 works on field-measured GPP, paper 2 on functional traits, and paper 3 presents a data-model comparison for GPP and checks the consistency between field-measured traits and GPP.

Paper 1 is built on in situ carbon measurements following the Global Ecosystem Monitoring protocol (Malhi *et al.*, 2021). Net primary productivity in this paper is from (Moore *et al.*, 2018). Paper 1 reported more field-measured site metadata and climate data and completed the in situ full carbon budget.

Paper 2 investigates plant ecophysiology traits, which were collected during the GEM-Traits project (Gvozdevaite, 2018; Gvozdevaite *et al.*, 2018; Oliveras *et al.*, 2020). More traits data were reported beyond the above citations.

Paper 3 synthesises field-measured data from the above two papers and involves many published global products, including MODIS (Running *et al.*, 2015), FLUXCOM (Jung *et al.*, 2019), TRENDY (Friedlingstein *et al.*, 2020) and ERA5-Land climate variables.

4 PAPER 1

CONTRASTING CARBON BUDGET ALONG FOREST ARIDITY GRADIENTS IN AFRICA AND AMAZONIA

"Specialists make the best generalists. You need to know one part of nature really, really well before you can come up with big new ideas."

Prof. Richard Corlett

(Ecologist at Xishuangbanna Tropical Botanic Garden)



View from the field camp outside Ankasa forest, Credit: Huanyuan Zhang-Zheng

4.1 Preface

The overall **aim of the thesis** is to elucidate West African forest GPP using thorough field measurements of carbon fluxes, plant traits and environmental variables. **Paper 1** is a carbon flux descriptive chapter which presents forest-inventory-based GPP and a thorough forest carbon budget of 14 one-hectare plots in Ghana, West Africa. Study plots were arranged along an aridity gradient because (1) aridity is the key environmental variable in West Africa and (2) the predicted drier climate in most tropical regions could result in forest dieback and further accelerate global warming.

4.1.1 The significance of the paper

In this paper, carbon budget from West African forests was compared to that from Amazonia forests, along an equivalent aridity gradient using the same protocol. The results show that strikingly, West African dry forests are more productive than lowland Amazonia wet evergreen forests, and than West African wetter forests. The above pattern, however, is not shown in global GPP modelling products because the West African forests GPP were severely underestimated. The paper also featured the discovery of the world's most productive forest measured to date.

The paper is of great interest to a wider audience, beyond carbon cycle specialists and to mass media, for several reasons. The study challenges conventional assumptions that wet evergreen tropical ecosystems are the most productive, and instead highlights West African forests as an extremely productive ecosystem. However, this ecosystem is underrepresented in the literature and subject to severe fragmentation and tree loss. The significant carbon storage and high productivity of the forests also suggest great conservation benefits, thereby attracting the attention of conservationists.

4.1.2 Author contributions

I am very grateful to the many people who have devoted themselves to field data collection over the past decade. There is a long story behind this paper. The study began with a grant from the UK Natural Environment Research Council (NE/1014705/1) in 2011, which proposed only two sites (ANK and BOB) with a strong focus on the role of carbon use efficiency in determining net primary production (NPP), without mentioning aridity. The third site (KOG) was added following Advanced Investigator Grants to Y.M. and R.V. from the European Research Council (GEM-TRAIT and Africa-GHG, respectively), which formed an aridity gradient. It appeared that the aridity gradient pattern was fascinating and become the central piece of a previous paper reporting NPP from these sites (Moore *et al.*, 2018). Several previous lab members, collaborators, and many field research scientists and assistants devoted a great deal of effort also to the collection of respiration data. Many co-authors cleaned and maintained the original respiration dataset, but it had not been analysed and interpreted. During the COVID lockdown, my planned fieldwork was cancelled. Instead, in 2020, I gathered, cleaned, and calculated the respiration flux and completed the carbon budget of these sites, with help from many co-authors. The original respiration dataset was in a challenging state due to the time lapse and the change of personnel. However, the humdrum of checking each field sheet and record (including 22,000 hemispherical photos) was quickly outpaced by the excitement of the surprising discovery of the most productive intact forests. **I became fascinated by West African forests because of this paper.**

The manuscript is now ready to be submitted to *Nature Geoscience*, but I am still waiting for some co-authors' replies.

4.1.3 Specific author contributions

Huanyuan Zhang-Zheng: Conceptualization; Formal Analysis; Investigation; Writing – original draft; Writing – review & editing.

Stephen Adu Bredu, Sam Moore: Conceptualization; Investigation; Resources.

Akwasi Duah-Gyamfi, Shalom D. Addo-Danso, Forzia Ibrahim, Armel T. Mbou, Agnes de Grandcourt, Riccardo Valentini, Giacomo Nicolini, Gloria Djagbletey, Kennedy Owusu-Afriyie, Agne Gvozdevaite, Maria C. Ruiz-Jaen: Investigation; Resources and data collections.

Cécile A.J. Girardin: Investigation; Formal Analysis; Writing – review & editing.

Sami Rifai, Cecilia Dalshjo, Terhi Riutta, Minxue Tang, Yuheng Sun: Formal Analysis; Data Curation.

Colin Prentice: Supervision, Writing – review & editing.

Imma Oliveras, Yadvinder Malhi: Conceptualization; Resources; Investigation; Supervision, Writing – review & editing.

CONTRASTING CARBON BUDGET ALONG FOREST ARIDITY GRADIENTS IN AFRICA AND AMAZONIA

Huanyuan **Zhang-Zheng**[1], Stephen **Adu Bredu**[3], Akwasi **Duah-Gyamfi**[3], Sam **Moore**[1], Shalom D. **Addo-Danso**[3], Forzia **Ibrahim**[3], Armel T. **Mbou**[4], Agnes **de Grandcourt**[4] Riccardo **Valentini**[4], Giacomo **Nicolini**[4], Gloria **Djagbletey**[3], Kelvin **Anim-Adjei**[3], Kennedy **Owusu-Afriyie**[3], Agne **Gvozdevaite**[1], Maria C. **Ruiz-Jaen**[6], Cécile A.J. **Girardin**[1], Sami **Rifai**[1], Cecilia **Dalshjo**[1], Terhi **Riutta**[1], Minxue **Tang**[5], Yuheng **Sun**[5], Iain Colin **Prentice** [5], Imma **Oliveras Menor**[1,2], Yadvinder **Malhi**[1],

1 Environmental Change Institute, School of Geography and the Environment, University of Oxford, Oxford, United Kingdom

2 AMAP (Botanique et Modelisation de l'Architecture des Plantes et des Végétations), CIRAD, CNRS, INRA, IRD,Université de Montpellier, Montpellier, France

3 Forestry Research Institute of Ghana, Council for Scientific and Industrial Research, Kumasi, Ghana

4 Centro Euro-Mediterraneo sui Cambiamenti Climatici, Leece, Italy

5 Georgina Mace Centre for the Living Planet, Department of Life Sciences, Imperial College London, Silwood Park Campus, Buckhurst Road, Ascot, SL5 7PY, UK

6 Subregional Office for Mesoamerica, Food and Agriculture Organization of the United Nations, Panama City, Panama

4.2 ABSTRACT

African tropical forests cover a vast area of the tropics and play a significant role in the global carbon cycle. However, there is a lack of in-situ measurements to understand the forests' gross primary productivity (GPP) and their allocation. Here we present the first

detailed field assessment of the carbon budget of African forests, by monitoring 14 one-hectare plots along an aridity gradient in Ghana, West Africa. When compared with an equivalent aridity gradient in Amazonia using the same measurement protocol, strikingly the studied West African forests generally had higher net primary productivity (NPP), higher GPP, and lower carbon use efficiency (CUE). The West African aridity gradient consistently shows the highest NPP, CUE, GPP, and autotrophic respiration at medium-aridity sites. Notably, NPP and GPP of the site (BOB) are the highest yet reported anywhere in the tropics using similar methods. They also allocated a larger proportion of GPP to canopy than the Amazonian forests, where we recorded a shorter canopy carbon turnover time. Our analysis suggests that the high productivity of the African forests is linked to their semi-deciduous characteristics. Yet these productive West-African forests are severely fragmented and under pressure from land use change and require urgent conservation measures to be implemented to avoid continued carbon loss. Further, these irreplaceable forests should be conserved for a multitude of benefits they provide to the local environment, to biodiversity and society.

Keywords: tropical forest, gross primary production, carbon allocation, autotrophic respiration, wet–dry gradients, West African, Amazonia,

4.3 Introduction

Tropical forests and savannas account for over 60% of global terrestrial gross primary productivity (GPP) (Beer et al., 2010). The partitioning of photosynthate into different components of autotrophic respiration (R_{auto}) and net primary production (NPP) (i.e. into short-lived tissues versus long-residence woody biomass), is an equally important but much less studied feature (DeLUCIA et al., 2007; Franklin et al., 2012; Litton et al., 2007). Unlike GPP, which can be estimated by multiple methods including eddy covariance measurements and remote sensing, R_{auto}, NPP, and their components still require intensive

field campaigns for quantification. As most carbon models start from GPP and calculate R_{auto} or carbon use efficiency (CUE = NPP/GPP) as a means to determine net primary productivity and equilibrium biomass, the dearth of field measurements on carbon allocation leads to simplified model assumptions or disagreement among models, restricting our ability to predict the effects of global change on the carbon dynamics of the biosphere (He et al., 2018; Ise et al., 2010; Purves & Pacala, 2008). For example, notwithstanding that a worldwide forest CUE of ca. 0.5 has been presumed in some studies (Enquist et al., 2007; Ise et al., 2010; Van Oijen et al., 2010), field measurements have suggested otherwise (Collalti & Prentice, 2019; DeLUCIA et al., 2007); especially for tropical old-growth forests where low CUE is commonly reported (0.23–0.45 for Amazonia (Doughty et al., 2018) and 0.34–0.43 for Asia (Kho, 2013; Mills et al., 2023; Tan et al., 2010)). There has this far no direct field quantification of CUE for any forests in Africa.

Field evidence regarding African tropical forests is particularly scarce. In the entire African tropical forest region, there has been only one eddy covariance tower (in Ankasa, Ghana), reporting three years of GPP (2011–2014) (Chiti et al., 2010; Fattore et al., 2014). Satellite-based GPP products struggle to provide reliable estimates of GPP of the region owing to the dense cloud cover, which extends across both wet and dry seasons (Fensholt & Proud, 2012; Sudmanns et al., 2020; Zhao et al., 2005). As there is no field assessment of GPP, R_{auto} and their allocation, consequently in carbon modelling or global analysis, African tropical forests are inevitably often omitted or parametrized based on data collected from other tropical forest regions,

However, it may be incorrect to assume that all tropical forest regions exhibit similar carbon dynamics and climate sensitivities. Some evidence suggests that African forests' carbon cycling could be very different to Amazonian Forest. For example, African and Amazonian tropical forests have experienced very different biogeographic and climatic

histories (Malhi et al., 2013). A satellite-based study found the trend of African NPP during 2000–2009 contrasted with that of Amazonian forests (Zhao & Running, 2010). Furthermore, a stable and positive carbon sink into stem biomass for African forests was reported to contrast with the declining trend in Amazonian forests, owing to the different mortality rates following drought events (Hubau et al., 2020). Bennett et al. (2021) suggested that African forests are more resistant to drought than other tropical forests, likely linked to the long history of greater climatic variation in the African tropics, compared to Amazonia. Moreover, Field measurements of NPP (Moore et al., 2018) revealed that along a wet-dry gradient in West Africa there was evidence that NPP was higher compared to equivalent gradients in Amazonia (Malhi et al., 2015).

Along wet-dry gradients in Amazonia, it has been reported that GPP declines toward drier sites, but not NPP, owing to the concomitant changes in CUE (Malhi et al., 2015). An equivalent gradient study in West Africa also noted no unimodal decline of NPP with increasing aridity (Moore et al., 2018), but GPP and CUE have not been investigated and compared to other tropical ecosystems for contextual understanding.

In this paper we report a more comprehensive analysis of carbon dynamics along the same West African aridity gradient and compare to previously published results for Amazonia to address the following questions: (1) is the higher NPP reported for the West African forests also reflected in higher GPP, or in higher CUE? (2) is the relationship between productivity and aridity similar along the West African and Amazonian Forest gradients? (3) Do the studied Amazonian and West African forests share similar carbon flux partitioning patterns?

4.4 Amazonia and West Africa comparison regarding productivity and respiration

Our comparison reinforces that the carbon flux of the studied West African forests is distinctly different to that previously reported for Amazonian tropical forests. Overall, the total NPP and R_{auto} were higher in West Africa than Amazonia along the aridity gradients (Table S 2 and Figure 2), albeit the wettest sites share similar values. The difference arises from differences in canopy NPP and leaf respiration rates (Figure 2). In contrast, stem woody productivity and rhizosphere respiration appear higher in the Amazonian studies, implying very different allocation patterns between the two studied regions (Figure 3). Overall, these differences lead to our estimates of GPP being much higher in the West African gradient than in Amazonia, particularly in the drier sites. As the two regions have similar LAI and biomass, the above lead to shorter carbon turnover time in West Africa. However, unlike in-situ estimates, FLUXCOM (climate-based extrapolation from global flux tower networks) and MODIS (satellite remote sensing) estimated West African forests to have lower GPP than Amazonia (Figure 4). This is also evident in other studies using vegetation models or satellite-based products (Anav et al., 2015; Beer et al., 2010; Li & Xiao, 2019). We found FLUXCOM consistently underestimated both Amazonia and West African forests GPP (Figure 4), and MODIS GPP was even lower. It seems likely that dynamic vegetation models also underestimate West African forests GPP because previous studies involving our wet rainforest site Ankasa (Chiti et al., 2010; Fattore et al., 2014) found model GPP estimates lower than the flux-tower GPP (yearly mean varying from 22 to 36 MgC/ha/year) that is smaller than in-situ measurements (40.1 MgC/ha/year) (Chiwara et al., 2018; Martín Belda et al., 2022; Wang et al., 2017). The above synthesis reveals acute data-model discrepancy in tropical forests productivity estimates, especially for West African forests, which require more detailed investigation.

4.5 Variation along the aridity gradient and variation within the site

It is striking to find that along aridity gradients in both Amazonia and West Africa, as CUE peaks at mid-aridity sites, NPP is generally maintained or possibly even enhanced in seasonally dry forests, before dropping off in very dry forests (Figure 2). This pattern mostly arises from patterns in leaf and fine root productivity. Woody stem productivity does show strong site-to-site variation, but no clear pattern along both the aridity gradients. Strikingly, along the African transect GPP, R_{auto} and NPP are highest in the mid-aridity site, a pattern not found in Amazonia. Along both transects, CUE peaks at mid-aridity plots. The pattern of GPP along the aridity gradient is well simulated in MODIS but not FLUXCOM (Figure 4). The study thereby highlighted that dry forests could be more productive than wet evergreen forests, as revealed in comparing West African dry forests (BOB) to wetter forests (ANK), and to Amazonia lowland forests (Figure 2).

Within-site comparisons can reveal the impact of local environmental factors. For example, the seasonally flooded swamp forest ANK03, despite having less stem biomass (135.36 MgC/ha) than the adjacent dry substrate forest (162.7 and 153.3 MgC/ha for ANK01 and ANK02), does not have significantly different NPP and GPP (Figure S 4). Similarly, the different history of logging in Bobiri (see method), and steep variation of biomass along forest-savanna transition Kogyae do not seem to result in any significant difference in either NPP or GPP (Figure S 4). There was also no discernable pattern when comparing photosynthate allocation between plots within any site (Figure 4). In contrast, previous studies reported that GPP and NPP change considerably from wet to dry sites in Amazonia (Araujo-Murakami et al., 2014; Doughty et al., 2015; Malhi et al., 2015) and along forest-savanna transition (Scalon et al., 2022). A modest variation of NPP with logging intensity was reported in Borneo (Riutta et al., 2018), but that was for much higher intensities of logging than at the Bobiri site. Such patterns were not seen for our Bobiri

study and another West-African study on logging (Morel et al., 2019). The above implies that aridity is the primary driver of productivity and its partitioning of these forests, than other local environmental factors. The lack of plot-to-plot variation increase the confidence of exceptionally high GPP measurements, and also open future research opportunity in west-African forest adaptation strategy to varying environments.

4.6 Contrasting patterns in carbon allocation

We found that our African forests' CUE appeared generally lower than previously reported values for Amazonian forests. Given that the Amazonia CUE is lower than the global average (see introduction), our finding further expands the global range of CUE and confirms that globally tropical forests are a low CUE ecosystem (Collalti & Prentice, 2019; Doughty et al., 2018). Among all plots, CUE has no correlation with GPP (Figure S 1), whereas both GPP and CUE significantly correlate with NPP. Although overall CUE explains less spatial variation in NPP than GPP, CUE does have considerable spatial variation and assuming a fixed CUE parameters in a model for both studied gradients would mis-represent spatial variation of NPP (Doughty et al., 2018).

More differences between Amazonia and West African forest carbon cycling were revealed in a further investigation of photosynthate allocation into canopy, fine root, and wood NPP and respiration (see Figure 3 for definition). Note that this is the partitioning of flux instead of the more commonly reported biomass allocation (Ceballos-Núñez et al., 2020). In both regions, the allocation pattern of autotrophic respiration is more homogeneous across plots than the allocation of NPP (i.e., points in Figure 3a are more clustered than Figure 3b). For NPP, the Ankasa wet rainforest site shows allocation patterns within the spectrum of Amazonian plots. The drier semi-deciduous site (Bobiri) consistently allocates more to the canopy than the reported Amazonian sites do. In contrast, the dry Kogyae site allocates consistently less to canopy and more to wood. For

autotrophic respiration, leaf respiration clearly separates West African plots from Amazonian plots (Figure 2, 3). The dry Kogyae forests allocate more to wood respiration and the semi deciduous Bobiri sites allocate more to the canopy, both of which match the NPP allocation trends. Overall, the carbon allocation of tropical forests to different components is highly variable between sites. Most variation can be seen in photosynthate allocated to the canopy, with a canopy respiration range from 24% to 63% and canopy NPP from 23% to 63%, substantially higher and more dynamic than that reported by previous extra-tropical meta-analyses (Litton et al., 2007).

The high variability in allocation patterns leads to questioning of the "fixed-ratio method" for intact forests carbon modelling (Franklin et al., 2012; Ostle et al., 2009). Despite the large spatial variation, NPP partitioning to the canopy is the most dominant portion in our study site, consistent with previous in situ evidence, but not shown in satellite-based products or vegetation models (Xia et al., 2019; Yang et al., 2021). Moreover, along both the Amazonia and West-African aridity gradients, spatial patterns in woody NPP do not represent the spatial pattern of total NPP or GPP (Figure 2). Previous studies also found canopy NPP could explain greater spatial variation of total NPP compared with stem NPP (Arag̃o et al., 2009; Malhi et al., 2011). The evidence gathered there highlights the great importance of CUE and canopy NPP, whereas previous literature has paid much more attention to GPP and stem NPP (Anderson-Teixeira et al., 2016); hence, future research is needed to balance the scale and complete the carbon cycle.

4.7 Why West African seasonally dry forest is more productive

As the wet evergreen forests in Amazonia Allpahuayo and West African Ankasa show similar levels of productivity (Figure 2), the reasons for the mean high productivity in the West African transect resides with the drier African plots (BOB and KOG), in particular, the most productive plot, BOB-02. The plot has a very high estimated GPP at 48.5 ± 3.2

and NPP at 21.3 ± 1.29 MgC/ha/year, the latest values reported this far for natural forests stands to our knowledge (Anderson-Teixeira et al., 2021) (although, it should be noted that farmland or logged forest may have even higher NPP (Morel et al., 2019; Riutta et al., 2018)). BOB02, compared to other plots in this study, has exceptionally high GPP, CUE, NPP, and R_{auto} simultaneously. All six plots in the Bobiri Forest reserve (now 54 km^2 only) show generally very high GPP (Figure S 2) so this high productivity is representative of the wider region. High NPP was also supported by another two one-hectare plots at Kakum, approximately 200 km to the south of Bobiri (Morel et al., 2019) and by a previous study focusing on aboveground NPP (John, 1973).

Since the most distinct difference between Bobiri forests and Amazonian forests is in carbon allocation to canopy (high leaf NPP and respiration), the high productivity of this mid-arid site should be associated with its special deciduous leaf phenology - remaining green all seasons but with only 5.2 ± 0.6 months leaf lifespan (Moore et al., 2018), substantially shorter than Amazonia (>12 months) (Flack-Prain et al., 2019). In other words, similar LAI and biomass but very different turnover time. Such a carbon strategy, however, entails higher leaf-level photosynthesis to provide more energy replacing leaves lost via turnover (Gibert et al., 2016). Species at BOB were indeed characterized by a high photosynthesis rate (Oliveras et al., 2020; Tomlinson et al., 2013). Like BOB02, another mid-arid plot in Amazonia, Kenia (KEN01), with the highest NPP along the Amazon aridity gradient, also featured a similar carbon strategy with more seasonality, higher CUE, and quicker carbon turnover. It is possible that BOB02 and KEN01 are recovering from previous disturbances (see Methods) (Araujo-Murakami et al., 2014; DeLUCIA et al., 2007; Malhi et al., 2009) or simply a common characteristic of semi-arid forests that were dominated by fast-growing pioneer species (Rocha et al., 2014). The high photosynthetic rate is consistent with short leaf lifespan and semi-deciduous phenology (Jin et al., 2016; Wright et al., 2004).

In short, our findings suggest that semi-deciduous sites might be the most productive tropical forests, even more than wet evergreen. The counterintuitive finding is in fact consistent with ecological theories. Gigantic trees dominate wet evergreen forests. Each maximize their own resource acquisition leading to a "tragedy of the commons status", where overall community resource-use efficiency is lower and hence less forest-total productivity (Farrior, 2014; McNickle et al., 2016; Schieving & Poorter, 1999). Whereas semi-arid forests experiencing frequent dry spells are subject to the intermediate disturbance hypothesis with higher mortality rates, species richness and productivity (Araujo-Murakami et al., 2014; Bongers et al., 2009). Previous study reveals that long-term drying trend has driven these mid-aridity forests toward more deciduousness (Aguirre-Gutiérrez et al., 2019; Fauset et al., 2012), making them more resilient to climate change than wet-evergreen Amazonia forests (Bennett et al., 2021; Hubau et al., 2020). Our analysis highlights that West-African forests have contrasting carbon strategy to Amazonian forests. However, as our sample sites are within one country, more evidence is required to achieve complete understanding of the special African forests carbon cycle.

We present the first complete carbon budget of African tropical forests to date by utilizing extensive field measurements across 14 one-ha plots, contributing towards a more comprehensive understanding of forest carbon allocation. The findings reveal that the productivity of West African dry forests could exceed that of Amazonian lowland forests but was previously underestimated. Furthermore, the study also featured the discovery of the world's most productive forests measured to date – Bobiri forest reserve. However, it should be noted that Bobiri forest is now a mere 54 km^2 patch. The West African tropical forests are severely fragmented (Norris et al., 2010) and increasingly face land use change pressures (Achard et al., 2014; Buchanan et al., 2021). The forests not only present significant carbon stores (Cuni-Sanchez et al., 2021) and high productivity (Figure 2) but as ancient and complex ecosystems, these forests are also adaptable and resilient to change

(Fauset et al., 2012; Watson et al., 2018). Avoiding deforestation of these irreplaceable ecosystems must become an urgent priority.

4.8 Figures

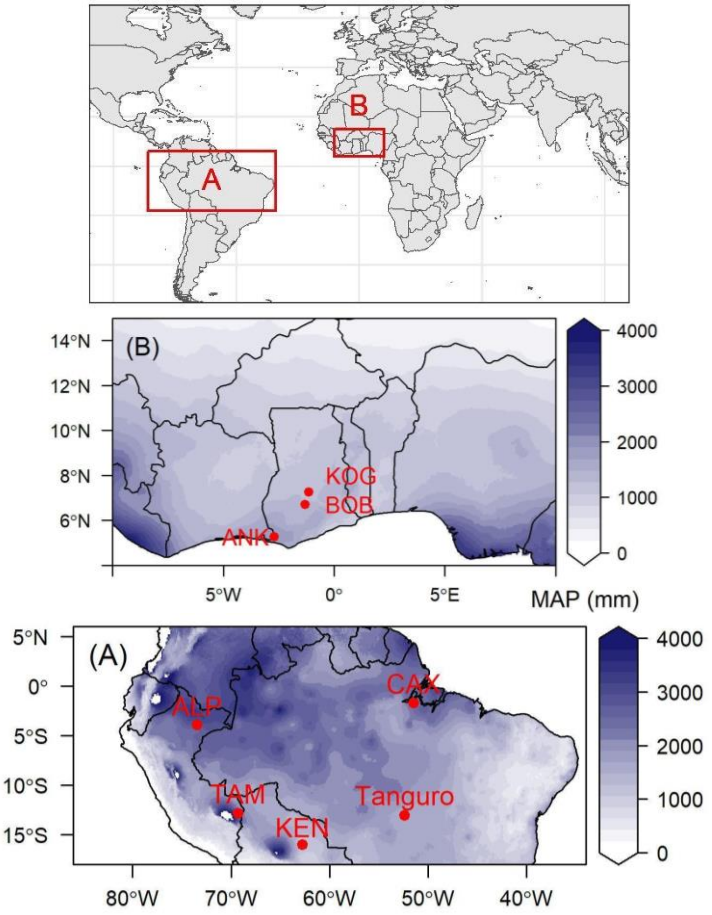


Figure 1 Map of study sites. (A) Amazonia aridity gradient and (B) West-African aridity gradient. Colour scale illustrate mean annual precipitation (MAP). Each red dot denotes a site. Each site contains multiple one-hectare plots (Table S1)

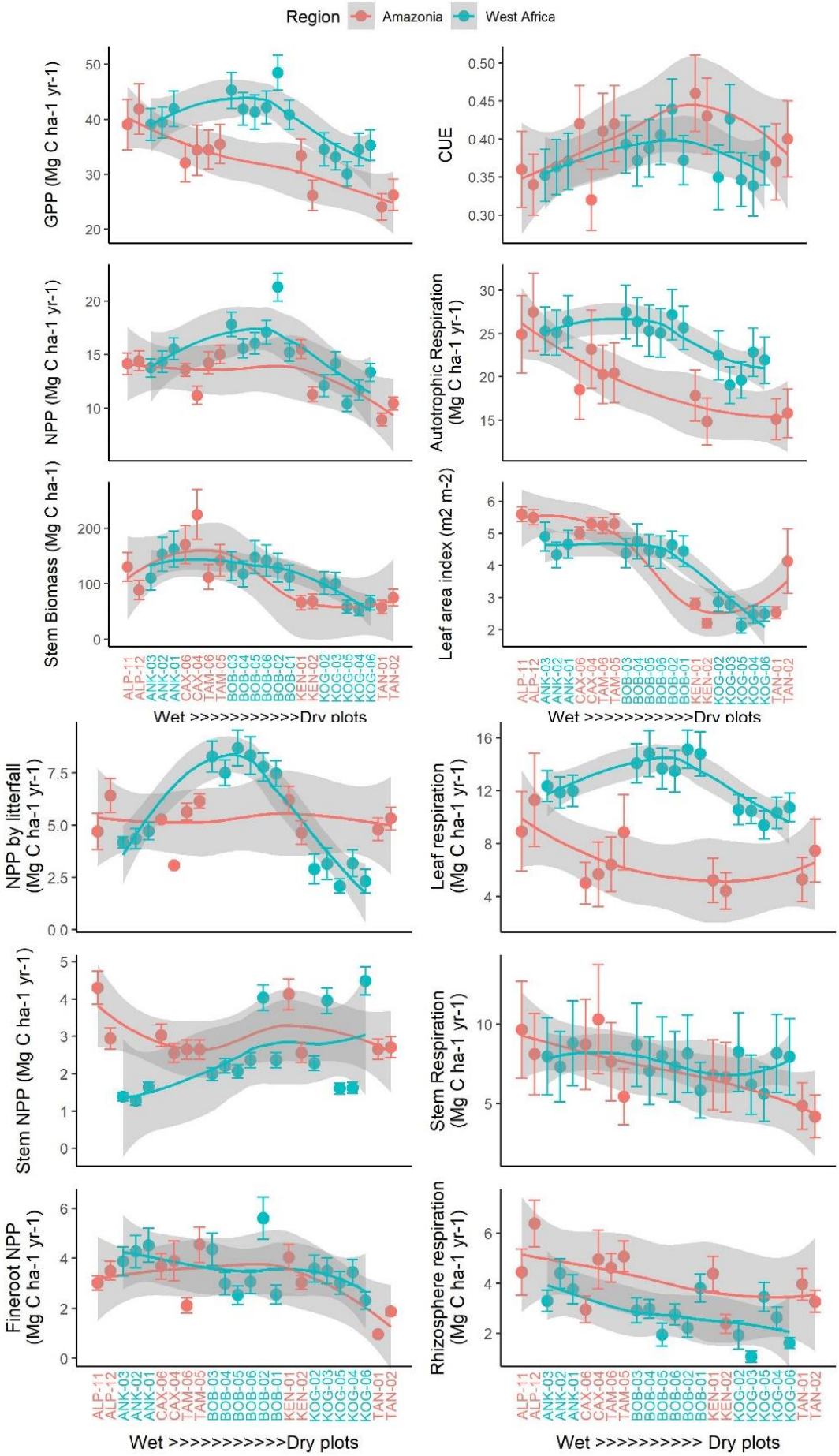

Region
Amazonia
West Africa
GPP (Mg C ha-1 yr-1)
CUE
NPP (Mg C ha-1 yr-1)
Autotrophic Respiration (Mg C ha-1 yr-1)
Stem Biomass (Mg C ha-1)
Leaf area index (m2 m-2)
ALP-11
ALP-12
ANK-03
ANK-02
ANK-01
CAX-06
CAX-04
TAM-06
TAM-05
BOB-03
BOB-04
BOB-05
BOB-06
BOB-02
BOB-01
KEN-01
KEN-02
KOG-02
KOG-03
KOG-05
KOG-04
KOG-06
TAN-01
TAN-02
Wet >>>>>>>>>>>>Dry plots
NPP by litterfall (Mg C ha-1 yr-1)
Leaf respiration (Mg C ha-1 yr-1)
Stem NPP (Mg C ha-1 yr-1)
Stem Respiration (Mg C ha-1 yr-1)
Fineroot NPP (Mg C ha-1 yr-1)
Rhizosphere respiration (Mg C ha-1 yr-1)
Wet >>>>>>>>>>>>Dry plots
Wet >>>>>>>>>>> Dry plots

Figure 2 Comparing in-situ estimates of various components of carbon fluxes between Amazonia plots (red) and West African plots (green). Local polynomial regression fitting lines (LOESS) are drawn for each region. See Table 1 for the definition of each carbon flux component. One dot represents one plot (one hectare). The error bars represent the uncertainty of estimates (see Supplementary Material 1 for uncertainty estimation). The curves and their uncertainties (grey zone) were given by Local polynomial regression. The x-axis is a factorial order of aridity. From wettest (left) to driest (right), plots were ranked by maximum climatological water deficit (MCWD mm year^{-1}). if not discernible by MCWD as some plots are too close, by in situ-measured surface soil moisture (Table S1).

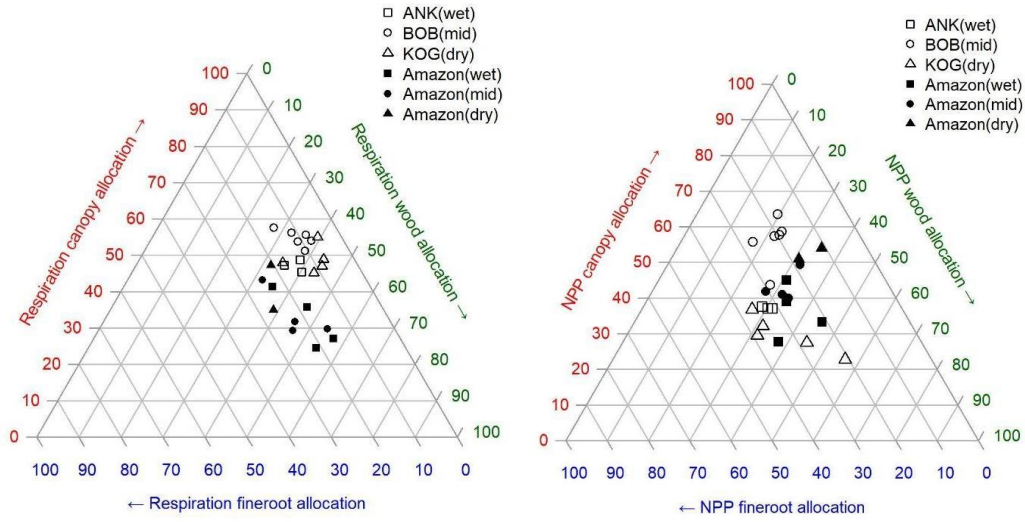


Figure 3 Percentage allocation of NPP and Autotrophic respiration. One dot represents one plot, for West African (hollow dot) and Amazonia (solid dot). The aridity of plots was illustrated with a dot shape. Allocation percentage should be read by following the arrow and ticks on each axis. For example, in the NPP diagram, the top hollow-round dot (BOB05) represents high allocation (63%) to canopy (red), 20% to wood (green), and 17% to fine roots (blue). The percentage of allocation was calculated as follows: NPP canopy allocation (%) * NPP = NPP_fine_litter_fall + NPP_herbivory; NPP wood allocation (%) * NPP = NPP_all_stem + NPP_coarseroot + NPP_branch; NPP fineroots allocation (%) * NPP = NPP_fineroot; Respiration canopy allocation (%) * R_autotrophic = R_leaf; Respiration wood allocation (%) * R_autotrophic = R_stem+R_coarse_root; Respiration fineroots allocation (%) * R_autotrophic = R_fine_root. See Method for the definition of each component.

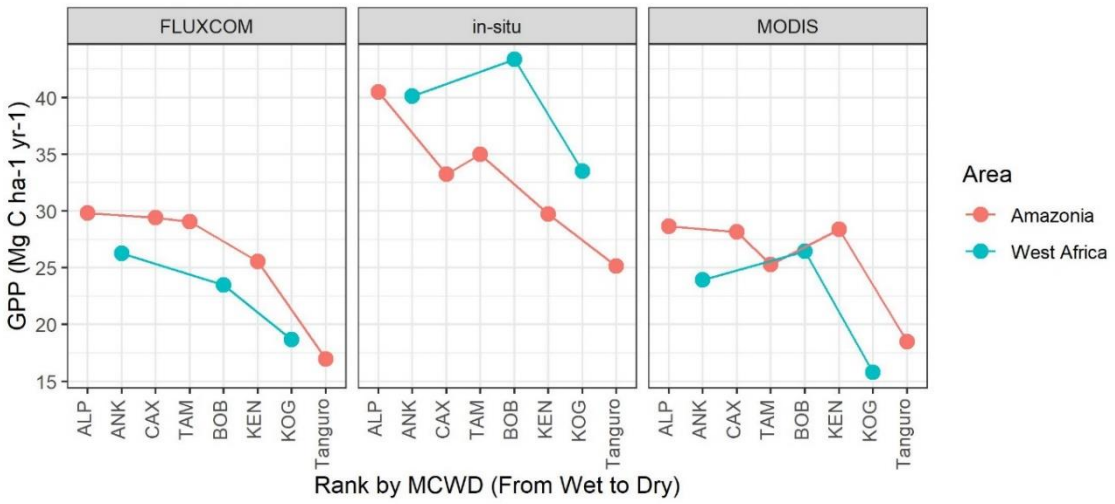


Figure 4 Comparing gross primary productivity (GPP, MgC ha-1 year-1) estimates of 5 sites in Amazonia (green dots) and 3 sites in West Africa (red dots) by FLUXCOM (left panel), in-situ (mid panel) and MODIS. The in-situ panel is equivalent to Figure 2 but on a site scale. One dot represents one site. Each site contains multiple one-hectare plots (Table S1)

4.9 Methods

4.9.1 The Ghanaian aridity gradient

As part of the Global Ecosystem Monitoring (GEM) network (Malhi et al., 2021), 14 one-hectare plots were established within three forest reserves in Ghana (Table S1, Figure 1) spanning an aridity gradient. There are three plots in the wettest forest reserve, Ankasa National Park (ANK), which receives a mean annual precipitation of 2050 mm. The medium-aridity forest reserve Bobiri (BOB) hosted six plots with a rainfall of 1500 mm. At the driest end, Kogyae Wildlife Reserve (KOG) had five plots with a rainfall of 1200 mm. These plots have a very similar mean annual temperature, but span a steep precipitation gradient, which provided a "natural laboratory" to investigate the stand-alone effect of aridity on forest productivity and respiration. Aridity of each plot is indicated by maximum climatological water deficit (MCWD mm/year) or, if not discernible by MCWD, by in situ-measured surface soil moisture (Table S1), in accord with soil hydrology

modelling of these sites (Paper 2). Along the aridity gradient, vegetation seasonality and deciduousness increased considerably toward the drier sites (Moore et al., 2018). Leaf area index and the number of trees decreased toward drier sites (Paper 2). More information about the study sites, on soil properties, hydrology and climate regime could be found at (Afreen et al., 2019; Caton Harrison et al., 2021; Moore et al., 2018; Oliveras et al., 2020). Forests in ANK and BOB have never been burnt but KOG experiences wildfire roughly every decade (Chiti et al., 2010; Janssen et al., 2018).

Although plots within the same forest reserve share very similar air temperature and precipitation, they differ dramatically in terms of soil moisture and composition of the vegetation community because of their soil properties, topography, and disturbance history. ANK is a humid rainforest and Pleistocene refuge with three plots spanning dry uplands (ANK01 and ANK02) and seasonally inundated riverine lowland (ANK03). BOB is a semi-deciduous forest where the plots span a gradient with selective logging history, spanning from the intact forest (BOB01) to forest lightly logged (2-3 stem/ha) in 1959 (BOB02 – 04) and in 2001 (BOB05 -06). KOG is a forest-mesic savanna transition where local soil factors appear to influence vegetation type from dry forest (KOG02) to savanna (KOG06) (Zhang-Zheng et al., 2023). Within any site (e.g., within ANK), there are common species between plots; however, the most abundant species may still differ, although there is almost no common species between sites.

4.9.2 Detailed carbon budget quantification

The study quantified the whole carbon cycle of 14 West African plots (one-hectare each) with a bottom-up method mostly following the GEM protocol (Malhi et al., 2021; Marthews et al., 2015). For each GPP component, a definition and brief description of the sampling method is provided in Table 1. The detailed sampling technique, calculation and scaling process, and references are explained in Supplementary Method. For completeness

and consistency, we sourced the estimate of some NPP components from another study (Moore et al., 2018). Carbon allocation (the partitioning of GPP) was illustrated with a ternary plot (Figure 3), drawn by R package "Ternary." The Z test was used to assess the difference among plots. Relevant statistics were reported in Table S2 and Figure S 4.

Our reported NPP and R_{auto} are completely independent measurements. The plot-to-plot variations (Figure 2) in NPP and R_{auto} are highly similar, and analogous allocation patterns (Figure 3) could also be found between NPP and R_{auto}, which reinforce the reliability of the findings. Furthermore, we found the sum of R_soil_heterotrophic and R_cwd was roughly equal to the sum of D_cwd, D_litter_fall, and D_root in each site (Figure S 3). This is an important cross-check to validate our carbon flux measurements because R and D are independent measurements, and they were expected to be equal in steady-state conditions.

The study also featured a comparison with detailed carbon budgets of Amazonian plots where the same sampling protocol was applied (Malhi et al., 2021). The carbon budget of these plots was sourced from (Malhi et al., 2015). The western Amazonian sites include Allpahuayo in NE Peru with no seasonality (del Aguila-Pasquel et al., 2014), Tambopata in SE Peru with moderate dry season (Malhi et al., 2014) and Bolivia featuring strong dry season (Araujo-Murakami et al., 2014) which is situated between humid Amazon Forest and chiquitano dry forest. The eastern Amazonian sites include Caxiuana, humid forests in NE Brazil (da Costa et al., 2014)and Tanguro dry forests in SE Brazil (Rocha et al., 2014), which sits close to the dry forest-savanna ecotone. See Table S 1 and references above for more characteristics of the sites.

4.9.3 FLUXCOM and MODIS

Using Google Earth Engine, we retrieved MODIS GPP from the collection MOD17A3HGF during 2001 to 2020. This collection of GPP has been cloud

contamination filtered and gap filled by the data providers. We chose the 'RS_METEO' version of FLUXCOM because the magnitude of GPP in this version does not involve uncertainty from MODIS FAPAR, which makes the comparison between FLUXCOM and MODIS GPP more independent. We extracted GPP of the studied plots using their coordinates and calculated mean per site.

Table 1 Abbreviation for components of NPP. See Supplementary Method for field protocol and calculation procedures. Data were retrieved from (Moore et al., 2018) except NPP_root_exudate.

Components of NPP	Meaning	Sampling period and interval
NPP_canopy	The sum of NPP_fine_litter_fall and NPP_herbivory	
NPP_fine_litter_fall	NPP by litterfall in Figure 2, measured by litter fall trap, it is the sum of leaf, twig, flower, fruit, seed and 'unidentified', not including NPP_herbivory and NPP_branch. The sum of flower, fruit and seed is called 'reproductive NPP'.	2011–2013(ANK) 2012–2015 (BOB&KOG), every 14 days
NPP_herbivory	NPP_leaf multiplied by 'the percentage of leaf bitten by animals', which were obtained from leaf scan.	2012–2013(ANK) 2012–2015 (BOB&KOG), every two months
NPP_branch	Measured with coarse woody debris census (i.e. branch litter larger than fine litter fall), it is representing the NPP that trees used to update their branch every few months. The branch is growing larger as the tree stature enlarge, meanwhile, the small branch is also updating themselves (e.g. because of wind damage), the former one is counted in NPP_all_stem, the later one is counted in NPP_branch	2012–2013(ANK) 2012–2015 (BOB&KOG), every three months
NPP_big_stem	Measured through stem diameter and tree height, for tree larger than 10cm diameter at breast height, representing the expanding of tree stem	2011–2013(ANK) 2011–2015 (BOB&KOG), every year
NPP_small_stem	Measured through stem diameter and tree height, for tree smaller than 10cm diameter at breast height, representing the expanding of tree stem	2011–2013(ANK) 2011–2015 (BOB&KOG), every year
NPP_all_stem	The sum of the above two. This is the 'Stem NPP' in the main figure	
NPP_coarseroot	Estimated by a root shoot ratio of 0.21 multiplied by NPP_all_stem, representing the expanding of tree coarse root	Estimated
NPP_fineroot	Measured using 'ingrowth core' technique, representing NPP in reproducing fine roots	2012–2013(ANK) 2012–2015(BOB&KOG), every three months
NPP_herbs	Measured by grass harvest, NPP of understory vegetation, mostly herb and grass	2014–2015(KOG only, there are little herbs in BOB and ANK), every three months
NPP_root_exudate	NPP of root exudates, estimated as a mean of several methods (Riutta et al., 2021). See Supplementary Method.	Estimated
NPP_AG	Aboveground NPP, sum of NPP_fine_litter_fall, NPP_herbivory, NPP_branch,NPP_all_stem and NPP_herbs	
NPP_BG	Belowground NPP, sum of NPP_fineroot, NPP_coarseroot and NPP_root_exudate	
NPP	The sum of NPP_AG and NPP_BG	

NPP_voc	NPP of volatile organic compound, not included in this study. It is thought to be a negligibly small proportion of total NPP (Malhi et al., 2011).	Not included

Table 2 Abbreviation for components of respiration and detritus flux. See Supplementary method for field protocol and calculation procedures.

Components	Meaning	Sampling period and interval
R_leaf	Respiration flux from leaf surface, calculated as R_dark * LAI	
LAI	Leaf area index, measured with hemispherical photo	2016-2017(ANK), 2012-2017 (BOB&KOG), every month
Rdark_shade	Measured leaf dark respiration for shade leaves	2014-2016 (ANK, BOB & KOG), every three months
Rdark_sun	Measured leaf dark respiration for sun leaves	2014-2016 (ANK, BOB & KOG), every three months
R_stem	Measured stem respiration	2016 (ANK), 2014-2016 (BOB & KOG), every month
R_soil	Soil respiration, including litter, but not coarse root respiration. The components were measured with EGM5 soil chamber, We assume that the soil respiration measurement (by installing a chamber on the ground) will capture fine litter respiration, soil organic matter respiration, rhizosphere respiration (including fine root respiration, mycorrhizal and priming effect etc), but will not capture coarse root respiration (Malhi et al., 2014). We then break this down into R_fine_litter, R_SOM and R_rhizosphere with partitioning experiments (Riutta et al., 2021).	2016 (ANK), 2013-2016 (BOB), 2014-2016 (KOG), every month
R_rhizosphere	Respiration associated with rhizosphere (like fine root, mycorrhizal or priming effect), see R_soil for method	Derived from the above with partitioning experiments
R_fine_litter	Respiration from litter layer above soil, see R_soil for method	Derived from the above with partitioning experiments
R_SOM	Respiration from soil organic matter, see R_soil for method	Derived from the above with partitioning experiments
R_soil_heterotrophic	The sum of R_fine_litter and R_SOM	Derived from the above with partitioning experiments
R_coarse_root	Coarse root respiration, estimated as root shoot ratio multipled by R_stem	Estimated
R_autotrophic	Termed R_{auto} in the main text. Total autotrophic respiration = R_stem+R_coarse_root+ R_fine_root + R_leaf	
R_heterotrophic	Heterotrophic respiration, The sum of R_cwd and R_soil_heterotrophic, by definition it should also include animal respiration and R_mycorrhizal but these were not included in this study.	

R_cwd	Respiration from coarse woody debris (any nacromass not included as fine litter), estimated in this study	Estimated
GPP	Gross primary production, as NPP + R_autotrophic	
CUE	Carbon use efficiency, as NPP/GPP	
NEP	Net ecosystem productivity (Same as net ecosystem exchange), as NPP- R_heterotrophic	
D_litter_fall	Detritus in the form of fine litter, from aboveground biomass to soil, equal to NPP_fine_litter	
D_CWD	Detritus in the form of coarse woody debris, from aboveground biomass to necromass, as NPP_all_stem +NPP_cwd	
D_root	Detritus from both coarse roots and fine roots to soil, as NPP_fineroot + NPP_coarseroot	
D_CWD_to_soil	Detritus from CWD to soil	

4.10 Acknowledgements

We thank Sophie Fauset, Roberto Salguero-Gómez, Simon Lewis, Jesus Aguirre Gutierrez, and David Bauman for valuable suggestions. Y.M. is supported by the Jackson Foundation. H.Z. received Henfrey Scholarship (by St Catherine's College, Oxford) and Tang Scholarship (by China-Oxford Scholarship Fund). This work is a product of the Global Ecosystems Monitoring (GEM) network (gem.tropicalforests.ox.ac.uk). Fieldwork was funded by grants from the UK Natural Environment Research Council (NE/ 1014705/1) and Advanced Investigator Grants to YM and RV from the European Research Council (GEM-TRAIT and Africa-GHG, respectively). We also acknowledge the Wildlife Division of the Forestry Commission in Ghana as well as the many field assistants who helped with data collection from the field.

4.11 Supplementary tables

Supplementary data 1: all_GPP_together_per_site_20221122.csv

Measurements of each carbon cycle component as a mean per plot

Supplementary data 2: all_GPP_together_per_plot_20221122.csv

Measurements of each carbon cycle component as a mean per site

4.12 Supplementary 1 Field measurements and processing procedure

The procedure was written to ensure reproducibility of results and thus includes many processing details.

Leaf area index (LAI) was estimated from hemispherical images taken with a Nikon 5100 camera and Nikon Fisheye Converter FC-E8 0.21x JAPAN near the center of each of the 25 subplots in each plot in each site, at a standard height of 1 m, and during overcast conditions. 22,000 photos were collected in total, every month during 2016-2017(ANK), 2012-2017 (BOB&KOG). Photos were processed using machine learning-based software 'ilastik' (Berg et al., 2019) for pixel classification and CANEYE (Demarez et al., 2008) for leaf area index calculations. The exposure procedure followed (Zhang et al., 2005) and GEM manual (Malhi et al., 2021) (http://gem.tropicalforests.ox.ac.uk). The following parameters were supplied to CANEYE.

(1) P1 = angle of view of the fish eye divided by the amount of pixels from the centroid of the fish eye circle to where the horizon is on the image.

(2) angle of view = 90 degrees, in which case, the edge of the photo is the horizon and the centroid of the image is the zenith.

(3) COI = 80, consideration of field is 80 degrees, we don't want the edge of the photo because it is not clear and sometimes obscure by tall grasses or saplings.

(4) Sub sample factor =1

(5) Fcover = 20 degrees, this is to calculate the percentage of black pixels within the central 20-degree ring. We used this to understand the relative openness of canopy for the given image. It is not relevant to LAI

(6) PAIsat = 10, When a pixel is completely black, mathematically, the leaf area index (LAI) is infinite. As we provide CANEYE 25 subplot images for each estimation of LAI, this means all 25 subplot images show black at a given pixel. To address this 'infinite' issue, we use a value of 10 for LAI in such cases. This value is based on the guess that, the densest point in a tropical forest should have an LAI of 10.

(7) Latitude 0 and Day of year a random number (not relevant for tropical site LAI)

Then, we extract output from CANEYE using software R. We chose the latest method of LAI calculation offered by CANEYE, 'CE V6.1 True PAI'. CANEYE reported one LAI value per method (4 methods) per plot per site per month, as a synthesis across 25 subplot images. As systematic error is dominating in LAI calculation, we take the standard deviation of LAI across four methods as the uncertainty for LAI.

Canopy respiration (R_leaf) is calculated as plot-mean LAI multiplied by plot-mean leaf dark respiration (Rdark), a leaf gas exchange measurement. To obtain the leaves, branches for both sun leaves and shade leaves were detached and immediately re-cut under water to restore hydraulic connectivity for subsequent gas exchange measurement. The leaves were fully darkened for 30 min prior to measuring Rdark. Rdark was measured using an open flow gas exchange system (LI-6400XT, Li-Cor Inc., Lincoln, NE, USA) and block temperature was kept constant throughout the sampling period at 30º C. The uncertainty of Rdark was calculated as the standard error of raw measurements (Paper 2). We convert measurements of Rdark from 30 degree to mean annual air temperature following (Mujawamariya et al., 2021). Rdark was measured for sun and shade leaves and from wet to dry seasons. We calculate a basal area community weighted mean for Rdark_sun and Rdark_shade. Then, we calculate canopy respiration per plot using: R_leaf

= Rdark_sun * F_sunlit + Rdark_shade* (1 – F_sunlit), where F_sunlit is the sunlit leaf area. It is calculated as Fsunlit = (1 – exp(− K∗LAI))/K where K is the light extinction coefficient (Doughty & Goulden, 2009). The final canopy total respiration was calculated as R_leaf * 0.67 to account for daytime light inhibition of leaf dark respiration (Malhi et al., 2009).

Above-ground live wood respiration (R_stem), was quantified at monthly intervals by measuring rates of CO_2 accumulation to chambers attached to the tree trunk, and scaling using stem surface area allometries. Bole respiration per unit surface area was measured using a wood respiration closed dynamic chamber method, from at least 50 trees covering dominating species distributed evenly throughout each plot at 1.3 m height with an IRGA (EGM-4) and soil respiration chamber (SRC-1) connected to a permanent collar. The uncertainty of bole respiration per unit surface area was calculated as the standard error of raw measurements. To recognise the large uncertainty of total stem surface area, mostly due to the simple allometries equation, we assigned an uncertainty of 30%.

Coarse root respiration (R_coarse_root) was not measured, by estimated by R_stem multiplied by 0.21 ± 0.10, following (Cairns et al., 1997; Jackson et al., 1996; Malhi et al., 2014).

Total soil CO_2 efflux (R_soil), called R_soil_no_coarseroot_with_litter in the raw data sheet, was measured every month at the same point in each of the 25 sub-plots on each plot. It was measured using a closed dynamic chamber method with an infra-red gas analyser and soil respiration chamber (EGM-4 IRGA and SRC-1 chamber, PP Systems, Hitchin, UK) sealed to a permanent collar in the soil. Coarse root respiration was assumed missed by the above method (Malhi et al., 2014). The uncertainty of R_soil_no_coarseroot_with_litter was calculated as the standard error of raw measurements.

Therefore, the R_soil_no_coarseroot_with_litter is composed of R_rhizosphere (including fine roots, mycorrhizal and exudates) respiration, soil organic matter derived respiration (R_soil_heterotrophic), and soil surface fine litter respiration (R_fine_litter). The percentage of each component was determined by using a partitioning experiment similar to that described in (Metcalfe et al., 2007; Riutta et al., 2021).

Root exudates NPP was not directly measured while mycorrhizal respiration was incorporated in R_rhizosphere in R_{auto}, bringing uncertainty to NPP and CUE. Following (Riutta et al., 2021), We estimated the root exudation rate from literature as (i) 6% of total NPP (Finzi et al., 2015) (ii) 59% of root NPP (Abramoff & Finzi, 2016), (iii) 37% of root respiration (calculated from data in (Sun et al., 2021))

Coarse woody debris respiration and dead wood respiration were not directly measured, which affects the estimates of carbon sink (net ecosystem exchange) but is irrelevant to GPP nor CUE. Study of Amazonia lowland intact forest found CWD respiration as 76% of CWD input, where a steady state (D_cwd = D_cwd_to_soil + R_cwd) was assumed (Chambers et al., 2001). However, the proportion of CWD respired could be rather variable (Yoon et al., 2015); a Recent study at Borneo lowland forest reported a 90% (Mills et al., 2023). In this study, we estimated R_cwd as (0.9+0.76)/2 = 0.83 of D_cwd, with ±0.1 uncertainty.

This study sources stem biomass (or called above ground coarse woody biomass, estimated from tree height and girth) and some NPP components from (Moore et al., 2018). However, it is worth noting that the study is limited in that some minor components (in terms of magnitude) of the carbon cycle were not covered by this study. For instance, Volatile organic compound NPP was found to be a very minor component of the carbon cycle of an Amazonian Forest (Malhi et al., 2009). Ground flora was neglected in ANK and BOB due to their relatively low abundance, and was included in KOG, a forest to

savanna transition zone. Epiphytes and liana were also not counted albeit their wide existence in the field, especially in BOB01.

When combining or multiplying different components of the carbon cycle, error was propagated following (Malhi et al., 2009).

4.13 Supplementary 2: Correlation between NPP and GPP

The following tests were performed as NPP were commonly calculated from GPP with a fixed proportion (known as CUE). The regression shows how well the spatial variation of GPP captured the spatial variation of NPP

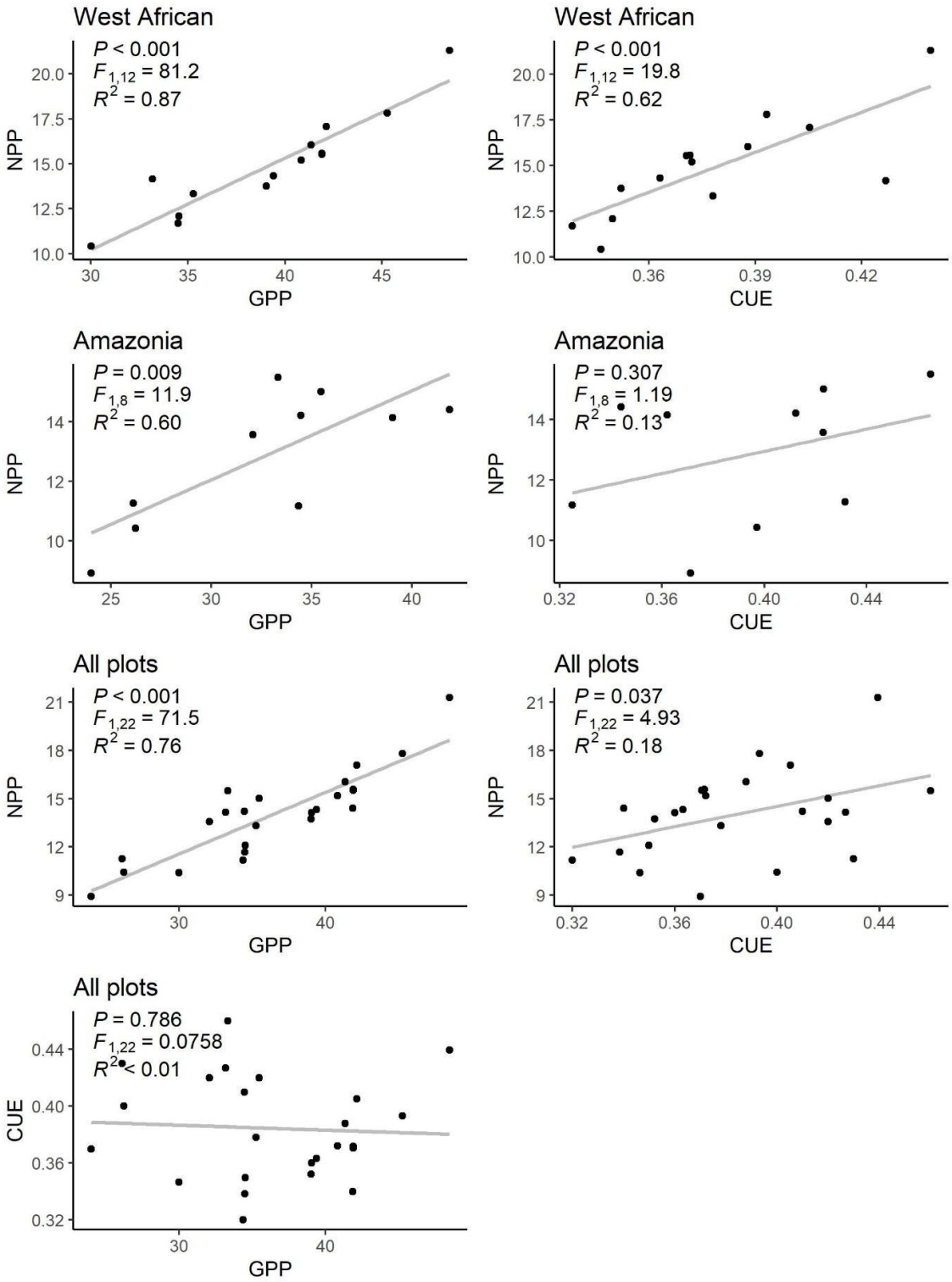


Figure S 1 Linear regression between gross primary productivity (GPP) and net primary productivity (NPP) both in unit (MgC ha^{-1} yr^{-1}), for West African plots, Amazonia plots and all plots together.

4.14 Supplementary 3 Plots information

Table S 1 Study plots information. These are all one-hectare plots.

Plot_code	RH (%)	Rdark shade	Rdark sun	vwc (%)	MCWD (mm)	MAT (°C)	MAP (mm)	Lat	Lon
ANK-01	91	-1.18	-1.69	5.96	-13	25	2050	5.267868	-2.693635
ANK-02	91	-1.25	-1.75	6.78	-13	25	2050	5.268485	-2.695035
ANK-03	91	-1.22	-1.71	11.63	-13	25	2050	5.27102	-2.69234
BOB-01	83.9	-1.57	-1.90	6.40	-374	25.7	1500	6.704713	-1.319068
BOB-02	83.9	-1.54	-1.83	7.87	-374	25.7	1500	6.69147	-1.338429
BOB-03	83.9	-1.56	-1.86	11.37	-374	25.7	1500	6.694531	-1.293695
BOB-04	83.9	-1.47	-1.88	9.42	-374	25.7	1500	6.69096	-1.317038
BOB-05	83.9	-1.47	-1.76	8.64	-374	25.7	1500	6.692606	-1.30727
BOB-06	83.9	-1.47	-1.75	8.19	-374	25.7	1500	6.691368	-1.307001
KOG-02	79.2	-1.59	-2.08	4.13	-412	26.4	1200	7.262316	-1.149953
KOG-03	79.2	-1.69	-2.12	2.90	-412	26.4	1200	7.306792	-1.156446
KOG-04	79.2	-1.78	-2.32	2.42	-412	26.4	1200	7.302644	-1.180213
KOG-05	79.2	-1.91	-2.39	2.54	-412	26.4	1200	7.305341	-1.164546
KOG-06	79.2	-1.90	-2.34	1.72	-412	26.4	1200	7.329423	-1.15578
ALP-11	89.2	-0.67	-0.56	26.8	-6	25.2	2689	-3.95	-73.4333
ALP-12	89.2	-0.79	-0.89	10.8	-6	25.2	2689	-3.9543	-73.4267
TAM-05	89.6	-0.79	-0.655	21.8	-259	24.4	1900	-12.8309	-69.2705
TAM-06	89.6	-0.495	-0.53	35.5	-259	24.4	1900	-12.8385	-69.296
KEN-01	80.8	-0.655	-0.815	19.7	-386	23.4	1310	-16.0158	-62.7301
KEN-02	80.8	no shade	-0.775	16	-386	23.4	1310	-16.0158	-62.7301
CAX-04	82.4	-0.365	-0.365	22.4	-203	25.8	2311	-1.716	-51.457
CAX-06	82.4	-0.44	-0.44	27.1	-203	25.8	2311	-1.7369	-51.46194
TAN-02	74.09	No data	No data	10.7	-482	25	1770	-13.0765	-52.3858
TAN-01	74.09	No data	No data	10.8	-482	25	1770	-13.0765	-52.3858

Note: (1) Soil properties of these sites are available at (Malhi et al., 2015; Moore et al., 2018); Leaf dark respiration, climate data and relative humidity are from (Araujo-Murakami et al., 2014; da Costa et al., 2014; del Aguila-Pasquel et al., 2014; Doughty et al., 2014; Malhi et al., 2014; Rocha et al., 2014). Climate data from ANK BOB and KOG are from (Moore et al., 2018). (2) At site CAX, leaf dark respiration is from (Metcalfe et al., 2010), information on sun/shade leaves were not provided. (3) For CAX, leaf dark respiration is standardized to 25 degrees. For ANK, BOB and KOG, leaf dark respiration is standardized to mean annual air temperature. Information on temperature standardization is lacking for the remaining sites. (4) Volumetric water content (vwc) at site ANK,

BOB and KOG are measurements of topsoil (12 cm) only, but vwc at site ALP, TAM, KEN, CAX, and TAN are measurements of top 30 cm. This data is provided for reference only and are not suggested for any quantitative analysis. (5) RH = relative humidity; Rdark = leaf dark respiration for shade or sun leaves; vwc= volumetric water content, indicating surface soil moisture; MCWD = maximum climatological water deficit; MAT= mean annual air temperature; MAP = mean annual air precipitation; Lat = latitude; Lon = longitude.

4.15 Supplementary 4 Thorough carbon budget quantification for West African carbon fluxes

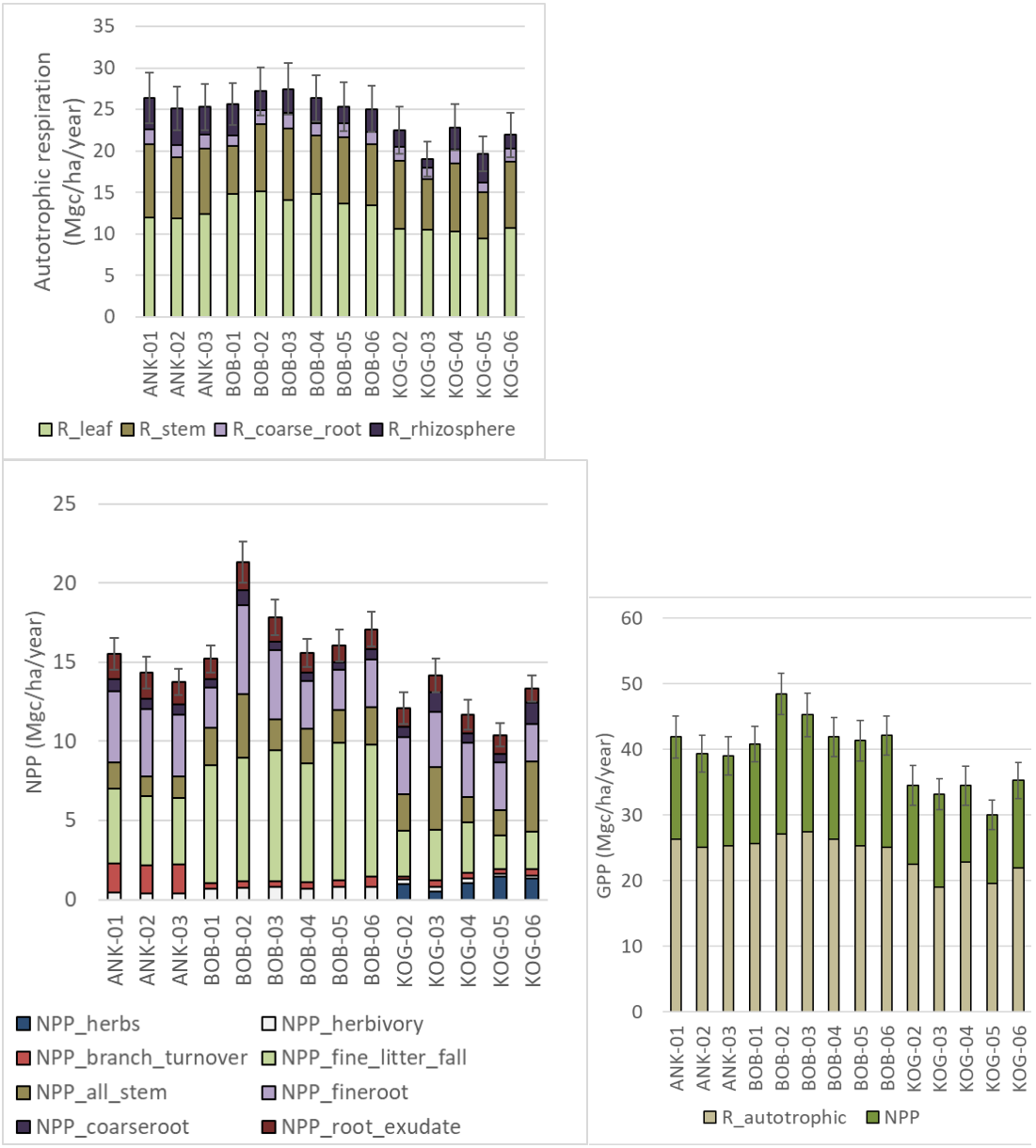
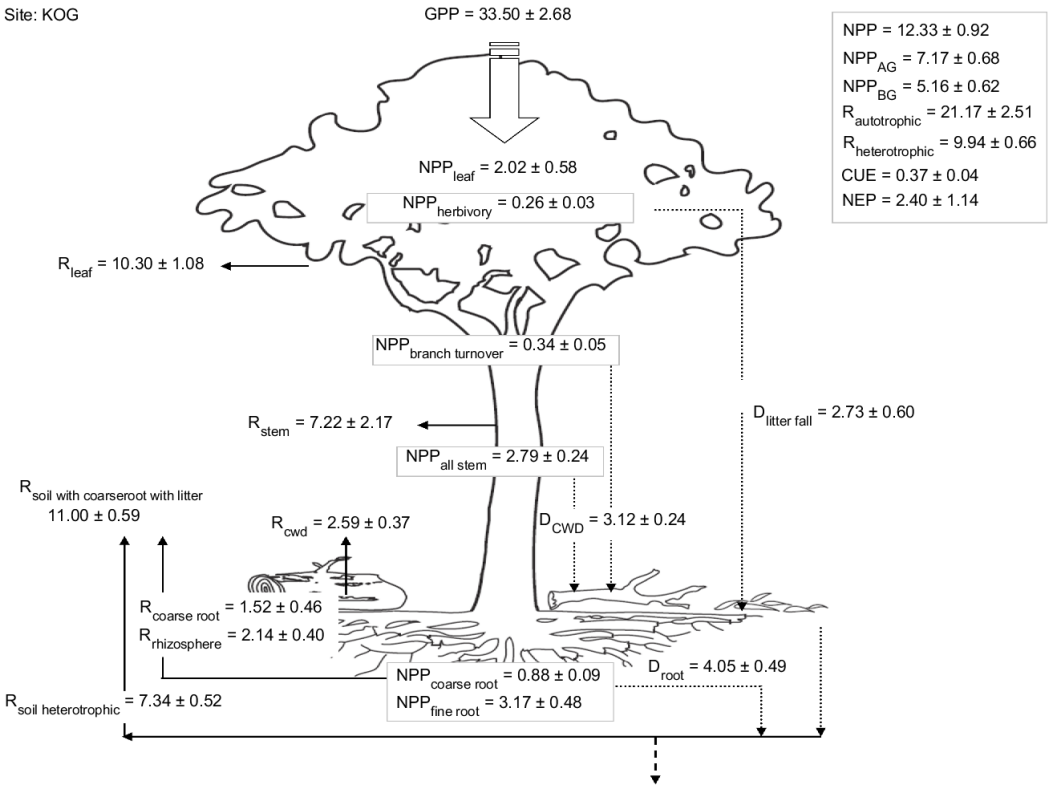


Figure S 2 Components of gross primary production (GPP), Autotrophic respiration (R_{auto}) and net primary production (NPP)


Site: KOG
GPP = 33.50 ± 2.68
NPP = 12.33 ± 0.92
NPP$_{AG}$ = 7.17 ± 0.68
NPP$_{BG}$ = 5.16 ± 0.62
R$_{autotrophic}$ = 21.17 ± 2.51
R$_{heterotrophic}$ = 9.94 ± 0.66
CUE = 0.37 ± 0.04
NEP = 2.40 ± 1.14
NPP$_{leaf}$ = 2.02 ± 0.58
NPP$_{herbivory}$ = 0.26 ± 0.03
R$_{leaf}$ = 10.30 ± 1.08
NPP$_{branch\ turnover}$ = 0.34 ± 0.05
R$_{stem}$ = 7.22 ± 2.17
D$_{litter\ fall}$ = 2.73 ± 0.60
NPP$_{all\ stem}$ = 2.79 ± 0.24
R$_{soil\ with\ coarseroot\ with\ litter}$ 11.00 ± 0.59
R$_{cwd}$ = 2.59 ± 0.37
D$_{CWD}$ = 3.12 ± 0.24
R$_{coarse\ root}$ = 1.52 ± 0.46
R$_{rhizosphere}$ = 2.14 ± 0.40
NPP$_{coarse\ root}$ = 0.88 ± 0.09
NPP$_{fine\ root}$ = 3.17 ± 0.48
D$_{root}$ = 4.05 ± 0.49
R$_{soil\ heterotrophic}$ = 7.34 ± 0.52
Site: BOB
GPP = 43.33 ± 3.03
NPP = 17.16 ± 1.05
NPP$_{AG}$ = 11.69 ± 0.77
NPP$_{BG}$ = 5.47 ± 0.69
R$_{autotrophic}$ = 26.16 ± 2.84
R$_{heterotrophic}$ = 13.63 ± 0.61
CUE = 0.39 ± 0.04
NEP = 3.53 ± 1.21
NPP$_{leaf}$ = 5.23 ± 0.46
NPP$_{herbivory}$ = 0.76 ± 0.07
R$_{leaf}$ = 14.32 ± 1.57
NPP$_{branch\ turnover}$ = 0.42 ± 0.07
R$_{stem}$ = 7.50 ± 2.26
D$_{litter\ fall}$ = 8.01 ± 0.73
NPP$_{all\ stem}$ = 2.50 ± 0.21
R$_{soil\ with\ coarseroot\ with\ litter}$ 15.55 ± 0.55
R$_{cwd}$ = 2.42 ± 0.35
D$_{CWD}$ = 2.92 ± 0.22
R$_{coarse\ root}$ = 1.58 ± 0.47
R$_{rhizosphere}$ = 2.77 ± 0.44
NPP$_{coarse\ root}$ = 0.61 ± 0.06
NPP$_{fine\ root}$ = 3.51 ± 0.53
D$_{root}$ = 4.12 ± 0.53
R$_{soil\ heterotrophic}$ = 11.21 ± 0.49

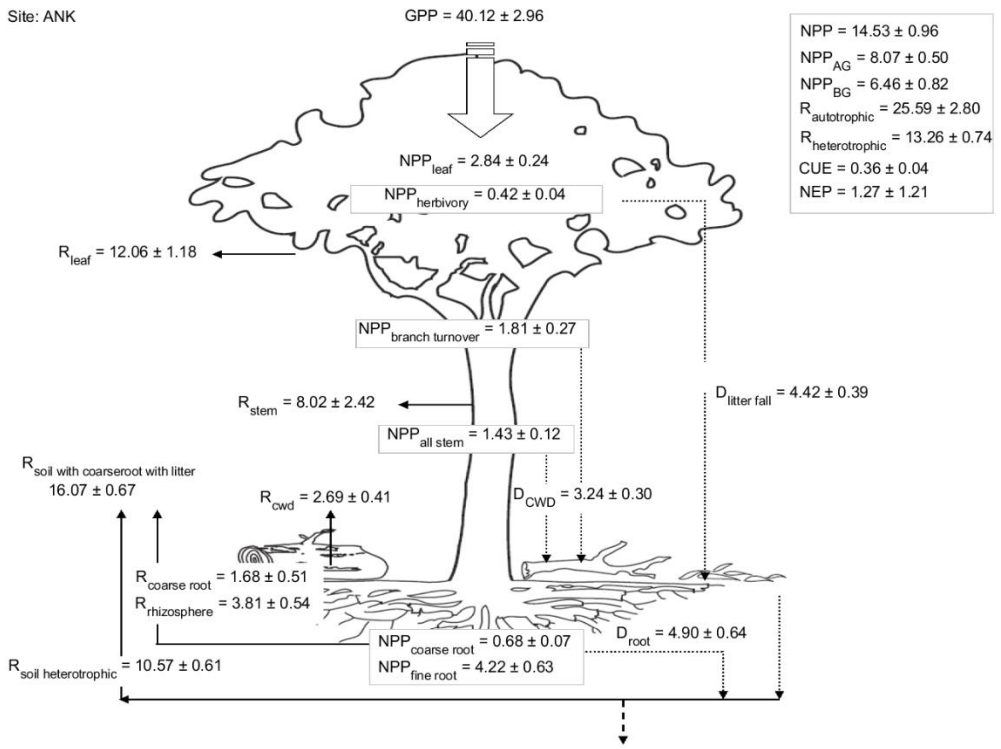


Figure S 3 Diagram showing the magnitude and pattern of key carbon fluxes for ANK (3 plots) BOB (6 plots) and KOG (5 plots)

Table S 2 Mean and Standard error (SE) of gross primary production (GPP) and its components across study plots for Amazonia and West African forests, the z-score and p-value test the difference between Amazonia and West African forests

	Amazonia Mean	Amazonia SE	West African Mean	West African SE	Z score	p-value
GPP	32.71	1.82	39.13	1.35	-2.83	0.00
CUE	0.39	0.01	0.38	0.01	0.92	0.36
NPP	12.86	0.71	14.87	0.74	-1.97	0.05
NPP_all_stem	3.01	0.21	2.37	0.28	1.86	0.06
NPP_fine_litter_fall	5.22	0.31	5.36	0.67	-0.18	0.86
R_autotrophic	19.84	1.35	24.26	0.71	-2.89	0.00
SoilMoisture	20.16	2.62	6.43	0.88	4.97	0.00
NPP_fineroot	3.06	0.35	3.54	0.24	-1.12	0.26
R_rhizosphere	4.24	0.37	2.77	0.25	3.31	0.00
R_leaf	6.87	0.70	12.40	0.51	-6.37	0.00
R_stem	7.23	0.64	7.51	0.27	-0.41	0.68

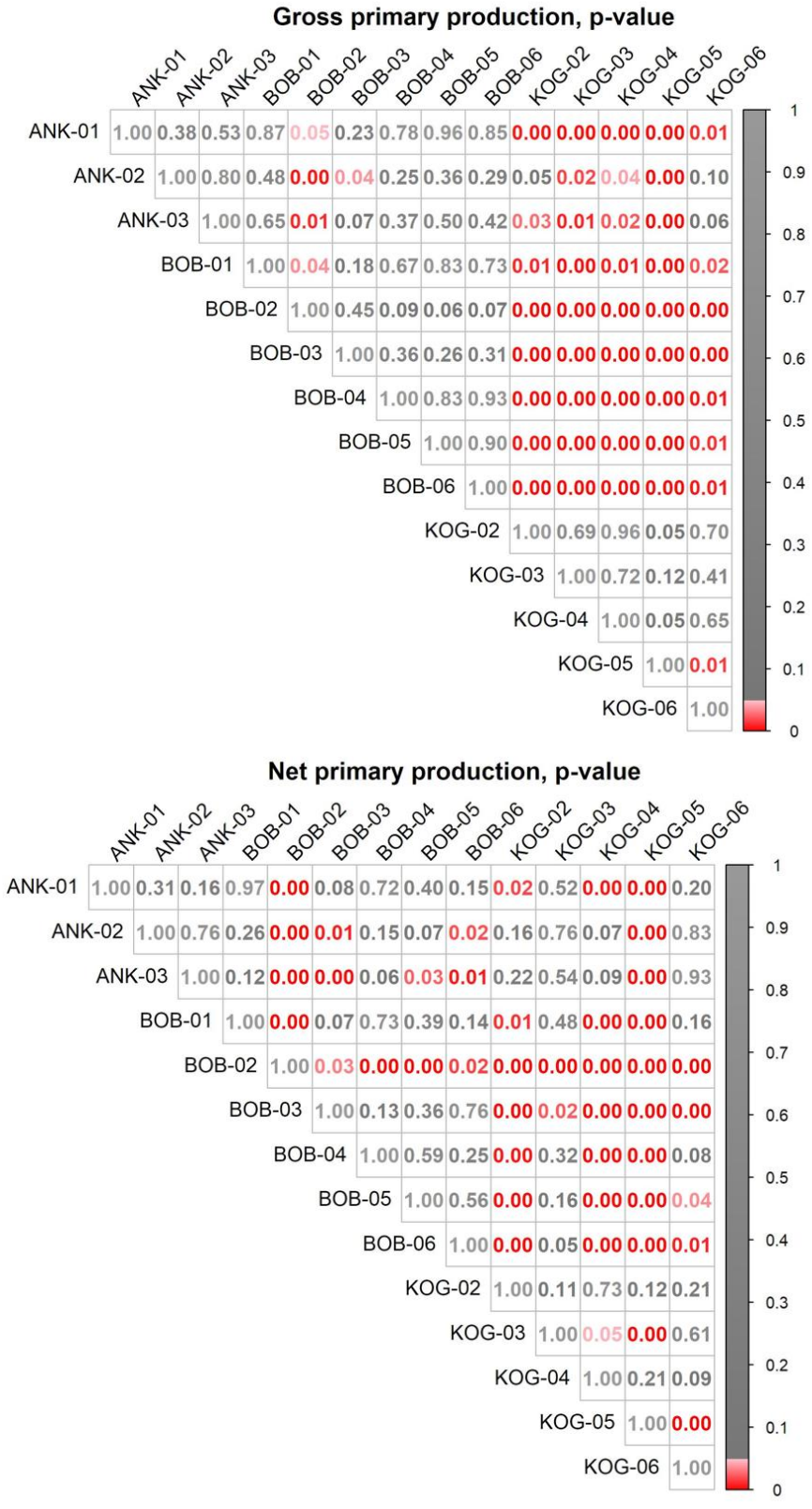


Figure S 4 Z-test was used to compare the difference between plots for net primary production (NPP) and gross primary production (GPP). P values between each plot were shown to illustrate significant (red, at 0.05 threshold) and insignificant (grey).

4.16 References for paper 1

Abramoff, R. Z., & Finzi, A. C. (2016). Seasonality and partitioning of Root allocation to rhizosphere soils in a midlatitude forest. *Ecosphere*, *7*(11). https://doi.org/10.1002/ecs2.1547

Achard, F., Beuchle, R., Mayaux, P., Stibig, H.-J., Bodart, C., Brink, A., Carboni, S., Desclée, B., Donnay, F., Eva, H. D., Lupi, A., Raši, R., Seliger, R., & Simonetti, D. (2014). Determination of tropical deforestation rates and related carbon losses from 1990 to 2010. *Global Change Biology*, *20*(8), 2540–2554. https://doi.org/https://doi.org/10.1111/gcb.12605

Afreen, T., Singh, H., & Singh, J. S. (2019). Influence of Changing Patterns of Precipitation and Temperature on Tropical Soil Ecosystem. *Tropical Ecosystems: Structure, Functions and Challenges in the Face of Global Change*, 11–26. https://doi.org/10.1007/978-981-13-8249-9_2

Aguirre-Gutiérrez, J., Oliveras, I., Rifai, S., Fauset, S., Adu-Bredu, S., Affum-Baffoe, K., Baker, T. R., Feldpausch, T. R., Gvozdevaite, A., Hubau, W., Kraft, N. J. B., Lewis, S. L., Moore, S., Niinemets, Ü., Peprah, T., Phillips, O. L., Ziemińska, K., Enquist, B., & Malhi, Y. (2019). Drier tropical forests are susceptible to functional changes in response to a long-term drought. *Ecology Letters*, *22*(5), 855–865. https://doi.org/https://doi.org/10.1111/ele.13243

Anav, A., Friedlingstein, P., Beer, C., Ciais, P., Harper, A., Jones, C., Murray-Tortarolo, G., Papale, D., Parazoo, N. C., Peylin, P., Piao, S., Sitch, S., Viovy, N., Wiltshire, A., & Zhao, M. (2015). Spatiotemporal patterns of terrestrial gross primary production: A review. In *Reviews of Geophysics* (Vol. 53, Issue 3). https://doi.org/10.1002/2015RG000483

Anderson-Teixeira, K. J., Herrmann, V., Morgan, R. B., Bond-Lamberty, B., Cook-Patton, S. C., Ferson, A. E., Muller-Landau, H. C., & Wang, M. M. H. (2021). Carbon cycling in mature and regrowth forests globally. *Environmental Research Letters*, *16*(5). https://doi.org/10.1088/1748-9326/abed01

Anderson-Teixeira, K. J., Wang, M. M. H., Mcgarvey, J. C., & Lebauer, D. S. (2016). Carbon dynamics of mature and regrowth tropical forests derived from a pantropical database (TropForC-db). *Global Change Biology*, *22*(5), 1690–1709. https://doi.org/10.1111/gcb.13226

Arag̃o, L. E. O. C., Malhi, Y., Metcalfe, D. B., Silva-Espejo, J. E., Jiménez, E., Navarrete, D., Almeida, S., Costa, A. C. L., Salinas, N., Phillips, O. L., Anderson, L. O., Alvarez, E., Baker, T. R., Goncalvez, P. H., Huamán-Ovalle, J., Mamani-Solórzano, M., Meir, P., Monteagudo, A., Patĩo, S., … Vásquez, R. (2009). Above- and below-ground net primary productivity across ten Amazonian forests on contrasting soils. *Biogeosciences*, *6*(12). https://doi.org/10.5194/bg-6-2759-2009

Araujo-Murakami, A., Doughty, C. E., Metcalfe, D. B., Silva-Espejo, J. E., Arroyo, L., Heredia, J. P., Flores, M., Sibler, R., Mendizabal, L. M., Pardo-Toledo, E., Vega, M., Moreno, L., Rojas-Landivar, V. D., Halladay, K., Girardin, C. A. J., Killeen, T. J., & Malhi, Y. (2014). The productivity, allocation and cycling of carbon in forests at the dry margin of the Amazon forest in Bolivia. *Plant Ecology and Diversity*, *7*(1–2), 55–69. https://doi.org/10.1080/17550874.2013.798364

Beer, C., Reichstein, M., Tomelleri, E., Ciais, P., Jung, M., Carvalhais, N., Rödenbeck, C., Arain, M. A., Baldocchi, D., & Bonan, G. B. (2010). Terrestrial gross carbon dioxide uptake: global distribution and covariation with climate. *Science*, *329*(5993), 834–838.

Bennett, A. C., Dargie, G. C., Cuni-Sanchez, A., Mukendi, J. T., Hubau, W., Mukinzi, J. M., Phillips, O. L., Malhi, Y., Sullivan, M. J. P., Cooper, D. L. M., Adu-Bredu, S.,

Affum-Baffoe, K., Amani, C. A., Banin, L. F., Beeckman, H., Begne, S. K., Bocko, Y. E., Boeckx, P., Bogaert, J., … Lewis, S. L. (2021). Resistance of African tropical forests to an extreme climate anomaly. *Proceedings of the National Academy of Sciences of the United States of America*, *118*(21). https://doi.org/10. 1073/pnas. 2003169118

Berg, S., Kutra, D., Kroeger, T., Straehle, C. N., Kausler, B. X., Haubold, C., Schiegg, M., Ales, J., Beier, T., Rudy, M., Eren, K., Cervantes, J. I., Xu, B., Beuttenmueller, F., Wolny, A., Zhang, C., Koethe, U., Hamprecht, F. A., & Kreshuk, A. (2019). ilastik: interactive machine learning for (bio)image analysis. *Nature Methods*, *16*(12). https://doi.org/10.1038/s41592-019-0582-9

Bongers, F., Poorter, L., Hawthorne, W. D., & Sheil, D. (2009). The intermediate disturbance hypothesis applies to tropical forests, but disturbance contributes little to tree diversity. *Ecology Letters*, *12*(8). https://doi.org/10.1111/j.1461-0248.2009.01329.x

Buchanan, G. M., Field, R. H., Bradbury, R. B., Luraschi, B., & Vickery, J. A. (2021). The impact of tree loss on carbon management in West Africa. *Carbon Management*, *12*(6), 623–633. https://doi.org/10.1080/17583004.2021.1994015

Cairns, M. A., Brown, S., Helmer, E. H., & Baumgardner, G. A. (1997). Root biomass allocation in the world's upland forests. *Oecologia*, *111*(1). https://doi.org/10.1007/s004420050201

Caton Harrison, T., Washington, R., Engelstaedter, S., Jones, R. G., & Savage, N. H. (2021). Influence of Orography Upon Summertime Low-Level Jet Dust Emission in the Central and Western Sahara. *Journal of Geophysical Research: Atmospheres*, *126*(23). https://doi.org/10.1029/2021JD035025

Ceballos-Núñez, V., Müller, M., & Sierra, C. A. (2020). Towards better representations of carbon allocation in vegetation: a conceptual framework and mathematical tool. *Theoretical Ecology*, *13*(3). https://doi.org/10.1007/s12080-020-00455-w

Chambers, J. Q., Schimel, J. P., & Nobre, A. D. (2001). Respiration from coarse wood litter in central Amazon forests. *Biogeochemistry*, *52*(2). https://doi.org/10.1023/A:1006473530673

Chiti, T., Certini, G., Grieco, E., & Valentini, R. (2010). The role of soil in storing carbon in tropical rainforests: The case of Ankasa Park, Ghana. *Plant and Soil*, *331*(1), 453–461. https://doi.org/10.1007/S11104-009-0265-X/TABLES/5

Chiwara, P., Ogutu, B. O., Dash, J., Milton, E. J., Ardö, J., Saunders, M., & Nicolini, G. (2018). Estimating terrestrial gross primary productivity in water limited ecosystems across Africa using the Southampton Carbon Flux (SCARF) model. *Science of the Total Environment*, *630*. https://doi.org/10.1016/j.scitotenv.2018.02.314

Collalti, A., & Prentice, I. C. (2019). Is NPP proportional to GPP? Waring's hypothesis 20 years on. *Tree Physiology*, *39*(8), 1473–1483. https://doi.org/10.1093/treephys/tpz034

Cuni-Sanchez, A., Sullivan, M. J. P., Platts, P. J., Lewis, S. L., Marchant, R., Imani, G., Hubau, W., Abiem, I., Adhikari, H., Albrecht, T., Altman, J., Amani, C., Aneseyee, A. B., Avitabile, V., Banin, L., Batumike, R., Bauters, M., Beeckman, H., Begne, S. K., … Zibera, E. (2021). High aboveground carbon stock of African tropical montane forests. *Nature*, *596*(7873). https://doi.org/10.1038/s41586-021-03728-4

da Costa, A. C. L., Metcalfe, D. B., Doughty, C. E., de Oliveira, A. A. R., Neto, G. F. C., da Costa, M. C., Silva Junior, J. de A., Aragão, L. E. O. C., Almeida, S., Galbraith, D. R., Rowland, L. M., Meir, P., & Malhi, Y. (2014). Ecosystem respiration and net primary productivity after 8-10 years of experimental through-fall reduction in an eastern Amazon forest. *Plant Ecology and Diversity*, *7*(1–2). https://doi.org/10.1080/17550874.2013.798366

del Aguila-Pasquel, J., Doughty, C. E., Metcalfe, D. B., Silva-Espejo, J. E., Girardin, C. A. J., Chung Gutierrez, J. A., Navarro-Aguilar, G. E., Quesada, C. A., Hidalgo, C. G., Reyna Huaymacari, J. M., Halladay, K., del Castillo Torres, D., Phillips, O., & Malhi, Y. (2014). The seasonal cycle of productivity, metabolism and carbon dynamics in a wet aseasonal forest in north-west Amazonia (Iquitos, Peru). *Plant Ecology and Diversity*, *7*(1–2), 71–83. https://doi.org/10.1080/17550874.2013.798365

DeLUCIA, E. H., Drake, J. E., Thomas, R. B., & Gonzalez-Meler, M. (2007). Forest carbon use efficiency: is respiration a constant fraction of gross primary production? *Global Change Biology*, *13*(6), 1157–1167.

Demarez, V., Duthoit, S., Baret, F., Weiss, M., & Dedieu, G. (2008). Estimation of leaf area and clumping indexes of crops with hemispherical photographs. *Agricultural and Forest Meteorology*, *148*(4). https://doi.org/10.1016/j.agrformet.2007.11.015

Doughty, C. E., Goldsmith, G. R., Raab, N., Girardin, C. A. J., Farfan-Amezquita, F., Huaraca-Huasco, W., Silva-Espejo, J. E., Araujo-Murakami, A., da Costa, A. C. L., Rocha, W., Galbraith, D., Meir, P., Metcalfe, D. B., & Malhi, Y. (2018). What controls variation in carbon use efficiency among Amazonian tropical forests? *Biotropica*, *50*(1), 16–25. https://doi.org/10.1111/btp.12504

Doughty, C. E., & Goulden, M. L. (2009). Seasonal patterns of tropical forest leaf area index and CO2 exchange. *Journal of Geophysical Research: Biogeosciences*, *114*(1). https://doi.org/10.1029/2007JG000590

Doughty, C. E., Metcalfe, D. B., da Costa, M. C., de Oliveira, A. A. R., Neto, G. F. C., Silva, J. A., Aragão, L. E. O. C., Almeida, S. S., Quesada, C. A., Girardin, C. A. J., Halladay, K., da Costa, A. C. L., & Malhi, Y. (2014). The production, allocation and cycling of carbon in a forest on fertile terra preta soil in eastern Amazonia compared with a forest on adjacent infertile soil. *Plant Ecology and Diversity*, *7*(1–2), 41–53. https://doi.org/10.1080/17550874.2013.798367

Doughty, C. E., Metcalfe, D. B., Girardin, C. A. J., Amezquita, F. F., Durand, L., Huaraca Huasco, W., Silva-Espejo, J. E., Araujo-Murakami, A., Da Costa, M. C., Da Costa, A. C. L., Rocha, W., Meir, P., Galbraith, D., & Malhi, Y. (2015). Source and sink carbon dynamics and carbon allocation in the Amazon basin. *Global Biogeochemical Cycles*, *29*(5). https://doi.org/10.1002/2014GB005028

Enquist, B. J., Kerkhoff, A. J., Huxman, T. E., & Economo, E. P. (2007). Adaptive differences in plant physiology and ecosystem paradoxes: Insights from metabolic scaling theory. *Global Change Biology*, *13*(3), 591–609. https://doi.org/10.1111/j.1365-2486.2006.01222.x

Farrior, C. E. (2014). Competitive optimization models, attempting to understand the diversity of life. In *New Phytologist* (Vol. 203, Issue 4). https://doi.org/10.1111/ nph.12940

Fattore, F., Bertolini, T., Materia, S., Gualdi, S., Thongo M'Bou, A., Nicolini, G., Valentini, R., De Grandcourt, A., Tedesco, D., & Castaldi, S. (2014). Seasonal trends of dry and bulk concentration of nitrogen compounds over a rain forest in Ghana. *Biogeosciences*, *11*(11). https://doi.org/10.5194/bg-11-3069-2014

Fauset, S., Baker, T. R., Lewis, S. L., Feldpausch, T. R., Affum-Baffoe, K., Foli, E. G., Hamer, K. C., & Swaine, M. D. (2012). Drought-induced shifts in the floristic and functional composition of tropical forests in Ghana. *Ecology Letters*, *15*(10). https://doi.org/10.1111/j.1461-0248.2012.01834.x

Fensholt, R., & Proud, S. R. (2012). Evaluation of Earth Observation based global long term vegetation trends - Comparing GIMMS and MODIS global NDVI time series. *Remote Sensing of Environment*, *119*, 131–147. https://doi.org/10.1016/j.rse. 2011. 12.015

Finzi, A. C., Abramoff, R. Z., Spiller, K. S., Brzostek, E. R., Darby, B. A., Kramer, M. A., & Phillips, R. P. (2015). Rhizosphere processes are quantitatively important

components of terrestrial carbon and nutrient cycles. *Global Change Biology*, *21*(5). https://doi.org/10.1111/gcb.12816

Flack-Prain, S., Meir, P., Malhi, Y., Smallman, T. L., & Williams, M. (2019). Leaf Area Index Changes Explain GPP Variation across an Amazon Drought Stress Gradient. *Biogeosciences Discussions*, *May*.

Franklin, O., Johansson, J., Dewar, R. C., Dieckmann, U., McMurtrie, R. E., Brännström, A. K., & Dybzinski, R. (2012). Modeling carbon allocation in trees: A search for principles. In *Tree Physiology* (Vol. 32, Issue 6). https://doi.org/10.1093/treephys/tpr138

Gibert, A., Gray, E. F., Westoby, M., Wright, I. J., & Falster, D. S. (2016). On the link between functional traits and growth rate: meta-analysis shows effects change with plant size, as predicted. *Journal of Ecology*, *104*(5). https://doi.org/10.1111/1365-2745.12594

He, Y., Piao, S., Li, X., Chen, A., & Qin, D. (2018). Global patterns of vegetation carbon use efficiency and their climate drivers deduced from MODIS satellite data and process-based models. *Agricultural and Forest Meteorology*, *256–257*(March), 150–158. https://doi.org/10.1016/j.agrformet.2018.03.009

Hubau, W., Lewis, S. L., Phillips, O. L., Affum-Baffoe, K., Beeckman, H., Cuní-Sanchez, A., Daniels, A. K., Ewango, C. E. N., Fauset, S., & Mukinzi, J. M. (2020). Asynchronous carbon sink saturation in African and Amazonian tropical forests. *Nature*, *579*(7797), 80–87.

Ise, T., Litton, C. M., Giardina, C. P., & Ito, A. (2010). Comparison of modeling approaches for carbon partitioning: Impact on estimates of global net primary production and equilibrium biomass of woody vegetation from MODIS GPP. *Journal of Geophysical Research: Biogeosciences*, *115*(4). https://doi.org/10.1029/2010JG001326

Jackson, R. B., Canadell, J., Ehleringer, J. R., Mooney, H. A., Sala, O. E., & Schulze, E. D. (1996). A global analysis of root distributions for terrestrial biomes. In *Oecologia* (Vol. 108, Issue 3). https://doi.org/10.1007/BF00333714

Janssen, T. A. J., Ametsitsi, G. K. D., Collins, M., Adu-Bredu, S., Oliveras, I., Mitchard, E. T. A., & Veenendaal, E. M. (2018). Extending the baseline of tropical dry forest loss in Ghana (1984–2015) reveals drivers of major deforestation inside a protected area. *Biological Conservation*, *218*, 163–172. https://doi.org/10.1016/J.BIOCON.2017.12.004

Jin, W., P., A. L., P., L. A., Natalia, R.-C., Matthew, H., T., W. K., Kaiyu, G., C., S. S., Bradley, C., Neill, P., V., T. J., Suelen, M., Hideki, K., L., F. M., Silva, C. K., Rodrigo, da S., M., B. P., G., D. D., E., H. T., … R., S. S. (2016). Leaf development and demography explain photosynthetic seasonality in Amazon evergreen forests. *Science*, *351*(6276), 972–976. https://doi.org/10.1126/science.aad5068

John, D. M. (1973). Accumulation and Decay of Litter and Net Production of Forest in Tropical West Africa. *Oikos*, *24*(3). https://doi.org/10.2307/3543819

Kho, L. (2013). *Carbon cycling in a Bornean tropical forest* [Oxford University, UK]. https://ora.ox.ac.uk/objects/uuid:bfa1f206-97bf-4bcd-a148-521506225c90

Li, X., & Xiao, J. (2019). Mapping photosynthesis solely from solar-induced chlorophyll fluorescence: A global, fine-resolution dataset of gross primary production derived from OCO-2. *Remote Sensing*, *11*(21). https://doi.org/10.3390/rs11212563

Litton, C. M., Raich, J. W., & Ryan, M. G. (2007). Carbon allocation in forest ecosystems. *Global Change Biology*, *13*(10), 2089–2109.

Malhi, Y., Adu-Bredu, S., Asare, R. A., Lewis, S. L., & Mayaux, P. (2013). African rainforests: Past, present and future. In *Philosophical Transactions of the Royal Society B: Biological Sciences* (Vol. 368, Issue 1625). https://doi.org/10. 1098/rstb.2012.0312

Malhi, Y., Aragão, L. E. O. C., Metcalfe, D. B., Paiva, R., Quesada, C. A., Almeida, S., Anderson, L., Brando, P., Chambers, J. Q., da Costa, A. C. L., Hutyra, L. R., Oliveira, P., Patiño, S., Pyle, E. H., Robertson, A. L., & Teixeira, L. M. (2009). Comprehensive assessment of carbon productivity, allocation and storage in three Amazonian forests. *Global Change Biology*, *15*(5), 1255–1274. https://doi.org/10.1111/j. 1365-2486.2008.01780.x

Malhi, Y., Doughty, C. E., Goldsmith, G. R., Metcalfe, D. B., Girardin, C. A. J., Marthews, T. R., del Aguila-Pasquel, J., Aragão, L. E. O. C., Araujo-Murakami, A., Brando, P., da Costa, A. C. L., Silva-Espejo, J. E., Farfán Amézquita, F., Galbraith, D. R., Quesada, C. A., Rocha, W., Salinas-Revilla, N., Silvério, D., Meir, P., & Phillips, O. L. (2015). The linkages between photosynthesis, productivity, growth and biomass in lowland Amazonian forests. *Global Change Biology*, *21*(6). https://doi.org/10.1111/gcb. 12859

Malhi, Y., Doughty, C., & Galbraith, D. (2011). The allocation of ecosystem net primary productivity in tropical forests. *Philosophical Transactions of the Royal Society B: Biological Sciences*, *366*(1582), 3225–3245. https://doi.org/10.1098/rstb.2011.0062

Malhi, Y., Farfán Amézquita, F., Doughty, C. E., Silva-Espejo, J. E., Girardin, C. A. J., Metcalfe, D. B., Aragão, L. E. O. C., Huaraca-Quispe, L. P., Alzamora-Taype, I., Eguiluz-Mora, L., Marthews, T. R., Halladay, K., Quesada, C. A., Robertson, A. L., Fisher, J. B., Zaragoza-Castells, J., Rojas-Villagra, C. M., Pelaez-Tapia, Y., Salinas, N., … Phillips, O. L. (2014). The productivity, metabolism and carbon cycle of two lowland tropical forest plots in south-western Amazonia, Peru. *Plant Ecology and Diversity*, *7*(1–2), 85–105. https://doi.org/10.1080/17550874.2013.820805

Malhi, Y., Girardin, C., Metcalfe, D. B., Doughty, C. E., Aragão, L. E. O. C., Rifai, S. W., Oliveras, I., Shenkin, A., Aguirre-Gutiérrez, J., Dahlsjö, C. A. L., Riutta, T., Berenguer, E., Moore, S., Huasco, W. H., Salinas, N., da Costa, A. C. L., Bentley, L. P., Adu-Bredu, S., Marthews, T. R., … Phillips, O. L. (2021). The Global Ecosystems Monitoring network: Monitoring ecosystem productivity and carbon cycling across the tropics. *Biological Conservation*, *253*, 108889. https://doi.org/10.1016/J.BIOCON. 2020.108889

Marthews, T., Riutta, T., Oliveras Menor, I., Urrutia, R., Moore, S., Metcalfe, D., Malhi, Y., Phillips, O., Huaraca Huasco, W., Ruiz Jaén, M., Girardin, C., Butt, N., & Cain, R. (2015). *Measuring Tropical Forest Carbon Allocation and Cycling: A RAINFOR-GEM Field Manual for Intensive Census Plots (v3.0)*. https://ora.ox.ac.uk/objects/ uuid:f33a0929-4675-43c6-91a3-8cbcda962775/files/ m18 44bb29c06f7d69207569648142e020

Martín Belda, D., Anthoni, P., Wårlind, D., Olin, S., Schurgers, G., Tang, J., Smith, B., & Arneth, A. (2022). LPJ-GUESS/LSMv1.0: A next generation Land Surface Model with high ecological realism. *Geosci. Model Dev. Discuss.*, *2022*, 1–61. https://doi.org/ 10.5194/gmd-2022-1

McNickle, G. G., Gonzalez-Meler, M. A., Lynch, D. J., Baltzer, J. L., & Brown, J. S. (2016). The world's biomes and primary production as a triple tragedy of the commons foraging game played among plants. *Proceedings of the Royal Society B: Biological Sciences*, *283*(1842). https://doi.org/10.1098/rspb.2016.1993

Metcalfe, D. B., Lobo-do-Vale, R., Chaves, M. M., Maroco, J. P., Aragão, L. E. O. C., Malhi, Y., Da Costa, A. L., Braga, A. P., Gonçalves, P. L., De Athaydes, J., Da Costa, M., Almeida, S. S., Campbell, C., Hurry, V., Williams, M., & Meir, P. (2010). Impacts of experimentally imposed drought on leaf respiration and morphology in an Amazon rain forest. *Functional Ecology*, *24*(3). https://doi.org/10.1111/j.1365-2435.2009.01683.x

Metcalfe, D. B., Meir, P., Aragão, L. E. O. C., Malhi, Y., da Costa, A. C. L., Braga, A., Gonçalves, P. H. L., de Athaydes, J., de Almeida, S. S., & Williams, M. (2007). Factors controlling spatio-temporal variation in carbon dioxide efflux from surface litter,

roots, and soil organic matter at four rain forest sites in the eastern Amazon. *Journal of Geophysical Research: Biogeosciences*, *112*(4). https://doi.org/10.1029/2007JG000443

Mills, M. B., Malhi, Y., Ewers, R. M., Kho, L. K., Teh, Y. A., Both, S., Burslem, D. F. R. P., Majalap, N., Nilus, R., Huasco, W. H., Cruz, R., Pillco, M. M., Turner, E. C., Reynolds, G., & Riutta, T. (2023). Tropical forests post-logging are a persistent net carbon source to the atmosphere. *Proceedings of the National Academy of Sciences of the United States of America*, *120*(3). https://doi.org/10.1073/pnas.2214462120

Moore, S., Adu-Bredu, S., Duah-Gyamfi, A., Addo-Danso, S. D., Ibrahim, F., Mbou, A. T., de Grandcourt, A., Valentini, R., Nicolini, G., Djagbletey, G., Owusu-Afriyie, K., Gvozdevaite, A., Oliveras, I., Ruiz-Jaen, M. C., & Malhi, Y. (2018). Forest biomass, productivity and carbon cycling along a rainfall gradient in West Africa. *Global Change Biology*, *24*(2), e496–e510. https://doi.org/10.1111/gcb.13907

Morel, A. C., Adu Sasu, M., Adu-Bredu, S., Quaye, M., Moore, C., Ashley Asare, R., Mason, J., Hirons, M., McDermott, C. L., Robinson, E. J. Z., Boyd, E., Norris, K., & Malhi, Y. (2019). Carbon dynamics, net primary productivity and human-appropriated net primary productivity across a forest–cocoa farm landscape in West Africa. *Global Change Biology*, *25*(8). https://doi.org/10.1111/gcb.14661

Mujawamariya, M., Wittemann, M., Manishimwe, A., Ntirugulirwa, B., Zibera, E., Nsabimana, D., Wallin, G., Uddling, J., & Dusenge, M. E. (2021). Complete or overcompensatory thermal acclimation of leaf dark respiration in African tropical trees. *New Phytologist*, *229*(5). https://doi.org/10.1111/nph.17038

Norris, K., Asase, A., Collen, B., Gockowksi, J., Mason, J., Phalan, B., & Wade, A. (2010). Biodiversity in a forest-agriculture mosaic – The changing face of West African rainforests. *Biological Conservation*, *143*(10), 2341–2350. https://doi.org/https://doi.org/10.1016/j.biocon.2009.12.032

Oliveras, I., Bentley, L., Fyllas, N. M., Gvozdevaite, A., Shenkin, A. F., Peprah, T., Morandi, P., Peixoto, K. S., Boakye, M., Adu-Bredu, S., Schwantes Marimon, B., Marimon Junior, B. H., Salinas, N., Martin, R., Asner, G., Díaz, S., Enquist, B. J., & Malhi, Y. (2020). The Influence of Taxonomy and Environment on Leaf Trait Variation Along Tropical Abiotic Gradients. *Frontiers in Forests and Global Change*, *3*, 18. https://doi.org/10.3389/FFGC.2020.00018/BIBTEX

Ostle, N. J., Smith, P., Fisher, R., Ian Woodward, F., Fisher, J. B., Smith, J. U., Galbraith, D., Levy, P., Meir, P., McNamara, N. P., & Bardgett, R. D. (2009). Integrating plant-soil interactions into global carbon cycle models. In *Journal of Ecology* (Vol. 97, Issue 5). https://doi.org/10.1111/j.1365-2745.2009.01547.x

Purves, D., & Pacala, S. (2008). Predictive models of forest dynamics. In *Science* (Vol. 320, Issue 5882). https://doi.org/10.1126/science.1155359

Riutta, T., Kho, L. K., Teh, Y. A., Ewers, R., Majalap, N., & Malhi, Y. (2021). Major and persistent shifts in below-ground carbon dynamics and soil respiration following logging in tropical forests. *Global Change Biology*, *27*(10), 2225–2240. https://doi.org/10.1111/gcb.15522

Riutta, T., Malhi, Y., Kho, L. K., Marthews, T. R., Huaraca Huasco, W., Khoo, M. S., Tan, S., Turner, E., Reynolds, G., Both, S., Burslem, D. F. R. P., Teh, Y. A., Vairappan, C. S., Majalap, N., & Ewers, R. M. (2018). Logging disturbance shifts net primary productivity and its allocation in Bornean tropical forests. *Global Change Biology*, *24*(7). https://doi.org/10.1111/gcb.14068

Rocha, W., Metcalfe, D. B., Doughty, C. E., Brando, P., Silvério, D., Halladay, K., Nepstad, D. C., Balch, J. K., & Malhi, Y. (2014). Ecosystem productivity and carbon cycling in intact and annually burnt forest at the dry southern limit of the Amazon rainforest (Mato Grosso, Brazil). *Plant Ecology and Diversity*, *7*(1–2). https://doi.org/10.1080/17550874.2013.798368

Scalon, M. C., Oliveras Menor, I., Freitag, R., Peixoto, K. S., Rifai, S. W., Marimon, B. S., Marimon Junior, B. H., & Malhi, Y. (2022). Contrasting strategies of nutrient demand and use between savanna and forest ecosystems in a neotropical transition zone. *Biogeosciences*, *19*(15), 3649–3661. https://doi.org/10.5194/bg-19-3649-2022

Schieving, F., & Poorter, H. (1999). Carbon gain in a multispecies canopy: The role of specific leaf area and photosynthetic nitrogen-use efficiency in the tragedy of the commons. *New Phytologist*, *143*(1). https://doi.org/10.1046/j.1469-8137.1999.00431.x

Sudmanns, M., Tiede, D., Augustin, H., & Lang, S. (2020). Assessing global Sentinel-2 coverage dynamics and data availability for operational Earth observation (EO) applications using the EO-Compass. *International Journal of Digital Earth*, *13*(7), 768–784. https://doi.org/10.1080/17538947.2019.1572799

Sun, L., Ataka, M., Han, M., Han, Y., Gan, D., Xu, T., Guo, Y., & Zhu, B. (2021). Root exudation as a major competitive fine-root functional trait of 18 coexisting species in a subtropical forest. *New Phytologist*, *229*(1). https://doi.org/10.1111/nph.16865

Tan, Z., Zhang, Y., Yu, G., Sha, L., Tang, J., Deng, X., & Song, Q. (2010). Carbon balance of a primary tropical seasonal rain forest. *Journal of Geophysical Research Atmospheres*, *115*(13). https://doi.org/10.1029/2009JD012913

Tomlinson, K. W., Poorter, L., Sterck, F. J., Borghetti, F., Ward, D., de Bie, S., & van Langevelde, F. (2013). Leaf adaptations of evergreen and deciduous trees of semi-arid and humid savannas on three continents. *Journal of Ecology*, *101*(2), 430–440.

Van Oijen, M., Schapendonk, A., & Höglind, M. (2010). On the relative magnitudes of photosynthesis, respiration, growth and carbon storage in vegetation. *Annals of Botany*, *105*(5), 793–797. http://www.jstor.org/stable/43576716

Wang, L., Zhu, H., Lin, A., Zou, L., Qin, W., & Du, Q. (2017). Evaluation of the latest MODIS GPP products across multiple biomes using global eddy covariance flux data. *Remote Sensing*, *9*(5). https://doi.org/10.3390/rs9050418

Watson, J. E. M., Evans, T., Venter, O., Williams, B., Tulloch, A., Stewart, C., Thompson, I., Ray, J. C., Murray, K., Salazar, A., McAlpine, C., Potapov, P., Walston, J., Robinson, J. G., Painter, M., Wilkie, D., Filardi, C., Laurance, W. F., Houghton, R. A., … Lindenmayer, D. (2018). The exceptional value of intact forest ecosystems. In *Nature Ecology and Evolution* (Vol. 2, Issue 4). https://doi.org/10.1038/s41559-018-0490-x

Wright, I. J., Reich, P. B., Westoby, M., Ackerly, D. D., Baruch, Z., Bongers, F., Cavender-Bares, J., Chapin, T., Cornellssen, J. H. C., Diemer, M., Flexas, J., Garnier, E., Groom, P. K., Gulias, J., Hikosaka, K., Lamont, B. B., Lee, T., Lee, W., Lusk, C., … Villar, R. (2004). The worldwide leaf economics spectrum. *Nature 2004 428:6985*, *428*(6985), 821–827. https://doi.org/10.1038/nature02403

Xia, J., Yuan, W., Lienert, S., Joos, F., Ciais, P., Viovy, N., Wang, Y. ping, Wang, X., Zhang, H., Chen, Y., & Tian, X. (2019). Global Patterns in Net Primary Production Allocation Regulated by Environmental Conditions and Forest Stand Age: A Model-Data Comparison. *Journal of Geophysical Research: Biogeosciences*, *124*(7). https://doi.org/10.1029/2018JG004777

Yang, H., Ciais, P., Wang, Y., Huang, Y., Wigneron, J. P., Bastos, A., Chave, J., Chang, J., E. Doughty, C., Fan, L., Goll, D., Joetzjer, E., Li, W., Lucas, R., Quegan, S., Le Toan, T., & Yu, K. (2021). Variations of carbon allocation and turnover time across tropical forests. *Global Ecology and Biogeography*, *30*(6). https://doi.org/10.1111/geb.13302

Yoon, T. K., Noh, N. J., Kim, S., Han, S., & Son, Y. (2015). Coarse woody debris respiration of Japanese red pine forests in Korea: controlling factors and contribution to the ecosystem carbon cycle. *Ecological Research*, *30*(4). https://doi.org/10. 1007/s11284-015-1275-1

Zhang, Y., Chen, J. M., & Miller, J. R. (2005). Determining digital hemispherical photograph exposure for leaf area index estimation. *Agricultural and Forest Meteorology*, *133*(1–4). https://doi.org/10.1016/j.agrformet.2005.09.009

Zhang-Zheng, H., Malhi, Y., Gvozdevaite, A., Peprah, T., Boackye, M., Ziemińska, K., Adu-Bredu, S., Aguirre-Gutiérrez, J., Sandoval, D., Prentice, C., & Oliveras, I. (2023). Photosynthetic and water transport strategies of plants along a tropical forest aridity gradient: a test of optimality theory. *BioRxiv*, 2023.01.10.523419. https://doi.org/10.1101/2023.01.10.523419

Zhao, M., Heinsch, F. A., Nemani, R. R., & Running, S. W. (2005). Improvements of the MODIS terrestrial gross and net primary production global data set. *Remote Sensing of Environment*, *95*(2). https://doi.org/10.1016/j.rse.2004.12.011

Zhao, M., & Running, S. W. (2010). Drought-Induced Reduction in GlobalTerrestrial Net Primary Productionfrom 2000 Through 2009. *Science*, *329*(5994), 940–943. https://doi.org/10.1126/science.1192666.

5 PAPER 2

PHOTOSYNTHETIC AND WATER TRANSPORT STRATEGIES OF PLANTS ALONG A TROPICAL FOREST ARIDITY GRADIENT: A TEST OF OPTIMALITY THEORY

"Everybody trusts the field data except its collector, nobody trusts a model except its modeller."

Prof. Mathew Williams

(Ecologist at The University of Edinburg)



A tree at study site Bobiri decides to shed only shade leaves, Credit: Huanyuan Zhang-Zheng

5.1 Preface

The overall **aim of the thesis** is to elucidate West African forest GPP using thorough field measurements of carbon fluxes, plant functional traits and environmental variables. **Paper 2** presents plant functional traits, including photosynthetic traits and explain their spatial pattern. **Paper 2** provides physiological understanding of the spatial pattern of GPP (presented in **Paper 1)** because photosynthesis forms the basis for estimating gross primary productivity (GPP) in most dynamic global vegetation models (DGVMs). Optimality theory was recently developed to predict photosynthetic traits and GPP from climate variables (see Research Background). **Paper 2** tests optimality theory at the study region and finds that the theory could well explain photosynthetic strategies along the tropical aridity gradient.

5.1.1 The significance of the paper

The paper contributes significantly to the field of study by summarizing our current theoretical expectations on the effect of aridity on 14 traits. It then disentangles the effect of aridity from temperature by testing the theoretical expectations along an aridity gradient, which clarifies the direct effects of aridity on photosynthesis. The paper is also timely, as many recent efforts have been devoted to proposing universal rules to explain worldwide photosynthetic strategies, but such rules have not been reviewed and tested along any aridity gradient. The paper synthesizes the state-of-the-art of optimality theories and explains their implications on plant strategies along an aridity gradient. As well as being interesting in itself, this work provides insights into how tropical forests may respond to intensified dry season climates.

5.1.2 Author contributions

I had originally planned fieldwork for this paper with a focus on hydraulic traits along the aridity gradient. However, the COVID pandemic impeded the fieldwork, and my supervisors (I.O. and Y.M.) thankfully provided many plants functional traits data pertaining to photosynthesis, previously collected mainly by A.G., T.P., and field collaborators. I.C.P. and I examined the implications of optimality theory on trait variation along a tropical aridity gradient and tested relevant hypotheses. During my informal chats with many other researchers, who are acknowledged but not co-authors, I received many constructive suggestions regarding the optimality theory framing of the paper. The manuscript is currently under review in *New Phytologist*.

5.1.3 Specific author contributions:

I.O., Y.M., I.C.P., and H.Z. designed the research and interpreted the results. D.S. did the hydraulic modelling. Y.M., A.G., T.P., M.B., K.Z., S.A.B., J.A.G., I.O., H.Z. contributed to data collection and analysis. H.Z. carried out the analyses and wrote the paper with inputs and revisions from all co-authors.

PHOTOSYNTHETIC AND WATER TRANSPORT STRATEGIES OF PLANTS ALONG A TROPICAL FOREST ARIDITY GRADIENT: A TEST OF OPTIMALITY THEORY

Huanyuan Zhang-Zheng1, Yadvinder Malhi1, Agne Gvozdevaite1, Theresa Peprah4, Mickey Boakye3, Kasia Ziemińska2, Stephen Adu-Bredu4, Jesús Aguirre-Gutiérrez1, David Sandoval 5, Iain Colin Prentice 5, Imma Oliveras Menor1,2,

1 Environmental Change Institute, School of Geography and the Environment, University of Oxford, Oxford, United Kingdom,

2 AMAP (Botanique et Modelisation de l'Architecture des Plantes et des Végétations), CIRAD, CNRS, INRA, IRD,Université de Montpellier, Montpellier, France

3 Department of Environmental Science, Policy, and Management, University of California, Berkeley, CA, 94720, USA

4 Forestry Research Institute of Ghana, Council for Scientific and Industrial Research, Kumasi, Ghana

5 Georgina Mace Centre for the Living Planet, Department of Life Sciences, Imperial College London, Silwood Park Campus, Buckhurst Road, Ascot, SL5 7PY, UK

5.2 Summary

(1) The research conducted, including the rationale

The direct effect of aridity on photosynthetic and water-transport strategies is not easy to discern in global analyses because of large-scale correlations between precipitation and temperature. We analyze tree traits collected along an aridity gradient in Ghana, West Africa, that shows little temperature variation, in an attempt to disentangle thermal and hydraulic influences on plant traits.

(2) Methods

Predictions derived from optimality theory of the variation of key plant traits along the gradient are tested with field measurements.

(3) Results

Most photosynthetic traits show trends consistent with optimality-theory predictions, including higher photosynthetic rates in the drier sites, and an association of higher photosynthetic rates with greater respiration rates and greater water transport. Leaf economic and hydraulic traits show less consistency with theory or global-scale pattern, especially predictions based on xylem efficiency safety trade-off. Nonetheless, the link between photosynthesis and water transport still holds: species (predominantly deciduous species found in drier sites) with both higher sapwood-to-leaf area ratio (A_S/A_L) and potential hydraulic conductivity (K_P), implying higher transpiration, tend to have both higher photosynthetic capacity, and lower leaf-internal CO_2.

(4) Conclusions

These results indicate that aridity is an independent driver of spatial patterns of photosynthetic traits, while plants show a diversity of water-transport strategies along the aridity gradient.

Plain language summary: Along an aridity gradient in Ghana, West-Africa, we used optimality theory to explain why higher photosynthetic rates should be found at drier places and how plants arrange water transportation to support quicker photosynthesis at the drier site. We also reported surprising data-theory inconsistency for some hydraulic traits along the aridity gradient where further research is needed.

Keywords

Optimality; photosynthesis; aridity; plant functional traits; plant hydraulics; xylem hydraulics

5.3 Introduction

Three key photosynthetic processes are frequently considered when seeking to understand plant photosynthesis strategies: light availability and electron transport; aridity and water transport; and CO_2 concentration and carboxylation (Farquhar et al., 2001). Plants capacities in these processes vary considerably along environmental gradients (Wang *et al.*, 2017a; Bahar *et al.*, 2017; Yang *et al.*, 2019; Oliveras *et al.*, 2020). Recently, many efforts have been made to propose universal rules to explain worldwide plant photosynthetic strategies, frequently cited as 'optimality theories', which could serve as a basic theoretical framework for vegetation carbon modelling and enable quantitative predictions of key photosynthetic traits (Franklin *et al.*, 2020; Harrison *et al.*, 2021).

One of the main challenges confronting these universal theories is to explain the 'pure' effect of aridity on photosynthesis (Rogers *et al.*, 2017). Such challenges become particularly pressing in the context of climate as greater atmospheric dryness (water vapour deficit, VPD) is predicted for most places (Neelin *et al.*, 2006; Grossiord *et al.*, 2020a; Bauman *et al.*, 2022), which may strongly influence photosynthesis and hence the carbon cycle (Canadell *et al.*, 2021). However, the theoretical expectation for the impact of aridity on plant traits based on optimality theories has not been summarized and tested. Most current earth systems models predict a negative relationship between photosynthesis (denoted by CO_2 assimilation rate per leaf area, A_{area}) and VPD simply due to the closing of stomata without incorporating the dynamics of photosynthetic capacity (denoted by electron-transport capacity, J_{max25} and Rubisco carboxylation capacity standardized to 25 degree celsius, V_{cmax25}) (Wang *et al.*, 2017a; Green *et al.*, 2020). On the contrary, a study focusing on Amazonia argued that higher VPD increases photosynthetic capacity which counteracts the reduced conductivity, leading to higher photosynthesis under drier climates (Restrepo-Coupe *et al.*, 2013; Green *et al.*, 2020). However, a global study found the above pattern only exists in wet ecosystems and higher VPD reduces photosynthesis overall (Fu

et al., 2022) although globally higher V_{cmax25} was indeed found for plants grown in drier sites (Peng *et al.*, 2021). Under experimental conditions, plants grown under low VPD show no difference in CO2 assimilation to plants grown under normal VPD (Cunningham, 2005).

With such mixed evidence in the literature, the stand-alone effect of aridity on photosynthesis still remains unclear. There are two particular challenges. First, on a large spatial scale, aridity can be confounded with temperature (especially when VPD is used as a metric of aridity). Temperature is a stronger driver of photosynthesis than aridity (Smith *et al.*, 2019; Peng *et al.*, 2021), but few studies try to disentangle aridity from temperature (Grossiord *et al.*, 2020a). Second, the effect of VPD can be confounded with soil water availability. Optimality theory predicted higher V_{cmax} and A_{area} under higher VPD (Smith *et al.*, 2019) but it is unclear how plants in drier environments arrange water transportation to support higher $A_{area.}$ A comprehensive theoretical framework is lacking to incorporate the effect of VPD on all leaf-level photosynthesis processes (light, water and CO_2) with full consideration of water delivery to leaves (Mencuccini *et al.*, 2019a).

Here, we examine a dataset of detailed traits measurements along an aridity gradient in West African forests to disentangle the effect of aridity on photosynthesis from temperature and to explain the effect with optimality theory. The key questions we address are: (1) do drier environments have higher photosynthesis rates and how do aridity and photosynthesis interact? (2) If photosynthetic rates are higher in arid environments, as predicted by optimality theory, how do plants arrange greater water transportation, given greater water stress in drier places? To answer these questions, we adopted a theory-data comparison approach where we first review the expectation of recent ‘universal’ theories and deduced 16 testable predictions (some of which have previously been tested but with confounding results). We then examined the consistency between each prediction and field measurement along the aridity gradient (Table 1). Consistency would give field-observed

patterns a mechanistic explanation and reinforce the stand-alone impact of aridity on the corresponding trait, while inconsistency would imply weakness of the theory and possible effect of environmental factors (like soil properties). Before closing the paper, we summarize the consistency and inconsistency with an integrated theoretical framework to address the 'pure' effect of aridity on photosynthesis.

5.4 Optimality theory review

'Optimality theory' was developed recently with the assumption that plants can optimize photosynthesis and minimize maintenance costs according to their living environments by optimizing investment in the above processes, which provides a universal explanation of the variation of photosynthetic strategies under different growing environments (Prentice *et al.*, 2014; Wang *et al.*, 2017b; Mencuccini *et al.*, 2019a; Stocker *et al.*, 2020; Xu *et al.*, 2021). Although the above-cited studies have tested the theories on global scales and along elevation gradients, discussion and validation of these theories along other abiotic gradients, such as aridity gradients, are still lacking. Therefore, we first review the implication of such theories on plants photosynthetic strategies along aridity gradients.

In drier sites, higher VPD increases potential transpiration per unit leaf area. As predicted by the 'least-cost hypothesis' (Wright *et al.*, 2001, 2003; Medlyn *et al.*, 2011; Prentice *et al.*, 2014), plants can compensate for high water costs in dry climates by keeping stomata relatively closed. Thus, in drier sites, plants are expected to have lower leaf internal CO_2 concentration (c_i), lower internal-to-external CO_2 ratio (c_i/c_a) and lower stomatal conductance (g_s). The 'coordination hypothesis' (Beerling & Quick, 1995; Maire *et al.*, 2012; Walker *et al.*, 2014) assumes equilibrium between Rubisco-limited photosynthesis rates (A_C) (depending on V_{cmax25} and c_i) and electron transport-limited photosynthesis rates (A_J) (depending on J_{max25} and leaf absorbed PPFD) (see the

quantitative expression in (Wang *et al.*, 2017b; Smith *et al.*, 2019; Stocker *et al.*, 2020)). To maintain such an equilibrium, plants in drier sites are expected to have larger V_{cmax25} to compensate for the lower c_i. Otherwise, A_C would be lower than A_J resulting in unused capacity for electron transport (J_{max25}). To sum up, lower c_i but higher V_{cmax25} is expected toward drier sites if J_{max25} stays constant (in which case A_J would be slightly lower due to smaller c_i).

In reality, toward drier sites, it is common to see higher leaf absorbed photosynthetic photon flux density (I_{abs}) because of less cloud cover and more open canopies. Considering an additional optimality criterion that J_{max25} is acclimated to I_{abs} (Smith *et al.*, 2019), supported by multiple experiments (Björkman, 1981; Ögren, 1993), we would expect higher J_{max25} in drier sites, which further encourages higher V_{cmax25} (see above paragraph). Higher J_{max25} and V_{cmax25} would give rise to higher A_C and A_J. All the above would lead to high leaf photosynthetic protein cost in dry sites, hence high leaf dark respiration (R_d), and high transpiration stream maintenance cost (see below for transpiration), hence higher stem respiration per leaf area (R_S) (Prentice *et al.*, 2014). Note that R_S is stem respiration per leaf area (R_{stem_leaf} hereafter), different from the commonly reported stem respiration per stem area (R_{stem_stem}). Some of the above predictions have been seen on global scale; for example, higher R_d has been found in drier sites (Wright *et al.*, 2001; Atkin *et al.*, 2015) and higher assimilation rate has been reported from drier sites (Maire *et al.*, 2015).

It is worth noting that V_{cmax25}, g_s and c_i in this paper are discussed as an overall value for a forest stand, disregarding diurnal variation and intraspecific variation (Stangl *et al.*, 2019; Han *et al.*, 2022). At the species or individual scales, there is a positive correlation between A_{sat} (light-saturated assimilation rate at 400 ppm), V_{cmax25}, g_s and c_i (Wright *et al.*, 2003; Prentice *et al.*, 2014), instead of the opposite trend of V_{cmax25} and c_i/c_a as discussed above regarding spatial variation only.

Photosynthesis strategies predicted by the optimality theory above can be linked with xylem water transportation strategies via stomatal behaviour, as given by Fick's law,

$$g_s = A_{area} / (ca - ci) \quad (1)$$

Where g_s is stomatal conductance (umol CO_2 $m^{-2}s^{-1}$), A_{area} is CO_2 assimilation rate per leaf area (umol CO_2 $m^{-2}s^{-1}$), and leaf internal (c_i, ppm) and external (c_a, ppm) CO_2 concentration.

We focus on daytime conditions that produce maximum rates of transpiration and photosynthesis, when water loss through stomata must equal water transport through xylem (Brodribb *et al.*, 2002; Xu *et al.*, 2021):

$$E = 1.6\, g_s\, VPD / P_{atm} = Ks\, \Delta\Psi_{max}\, A_S/A_L / h \quad (2)$$

Where E is the transpiration rate (mol m–2s–1), P_{atm} is atmospheric pressure (MPa), K_S is the sapwood-specific hydraulic conductivity (mol $m^{-1}s^{-1}$ MPa^{-1}); A_S/A_L is the ratio of sapwood to leaf area (cm^2m^{-2}) $\Delta\Psi_{max}$ is the maximum decrease in water potential from soil to leaves (MPa) and h is the transpiration stream pathlength (m), roughly equivalent to plant height.

Combining the above two equations we obtain a link between water transportation and photosynthesis:

$$K_s\ \Delta\Psi_{max}\ A_S/A_L\ / h = 1.6\ VPD\ A_{area} / (c_a - c_i) /P_{atm} = E \quad (3)$$

Note that here we focus on overall forest-stand scale and disregard diurnal or seasonal variation. Relationships could be very different at other scales (Mencuccini *et al.*, 2019a).

In drier sites with higher VPD, despite less open stomata (less g_s and less c_i), there should inevitably be a larger E (Granier *et al.*, 1996) and more negative $\Delta\Psi_{max}$ (Gleason *et al.*, 2013); therefore smaller maximum tree height, and more negative turgor loss point (TLP, Mpa) in drier sites to increase hydraulic resistance (note that TLP must be more negative than $\Delta\Psi_{max}$) (Ryan & Yoder, 1997; Bartlett *et al.*, 2012). Equation 3 implies that in drier sites with high VPD, plants require a larger A_S/A_L and/or larger K_S in order to

support the same amount of photosynthesis with enhanced transpiration. Following the xylem safety efficiency trade-off (Manzoni *et al.*, 2013; Gleason *et al.*, 2016; Bittencourt *et al.*, 2016; Grossiord *et al.*, 2020b) (although arguments against this trade-off exist, here we present testable hypotheses expected by the trade-off), plants at drier sites would be expected to have lower hydraulic efficiency and lower hydraulic conductivity. Lower hydraulic conductivity is often associated with smaller vessel diameter, higher vessel density and higher wood density (Poorter *et al.*, 2010; Schuldt *et al.*, 2013; Hoeber *et al.*, 2014). Such patterns have been observed along an Australian aridity gradient (Gleason *et al.*, 2013; Pfautsch *et al.*, 2016), but no effect of aridity on vessel diameter was reported (Olson & Rosell, 2013; Olson *et al.*, 2014). Plants in drier sites should have increased hydraulic safety - more negative TLP and more negative P_{50} (water potential at 50% loss of conductivity) (Hacke *et al.*, 2001; Martínez-Vilalta *et al.*, 2009; Gleason *et al.*, 2013; Togashi *et al.*, 2015; Liu *et al.*, 2019; López *et al.*, 2021). In short, toward drier sites, we would expect to see, higher A_S/A_L and more negative TLP. The safety-efficiency trade-off implies lower K_S, smaller vessel diameter, higher vessel density and higher wood density.

The trade-off between K_S and A_S/A_L is also embedded in the variance of traits in equation 3. K_S and A_S/A_L could vary by two orders of magnitude (100-fold variation) (Mencuccini *et al.*, 2019b) on a global scale, while c_i/c_a and A_{area} vary much less (c_i/c_a: 2-fold; A_{area}: 10 fold) (Wright *et al.*, 2004; Wang *et al.*, 2017b). This leads to a trade-off between K_S and A_S/A_L (i.e. K_S * A_S/A_L should vary less than either of them). However, given that there are also variations of c_i/c_a, A_{area}, h and $\Delta\Psi_{max}$, it is possible that different species range along a spectrum from high A_{area} and E to low A_{area} and E while always satisfying equation 3 (Prentice *et al.*, 2014).

In short, the above review leads to an integrated hypothesis that plants in drier (normally also brighter) sites tend to develop a photosynthesis strategy with less stomatal conductance and hence lower ci, stronger photosynthetic capacities (larger Vc_{max25}, J_{max25}

and A_{area}) with more maintenance cost (higher R_d and R_S), higher maximum carbon assimilation rate and larger maximum evapotranspiration which the water transport system would adjust to with higher A_S/A_L, lower K_S, lower tree height and more negative TLP. Information on leaf economic traits is provided in Appendix 3. We break the above prediction down into 16 testable hypotheses (Table 1) and test each of them along a forest aridity gradient.

5.5 Materials and Methods

5.5.1 Study sites - the aridity gradient

This study presents and analyses physiological traits data collected from seven one-hectare forest and savanna plots distributed along a wet to dry rainfall gradient across three sites, Ankasa (ANK, moist rainforest), Bobiri (BOB, semi-deciduous forest) and Kogyae (KOG, dry forest and mesic savanna), in Ghana, West Africa (Figure S 1 Figure S 2) (Moore *et al.*, 2018; Oliveras *et al.*, 2020), as part of the Global Ecosystem Monitoring (GEM) network (Malhi *et al.*, 2021). These sites share very similar mean annual temperature but span a steep gradient of aridity (Figure 1), which provided a "natural laboratory" to disentangle the hydraulic aspect of plant traits variation from temperature. Light increases toward drier sites (Table S 1). There is no seasonal variation of temperature but with strong seasonality of rainfall (Figure S10 S11).

Although one-hectare plots (e.g. BOB-02) within the same site (e.g. BOB) share very similar air temperature and precipitation, they can differ in terms of soil moisture supply due to small-scale variations in soil properties and topography (Table S1). Along the aridity gradient, there are also variations in soil and vegetation type, with vegetation seasonality and deciduousness increasing considerably towards drier sites (Moore *et al.*, 2018). More information about the soil properties and climate of all three sites can be

found in (Domingues *et al.*, 2010; Chiti *et al.*, 2010; Moore *et al.*, 2018). Moreover, the swampy rainforest (ANK03) is partly inundated during the wet season unlike ANK01, which is located on a hill and never inundated. From KOG02 (dry forest), KOG04 to KOG05 (savanna), forest plots become more deciduous with a smaller number of trees. Within any site, there are many common species between plots but species composition (e.g., top five abundant species) could still be very different. There are almost no common abundant species between the three sites (ANK, BOB and KOG).

5.5.2 Aridity index and soil moisture stress

At site scales, we calculated an aridity index as the ratio of annual potential evapotranspiration (PET) to mean annual precipitation (MAP). To understand soil moisture stress experienced by plants, we reported not only measured surface (12 cm depth) soil volumetric water content, but also hydraulic simulations on plot scales with SPLASH v2.0 (Sandoval & Prentice, 2020). This model requires three sets of input data: (1) field observed climate data at site scale during 2011-2016 (2) soil properties measured following the RAINFOR protocols (Quesada *et al.*, 2010); (3) terrain data: root zone was assumed 2m, while upslope drainage area, slope inclination and orientation were extracted from a global dataset (Yamazaki *et al.*, 2019). We considered two modelled indices: the relative soil moisture saturation (Θ) was defined as the volumetric water content (θ) normalized by the volumetric water content at saturation (θ_{SAT}); a vegetation water stress index (α) was estimated as the ratio of annual actual evapotranspiration (AET) to PET.

5.5.3 Functional trait data measurements

Leaf traits field campaigns to measure leaf traits were conducted using a standardized protocol between October 2015 and September 2016 in all plots (Oliveras *et al.*, 2020), covering both dry and wet seasons (see Appendix 1 for sampling protocol). We selected species that contributed to up to 80% of the basal area of each plot and sampled the three

largest individuals for each species. From each selected individual, we sampled a sun and a shade branch, and from each branch, we used three leaves and three wood segments to measure leaf and wood traits, respectively. Only sunlit samples were used in this analysis because temperature and light of the shade leaves vary considerably from plot to plot which dilutes the focus on the effect of aridity. As equation 3 focuses on daytime conditions with maximum transpiration, we use K_P (potential sapwood-specific hydraulic conductivity) as a proxy of K_S (sapwood-specific hydraulic conductivity) and plant stature (H_{max}) as a proxy of path length (h). K_P was calculated from vessel density and vessel diameter following (Poorter *et al.*, 2010). Leaf area index and net primary productivity were retrieved from (Moore *et al.*, 2018).

Following (Prentice *et al.*, 2014), we calculated stem respiration per leaf area (Rs_leaf) instead of the commonly presented Rs_stem, as a 'maintenance cost of photosynthesis' (See Appendix 1). To our knowledge, Rs_leaf has not previously been presented with in-situ data in the literature. Here we argue the importance to understand stem respiration from per leaf area perspectives because (1) higher stem respiration per stem area has been found in wetter sites (Yang *et al.*, 2016), contradictory to theoretical expectation (Prentice *et al.*, 2014) (2) consistency with photosynthetic traits which were commonly reported per leaf area.

All data reported in this study were field-measured except for wood density, which was obtained from a global species database (Zanne *et al.*, 2009). Global scale sapwood-to-leaf-area ratio in Figure S6 and S4 are sourced from (Mencuccini *et al.*, 2019b). Global scale vessel diameter used in Figure S4 is sourced from (Choat *et al.*, 2012). Multiple sources of data were joined using species name.

5.5.4 Statistical analysis

Hypotheses 1-14 (Table 1) were tested by significant differences between wet and dry sites. Principal component analysis (PCA) and standardized major axis regression are used to understand the relationship between K_S, A_S/A_L and photosynthesis traits (Hypothesis 15-16).

We performed a plot-to-plot comparison in answering Hypotheses 1 to 14 as follows: (1) The distribution was visually inspected with histograms and transformations were applied if necessary. (2) Outliers were checked with the R package *outliers::scores*, 'iqr' method with threshold 1.5. This removed leaves/trees with extreme values but made the community-weighted mean a better representation of the whole plot. (3) Community-weighted means were calculated based on the basal area of each species. Standard error was calculated with the same weights (Madansky & Alexander, 2017). (4) Significance of differences in plot-to-plot community-weighted means were then tested with *lm*(), *glht*(), and *cld*(). (See Rscript *community_weighted_mean_Ghana_log_YS.R* for a full description). In testing Hypotheses 1-14, a hypothesis was accepted if KOG (dry region) was significantly different to ANK (wet region) while BOB (middle aridity) sat in between (Figure 1). (5) Variance partitioning was done with *vegan::varpart()*, following the 'RDA' method with the expression: *varpart* (Trait, ~ Plot, ~ Species, data = Trait). Variance partitioning reveals whether the change of traits along the aridity gradient was driven by intraspecific or interspecific variation. Note that plots within one site share common species (e.g. ANK01 to ANK03), but species composition is very different between site (e.g. ANK01 to KOG02). Variance partitioning is also used to diagnose whether the intra-specific variation or measurement errors are overwhelming. To double-check the impact of intraspecific variation, we recalculated a community-weighted mean by assuming that the same species share the same value of trait (i.e. remove intraspecific variation) and extrapolated traits value to forest plots without trait measurements (Appendix 5)

For hypothesis 16, we applied Principal Component Analysis (PCA) with *FactoMineR::PCA*(), (See Rscript ~/link_hydraulic_photosynthesis/PCA.R). A_{sat}, K_P, A_S/A_L and Vc_{max25} were log10 transformed. We avoid standardization by setting 'scale.unit' as False in function PCA() so that the variance of a trait was reflected by the length of an arrow in Figure 2. Trait-trait correlations (bivariate plot) were calculated (Rscript *Compare_with_Others.R*). For hypothesis 15, the slopes and significance of correlation were calculated using Standard Major Axis Regression (*function smatr::sma*()), which is preferable to ordinary least squares regression in summarizing the relationship between two plant traits (Wright *et al.*, 2005; Warton *et al.*, 2012) as it considers uncertainties of both axes. All analyses were done at the species level (i.e. each point in Figure 2 represents a species) to compare with other studies and join among datasets. Hypothesis 15 was also tested at the global scale because K_S was reported to negatively correlate with A_S/A_L but there is no report on the global correlation between K_P and A_S/A_L (Appendix 4).

5.6 Results

5.6.1 Aridity gradient

The values of the aridity index (PET/MAP) (site scale) revealed a clear aridity gradient from ANK (moist rainforest site) to BOB (mid) and KOG (dry) (Table S 2). The same order could be arrived at with VPD or maximum cumulative water deficit (MCWD). The standard deviation of monthly VPD also suggested that the seasonality was weaker in ANK and increased towards KOG.

On the other hand, the simulations of relative soil moisture saturation (Θ) and vegetation water stress index (α) (plot scale) showed that plants at BOB was the least soil moisture stressed, followed by ANK and KOG. BOB-02 had the highest values in these

two metrics, different to surface soil moisture (Figure 1). The model reported the highest runoff at ANK-03, capturing to some degree the seasonal flooding, as also observed in the field. The different patterns of Θ (or α) to aridity index along the aridity gradient were caused by the soil characteristics which in turn define water holding capacity (WHC) and hydraulic conductivity; for example, the plots in BOB were atmospherically drier (higher PET/MAP) than in ANK but they could hold more water (higher Θ). Especially in BOB-02, the infiltration rate was strongly reduced (60 mm/hr, less than half of ANK plots), and hence water can stay more time in the root zone while percolating. This acts as a buffer against the evaporative demand, maintaining water availability during dry months. The hydrological modelling outputs also matched with field observation of plot vegetation characteristics (see Methods, Figure S1 S2).

For presentation (Figure 1), we rank sites by aridity index and then plots within sites by soil moisture stress.

5.6.2 The effect of aridity on traits

From a photosynthesis perspective, along the aridity gradient, we saw consistency between theoretical prediction and field measurements (Table 1) for all traits from wet to dry: c_i/c_a (0.85 to 0.71), Vc_{max25} (21.58 to 46.48 umol CO_2 m^{-2} s^{-1}), J_{max25} (38.48 to 91.44 umol CO_2 m^{-2} s^{-1}), R_d (-1.66 to -2.41 umol CO_2 m^{-2} s^{-1}), R_S (3.76 to 11.70 umol CO_2 m^{-2} s^{-1}), A_{sat} (4.56 to 7.72 umol CO_2 m^{-2} s^{-1}) and A_{max} (15.88 to 22.86 umol CO_2 m^{-2} s^{-1}).

From a water transpiration perspective, the hypotheses were consistent with field measurements for leaf traits. A_S/A_L was higher in drier sites (359.62 to 901.66 cm^{-2} m^{-2}) and TLP was more negative in drier sites (-1.33 to -1.63 Mpa). However, no consistency was found between theoretical expectations and field measurements for any xylem-related traits. Along the aridity gradient, there was an increasing trend of field K_P toward drier sites (from 28.62 to 59.29 kg m-1 Mpa-1 s^{-1}), against the xylem safety-efficiency trade-off.

Behind the above trend, vessel diameter and vessel density also contradicted the hypotheses. Vessel diameter did not change along the aridity gradient, while vessel density increased toward drier sites (from 44.57 to 69.69 mm^{-2}). The drier sites (KOG) had higher K_P, higher twig density and higher wood density than the wetter sites on site scales, but we also found K_P negatively correlated with twig density on species scales (see Appendix 4). ANK-01 had very high wood density and twig density which breaks the increasing trend formed by other plots. To conclude, the trends of all photosynthetic traits were successfully predicted by theories based on VPD alone. As leaf economy traits, soil nutrients and soil moisture (Θ or α) overall did not have a clear trend along the gradient, considering nutrient and water deliveries to leaves does not seem to aid the prediction of variation of photosynthetic traits along the aridity gradient.

With variance partitioning, we found that the plot-to-plot trends of all traits were dominated by inter-specific rather than intra-specific variation (i.e., components [a] are smaller than [b] in Appendix 5) (i.e. the change of species composition). The analogous patterns between twig and wood density along the aridity gradient also supported species turnover since twig density was field measured and wood density was parsed from a global database by species (Zanne *et al.*, 2009). To double-check the conclusion of predominant interspecific variation, we recalculated community weighted means by assuming that the same species share the same value of trait (i.e. remove intraspecific variation) and extrapolated trait values to forest plots without trait measurements. We found that the conclusions in Table 1 still hold after extrapolation (Appendix 5). The trend of trait variation from plot to plot could be well re-constructed on a species basis, which hints at the possibility of extrapolation to other sites with species composition information or upscaling to larger scales. Nonetheless, for within plot variance, intraspecific variation or measurement errors (component [d]) were large for most traits: accounting for 95% of turgor loss point variance, followed by Vc_{max25} (74%) and J_{max25} (66%).

5.6.3 The coordination between photosynthesis and water transportation

Data from our West African aridity gradient reveal a weak positive correlation between K_P and A_S/A_L, contradictory to Hypothesis 15, and inconsistent with the negative correlation that emerged on global scales (Appendix 4). A_S/A_L for the Ghanaian aridity gradient was higher than the pantropical average. For hypothesis 16, we further explore the link between A_S/A_L, K_P and photosynthetic trait using PCA. Species with both high A_S/A_L and K_P tend to have higher Vc_{max25} and lower c_i/c_a. Such species tend to be deciduous and appear more in drier plots (Figure 2). There was a larger variance of hydraulic traits compared to photosynthetic traits. The pattern is consistent if we redo the above PCA with A_{sat} instead of Vc_{max25} (Appendix 4). This finding supports hypothesis 16 (Table 1) as well as equation 3.

5.7 Discussion

5.7.1 The trend of traits along the aridity gradient

Although most hypotheses (Table 1) have been tested with spatially varying aridity at multiple scales (Harrison *et al.*, 2021), testing them along the Ghana aridity gradient helps to scrutinize the pattern in the absence of temperature variation. The patterns of all photosynthetic traits measured along the aridity gradient (c_i/c_a, J_{max25}, Vc_{max25}, D_{resp}, R_S, A_{sat}, A_{max}, namely hypotheses 1-7) are consistent with the theoretical expectations, which underscores that aridity is a direct and critical driver of photosynthetic traits, in absence of confounding effect with temperature. The increase of photosynthetic capacity towards drier sites is useful in explaining multiple previous observations, including that (1) savanna has higher photosynthesis rates than wet evergreen forest (Gvozdevaite, 2018; Oliveras *et al.*, 2020) (2) woody savanna has sparse canopy but similar net primary productivity to wet evergreen forest (Figure 1) (Moore *et al.*, 2018). As leaf area index decrease toward dry sites and photosynthesis rate increase, the mid-aridity site is the most productive. (3) for

wet Amazonia forests, leaves flushed in dry season have higher photosynthetic capacities which increase forest productivity (Wu *et al.*, 2020; Green *et al.*, 2020).

From a water transportation perspective, forests in drier sites have higher TLP, lower H_{max} and higher A_S/A_L (agreed with hypotheses 8-10), in support of a greater mid-day transpiration stream. However, hypotheses derived from the safety-efficiency trade-off (hypotheses for K_P and vessel diameter) were not in agreement with measurements along the aridity gradient. It is possible that the trade-off may work well for single-species studies (Pritzkow *et al.*, 2020) and become weak on large scales and across species (Gleason *et al.*, 2016; Grossiord *et al.*, 2020b). Much higher deciduousness in KOG (dry site) than in the wet sites may play a role as higher hydraulic efficiency was reported from deciduous species or more deciduous forests (Choat *et al.*, 2005; Chen *et al.*, 2008; Liu *et al.*, 2021). We reported a negative correlation between A_S/A_L and K_P at global scales but a positive correlation along the aridity gradient (Appendix 4). One of the reasons for these contrasting opposite correlations may lie in a geographical sampling bias – the global dataset with scarce data points from West Africa compared with the Ghanaian dataset. The other possibility could be a confounding effect by temperature or vegetation type at the global scale (a Simpson's paradox); for example, a negative correlation between A_S/A_L and K_S was reported globally (Mencuccini *et al.*, 2019b) and on continental (Australia) scales (Gleason *et al.*, 2012), but an insignificant correlation was also reported for tropical forest stands on local scales without varying temperature (Poorter *et al.*, 2010; Schuldt *et al.*, 2013; Hoeber *et al.*, 2014).

By assuming that traits with a clear and strong trend along the aridity gradient are more tightly bound with aridity (Figure 1), c_i/c_a, TLP and A_S/A_L were found to be the most aridity-driven traits. The runners-up are R_d, R_S, $J_{max25,}$ and Vc_{max25}, which was thought acclimated to c_i/c_a and light intensity (Wang *et al.*, 2017b). Although c_i/c_a, Vc_{max25}, K_P and A_S/A_L all vary from wet to dry sites, we further illustrate that, surprisingly, it is

photosynthetic traits instead of hydraulic traits that contrast species from wet to dry sites (also from evergreen to deciduous) (Figure 2). Given that large photosynthetic trait variation from wet to dry plot was induced by species turnover (Appendix 5), our studies hint that facing a drier climate, if allowed time, West African forests photosynthesis could adapt to a drier climate by changing species abundance with possibly more deciduousness and higher photosynthesis capacity albeit less stomatal openness (Aguirre-Gutiérrez *et al.*, 2019). Without consideration of the positive effect of aridity on photosynthetic capacity, models could possibly underestimate forest productivity under future drier climates.

5.7.2 Combining photosynthesis and hydraulic hypotheses

Overall, optimality theory can well explain plant photosynthesis strategies along the aridity gradient and we also expand the theory to consider water transportation. Namely, species in drier sites (with more deciduousness) tend to develop a photosynthesis strategy with less stomata openness (c_i/c_a), stronger photosynthetic capacities (J_{max25} and Vc_{max25}) with more maintenance cost (higher R_d and R_S), higher photosynthesis rate (A_{sat}) and larger maximum transpiration, supported by large K_P and large A_S/A_L. The product of A_S/A_L and K_P is a proxy of water delivery per leaf area, which was previously found well correlated with proxies of photosynthesis rate: A_{sat} (Santiago *et al.*, 2004), quantum yield of electron transport (Brodribb & Feild, 2000) and electron transfer rate (Brodribb *et al.*, 2002). The large variance of wood traits (considerably larger than leaf traits) (Mencuccini *et al.*, 2019b), hints that plants might have a wide range of choices of traits combinations to provide adequate water transportation (Sperry *et al.*, 2002; Prentice *et al.*, 2014) in drier sites to support faster photosynthesis. Further investigations into xylem functioning are required to understand how larger water transportation was achieved in drier sites. Notably, we successfully predicted plants photosynthesis strategies along the aridity gradient (hypothesis 1-7) based solely on VPD without incorporating leaf economic traits nor soil

moisture. Nonetheless, our theoretical deduction implicitly assumes that plants in the drier site could arrange water transportation (e.g., high A_S/A_L and high K_P, Figure 2) and have adequate access to belowground water. Regarding the ongoing discussion on the impact of VPD versus soil moisture, soil moisture may be playing a role at other temporal scales (e.g., daily) (Liu *et al.*, 2020; Fu *et al.*, 2022) or under extreme soil drought (Sperry *et al.*, 2002).

5.7.3 Conclusion

Along the aridity gradient, we found that species with both higher A_S/A_L and K_P (greater potential mid-day transpiration steam) tend to have higher Vc_{max25} and lower c_i/c_a, which appears more in drier sites with more deciduous species. With such a working example in West Africa, the study not only underscores the importance of incorporating the positive effect of aridity on photosynthesis capacity in carbon modelling but also simplifies the coupling between carbon and water cycle: future modelling studies, following our theoretical framework, could estimate site-time-averaged leaf-level photosynthesis simply from VPD only and consider soil moisture (or water availability) in simulating forest stands dynamic such as drought-induced mortality or seasonality (Hubau *et al.*, 2020; Bauman *et al.*, 2022).

5.8 Data availability

Figures could be downloaded from

https://github.com/Hzhang-ouce/Ghana_rainfall_trait_variation_optimality_github.

To reproduce figures, data and R codes mentioned in the main text could also be found in the above repository.

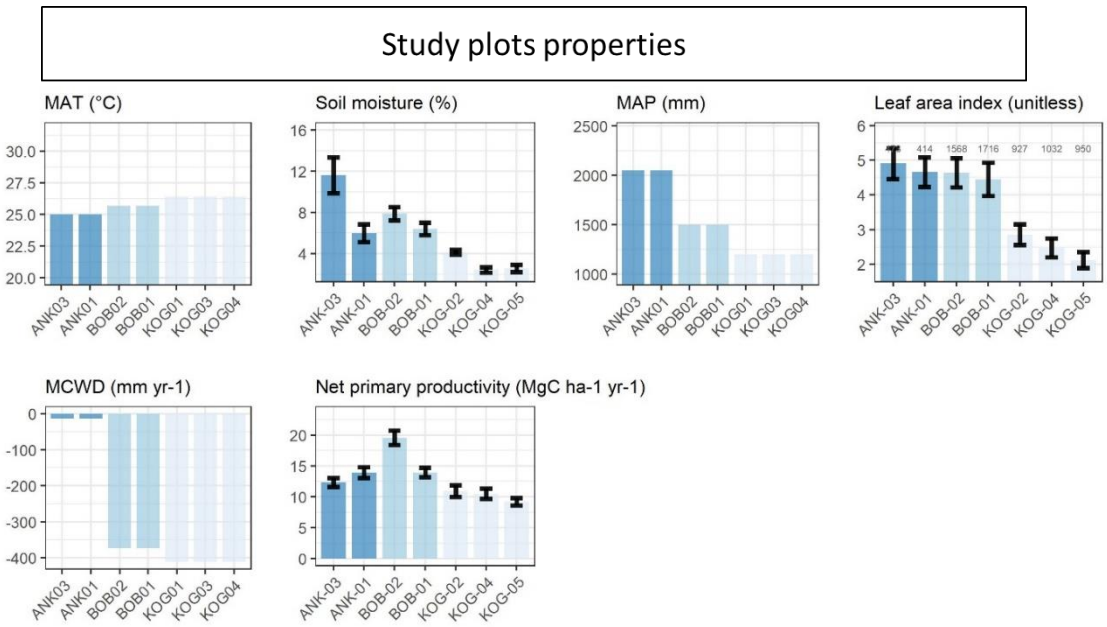
5.9 Acknowledgements

We thank Natascha Luijken, Ya-Jun Chen, Yu-Heng Sun, Maurizio Mencuccini, Akwasi DGyamfi, Guillaume Delhaye, Dong Ning, Han Wang, Roberto Salguero-Gómez and Sophie Fauset for valuable discussion and assistance with data processing. Y.M. is supported by the Jackson Foundation. H.Z. received Henfrey Scholarship (from St Catherine's College, Oxford) and Tang Scholarship (from China-Oxford Scholarship Fund). The field data collection was funded by a grant award (ERC GEM-TRAIT, grant no. ERC-2012-ADG_20120216) to Y.M., with additional support for the fieldwork from a Royal Society-Leverhulme Africa Capacity Building Award and Marie Curie Fellowship to I.O. (FP7-2012-IEF-327990-TipTropTrans).

Table 1 Traits name, unit, hypotheses and findings from field measurements along the rainfall gradient, Green color denotes consistency between theory and our field data. Orange color denote inconsistency.

#	Hypotheses	Data	Consistent
	Variables associated with photosynthesis and respiration (Optimality theory)		
1	Toward drier sites, the ratio between leaf-internal and ambient CO_2 (c_i/c_a, %) (from 13C) **decreases**.	Decrease	✓
2	Toward drier sites, Rubisco carboxylation capacity at 25 C° (Vc_{max25}, umol CO_2 m^{-2} s^{-1}) **increases**.	Slight increase	✓
3	Toward drier sites, electron transport capacity at 25 C° (J_{max25}, umol CO_2 m^{-2} s^{-1}) **increases**.	Slight increase	✓
4	Toward drier sites, light saturated assimilation rate at 400 ppm (A_{sat}, umol CO_2 m^{-2} s^{-1}) **increases**.	Increases	✓
5	Toward drier sites, light saturated assimilation rate at 2000 ppm (A_{max}, umol CO_2 m^{-2} s^{-1}) **increases.**	Increase	✓
6	Toward drier sites, leaf dark respiration (R_d, umol CO_2 m^{-2} s^{-1}) **increases**.	Increase	✓
7	Toward drier sites, specific stem respiration (R_S, umol CO_2 m^{-2} s^{-1}) **increases.**	Increase	✓
	Variables associated with water transportation		
8	Toward drier sites, Sapwood to leaf area ratio (Huber value) (A_S/A_L, cm^{-2} m^{-2}) **increases.**	Increase	✓
9	Toward drier sites, turgor loss point (TLP, MPa) becomes more negative.	More negative	✓

10	Toward drier sites, plant stature, calculated as maximum tree height of a species (H_{max}, m) **decreases**.	Slight decrease	✓
11	Toward drier sites, wood density (g cm-3) and twig density (g cm-3) **increase** (if following the safety-efficiency trade-off).	Slight increase	✓
12	Toward drier sites, potential specific hydraulic conductivity (K_P, kg m^{-1} Mpa-1 s^{-1}) **decreases** (if following the safety-efficiency trade-off).	Slight increase	
13	Toward drier sites, vessel diameter (micron) **decreases.** (if following the safety-efficiency trade-off).	No trend	
14	Toward drier sites, vessel density (mm^{-2}) **decreases.** (if following the safety-efficiency trade-off).	Increase	
15	A_S/A_L and K_P are negatively correlated. (If following safety-efficiency trade-off, and global scale analysis – see introduction)	Positive correlation	
16	For species with high A_S/A_L and K_P, there is high Vc_{max} (or high A_{sat})	See Figure 3	✓
	'Data' column summarizes patterns in Figure 1. A trend of trait is qualitatively recognized if KOG (dry region) is significantly different to ANK (wet region) while BOB ranks between. 'Slight increase' suggests that the pattern fits the above criteria broadly albeit one plot behaves inconsistently. Colours indicate results that are consistent (green), weakly consistent (light green) and inconsistent (orange) with theoretical expectations. Ticks in the column 'consistent' indicate consistency between hypotheses and data		



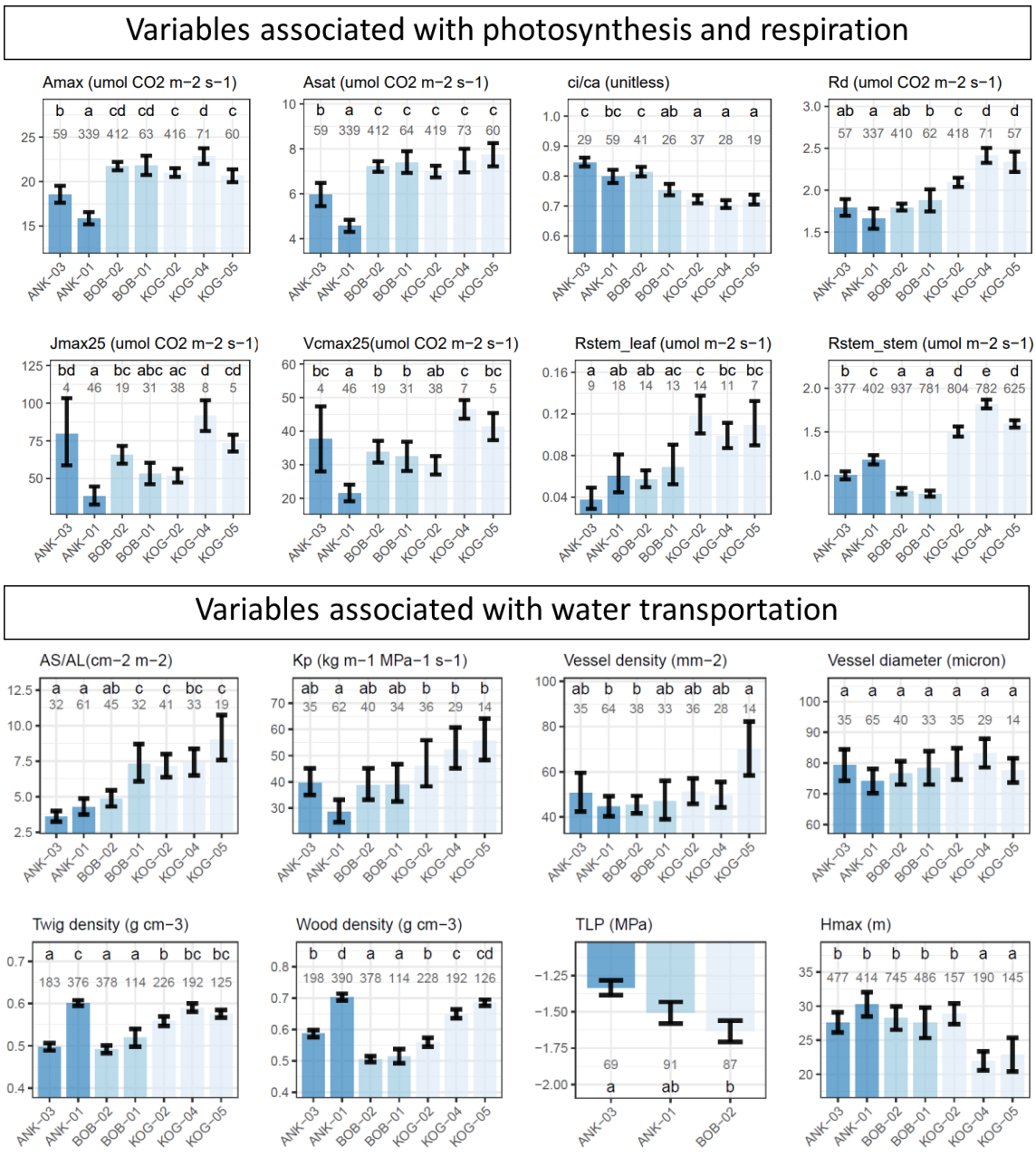


Figure 1 Plot scale community weighted mean (with standard error) from the wettest (left) to the driest (right) plot. Here we show Maximum Cumulative Water Deficit (MCWD), Mean annual air temperature (MAT), mean annual precipitation (MAP) and soil volumetric water content at 12 cm depth (Soil moisture), leaf area index (LAI) and Net primary productivity (NPP). See Table 1 for the list of plant traits. Forest plots are arrayed from left to right in order of increasing aridity according to the aridity gradient description described in the text. The number denotes the number of samples, which could be a leaf, a branch, a tree or a species depending on the variable. The letters denote significance (P<0.05) in plot-to-plot difference.

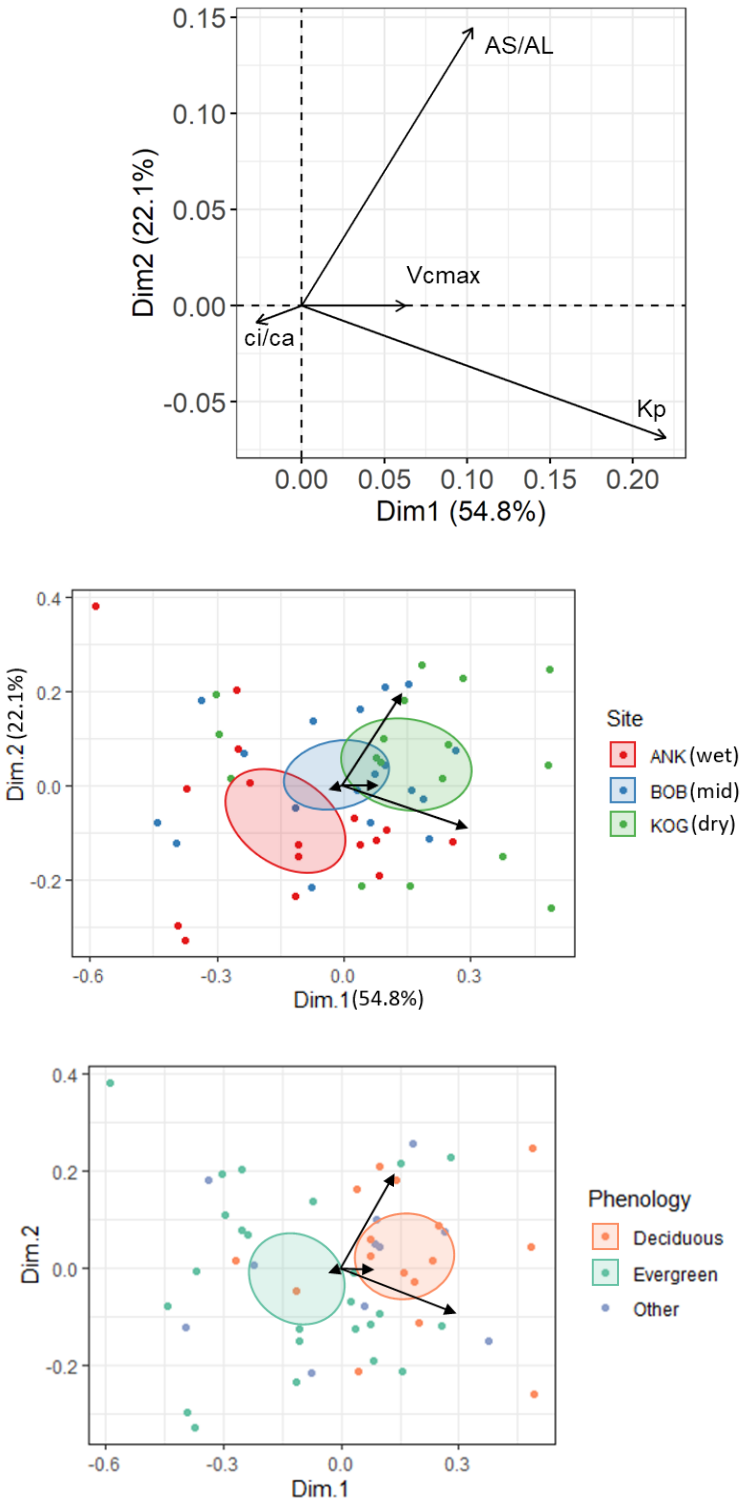


Figure 2 Principal components analysis for Huber value (A_S/A_L), the ratio between leaf internal and ambient CO_2 (c_i/c_a), Rubisco carboxylation capacity at 25 degree (Vc_{max25}) and potential specific conductivity (K_P) on species scale. Values are transformed to achieve normal distribution but not standardized to equal variance; therefore the length of arrows denotes the variance of the specific trait. The ellipses for each site are confidence ellipses around group mean points. The PCA axes in all figures are identical. Note that the three figures display the same PCA, but with a different classification of scatter points.

5.10 Appendix 1 Field sampling protocol

c_i/c_a (unitless) were estimated from leaf δ13C measurements (the stable isotope ratio relative to a standard material). We first estimated Δ13C as the difference between the leaf stable isotope ratio and the atmospheric stable isotope ratio at that place and time according to (Cornwell *et al.*, 2016). Then we estimated c_i/c_a by equation 11 in (Peng *et al.*, 2020).

Soil volumetric water content (%) was measured in the field over the depth 0–12 cm.

For LMA (m^{-2} kg^{-1}), A_{sat} (umol CO_2 m^{-2} s^{-1}) and A_{max} (umol CO_2 m^{-2} s^{-1}), see supporting information in (Oliveras *et al.*, 2020).

For P_{area} (g m^{-2}), N_{area} (g m^{-2}), N_{mass} (g/kg), P_{mass} (g/kg), R_d (umol CO_2 m^{-2} s^{-1}), J_{max25} (umol CO_2 m^{-2} s^{-1}) and Vc_{max25} (umol CO_2 m^{-2} s^{-1}), please see chapter 4 of (Gvozdevaite, 2018).

For A_S/A_L (cm^{-2} m^{-2}), twig density (g cm^{-3}), vessel density (mm^{-2}), vessel diameter (micron) and K_P (kg m^{-1} MPa^{-1} s^{-1}), H_{max} (m) please see supplementary of (Aguirre-Gutiérrez *et al.*, 2019)

For TLP (MPa), see chapter four of (Raab, 2020)

Wood density was provided by Forestplot.net who sourced information from (Zanne *et al.*, 2009). In appendix 4, we also compared data collected from Ghana with A_S/A_L from (Mencuccini *et al.*, 2019b) and vessel diameter from xylem functional traits database (Choat *et al.*, 2012).

Stem respiration per steam area (Rs_stem) was measured using a closed dynamic chamber method, from 25 trees distributed evenly throughout each plot at 1.3 m height with an IRGA (EGM-4) and soil respiration chamber (SRC-1) connected to a permanent collar, sealed to the tree bole surface. On plot scale, Rs_stem was multiplied by A_S/A_L to calculate stem respiration per leaf area (Rs_leaf).

5.11 Appendix 2 Study Sites, the aridity gradient

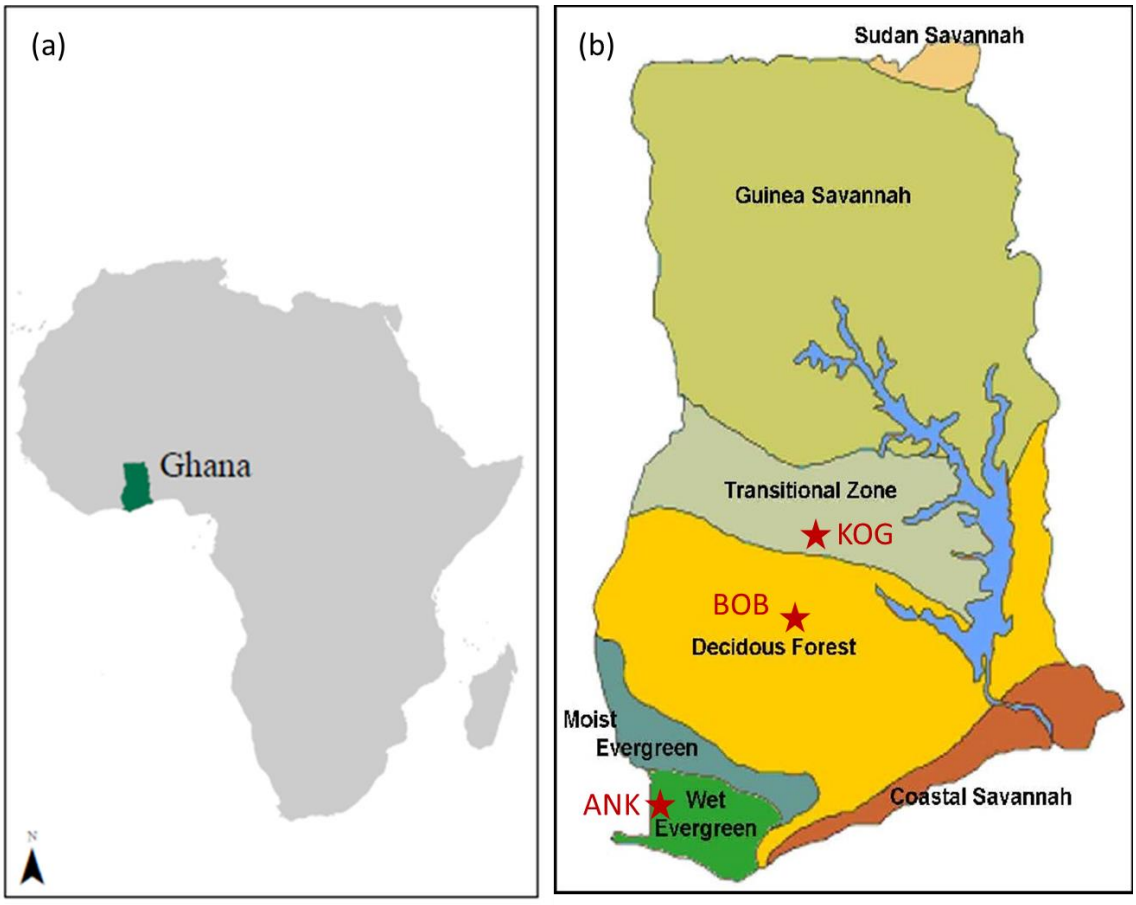


Figure S 1Map of the location of (a) Ghana within the African continent (b) and the study plots and forest types in Ghana (Appiah et al., 2014).



Figure S 2 Photo of KOG02 (dry site), KOG05(dry site), ANK03 (wet site), and BOB01 (mid site). All photos taken in January 2022 by Huanyuan Zhang-Zheng

Table S 1Summary information of plot characteristics

| | | Wet >>>>

Table S 2 Rsplash model outputs, which simulate hydrology from climate, typography and soil property. vwc_mean and vwc_sd are mean and standard deviation of soil volumetric water content (unitless fraction); Se_mean and Se_sd are the mean and standard deviation of relative soil moisture saturation (Θ) (unitless fraction); Alpha_mean and Alpha_sd are mean and standard deviation of vegetation water stress index (α) (unitless fraction); Aet is actual evapotranspiration (mm year-1); Pet is potential evapotranspiration (mm/year); ro is runoff (mm/year); cond is condensation (mm/year); MAP is mean annual precipitation (mm/year), MAT is mean annual air temperature (degree Celsius), VPD is vapor pressure deficit (kpa, annual stats); SAT: volumetric water content at saturation m^3/m^{-3}; perc: percolation or deep drainage, or vertical drainage (mm/year); FC is volumetric water content at 33kPa (field capacity) m^3/m^3; WP, volumetric water content at 1500kPa (permanent wilting point) m^3/m^3; AWC: plant available volumetric water content (FC-WP); Ksat, Saturated hydraulic conductivity (mm/hr)

Plot	**ANK-01**	**ANK-03**	**BOB-01**	**BOB-02**	**KOG-02**	**KOG-04**	**KOG-05**
Site	Ankasa	Ankasa	Bobiri	Bobiri	Kogyae	Kogyae	Kogyae
vwc_mean	0.173647	0.309652	0.288372	0.417	0.174785	0.152259	0.134706
vwc_sd	0.017241	0.085336	0.032128	0.045303	0.029734	0.02364	0.018203
Se_mean	0.379521	0.581384	0.580031	0.786519	0.3387	0.301315	0.272344
Se_sd	0.037682	0.160223	0.064623	0.085447	0.057618	0.046783	0.036803
alpha_mean	0.630998	0.583154	0.655883	0.70185	0.401261	0.366604	0.338958
alpha_sd	0.024953	0.038648	0.02599	0.005342	0.013719	0.010825	0.00929
aet	863.1792	805.3301	951.0688	1016.294	658.4057	606.0918	559.005
pet	1366.693	1378.178	1448.611	1447.996	1641.281	1654.57	1651.407
ro	0	177.2069	0	70.2051	0	0	0
cond	35.00537	32.64697	34.66683	34.9216	47.13504	44.43666	45.14205
perc	48.78369	140.6087	12.80651	156.903	272.1005	192.8297	71.75027
MAP_mean	2183.329	2183.329	1297.797	1297.797	1327.496	1327.496	1327.496
MAP_sd	548.3388	548.3388	96.80984	96.80984	91.86095	91.86095	91.86095
MAT_mean	25.02057	25.02057	26.04887	26.04887	26.75565	26.75565	26.75565
MAT_sd	0.114074	0.114074	0.320538	0.320538	0.277137	0.277137	0.277137
VPD_mean	0.099453	0.099453	0.465912	0.465912	0.756213	0.756213	0.756213
VPD_sd	0.108151	0.108151	0.290293	0.290293	0.726797	0.726797	0.726797
PET/MAP	0.625968	0.631228	1.116207	1.115734	1.236373	1.246384	1.244001
SAT	0.293072	0.517389	0.453959	0.484107	0.515887	0.505159	0.494013
FC	0.130408	0.252317	0.216695	0.276332	0.198493	0.194701	0.190016
WP	0.061419	0.103204	0.096532	0.141651	0.057346	0.059782	0.061278
AWC	0.107705	0.1535	0.1316	0.1475	0.141191	0.134961	0.128895
Ksat	87.86493	115.5978	96.32671	60.17225	205.6295	188.7933	174.9063

5.12 Appendix 3 Information associated with leaf economy

It has been shown that assimilation rate and Vc_{max25} are positively correlated with leaf nitrogen by area (N_{area}) and by dry mass (N_{mass}) (Wright *et al.*, 2004; Niinemets *et al.*, 2009; Walker *et al.*, 2014). On a site scale, N_{area} and N_{mass} tend to be higher in drier and brighter sites (Dong *et al.*, 2017, 2020). All the above suggests that N_{mass} should increase toward drier sites along the aridity gradient. Leaf phosphorus by dry mass (P_{mass}) also tends to be higher in drier sites (Maire *et al.*, 2015; Gvozdevaite *et al.*, 2018), and. it has been predicted that LMA should increase with light and aridity (Wright *et al.*, 2005; Poorter *et al.*, 2010).

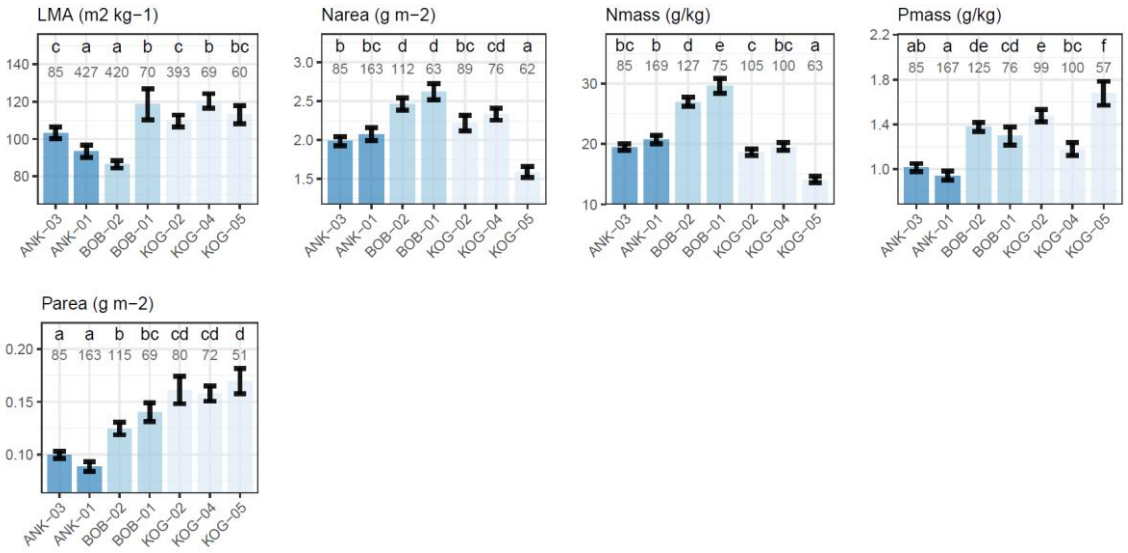


Figure S 3 Community weighted mean (with standard error) of variables associated with leaf economy from wet to dry plots. Plots were ordered from left to right according to the description in the first paragraph of results. The number denotes the number of samples, which could be a leaf, a branch or a tree etc. The letters denote significance (P<0.05) in plot-to-plot difference. These are reported and discussed in previous paper (Oliveras et al., 2020), data here are provided for completeness and for future researchers 'convenience.

5.13 Appendix 4 Report on hypothesis 15

We hypothesized that the product of K_P (specific xylem hydraulic conductivity) and A_S/A_L (sapwood to leaf area) vary less than K_P or A_S/A_L themselves, and there is a trade-off (negative correlation) between K_P and A_S/A_L. As the trade-off between K_S (well

associated with K_P) and A_S/A_L has been observed on a global scale (Mencuccini *et al.*, 2019b), here we also plot K_P versus A_S/A_L for readers' convenience in comparison with measurements from Ghana aridity gradient. We estimated K_P for species reported in (Mencuccini *et al.*, 2019b) by collecting vessel diameter and vessel density from XFT database (Choat *et al.*, 2012), with the same calculation method as K_P of Ghana aridity gradient.

For Ghana, both hypotheses were rejected, as we see a positive correlation between K_P and A_S/A_L (slope = 0.95, R-squared: 0.0598, P-value: 0.0224) and the coefficient of variance is found largest for $K_P * A_S/A_L$.

For a global dataset (Mencuccini et al., 2019), there is a negative correlation between K_P and A_S/A_L (slope =-0.638, R-squared: 0.153, P-value: <0.001) which agreed with the hypothesis but the coefficient of variance of $K_P * A_S/A_L$ is still larger than that of either K_P or A_S/A_L.

Therefore, hypothesis 15 in Table 1 is rejected in this study. The negative correlation between K_P and A_S/A_L emerge on global scale probably because of confounding effect with other environmental variables. The different patterns that emerged at different scales could also result from a Simpson's paradox. For example, the drier sites (KOG) have higher K_P, higher twig density and higher wood density than the wetter sites on site scale (Figure 2), but we also found K_P negatively correlated with twig density on species scale (Figure S5).

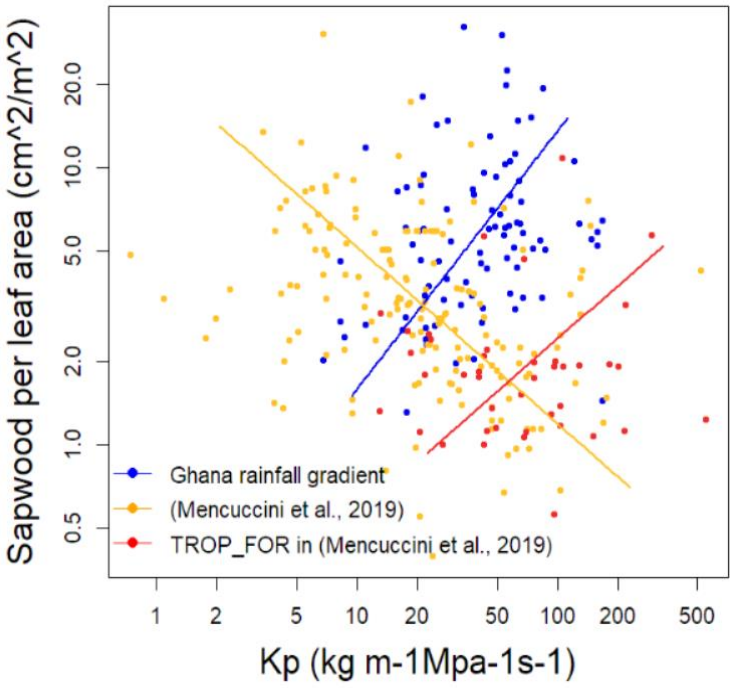


Figure S 4 The correlation between sapwood to leaf area (A_S/A_L) and potential sapwood hydraulic conductivity (K_P) for Ghana aridity gradient (ANK, BOB and KOG all together) and species included in (Mencuccini et al., 2019b). The figure was drawn on species scale (one scatter point is one species).

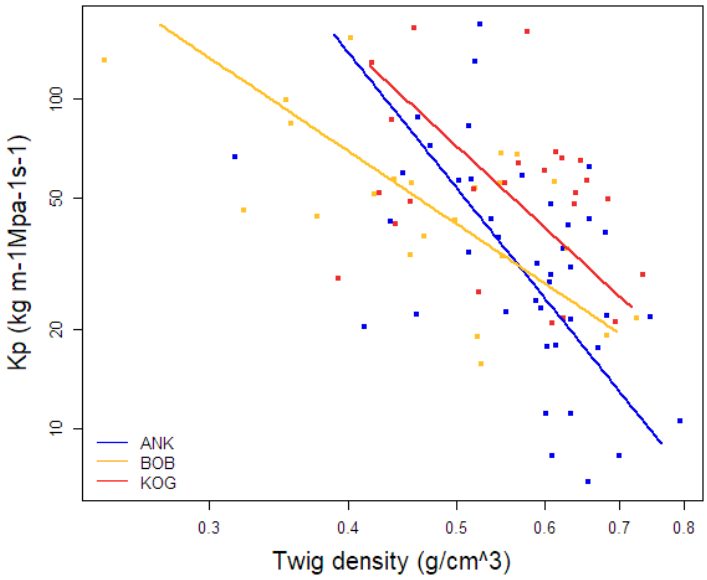


Figure S 5 The correlation between twig density (g/cm^3) and potential sapwood hydraulic conductivity (K_P) for site ANK, BOB and KOG. The figure was drawn on species scale (one scatter point is one species).

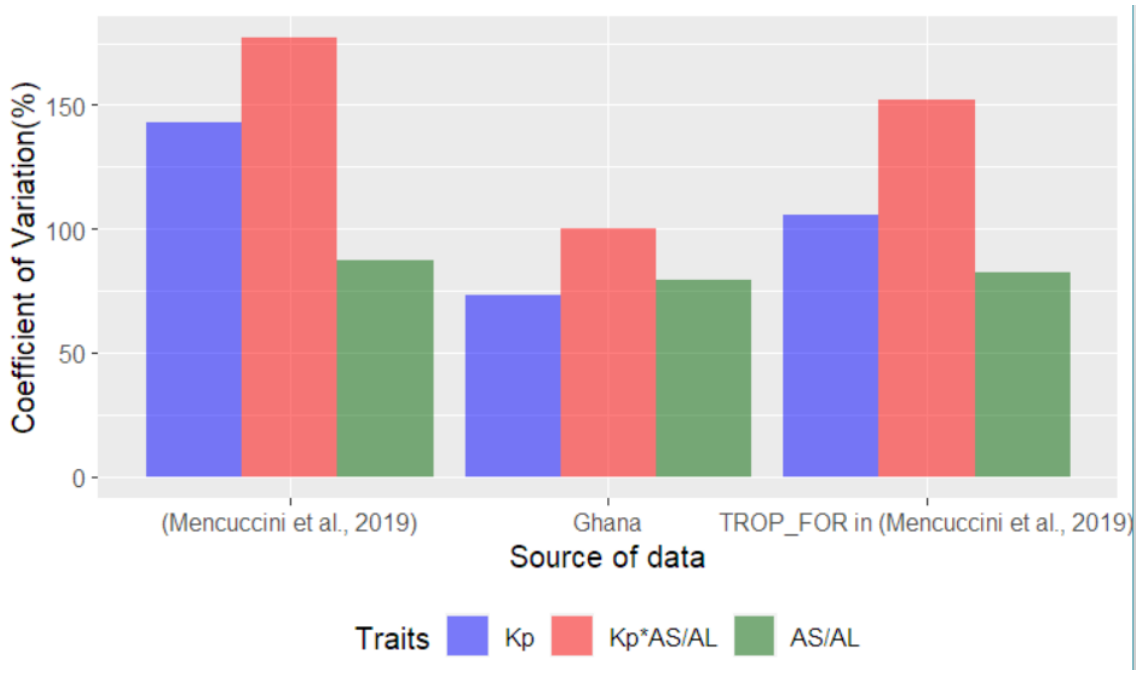


Figure S 6 Coefficient of variation (%) for data points shown in figure S6, potential sapwood hydraulic conductivity (K_P), sapwood area to leaf area (A_S/A_L) and the product of K_P and A_S/A_L

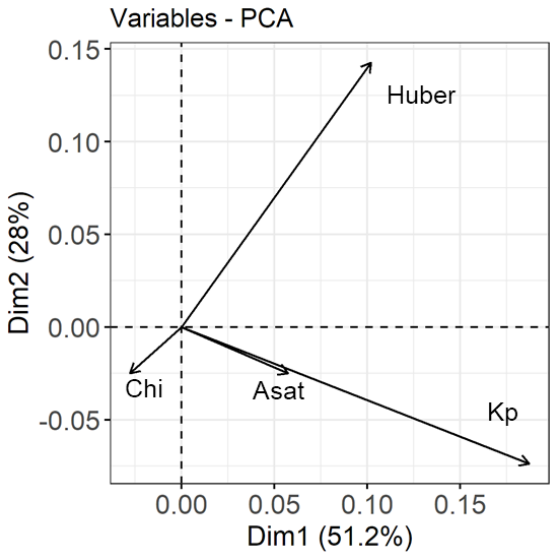




Figure S 7 Principal components analysis for A_S/A_L, c_i/c_a, A_{sat} and K_P. Please also see Figure 2

5.14 Appendix 5 Trait extrapolation and Variance partitioning

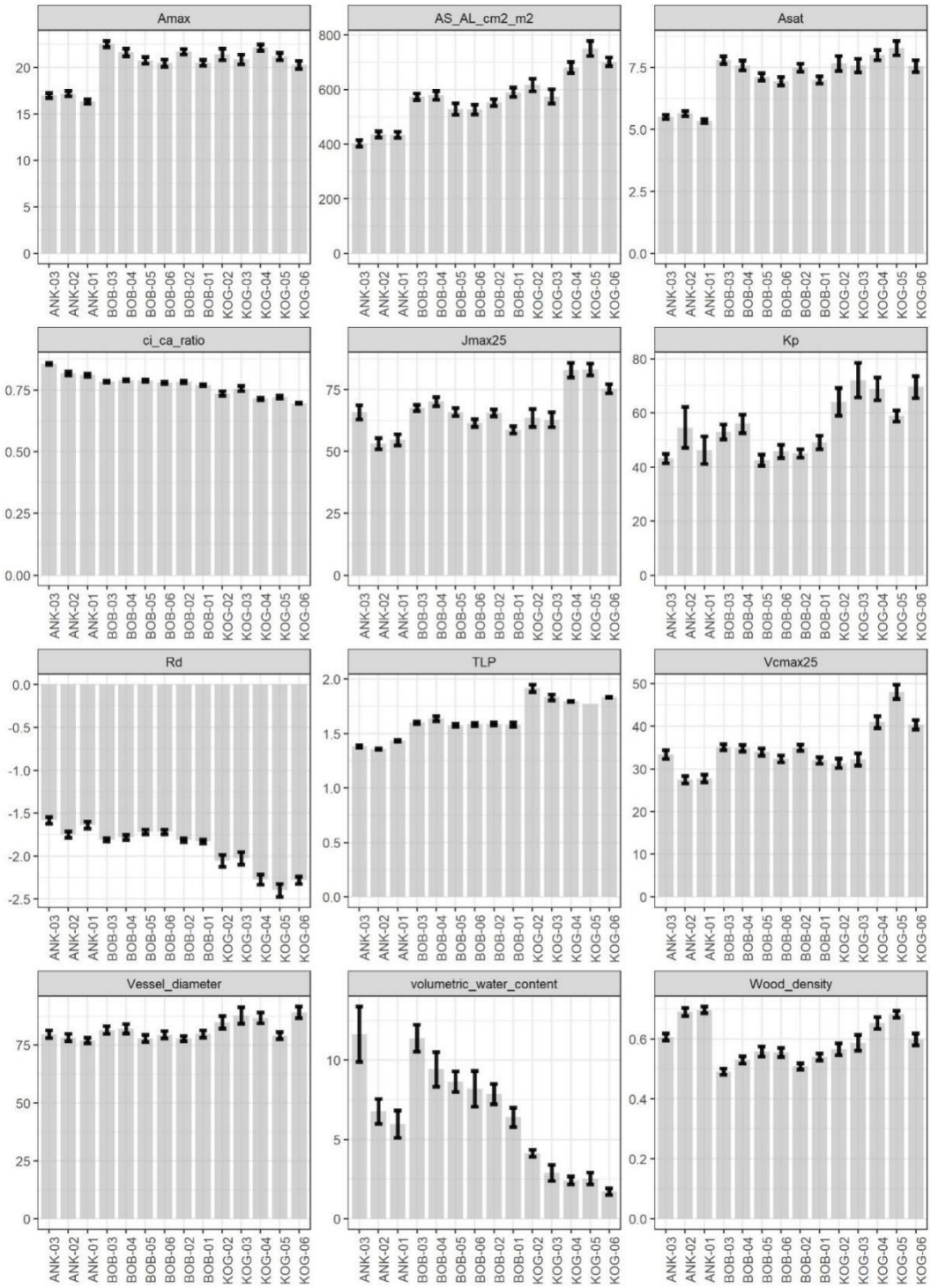
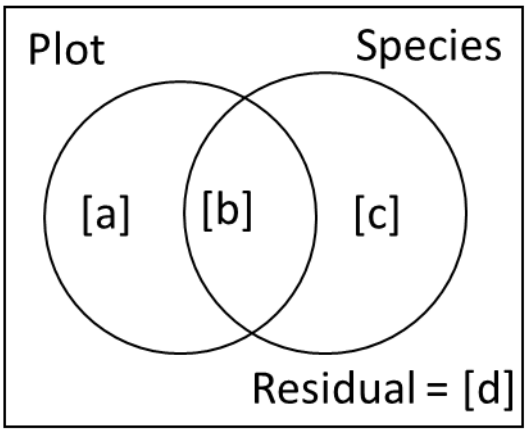


Figure S 8 Same as Figure 1 but here we extrapolate traits to more sites by assuming the same species share the same trait value, which removes intraspecific variation. The above figure tells the same story as Figure one and hence we conclude that the trait variation pattern (as summarized in Table 1) along the aridity gradient was driven by changing-species instead of intra-specific variation.

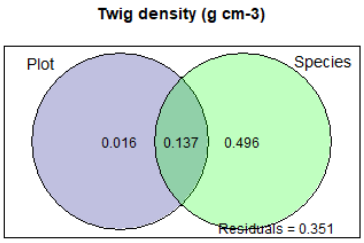


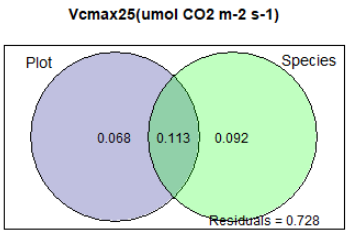
[a] Variance incurred by changing plot for the same species

[b] Variance incurred by changing plot and changing species

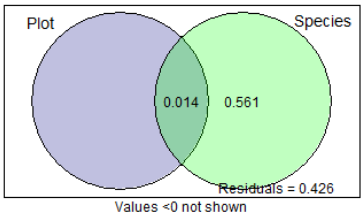
[c] Variance incurred by changing Species but not plot (inter-specific variance in a plot)

[d] Variance incurred by anything else but not changing plot and not changing species. It includes intra-specific variation (e.g., changing measurement leaves) and measurement error because for most of the traits, [d] exist only when multiple measurements were collected for one species. If the changing species induced variance [c] is larger than [d], it is safe to conclude that the variation of trait (overall in Ghana) is dominated by changing species, instead of intra-specific variation



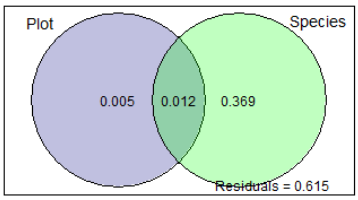


Vessel diameter (micron)

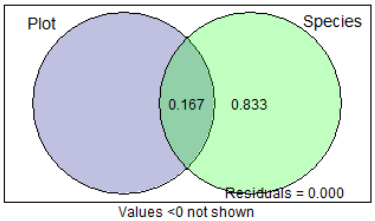


Values <0 not shown

Vessel density (mm-2)

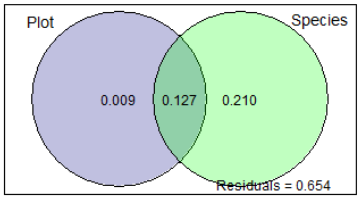


Wood density (g cm-3)

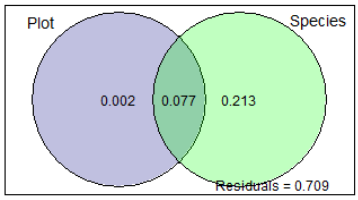


Values <0 not shown

Amax (umol CO2 m-2 s-1)



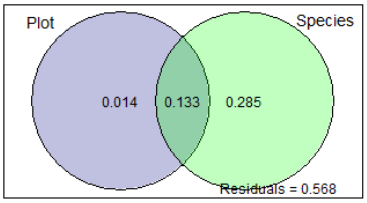
Asat (umol CO2 m-2 s-1)



ci/ca (unitless)



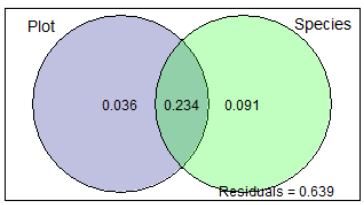
Rd (umol CO2 m-2 s-1)



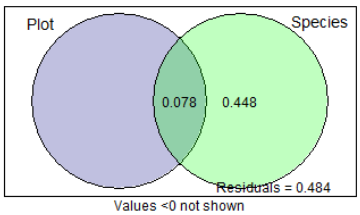
AS/AL(cm-2 m-2)



Jmax25 (umol CO2 m-2 s-1)



Kp (kg m-1 MPa-1 s-1)



Values <0 not shown

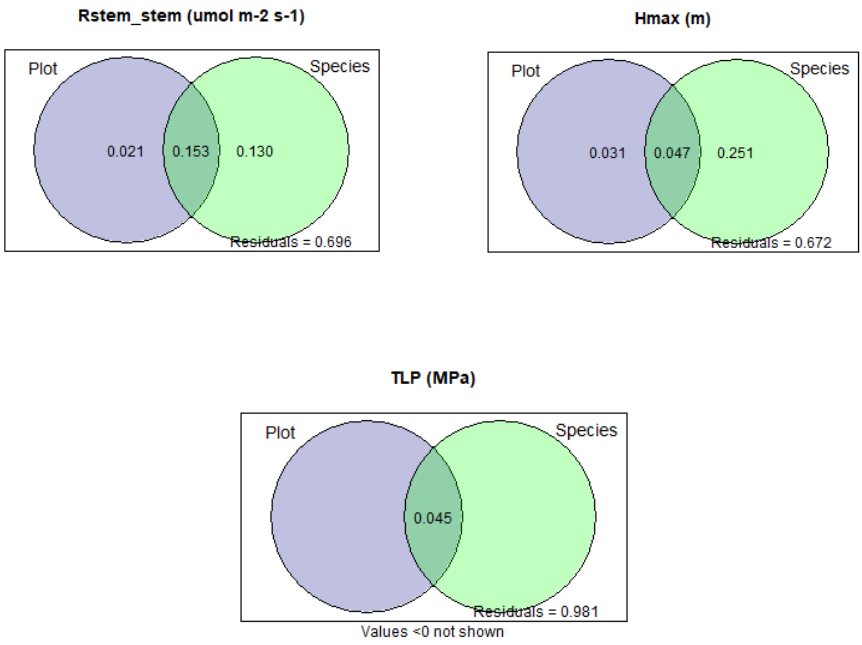


Figure S 9 Variance partitioning into plot and species. Please see table 1 for definition of traits. Meanings of each number in the circles are explained in the top panel. Note that Vc_{max25}, LMA N_{area} and P_{area} from the same plots were published in (Agne 2018), and A_{sat} A_{max} LMA, N_{mass} and P_{mass} from the same plots were published in (Oliveras et al., 2020). Values are not mathematically identical due to (1) different methods of variance partitioning and (2) one more year sampling than the previous publications.

5.15 Appendix 6 Other figures

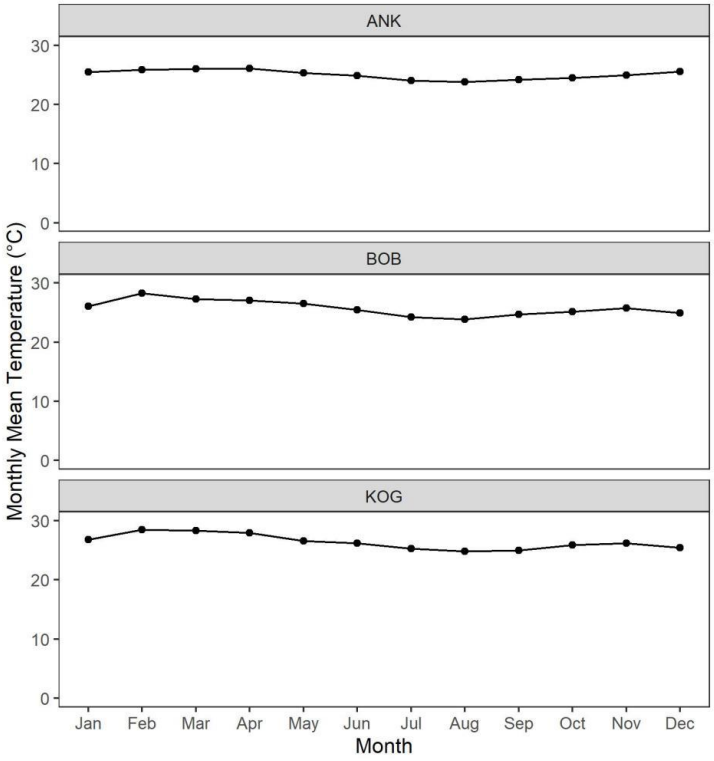


Figure S 10 Monthly mean temperature at study sites ANK (wet site), BOB (mid site) and KOG (dry site), measured by in-situ climatological stations.

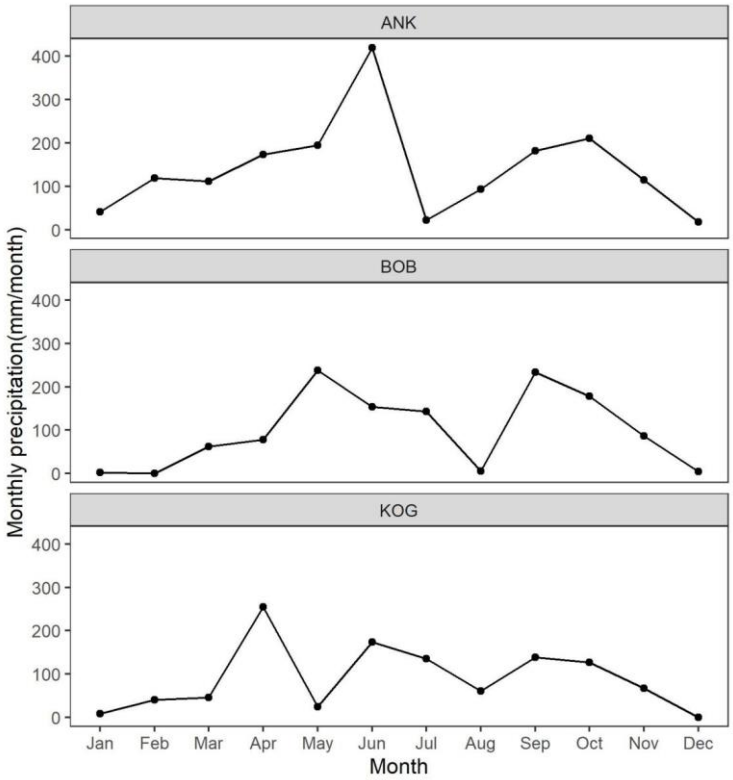


Figure S 11 Monthly precipitation (mm/month) at study sites ANK (wet site, measured in 2011), BOB (mid site, measured in 2013) and KOG (dry site, measured in 2014), measured by in-situ climatological stations.

5.16 References for paper 2

Aguirre-Gutiérrez J, Oliveras I, Rifai S, Fauset S, Adu-Bredu S, Affum-Baffoe K, Baker TR, Feldpausch TR, Gvozdevaite A, Hubau W, *et al.* 2019. Drier tropical forests are susceptible to functional changes in response to a long-term drought. *Ecology Letters* **22**: 855–865.

Appiah D, Osman B, Boafo J. **2014**. Land Use and Misuse; Human Appropriation of Land Ecosystems Services in Ghana. *International Journal of Ecosystem* **4**: 24–33.

Atkin OK, Bloomfield KJ, Reich PB, Tjoelker MG, Asner GP, Bonal D, Bönisch G, Bradford MG, Cernusak LA, Cosio EG, *et al.* 2015. Global variability in leaf respiration in relation to climate, plant functional types and leaf traits. *New Phytologist* **206**: 614–636.

Bahar NHA, Ishida FY, Weerasinghe LK, Guerrieri R, O'Sullivan OS, Bloomfield KJ, Asner GP, Martin RE, Lloyd J, Malhi Y, *et al.* 2017. Leaf-level photosynthetic capacity in lowland Amazonian and high-elevation Andean tropical moist forests of Peru. *New Phytologist* **214**: 1002–1018.

Bartlett MK, Scoffoni C, Sack L. **2012**. The determinants of leaf turgor loss point and prediction of drought tolerance of species and biomes: A global meta-analysis. *Ecology Letters* **15**.

Bauman D, Fortunel C, Delhaye G, Malhi Y, Cernusak LA, Bentley LP, Rifai SW, Aguirre-Gutiérrez J, Menor IO, Phillips OL, *et al.* 2022. Tropical tree mortality has increased with rising atmospheric water stress. *Nature*.

Beerling DJ, Quick WP. **1995**. A new technique for estimating rates of carboxylation and electron transport in leaves of C3 plants for use in dynamic global vegetation models. *Global Change Biology* **1**: 289–294.

Bittencourt PRL, Pereira L, Oliveira RS. **2016**. On xylem hydraulic efficiencies, wood space-use and the safety–efficiency tradeoff. *New Phytologist* **211**: 1152–1155.

Björkman O. **1981**. Responses to Different Quantum Flux Densities. *Physiological Plant Ecology I*: 57–107.

Brodribb TJ, Feild TS. **2000**. Stem hydraulic supply is linked to leaf photosynthetic capacity: evidence from New Caledonian and Tasmanian rainforests. *Plant, Cell & Environment* **23**: 1381–1388.

Brodribb TJ, Holbrook NM, Gutierrez M v. **2002**. Hydraulic and photosynthetic co-ordination in seasonally dry tropical forest trees. *Plant, Cell & Environment* **25**: 1435–1444.

Canadell JG, Monteiro PMS, Costa MH, Cunha LC da, Cox PM, Eliseev A v., Henson S, Ishii M, Jaccard S, Koven C, *et al.* 2021. Global carbon and other biogeochemical cycles and feedbacks. In: Climate Change 2021: The Physical Science Basis. Contribution of Working Group I to the Sixth Assessment Report of the Intergovernmental Panel on Climate Change.

Chen J-W, Zhang Q, Cao K-F. **2008**. Inter-species variation of photosynthetic and xylem hydraulic traits in the deciduous and evergreen Euphorbiaceae tree species from a seasonally tropical forest in south-western China. *Ecological Research* **24**: 65.

Chiti T, Certini G, Grieco E, Valentini R. **2010**. The role of soil in storing carbon in tropical rainforests: The case of Ankasa Park, Ghana. *Plant and Soil* **331**: 453–461.

Choat B, Ball MC, Luly JG, Holtum JAM. **2005**. Hydraulic architecture of deciduous and evergreen dry rainforest tree species from north-eastern Australia. *Trees* **19**: 305–311.

Choat B, Jansen S, Brodribb TJ, Cochard H, Delzon S, Bhaskar R, Bucci SJ, Feild TS, Gleason SM, Hacke UG, *et al.* 2012. Global convergence in the vulnerability of forests to drought. *Nature 2012 491:7426* **491**: 752–755.

Cornwell WK, Wright I, Turner J, Maire V, Barbour M, Cernusak L, Dawson T, Ellsworth D, Farquhar G, Griffiths H. 2016. A global dataset of leaf delta 13C values. *Scientific Data*.

Cunningham SC. 2005. Photosynthetic responses to vapour pressure deficit in temperate and tropical evergreen rainforest trees of Australia. *Oecologia* **142**: 521–528.

Dai Z, Edwards GE, Ku MSB. 1992. Control of photosynthesis and stomatal conductance in Ricinus communis L.(castor bean) by leaf to air vapor pressure deficit. *Plant physiology* **99**: 1426.

Domingues TF, Meir P, Feldpausch TR, Saiz G, Veenendaal EM, Schrodt F, Bird M, Djagbletey G, Hien F, Compaore H, *et al.* 2010. Co-limitation of photosynthetic capacity by nitrogen and phosphorus in West Africa woodlands. *Plant, Cell & Environment* **33**: 959–980.

Dong N, Prentice IC, Evans BJ, Caddy-Retalic S, Lowe AJ, Wright IJ, Colin Prentice I, Evans BJ, Caddy-Retalic S, Lowe AJ, *et al.* 2017. Leaf nitrogen from first principles: Field evidence for adaptive variation with climate. *Biogeosciences* **14**: 481–495.

Dong N, Prentice IC, Wright IJ, Evans BJ, Togashi HF, Caddy-Retalic S, McInerney FA, Sparrow B, Leitch E, Lowe AJ. 2020. Components of leaf-trait variation along environmental gradients. *New Phytologist* **228**: 82–94.

Franklin O, Harrison SP, Dewar R, Farrior CE, Brännström Å, Dieckmann U, Pietsch S, Falster D, Cramer W, Loreau M, *et al.* 2020. Organizing principles for vegetation dynamics. *Nature Plants* **6**: 444–453.

Fu Z, Ciais P, Prentice IC, Gentine P, Makowski D, Bastos A, Luo X, Green JK, Stoy PC, Yang H, *et al.* 2022. Atmospheric dryness reduces photosynthesis along a large range of soil water deficits. *Nature Communications 2022 13:1* **13**: 1–10.

Gleason SM, Butler DW, Waryszak P. 2013. Shifts in leaf and stem hydraulic traits across aridity gradients in eastern Australia. *International Journal of Plant Sciences* **174**: 1292–1301.

Gleason SM, Butler DW, Ziemińska K, Waryszak P, Westoby M. 2012. Stem xylem conductivity is key to plant water balance across Australian angiosperm species. *Functional Ecology* **26**: 343–352.

Gleason SM, Westoby M, Jansen S, Choat B, Hacke UG, Pratt RB, Bhaskar R, Brodribb TJ, Bucci SJ, Cao KF, *et al.* 2016. Weak tradeoff between xylem safety and xylem-specific hydraulic efficiency across the world's woody plant species. *New Phytologist* **209**: 123–136.

Granier A, Hue R, Barigah ST. 1996. Transpiration of natural rain forest and its dependence on climatic factors. *Agricultural and Forest Meteorology* **78**: 19–29.

Green JK, Berry J, Ciais P, Zhang Y, Gentine P. 2020. Amazon rainforest photosynthesis increases in response to atmospheric dryness. *Science Advances* **6**.

Grossiord C, Buckley TN, Cernusak LA, Novick KA, Poulter B, Siegwolf RTW, Sperry JS, McDowell NG. 2020a. Plant responses to rising vapor pressure deficit. *New Phytologist* **226**: 1550–1566.

Grossiord C, Ulrich DEM, Vilagrosa A. 2020b. Controls of the hydraulic safety–efficiency trade-off. *Tree Physiology* **40**: 573–576.

Gvozdevaite A. 2018. The role of economic, venation and morphological leaf traits in plant and ecosystem function along forest-savanna gradients in the tropics.

Gvozdevaite A, Oliveras I, Domingues TF, Peprah T, Boakye M, Afriyie L, da Silva Peixoto K, de Farias J, Almeida de Oliveira E, Almeida Farias CC, *et al.* 2018.

Leaf-level photosynthetic capacity dynamics in relation to soil and foliar nutrients along forest–savanna boundaries in Ghana and Brazil. *Tree Physiology* **38**: 1912–1925.

Hacke UG, Sperry JS, Pockman WT, Davis SD, McCulloh KA. **2001**. Trends in wood density and structure are linked to prevention of xylem implosion by negative pressure. *Oecologia 2000 126:4* **126**: 457–461.

Han T, Feng Q, Yu T, Yang X, Zhang X, Li K. **2022**. Characteristic of Stomatal Conductance and Optimal Stomatal Behaviour in an Arid Oasis of Northwestern China. *Sustainability 2022, Vol. 14, Page 968* **14**: 968.

Harrison SP, Cramer W, Franklin O, Prentice IC, Wang H, Brännström Å, de Boer H, Dieckmann U, Joshi J, Keenan TF, *et al.* 2021. Eco-evolutionary optimality as a means to improve vegetation and land-surface models. *New Phytologist* **231**: 2125–2141.

Hoeber S, Leuschner C, Köhler L, Arias-Aguilar D, Schuldt B. **2014**. The importance of hydraulic conductivity and wood density to growth performance in eight tree species from a tropical semi-dry climate. *Forest Ecology and Management* **330**: 126–136.

Hubau W, Lewis SL, Phillips OL, Affum-Baffoe K, Beeckman H, Cuní-Sanchez A, Daniels AK, Ewango CEN, Fauset S, Mukinzi JM. **2020**. Asynchronous carbon sink saturation in African and Amazonian tropical forests. *Nature* **579**: 80–87.

Liu H, Gleason SM, Hao G, Hua L, He P, Goldstein G, Ye Q. **2019**. Hydraulic traits are coordinated with maximum plant height at the global scale. *Science Advances* **5**: eaav1332.

Liu L, Gudmundsson L, Hauser M, Qin D, Li S, Seneviratne SI. **2020**. Soil moisture dominates dryness stress on ecosystem production globally. *Nature Communications* **11**: 4892.

Liu H, Ye Q, Gleason SM, He P, Yin D. **2021**. Weak tradeoff between xylem hydraulic efficiency and safety: climatic seasonality matters. *New Phytologist* **229**: 1440–1452.

Long SP, Woolhouse HW. **1978**. The responses of net photosynthesis to vapour pressure deficit and CO_2 concentration in Spartina townsendii (sensu lato), a C4 species from a cool temperate climate. *Journal of Experimental Botany* **29**: 567–577.

López R, Cano FJ, Martin-Stpaul NK, Cochard H, Choat B. **2021**. Coordination of stem and leaf traits define different strategies to regulate water loss and tolerance ranges to aridity. *New Phytologist* **230**: 497–509.

Maire V, Martre P, Kattge J, Gastal F, Esser G, Fontaine S, Soussana J-F. **2012**. The coordination of leaf photosynthesis links C and N fluxes in C3 plant species. *PloS one* **7**: e38345.

Maire V, Wright IJ, Prentice IC, Batjes NH, Bhaskar R, van Bodegom PM, Cornwell WK, Ellsworth D, Niinemets Ü, Ordonez A. **2015**. Global effects of soil and climate on leaf photosynthetic traits and rates. *Global Ecology and Biogeography* **24**: 706–717.

Malhi Y, Girardin C, Metcalfe DB, Doughty CE, Aragão LEOC, Rifai SW, Oliveras I, Shenkin A, Aguirre-Gutiérrez J, Dahlsjö CAL, *et al.* 2021. The Global Ecosystems Monitoring network: Monitoring ecosystem productivity and carbon cycling across the tropics. *Biological Conservation* **253**: 108889.

Manzoni S, Vico G, Katul G, Palmroth S, Jackson RB, Porporato A. **2013**. Hydraulic limits on maximum plant transpiration and the emergence of the safety–efficiency trade-off. *New Phytologist* **198**: 169–178.

Martínez-Vilalta J, Cochard H, Mencuccini M, Sterck F, Herrero A, Korhonen JFJ, Llorens P, Nikinmaa E, Nolè A, Poyatos R, *et al.* 2009. Hydraulic adjustment of Scots pine across Europe. *The New phytologist* **184**: 353–364.

Medlyn BE, Duursma RA, Eamus D, Ellsworth DS, Prentice IC, Barton CVM, Crous KY, de Angelis P, Freeman M, Wingate L. **2011**. Reconciling the optimal and

empirical approaches to modelling stomatal conductance. *Global Change Biology* **17**: 2134–2144.

Mencuccini M, Manzoni S, Christoffersen B. **2019a**. Modelling water fluxes in plants: from tissues to biosphere. *New Phytologist* **222**: 1207–1222.

Mencuccini M, Rosas T, Rowland L, Choat B, Cornelissen H, Jansen S, Kramer K, Lapenis A, Manzoni S, Niinemets Ü, *et al.* 2019b. Leaf economics and plant hydraulics drive leaf : wood area ratios. *New Phytologist* **224**: 1544–1556.

Moore S, Adu-Bredu S, Duah-Gyamfi A, Addo-Danso SD, Ibrahim F, Mbou AT, de Grandcourt A, Valentini R, Nicolini G, Djagbletey G, *et al.* 2018. Forest biomass, productivity and carbon cycling along a rainfall gradient in West Africa. *Global Change Biology* **24**: e496–e510.

Neelin JD, Münnich M, Su H, Meyerson JE, Holloway CE. **2006**. Tropical drying trends in global warming models and observations. *Proceedings of the National Academy of Sciences* **103**: 6110–6115.

Niinemets Ü, Wright IJ, Evans JR. **2009**. Leaf mesophyll diffusion conductance in 35 Australian sclerophylls covering a broad range of foliage structural and physiological variation. *Journal of Experimental Botany* **60**: 2433–2449.

Ögren E. **1993**. Convexity of the Photosynthetic Light-Response Curve in Relation to Intensity and Direction of Light during Growth. *Plant physiology* **101**: 1013–1019.

Oliveras I, Bentley L, Fyllas NM, Gvozdevaite A, Shenkin AF, Peprah T, Morandi P, Peixoto KS, Boakye M, Adu-Bredu S, *et al.* 2020. The Influence of Taxonomy and Environment on Leaf Trait Variation Along Tropical Abiotic Gradients. *Frontiers in Forests and Global Change* **3**: 18.

Olson ME, Anfodillo T, Rosell JA, Petit G, Crivellaro A, Isnard S, León-Gómez C, Alvarado-Cárdenas LO, Castorena M. **2014**. Universal hydraulics of the flowering plants: vessel diameter scales with stem length across angiosperm lineages, habits and climates. *Ecology Letters* **17**: 988–997.

Olson ME, Rosell JA. **2013**. Vessel diameter–stem diameter scaling across woody angiosperms and the ecological causes of xylem vessel diameter variation. *New Phytologist* **197**: 1204–1213.

Peng Y, Bloomfield KJ, Cernusak LA, Domingues TF, Colin Prentice I. **2021**. Global climate and nutrient controls of photosynthetic capacity. *Communications Biology 2021 4:1* **4**: 1–9.

Peng Y, Bloomfield KJ, Prentice IC. **2020**. A theory of plant function helps to explain leaf-trait and productivity responses to elevation. *New Phytologist* **226**: 1274–1284.

Pfautsch S, Harbusch M, Wesolowski A, Smith R, Macfarlane C, Tjoelker MG, Reich PB, Adams MA. **2016**. Climate determines vascular traits in the ecologically diverse genus Eucalyptus. *Ecology Letters* **19**: 240–248.

Poorter L, McDonald I, Alarcón A, Fichtler E, Licona JC, Peña-Claros M, Sterck F, Villegas Z, Sass-Klaassen U. **2010**. The importance of wood traits and hydraulic conductance for the performance and life history strategies of 42 rainforest tree species. *New Phytologist*.

Prentice IC, Dong N, Gleason SM, Maire V, Wright IJ. **2014**. Balancing the costs of carbon gain and water transport: testing a new theoretical framework for plant functional ecology. *Ecology Letters* **17**: 82–91.

Pritzkow C, Williamson V, Szota C, Trouvé R, Arndt SK. **2020**. Phenotypic plasticity and genetic adaptation of functional traits influences intra-specific variation in hydraulic efficiency and safety. *Tree Physiology* **40**: 215–229.

Quesada CA, Lloyd J, Schwarz M, Patiño S, Baker TR, Czimczik C, Fyllas NM, Martinelli L, Nardoto GB, Schmerler J, *et al.* 2010. Variations in chemical and physical properties of Amazon forest soils in relation to their genesis. *Biogeosciences* **7**.

Raab N. 2020. Non-structural carbohydrates and leaf ecophysiology in tropical and temperate forests.

Restrepo-Coupe N, da Rocha HR, Hutyra LR, da Araujo AC, Borma LS, Christoffersen B, Cabral OMR, de Camargo PB, Cardoso FL, da Costa ACL, *et al.* 2013. What drives the seasonality of photosynthesis across the Amazon basin? A cross-site analysis of eddy flux tower measurements from the Brasil flux network. *Agricultural and Forest Meteorology* **182–183**: 128–144.

Rogers A, Medlyn BE, Dukes JS, Bonan G, von Caemmerer S, Dietze MC, Kattge J, Leakey ADB, Mercado LM, Niinemets Ü, *et al.* 2017. A roadmap for improving the representation of photosynthesis in Earth system models. *New Phytologist* **213**: 22–42.

Ryan MG, Yoder BJ. 1997. Hydraulic Limits to Tree Height and Tree Growth. *BioScience* **47**.

Sandoval D, Prentice IC. 2020. Simple process-led algorithms for simulating habitats (SPLASH v.2.0): robust calculations of water and energy fluxes in complex terrain. *EGU General Assembly 2020* .

Santiago LS, Goldstein G, Meinzer FC, Fisher JB, Machado K, Woodruff D, Jones T. 2004. Leaf photosynthetic traits scale with hydraulic conductivity and wood density in Panamanian forest canopy trees. *Oecologia* **140**: 543–550.

Schuldt B, Leuschner C, Brock N, Horna V. 2013. Changes in wood density, wood anatomy and hydraulic properties of the xylem along the root-to-shoot flow path in tropical rainforest trees. *Tree physiology* **33**: 161–174.

Smith NG, Keenan TF, Prentice IC, Wang H, Wright IJ, Niinemets U, Crous KY, Domingues TF, Guerrieri R, Ishida FY, *et al.* 2019. Global photosynthetic capacity is optimized to the environment.

Sperry JS, Hacke UG, Oren R, Comstock JP. 2002. Water deficits and hydraulic limits to leaf water supply. *Plant, Cell & Environment* **25**: 251–263.

Stangl ZR, Tarvainen L, Wallin G, Ubierna N, Räntfors M, Marshall JD. 2019. Diurnal variation in mesophyll conductance and its influence on modelled water-use efficiency in a mature boreal Pinus sylvestris stand. *Photosynthesis Research* **141**: 53–63.

Stocker BD, Wang H, Smith NG, Harrison SP, Keenan TF, Sandoval D, Davis T, Prentice IC. 2020. P-model v1.0: An optimality-based light use efficiency model for simulating ecosystem gross primary production. *Geoscientific Model Development* **13**: 1545–1581.

Togashi HF, Prentice IC, Evans BJ, Forrester DI, Drake P, Feikema P, Brooksbank K, Eamus D, Taylor D. 2015. Morphological and moisture availability controls of the leaf area-to-sapwood area ratio: analysis of measurements on A ustralian trees. *Ecology and Evolution* **5**: 1263–1270.

Walker AP, Beckerman AP, Gu L, Kattge J, Cernusak LA, Domingues TF, Scales JC, Wohlfahrt G, Wullschleger SD, Woodward FI. 2014. The relationship of leaf photosynthetic traits – Vc_{max} and J_{max} – to leaf nitrogen, leaf phosphorus, and specific leaf area: a meta-analysis and modeling study. *Ecology and Evolution* **4**: 3218–3235.

Wang H, Prentice IC, Davis TW, Keenan TF, Wright IJ, Peng C. 2017a. Photosynthetic responses to altitude: an explanation based on optimality principles. *New Phytologist* **213**: 976–982.

Wang H, Prentice IC, Keenan TF, Davis TW, Wright IJ, Cornwell WK, Evans BJ, Peng C. 2017b. Towards a universal model for carbon dioxide uptake by plants. *Nature Plants 2017 3:9* **3**: 734–741.

Warton DI, Duursma RA, Falster DS, Taskinen S. **2012**. smatr 3-an R package for estimation and inference about allometric lines. *Methods in ecology and evolution* **3**: 257–259.

Wright IJ, Reich PB, Cornelissen JHC, Falster DS, Groom PK, Hikosaka K, Lee W, Lusk CH, Niinemets Ü, Oleksyn J. **2005**. Modulation of leaf economic traits and trait relationships by climate. *Global Ecology and Biogeography* **14**: 411–421.

Wright IJ, Reich PB, Westoby M. **2001**. Strategy shifts in leaf physiology, structure and nutrient content between species of high- and low-rainfall and high- and low-nutrient habitats. *Functional Ecology* **15**: 423–434.

Wright IJ, Reich PB, Westoby M. **2003**. Least-cost input mixtures of water and nitrogen for photosynthesis. *The American naturalist* **161**: 98–111.

Wright IJ, Reich PB, Westoby M, Ackerly DD, Baruch Z, Bongers F, Cavender-Bares J, Chapin T, Cornellssen JHC, Diemer M, *et al.* 2004. The worldwide leaf economics spectrum. *Nature 2004 428:6985* **428**: 821–827.

Wu J, Serbin SP, Ely KS, Wolfe BT, Dickman LT, Grossiord C, Michaletz ST, Collins AD, Detto M, McDowell NG, *et al.* 2020. The response of stomatal conductance to seasonal drought in tropical forests. *Global Change Biology* **26**: 823–839.

Xu H, Wang H, Prentice IC, Harrison SP, Wright IJ. **2021**. Coordination of plant hydraulic and photosynthetic traits: confronting optimality theory with field measurements. *New Phytologist* **232**: 1286–1296.

Yamazaki D, Ikeshima D, Sosa J, Bates PD, Allen GH, Pavelsky TM. **2019**. MERIT Hydro: A high-resolution global hydrography map based on latest topography dataset. *Water Resources Research* **55**: 5053–5073.

Yang J, He Y, Aubrey DP, Zhuang Q, Teskey RO. **2016**. Global patterns and predictors of stem CO_2 efflux in forest ecosystems. *Global Change Biology* **22**: 1433–1444.

Yang Y, Wang H, Harrison SP, Prentice IC, Wright IJ, Peng C, Lin G. **2019**. Quantifying leaf-trait covariation and its controls across climates and biomes. *New Phytologist* **221**: 155–168.

Zanne AE, Lopez-Gonzalez G, Coomes DA, Ilic J, Jansen S, Lewis SL, Miller RB, Swenson NG, Wiemann MC, Chave J. **2009**. Data from: Towards a worldwide wood economics spectrum.

6 PAPER 3

WHY MODELS UNDERESTIMATE TROPICAL FOREST PRODUCTIVITY: A CASE STUDY IN WEST AFRICA

"I prefer this research plan, because it is simpler."

Prof. Iain Colin Prentice

(Ecologist at Imperial College London)



A tree in Bobiri forest is sprouting while shedding, Credit: Huanyuan Zhang-Zheng

6.1 Preface

Paper 1 observed exceptionally high GPP at West African forests (higher than Amazonia) and reveal that West African forest GPP has been underestimated in many global GPP products or models. Thus, the aim of **Paper 3 is to investigate the cause of GPP data-model discrepancy**. As models are designed based on current ecological theory (Franklin *et al.*, 2020), a large discrepancy signals a lack of physiological explanation for the high productivity of West African forests. Although **Paper 2** qualitatively explains photosynthetic strategies along the aridity gradient, it is not known whether the in situ GPP is quantitatively consistent with field measured photosynthetic traits and other forests properties. Therefore, along with the investigation into the GPP data-model discrepancy (the first research aim), Paper 3 joins observed GPP (Paper 1) and plant traits (Paper 2) to explain that the high GPP is consistent with leaf photosynthetic traits and other forest in situ measurements (the second research aim).

6.1.1 The significance of the paper

The estimation of GPP is an important "first step" in many carbon cycling models. The paper highlights the necessity, and more importantly, approaches to better represent the GPP of African tropical forests. The paper also makes methodological advances by demonstrating consistency between observed GPP and recalculated GPP based on field-measured photosynthetic traits and fAPAR. By showing that West African forests are very productive but have been previously overlooked, the study calls for urgent conservation as the forests are highly fragmented and still suffer from tree loss.

6.1.2 Author contributions

I proposed the prototype of this study in my DPhil application materials. The proposed study was the first of three modelling papers back then (the other two are now sitting in 6.3 Future works). However, I realized later that there were two other important

empirical papers to write before this study became possible. The final study design has benefited greatly from the suggestions of I.C.P. and Y.M. With the help of B.S. and E.T., I informed P-model with field-measured photosynthetic traits. The most exciting step in this paper was finding consistency between traits and GPP, which were independently measured in the field. This consistency reinforces the reliability of both datasets (and clears my self-doubt from the previous two papers). With X.D.'s help, I retrieved GPP data from MODIS, FLUXCOM, and TRENDY.

The manuscript is now ready to be submitted to *Global Change Biology*, but I am waiting for paper 1 (the background of paper 3) to be submitted.

6.1.3 Specific author contributions:

H.Z., I.C.P., Y.M., conceived the study. S.A.B., A.D., A.G., S.M., I.O. collected field data. R.D., E.T., B.S., H.Z. did the modelling works. H.Z., X.D. carried out data analysis. H.Z. wrote the paper with inputs and revisions from all co-authors.

WHY MODELS UNDERESTIMATE TROPICAL FOREST PRODUCTIVITY: A CASE STUDY IN WEST AFRICA

Huanyuan Zhang-Zheng1, Yadvinder Malhi1, Ruijie Ding 5, Xiongjie Deng1, Eleanor Thomson 1, Benjamin Stocker 3, Stephen Adu Bredu4, Akwasi Duah-Gyamfi4, Agne Gvozdevaite1, Sam Moore 1, Imma Oliveras Menor 1,2, Colin Prentice 5

1 Environmental Change Institute, School of Geography and the Environment, University of Oxford, Oxford, United Kingdom,

2 AMAP (Botanique et Modelisation de l'Architecture des Plantes et des Végétations), CIRAD, CNRS, INRA, IRD,Université de Montpellier, Montpellier, France

3 Institute of Geography, University of Bern, Hallerstrasse 12, 3012 Bern, Switzerland

4 Forestry Research Institute of Ghana, Council for Scientific and Industrial Research, Kumasi, Ghana

5 Georgina Mace Centre for the Living Planet, Department of Life Sciences, Imperial College London, Silwood Park Campus, Buckhurst Road, Ascot, SL5 7PY, UK

6.2 Abstract

Current models for gross primary production (GPP) suggest that forests in tropical West Africa are far less productive than those in lowland Amazonia. However, recent field observations show that West African forests have among the highest tropical forest productivity yet observed. We explore possible reasons for this data-model mismatch. *In situ* GPP measurements are compared to multiple global GPP models at three forest sites in Ghana, West-Africa. The underestimation of GPP largely disappears when the Farquhar–

von Caemmerer–Berry model is informed by field-measured values of (a) fractional absorbed photosynthetic radiation (fAPAR), and (b) photosynthetic traits, which are shown to be consistent with values predicted from the light environments and climates of the sites using optimality principles. Satellites systematically underestimate fAPAR due to extreme cloud cover in the wet season. The forest sites lie within a matrix dominated by croplands; but most models correctly predict the surrounding agricultural lands to be as productive as the forests, so the problem is not caused by the failure of coarse-resolution models to resolve small forest patches. An exception however is MODIS, which assigns unrealistically low GPP to agricultural lands, and could severely underestimate the region's GPP. The study highlights the underestimation of tropical forests GPP and hints at the area for model improvement.

Keywords: MODIS; carbon model; Tropical forests; Gross primary production; fAPAR; light use efficiency; photosynthetic traits

6.3 Introduction

Carbon exchanges between terrestrial ecosystems, especially tropical forests, and the atmosphere are a major element of the global carbon cycle. As the world's most productive terrestrial ecosystems (Grace *et al.*, 2001), tropical forests have been estimated to account for around 44% of global forest biomass and 43% of global gross primary production (GPP) (Pan *et al.*, 2011; Liu *et al.*, 2015). Nonetheless, confidence in estimates of tropical forest productivity remains low (Ciais *et al.*, 2014, p. 499; Pugh *et al.*, 2018). There is still a large variation among models regarding the magnitude and spatial pattern of tropical GPP (Jung *et al.*, 2011; Anav *et al.*, 2015; Yang *et al.*, 2022). Multiple global-scale forest GPP studies have indicated that the largest uncertainty applies to tropical forests (Bonan *et al.*, 2011; Frankenberg *et al.*, 2011; Chen *et al.*, 2017; Badgley *et al.*, 2019). This is likely

an inevitable consequence of the paucity of carbon cycling data in the tropics relative to temperate regions (Hickler *et al.*, 2008; Wood, Cavaleri and Reed, 2012; Babst *et al.*, 2021; Zhang and Ye, 2021). For instance, many previous studies found particularly large GPP data-model discrepancy for tropical forests between flux towers and models (or satellite GPP products) (Joiner *et al.*, 2018; Zhang and Ye, 2021; Tian *et al.*, 2023), but investigation into the cause of discrepancy was not attempted due to the lack of in-situ auxiliary measurements of plant traits and forest characteristics (Seiler *et al.*, 2022). Large unresolved data-model discrepancy suggests fundamental challenges in our understanding of tropical forest productivity and its geography.

The uncertainty in estimates of tropical forest productivity is particularly large in West Africa (Ardö, 2015). The first in-situ quantification of GPP in West African forests, conducted recently, yielded the highest GPP value recorded anywhere – surpassing values measured in Amazonia (Paper 1 of this thesis). However, this high GPP is underestimated by about 60% in both the MODIS and FLUXCOM products (Paper 1 of this thesis). As models are designed based on current ecological theory (Franklin *et al.*, 2020), such a large discrepancy signals a lack of physiological explanation for the high productivity. Here we set out to investigate the possible reasons behind the GPP data-model discrepancy which also explains the high productivity, with a view to provide information that could be used to improve the models currently used to assess primary production in forests.

The investigation is conducted in three steps. (1) We first thoroughly compare forest inventory-based GPP to multiple models and satellite-based products, to quantify the data-model discrepancy. (2) Then, before the cause of data-model discrepancy could be examined, we investigate whether the high productivity was also reflected in leaf photosynthetic traits and other field measurements. The investigation was made possible by extensive field measurements of environmental variables, plant traits, and carbon fluxes at the same sites (Gvozdevaite *et al.*, 2018; Moore *et al.*, 2018; Oliveras *et al.*, 2020). (3)

Finally, we investigated the data-model discrepancy in the West-African region by substituting model inputs (or parameters) with field measurements according to hypotheses explained below (see also Method and Table 1). Using study sites in Ghana West Africa as an example, the study not only identifies key areas for model improvement but also provides an ecological explanation for the remarkably high GPP observed in the field.

Most vegetation models estimate GPP using key inputs including photosynthetic photon flux density (PPFD, or shortwave radiation), light use efficiency (LUE, or equivalently photosynthetic capacity), fraction of absorbed photosynthetically active radiation (fAPAR, or leaf area index), and plant functional types (PFTs) prescription (see also Equation 1). Therefore, for the cause of data-model discrepancy (Objective 3). We hypothesize that the large data-model discrepancy for GPP could stem from key input variables: (1) incorrect LUE; (2) incorrect fAPAR; or (3) confusion between forest and crop functional types. Multiple experiments are designed to test each hypothesis (Table 1).

6.4 Methods

6.4.1 Analysis for objective 1: Compare forest inventory-based GPP to models' GPP (Figure 2)

We compared in-situ measurements of GPP with values estimated by the TRENDY ensemble of dynamic global vegetation models (DGVMs) (Friedlingstein et al., 2019), and two data-driven models, FLUXCOM (Jung et al., 2019) and MODIS (Running, Mu and Zhao, 2015), and an optimality-based model (P-model v1.0). There are many other GPP products (see a list at (Zhang and Ye, 2021)). The above choices are the most extensively used representative from each method category.

The TRENDY ensemble is a collection of 15 models which calculate functional aspects of vegetation, including fAPAR or leaf area index (LAI) which determines light absorption, from environmental variables, without using any remotely sensed data as input.

Most of these models calculate leaf-level photosynthesis via the Farquhar-von Caemmerer-Berry (FvCB) photosynthesis model (Farquhar, von Caemmerer and Berry, 1980), which requires specification of traits that vary greatly in space and time: the maximum carboxylation rate (Vc_{max}), the maximum electron transport rate (J_{max}), and parameters of one or other of the semi-empirical schemes that are commonly used to estimate stomatal conductance (g_s) (Rogers *et al.*, 2017). Leaf-level photosynthesis is scaled up to the canopy, and thus to GPP, by methods that vary in complexity – but all depend on the modelled LAI or fAPAR.

FLUXCOM and MODIS, by contrast, are data-driven models that do not depend on the FvCB model. FLUXCOM GPP is a machine learning application based on eddy-covariance estimates of GPP at worldwide flux towers as the key input, with environmental covariates that include satellite-based fAPAR, and PPFD.

MODIS GPP (Running, Mu and Zhao, 2015) is a light use efficiency model (Hilker *et al.*, 2008; Sun *et al.*, 2014) that it calculates GPP as follows:

$$GPP = fAPAR \times LUE \times PPFD \quad (1)$$

where PPFD is photosynthetic photon flux density, commonly calculated from shortwave radiation; and LUE is the light use efficiency. The MODIS GPP algorithm calculates LUE as a prescribed (per biome) maximum light use efficiency, multiplied by reduction factors that are defined *a priori* as biome-specific functions of temperature and vapour pressure deficit.

The P-model, uniquely, is a LUE model (also using Equation 1) but it calculates LUE based on the FvCB model, using optimality principles (Harrison *et al.*, 2021) to determine the spatial and temporal variation in Vc_{max}, J_{max} and the ratio (ci/ca) of leaf-internal to ambient CO_2 (Stocker *et al.*, 2020). ci/ca results from the combined effects of photosynthetic rate and stomatal conductance, which are co-regulated by plants. Leaf-level photosynthesis is scaled up to the canopy with the help of the big-leaf approximation

(Friend, 2001) and driven by satellite fAPAR data. The P-model thus combines the mechanistic basis of photosynthesis as represented in DGVMs with the simplicity of LUE models. The P-model also dispenses with the need to consider plant functional type (PFT) or biome distinctions (apart from the difference between C_3 and C_4 plants); the differences in photosynthetic traits among C_3 PFTs are implicitly predicted as a consequence of their habitat preferences alone. The validity of these predictions has been supported by global-scale comparisons (H. Wang, Prentice, Keenan, *et al.*, 2017; Smith *et al.*, 2019; Peng *et al.*, 2021).

6.4.2 Analysis for objective 2: consistency between the in-situ GPP, and other in-situ measurements

Before investigating the cause of GPP data-model discrepancy, it is necessary to first investigate whether in-situ GPP could be reproduced by FvCB model (within P-model) informed by fully field-measured inputs – PPFD, fAPAR and LUE (derived from measurements of ci/ca, A_{sat}, A_{max}). The above GPP experiment was called 'P-model_PfL'. A match would indicate consistency between the independent field measurements of traits and the in-situ measured GPP.

If a match is found between P-model_PfL GPP and in-situ GPP, we could further investigate the cause of GPP data-model discrepancy by designing more experiments using P-model with different inputs (see below and Table 1). The difference between P-model_PfL and in-situ GPP is labelled as the **'unresolved discrepancy'** in Figure 3**.**

6.4.3 Analysis for objective 3: Cause of GPP data-model discrepancy

Following equation 1 (also see Introduction), we hypothesize that the large data-model discrepancy for GPP could stem from: (1) incorrect LUE and/or PPFD; (2) incorrect fAPAR; or (3) confusion between forest and crop functional types.

The following explanation is illustrated in Table 1.

To test hypothesis 1 (incorrect LUE and/or PPFD explains the mismatch), we used P-model to predict photosynthetic capacity (Vc_{max}, J_{max}) and LUE using optimality theory based on climate variables alone. P-model then calculates a 'P-model_Pf' GPP using the above optimality-based predictions, combined with field-measured PPFD and fAPAR. As the only difference between ' P-model_Pf' and 'P-model_PfL' GPP is in light use efficiency (optimality versus in-situ), we label the difference in GPP as **'data-model discrepancy resolved by field traits'.**

Next, the model calculates a 'P-model_P' GPP also using measured PPFD, and the above optimality-theory predicted LUE, but with MODIS fAPAR rather than in-situ measured fAPAR as input. This 'P-model_P' GPP is compared to MODIS GPP. We note that a small proportion of the difference between MODIS GPP and P-model_P might originate from different PPFD inputs, because P-model_P uses field PPFD whereas MODIS GPP uses PPFD from NASA GMAO (Global Modelling and Assimilation Office) (Table 1) (Running, Mu and Zhao, 2015); however, the differences are expected to be slight (see Figure S 3). The primary difference between 'P-model_P' GPP and MODIS GPP is in LUE (predicted by optimality theory versus lookup table), hence the difference is labelled as **'data-model discrepancy resolved by optimality'**.

To test hypothesis 2 (incorrect fAPAR explains the mismatch), we compared 'P-model_P' to 'P-model_Pf'. The only difference between these two is in fAPAR (in-situ versus MODIS). We referred to the difference as **'data-model discrepancy resolved by fapar'.**

Equivalently, one could directly compare Vc_{max}, J_{max}, fAPAR and LUE from multiple sources (some presented in Figure S 2 and Figure S 3). However, LUE and GMAO PPFD used in MOD17 GPP were not publicly available and were difficult to reproduce, so we did not include them. Since the data-model discrepancies in these variables all cascade into GPP, we focus on visualizing the discrepancies in GPP in Figure 3.

Hypothesis 3 (confusion of land cover classification) is based on the fact that the GPP estimated from in-situ measurements, which is the mean of data from several one-hectare plots, differs in scale from the GPP estimated by the TRENDY models, FLUXCOM and MODIS (as visualized in figure S1). West African forests are extremely fragmented, and some forest patches are smaller than the grid cell size of the models. For example, one of the study forests, BOB, measures only about 7 x15 km (Figure S 1), surrounded by cocoa farmland. To illustrate this, we drew a map of MODIS GPP (with a resolution of 500m) over the BOB site, covering an area similar to a single 0.5˚ x 0.5˚ grid cell of the TRENDY models. Since each grid cell of the TRENDY models is a composite of multiple PFTs (often represented by different fractions in different models) and models report GPP per PFT, we also show the modelled PFT composition of the grid cells and compare 'forest-only' GPP to the grid cell average (Figure S 4).

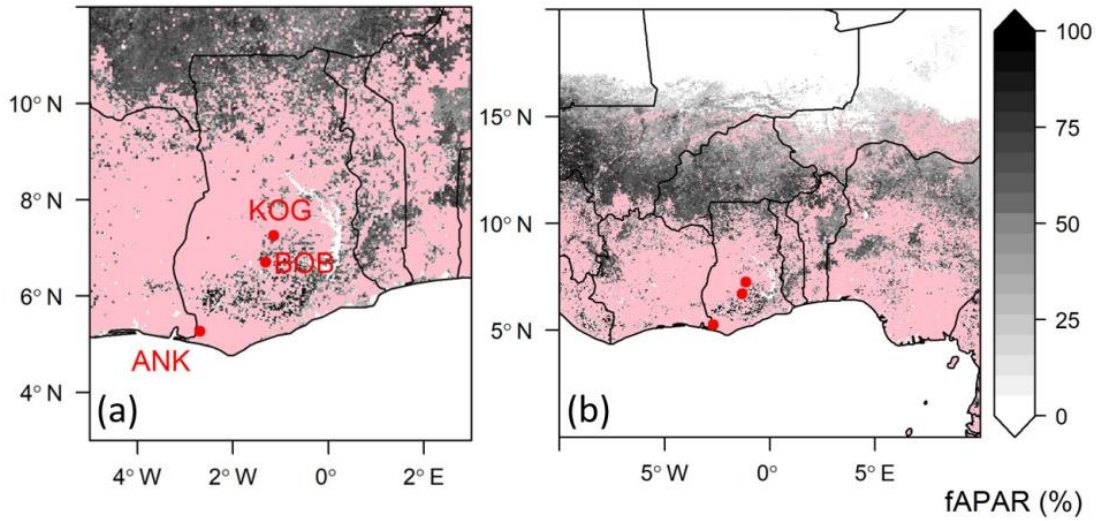


Figure 1 Map of the three study sites in Ghana, West-Africa (b). Grey scales show MODIS fAPAR, on 2016-09-07. Pinks area are pixels contaminated by cloud, which were flagged as 'Significant clouds were present' in MODIS MOD15A2H product. Each red dot denotes a site. Each site contains multiple one-hectare plots (see Method). More meta-data of these sites are provided in supplementary. Map (b) shows that the cloudiness issue is affecting a large area of West African forests.

6.4.4 Study sites

The three study sites span a wet-to-dry rainfall gradient from Ankasa (ANK) with a mean annual precipitation of 2050 mm, to Bobiri (BOB) with 1500 mm, and Kogyae (KOG) with 1200 mm. ANK is occupied by moist rainforest, BOB by semi-deciduous forest, and KOG by dry forest and mesic savanna.

6.4.5 Field measurements of GPP and traits

Observed GPP was estimated in the field using the Global Ecosystem Monitoring protocol, which sums measurements of the components of NPP and autotrophic respiration to calculate GPP (Malhi et al 2021) and is reported in Paper 1. In-situ GPP was originally quantified on plot scale. There were three one-hectare plots at site ANK, six at site BOB, and five at site KOG. This study was conducted at site rather than plot scale because plots at the same site share identical climate variables and fall into one model grid cell. Nonetheless, plots at the same site have different soil property and fall into different grid cells of MODIS product (Figure S 1). We therefore calculated, for each site, the mean and standard error of measured GPP across plots.

fAPAR was estimated using hemispherical photography, taken each month in each plot between 2012 and 2017. Photos were processed using machine learning-based software 'ilastik' (Berg *et al.*, 2019) for pixel classification and CANEYE (Weiss and Baret, 2017) for fAPAR calculations (Supplementary Method).

Traits based LUE was derived from community-weighted mean light-saturated photosynthetic rate (A_{sat}), light- and CO_2 -saturated photosynthetic rate (A_{max}), which were reported in (Paper 2).

Each field measured A_{sat} and A_{max} was derived into Vc_{max} and J_{max} at mean annual air temperature using R package 'plantecophys' (Duursma, 2015; De Kauwe *et al.*, 2016), but modified to bridge with R package 'rpmodel' (Supplementary Method) (Stocker *et al.*, 2020). Measurements were made every three months from 2014 to 2016 to cover both wet

and dry seasons. Although we measured both shade and sun leaves, we used sun leaves only in this study (consistent with common practice in field studies of photosynthetic traits). We used above canopy PPFD as model input and we note that only sun leaves acclimate to this level of PPFD; shade leaves acclimate to darker environments and have consistently lower A_{sat} than sun leaves (Keenan and Niinemets, 2016).

6.4.6 LUE, climate variables and ci/ca

P-model, an optimality theory based model, was used to provide the optimality-estimated LUE, ci/ca and GPP (Table 1) via R package 'rpmodel' (Stocker *et al.*, 2020), for expeirments P-model_Pf, P-model_P and P-model_Null.

Instead of optimality-estimated LUE, we informed P-model with several field-measured input data, including PPFD, climate variables, fAPAR, and LUE (see Method above). The GPP calculated here was called 'P-model_PfL'.

ci/ca was estimated from leaf $\delta^{13}C$ measurements, using method described in (Peng, Bloomfield and Prentice, 2020). This isotope based ci/ca was compared to P-model predicted ci/ca (Figure S 3).

The P-model requires several climate variables as input, and this can be a source of uncertainty in modelled GPP. To address this, we compared the temperature and relative humidity from local weather stations to products commonly used by vegetation models. We selected relative humidity and temperature provided by ERA-interim, using which we also calculated optimality-estimated ci/ca via 'rpmodel'. We derived PPFD from shortwave radiation retrieved from ERA5-Land, following (H. Wang, Prentice, Keenan, *et al.*, 2017). ERA-interim and ERA5-Land were selected because these products have very high resolution which could well tell the difference between sites.

Data-model comparisons of many climate variables have been done in previous literature (Burton, Rifai and Malhi, 2018), which found ERA-interim the best product for

Africa. As we found very small data-model discrepancy in climate variables (See Results), we used ERA-interim temperature, vapour pressure and optimality-estimated ci/ca for all GPP experiments in this study to maintain consistency and ensure a fair comparison between P-model and other models, while the choice of PPFD data set was specific to the experiment (see simulation schematic in Table 1).

6.4.7 Processing MODIS fAPAR and GPP

Using Google Earth Engine, we retrieved MODIS GPP from the collection MOD17A2H and retrieved MODIS fAPAR from MOD15A2H during 2001 to 2020. We extracted GPP and fAPAR of the 14 plots using their coordinates and calculated annual (Figure 2 and Figure 3) and monthly mean (Figure 4) per site. Note that plots in the same site fall into one grid cell of model (about 50 x 50 km, or 0.5° x 0.5°), but into different grid cells of MODIS due to higher resolution of MODIS (500m). The scale difference is illustrated in Figure S 1. To remove cloud-contaminated GPP and fAPAR, we selected only data flagged as 'Significant clouds NOT present (clear)' or 'Mixed cloud present on pixel'. Since MODIS GPP and fAPAR share the same data flag, the above approach ensures that the fAPAR used in P-model_P and P-model_null is identical to that used in MODIS GPP (Figure 3) ensuring fair comparison between them. The issue of cloud contamination is visualized in Figure 1 and Figure 4.

6.4.8 FLUXCOM and TRENDY GPP

There is a flux tower at ANK (GH-Ank), but not at BOB or KOG. Therefore, we compared in-situ measured GPP at the three sites with FLUXCOM. We chose the 'RS_METEO' version of FLUXCOM because the magnitude of GPP in this version does not involve uncertainty from MODIS fAPAR, which makes the comparison between FLUXCOM and MODIS GPP more independent. For TRENDY, we analysed the model outputs in version 9 (Friedlingstein *et al.*, 2020) under the S2 protocol, in which climate

and CO_2 change while land use is kept constant. Note that models still include ‘C4 crop land’ as one of the plant functional types (PFTs), but the cover of ‘C4 crop land’ is kept constant. We retrieved total GPP (sum of all PFTs) of the grid cell and also a forest-only GPP. For both TRENDY and FLUXCOM, we extracted the grid cells where the three study sites stand, as an average from 2009 to 2019.

6.5 Result

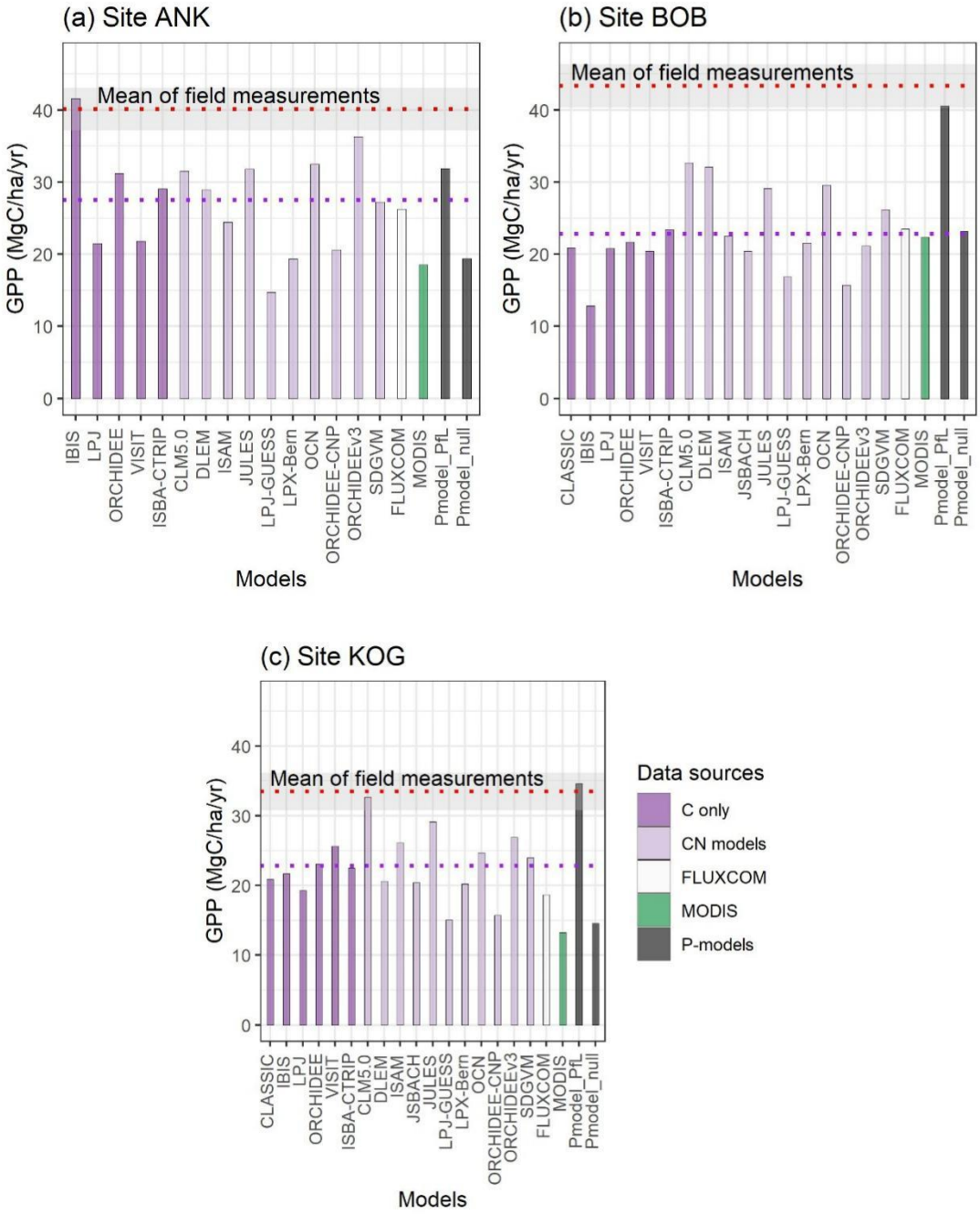


Figure 2 Intercomparison of gross primary productivity (GPP, MgC ha–1 year–1) from various independent sources. The red dotted lines denote GPP based on in-situ measurements and the grey areas denote uncertainty. Bar denotes Carbon only models (dark purple), Carbon-Nitrogen coupled models (light purple), FLUXCOM (white) and MODIS (green). Purple dotted line denotes average across all models.

	GPP	=	PPFD	×	fAPAR	×	LUE
Experiments	Pmodel_PfL		**Measured**		**Measured**		**From measured traits**
	Pmodel_Pf		**Measured**		**Measured**		Optimality-estimated
	Pmodel_P		**Measured**		MODIS fAPAR		Optimality-estimated
	Pmodel_null (in Figure 1)		ERA-Interim		MODIS fAPAR		Optimality-estimated
	MODIS		GMAO		MODIS fAPAR		Look-up table

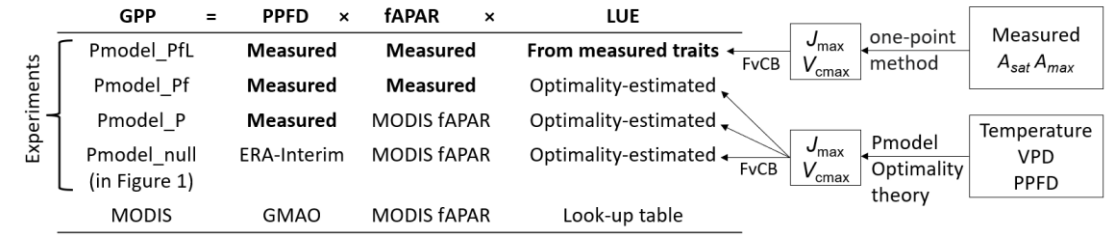


Table 1 The table shows input data for experiments in Figure 3. Input using field measurements are in bold. The schematic shows the calculation of LUE for the four experiments .

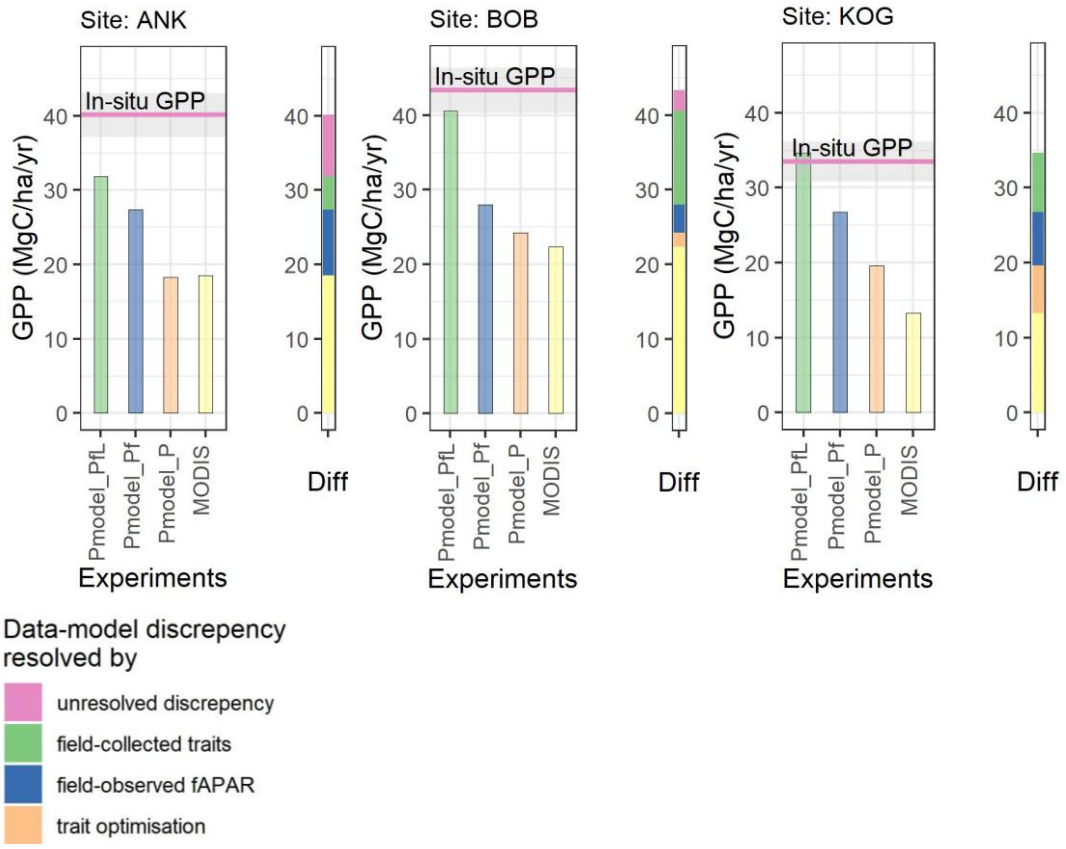


Figure 3 Partitioning of GPP data-model discrepancy, by comparing between different experiments. The left panel displays field-measured GPP (pink line with grey zone showing uncertainty) and multiple GPP experiments (bars). Pmodel_PfL, Pmodel_Pf and Pmodel_P are GPP experiments which are all simulated using P-model but with different inputs (see Table 1 and Methods). Both P-model and MODIS GPP were calculated from equation (1), enabling direct comparison. The right panel, a 'Diff' bar, illustrates the difference in GPP between experiments, which represents the sources of GPP data-model discrepancy. For example, the GPP difference between Pmodel_Pf and Pmodel_P experiments (Figrue 3) is caused by the sole difference in input variables - fAPAR. Therefore, the difference between them (blue) is GPP data-model discrepancy caused by fAPAR. The difference (orange) between Pmodel_P and MODIS is GPP data-model discrepancy caused mainly by the difference between optimality-based LUE and MODIS LUE. The difference (green) between Pmodel_PfL and Pmodel_Pf is GPP data-model discrepancy caused by the difference between measured LUE and optimality-based LUE.

6.5.1 Intercomparison of GPP estimates

Considerable discrepancies in GPP are found among DGVMs, FLUXCOM, MODIS, P-model, and in-situ measurements for all sites, with a pattern that is consistent from site to site (Figure 2). At each site, in-situ measured GPP exceeds GPP estimated by other methods. Overall, the DGVMs models' average GPP is higher than FLUXCOM, which in turn is higher than MODIS GPP. Nonetheless at BOB, the DGVM average, FLUXCOM, and MODIS report almost equal GPP – but still less than the measured GPP. There are substantial disagreements between different DGVMs; for example, at ANK, the models' simulated GPP ranged from 15 to 42 (in-situ GPP at 40) MgC/ha/year. The largest data-model discrepancy between DGVMs and in-situ GPP is seen at BOB (22.8 versus 43.3 MgC/ha/year). The discrepancy between in-situ and MODIS GPP is about 20 MgC/ha/year at all sites.

6.5.2 The match between trait-based GPP and in-situ GPP

Using field observed PPFD, fAPAR, and LUE as input, P-model could estimate a GPP (i.e., experiment P-model_PfL) slightly lower but still within the uncertainty range of in-situ GPP at BOB and KOG sites. However, at the ANK site, P-model_PfL was slightly outside the uncertainty range of in-situ GPP, although it was not the primary factor contributing to the data-model discrepancy at the site (Figure 3).

6.5.3 Measured and modelled photosynthetic trait

Photosynthetic capacity estimated by P-model is lower, although close to in-situ photosynthetic capacity (Figure S 2) implying underestimated LUE. As a consequence, P-model_Pf is lower than P-model_PfL consistently at all sites.

GPP is substantially underestimated when in-situ fAPAR is replaced with MODIS fAPAR, resulting in a considerable difference between P-model_Pf GPP and P-model_P at any site. Especially at ANK, fAPAR is found to be the largest contributor to GPP data-

model discrepancy. A further investigation into MODIS fAPAR (Figure 4) shows that during the rainy season, MODIS fAPAR decreases along with increasing cloud cover (up to 90% of pixels), whereas field fAPAR peaks (denser canopy) during the rainy season. In short, MODIS fAPAR shows an opposite trend to field fAPAR due to cloudiness. Filtering fAPAR values according to cloudiness or gap-filling bad data points, however, removes most of the values from the rainy season, leading to an underestimated mean annual fAPAR. The above issue could affect a major proportion of the African tropical forest (Figure 1).

Although at site ANK, MODIS and P-model_P GPP are almost identical, for site BOB and KOG, MODIS is much lower than P-model_P GPP. The difference could be sourced from PPFD (Figure S 3) or that the optimality-based LUE is higher than MODIS LUE (from the look-up table). Given that P-model_null (using ERA5 PPFD) is higher than MODIS fAPAR at any site (Figure 2), it is more possible that optimality theory tends to estimate an LUE higher than LUE in MODIS GPP.

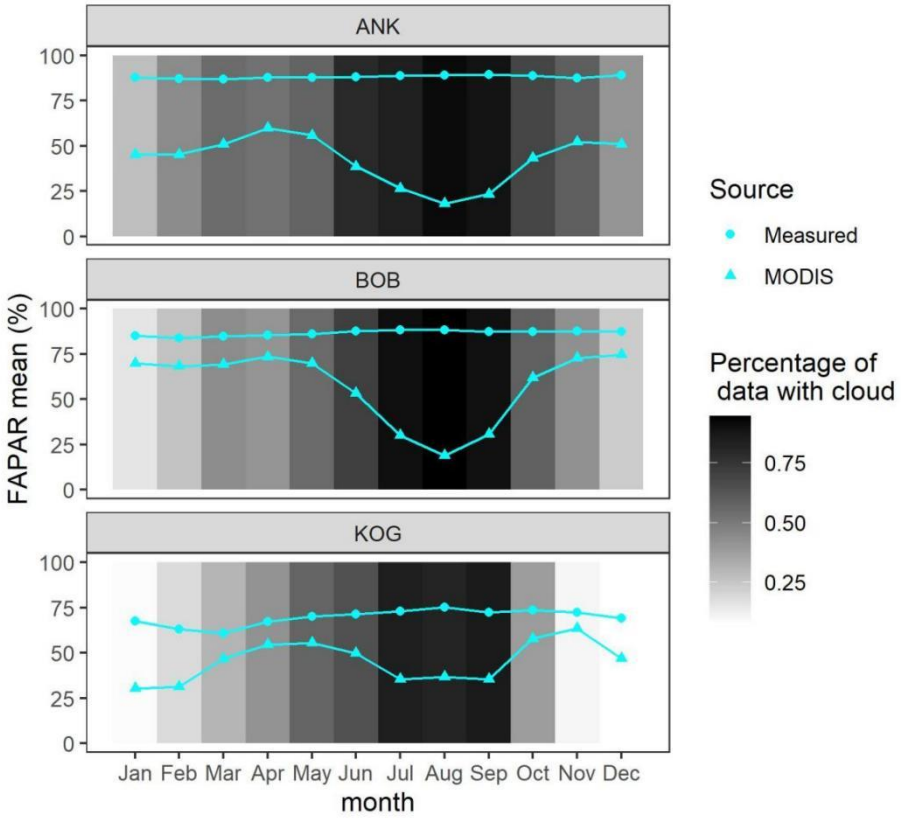


Figure 4 The seasonal variation of the fraction of absorbed photosynthetically active radiation (fAPAR) retrieved from MODIS MOD15A2Hv006 (triangle) and in-situ measured using hemispherical photography (dot), at the three study sites (ANK, BOB and KOG), as an average across multiple years. Note that fAPAR in the above figure was displayed without cloud contamination filtering (nor gap-filling), but MODIS fAPAR used in Table 1 is filtered. Grey scale shows the percentage of records contaminated by clouds.

6.5.4 Scaling and plant functional type

At BOB the entire forest is smaller than a single grid cell in a DGVM. MODIS GPP estimates that the surrounding cocoa farm has only half the productivity of the forests. Therefore, the mean of the whole map (19.6 MgC/ha/year) appears to be smaller than the forests (23 MgC/ha/year) (Figure S 1). It is important to note that field studies on net primary production (NPP) indicate that cocoa farms are as productive as adjacent forests (Morel *et al.*, 2019).

For all of the study sites, most TRENDY models treat the grid cell as a composite of 'forest' or 'C4 grass/crop', although the fraction of forests varies considerably among models. Furthermore, most TRENDY models correctly estimate that 'C4 grass/crop' is as productive as forests (different from MODIS) and hence, forest-only GPP is similar to the mean of the whole pixel (Figure S 4).

Therefore, we have concluded that the GPP data-model discrepancy between TRENDY and in-situ GPP cannot be explained by scaling or PFT issues (rejecting hypothesis 3). The data-model discrepancy between MODIS and in-situ GPP at the 0.5˚ scale, however, is compounded by MODIS' estimation of low productivity in croplands.

6.5.5 Data-model consistency in climate variables

The data-model differences we found for temperature, relative humidity, PPFD and ci/ca were very small and not likely to contribute significantly to the GPP data-model discrepancy (Figure S 3).

6.6 Discussion

6.6.1 Main sources of GPP data-model discrepancy

We not only demonstrate a significant data-model discrepancy in West-African forest GPP but also reveal the main sources of this discrepancy. At the Ankasa wet rainforest site, we found that underestimation of fAPAR is the major contributor to GPP data-model discrepancy. At the Bobiri (semideciduous) and Kogyae (dry forest) sites, too low values of photosynthetic traits (leading to a bias in light use efficiency) are the primary source of GPP data-model discrepancy, which can be partly explained using optimality theory predictions. Additionally, fAPAR accounts for a large proportion of GPP data-model discrepancy at Kogyae but not at Bobiri. Through this analysis we are able to fully account for the data-model discrepancy at Kogaye and Bobiri, with a modest unresolved data-model discrepancy still persisting at Ankasa.

6.6.2 Why do models underestimate GPP in West African tropical forests?

Focusing on three sites (comprising 14 one-hectare plots) in Ghana, we have utilized the first in-situ quantification of African forest GPP and conduct a systematic data-model comparison. Despite the uncertainty of the in-situ GPP, it is more likely that FLUXCOM, MODIS, TRENDY models, and P-model_0 underestimate West African forest productivity than that the in-situ GPP measurements overestimate it. This is because (1) the in-situ GPP is an average across multiple plots spanning several years, and its high productivity is supported by other field studies (Morel *et al.*, 2019); (2) West-African forests were characterised with a high CO_2 assimilation rate or high photosynthetic capacity, in comparison to wet-evergreen tropical forests (Domingues *et al.*, 2010; Tomlinson *et al.*, 2013; Oliveras *et al.*, 2020); Moreover, P-model could simulate a GPP close to in-situ GPP if informed by field-measured traits (Figure 3), which signals a broad

consistency between the high GPP and measured photosynthetic traits. (3) the cause of the models' underestimation can be well explained by errors in modelled LUE and satellite-derived fAPAR (Figure 3).

Some degree of model underestimation of GPP may even be a pan-tropical feature. Intercomparison of GPP and NPP in previous study (Xu *et al.*, 2015; Rödig *et al.*, 2018) has also revealed data-model discrepancies for Amazonian lowland forests. In this study, we found that the data-model discrepancy was due to fAPAR and LUE. The cloudiness issue, leading to low satellite-based fAPAR, has been described as a pan-tropical phenomenon for many remotely sensed products (Zhao *et al.*, 2005; Fensholt and Proud, 2012; Fuster *et al.*, 2020; Sudmanns *et al.*, 2020). Bias in MODIS fAPAR (or LAI, NDVI) will inevitably cascade into models or analyses that use MODIS fAPAR as a predictor, including FLUXCOM. L. Wang *et al.*, (2017) similar to our findings, indicated that fAPAR (and not meteorological data) is the main cause of MODIS GPP underestimation in both African and Amazonian forests.

The LUE discrepancy however is likely to be a West African regional issue, since a previous study found higher A_{sat} and A_{max} values in West African species than Amazonian (Tomlinson *et al.*, 2013). There are higher A_{sat} and A_{max} from BOB and KOG (drier sites), but not ANK (the wet evergreen forest more similar to lowland Amazonia) (Oliveras *et al.*, 2020; Paper 2), making LUE the dominating source of GPP bias in BOB and KOG but less dominant in ANK. The high photosynthetic capacity in semi-arid forest or savanna is consistent with other field studies in West Africa (Domingues *et al.*, 2010). Vc_{max} inferred from remotely sensed leaf chlorophyll data, and Vc_{max} predicted by the P model, both show exceptionally high values in West Africa and parts of India – substantially higher than in Amazonia or SE Asia (Chen *et al.*, 2022; Dong *et al.*, 2022), where plants photosynthesis may be optimized to high light, temperature and VPD. Whereas, the substantial spatial

dynamic of Vc_{max} has not been incorporated in most TRENDY models (Rogers *et al.*, 2017) which could lead to underestimation of GPP at such regions.

6.6.3 The importance of field evidence in productivity estimation

The availability of comprehensive field measurements allows us to trace and quantify the sources of data-model discrepancy in the GPP of West-African forests. We find that fAPAR and LUE are the dominant sources of data-model discrepancy, rather than model structure or climate variables. These findings reflect the lack of field measurements of West-African forest photosynthetic traits and leaf area index (fAPAR), while the environmental variables of the study regions are better represented. FLUXCOM also struggles with the number of field stations in the study region. There is only one flux tower for West-African forests (Tower GH-ank), which reports three years of GPP varying dramatically (L. Wang *et al.*, 2017). The mean GPP across three years appears to be lower than the in-situ GPP, which may be associated with raw data quality (Pastorello *et al.*, 2020), technical issues (Hayek *et al.*, 2018; Billesbach *et al.*, 2019), and challenging subcanopy CO_2 storage estimation (de Araújo *et al.*, 2010; Fu *et al.*, 2018). During FLUXCOM extrapolation, the machine learning algorithm would not incorporate the higher photosynthetic capacity at BOB and would simply find BOB less productive than ANK (opposite in-situ GPP pattern) due to less precipitation (Figure 3). Beyond pointing out the sources of data-model discrepancy, this study also highlights that such issues could be fixed if models were informed with field-measured fAPAR and LUE derived from measured traits. The data-model discrepancy could also be partially (although not completely) resolved with GLASS fAPAR products (L. Wang *et al.*, 2017) or using predicted LUE by optimality theory (Table 1), which highlight the importance of using 'trait-based approaches' photosynthesis parameters instead of PFTs prescription (Wullschleger *et al.*, 2014; Rogers *et al.*, 2017). Given that GLASS, optimality-based

LUE, and FLUXCOM all require validation with field evidence, the study suggests that providing models with ample field evidence and ensuring strong fidelity to field measurements is critical in improving current carbon cycle simulations (Prentice *et al.*, 2015).

6.6.4 Implication for carbon modelling of West-African forests

Researchers studying African forests in the future should exercise caution when using satellite information, as satellite data are strongly biased during the rainy season in this region due to high cloudiness. Additionally, West-African forests are highly fragmented (Buchanan *et al.*, 2021) (Figure S 1), so modellers should bear in mind that resample satellite products to a coarser resolution (e.g., from 500m to 50km) would mix forests with farmland which could be similar in productivity but differ in other aspects of carbon cycling (Figure S 4) (Morel *et al.*, 2019).

The study has shown that the P-model can satisfactorily predict ci/ca, Vc_{max} and J_{max} – essential parameters for the FvCB model. The data also support the coordination of the Rubiscio- and electron transport-limited photosynthetic rates, A_C and A_J, which is one of the optimality principles underlying the P-model (Figure S 2). However, the reasons why almost all TRENDY models underestimated West-African GPP have not been fully elucidated. While much criticism of TRENDY models has centred on issues such as the representation of nutrient limitation or inaccurate characterizations of plant functional types, our study suggests that neither of these factors is likely to be the main reason for the underestimation of GPP. Although it is challenging to unbox each model and investigate their Vc_{max}, J_{max} or LUE, our analysis suggests that the underestimation of GPP may source from the underestimation of Vc_{max}, J_{max} or LUE. Allowing Vc_{max}, J_{max} or LUE to acclimate to brighter and drier environment should improve simulation of GPP at semi-arid forest and savanna.

6.6.5 Conclusion

In conclusion, the study not only reveals underestimation of West African forest productivity but also explains why this underestimation occurs. The unique data-model comparison approach proposed in this study may also have greater potential as it successfully shows (1) consistency between field measured photosynthetic traits and bottom-up GPP (2) the source of data-model discrepancy by designing multiple experiments with a minimal photosynthesis model (P-model). The study also demonstrates that to gain insight, thorough field measurements of forest plots are valuable and application of simple models (that can be easily understood and tuned) are key for ecological hypothesis testing. However, further investigation is still needed until a better (likely higher) estimation of African GPP could be given. The study is limited in terms of spatial cover. We therefore encourage future study to focus on drier African ecosystem where C4 grasses are abundant with more LUE (Chen *et al.*, 2021) but less cloudiness (Figure 1).

6.7 Supplementary Method – Manual for reproducing results

The purpose of the supplementary material is to guarantee the reproducibility of all parameters used in our modelling work. As a result, it prioritizes technical details over readability, serving as a technical manual of the "Methods" chapter in the main text.

6.7.1 To reproduce Figure S3

(Codes in Zenodo deposit 1_prepare_climate_data and 3. supplementary_compare_climate_variable)

ci/ca was estimated from leaf $\delta^{13}C$ measurements. We initially estimated the difference between the leaf stable isotope ratio and the atmospheric stable isotope ratio at that place and time ($\Delta^{13}C$) from $\delta^{13}C$, using the method described by Cornwell et al. (2016). Subsequently, we calculated ci/ca from $\Delta^{13}C$ using equation 11 in Peng et al.

(2020). The community-weighted mean and standard error were then calculated based on 238 measurements. This isotope based ci/ca was compared to P-model predicted ci/ca explained in 5.2.2 P-model experiment (Figure S3).

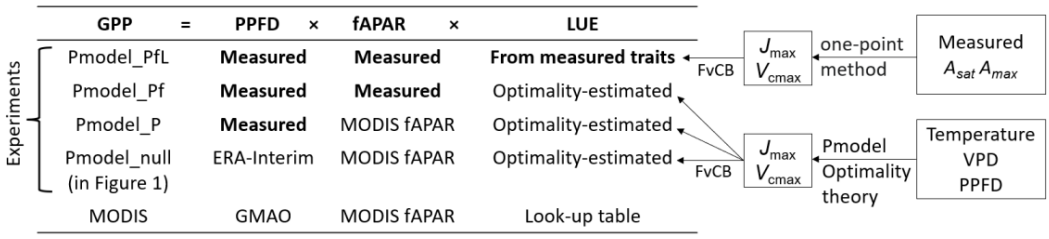
The P-model requires several climate variables as input, and this can be a source of uncertainty in modelled GPP. To address this, we compared the temperature and relative humidity from local weather stations to products commonly used by vegetation models. We selected relative humidity and temperature provided by ERA-interim and shortwave radiation retrieved from ERA5-Land. However, the data-model differences we found for temperature, relative humidity and ci/ca (calculated from temperature and vapour pressure) were very small and not likely to contribute significantly to the GPP data-model discrepancy (Figure S3). Moreover, data-model comparisons of many climate variables have been done in previous literature (Burton, Rifai and Malhi, 2018). Therefore, we used CRU temperature, vapour pressure and calculated ci/ca for all GPP experiments in this study to maintain consistency and ensure a fair comparison with other models (Figure 2), while the choice of PPFD data set was specific to the experiment (Table 1).

For satellite based fAPAR, we extracted MODIS fAPAR (MOD15A2H) of the 14 plots from 2001 to 2020 and averaged them into mean fAPAR per site. To remove cloud contaminated fAPAR, we selected only CLOUDSTATE=00 and =10. Since MODIS GPP and fAPAR share the same CLOUDSTATE, this ensures that the fAPAR used in P-model_P is identical to that used in MODIS GPP (Table 1). The issue of cloud contamination is visualized in Figure 1 and Figure 3. Field measured fAPAR is explained in 5.2.1.

6.7.2 To reproduce Figure 3 and Figure S2

(Codes in Zenodo deposit 4.Figure_two_GPP_from_measured_Vc_{max})

This chapter explain how to calculate GPP for each P-model experiment as shown below (which is Table 1).



6.7.3 Experiment P-model_PfL

We used measured mean fAPAR, light-saturated photosynthetic rate (A_{sat}), light- and CO_2-saturated photosynthetic rate (A_{max}), ci/ca, and climate variables for each site as inputs to the P-model in order to calculate 'P-model_PfL GPP' for each site. Vc_{max}, J_{max} and LUE can also be calculated from the above measurements. We chose field measured A_{sat} and A_{max} instead of field measured Vc_{max}, J_{max} because the former is simpler to measure. We have multi-seasonal samplings and lots of replicates for A_{sat} and A_{max} (which do have strong seasonal variation) (Jin *et al.*, 2016).

fAPAR was estimated using hemispherical photography. hemispherical images taken with a Nikon 5100 camera and Nikon Fisheye Converter FC-E8 0.21x JAPAN near the center of each of the 25 subplots in each plot in each site, at a standard height of 1 m, and during overcast conditions. 22,000 photos were collected in total, every month during 2016-2017(ANK), 2012-2017 (BOB&KOG). Photos were processed using machine learning-based software 'ilastik' (Berg *et al.*, 2019) for pixel classification and CANEYE (Weiss and Baret, 2017)for leaf area index calculations. The exposure procedure followed (Zhang, Chen and Miller, 2005) and GEM manual (Malhi *et al.*, 2021) (http://gem.tropicalforests.ox.ac.uk). The following parameters were supplied to CANEYE to calculate both leaf area index (LAI) and fAPAR

(8) P1 = angle of view of the fish eye divided by the amount of pixels from centroid of the fish eye circle to where horizon is on the image.

(9) angle of view = 90 degree, in which case, the edge of the photo is the horizon and the centroid of the image is zenith.

(10) COI = 80, consideration of field is 80 degrees, we don't want the edge of the photo because it is not clear and sometime obscure by tall grasses or saplings.

(11) Sub sample factor =1

(12) Fcover = 20 degree, this is to calculate the percentage of black pixels within central 20-degree ring. We used this to understand the relative openness of canopy for the given image. It is not relevant to LAI

(13) PAIsat = 10, When a pixel is completely black, mathematically, the leaf area index (LAI) is infinite. As we provide CANEYE 25 subplot images for each estimation of LAI, this means all 25 subplot images show black at a given pixel. To address this 'infinite'issue, we uses a value of 10 for LAI in such cases. This value is based on the guess that, the densest point in a tropical forest should had an LAI of 10.

(14) Latitude 0 and Day of year a random number (not relevant for tropical site LAI)

CANEYE reported a diffuse fAPAR and a direct fAPAR. We calculated overall fAPAR as 0.8*Diffuse_fapar +0.2*Direct_fapar (Zhang *et al.*, 2020). We used 0.8 and 0.2 because We assumed that 80% of days in the study region is cloudy.

To measure A_{sat} and A_{max}, we used an open-flow gas exchange system (LI-6400XT, Li-Cor Inc., Lincoln, NE, USA). To ensure a proper representation of the forest stand, we sampled tree species that constituted approximately 80% of the plot basal area. For each species, we selected three mature and canopy emergent trees, and cut one fully sunlit and one shaded branch per tree using a single rope climbing technique. We immediately placed and recut the cut branch under water, and measured the maximum rate of net CO_2

assimilation at 400 ppm CO_2 (A_{sat}) and 2000 ppm CO_2 (A_{max}) on three leaves per branch. The PPFD was set to 2000 µmol m^{-2} s^{-1} and block temperature was kept constant at 30 ºC. Each measurement was derived into Vc_{max} and J_{max} at growth temperature (Peng, Bloomfield and Prentice, 2020) using R package 'plantecophys' (Duursma, 2015; De Kauwe *et al.*, 2016). Measurements were made every three months from 2014 to 2016 to cover both wet and dry seasons. Although we measured both shade and sun leaves, we used sun leaves only in this study (consistent with common practice in field studies of photosynthetic traits). We used above canopy PPFD as model input and we note that only sun leaves acclimate to this level of PPFD; shade leaves acclimate to darker environments and have consistently lower A_{sat} than sun leaves (Keenan and Niinemets, 2016). We filtered outliers with the R package 'outliers::scores', 'iqr' method with threshold 1.5. Then measurements from 1394 leaves were used to calculate community-weighted means based on the basal area of each species. The same weights were applied in calculating standard errors (Madansky and Alexander, 2017).

6.7.4 LUE was calculated from A_{sat} and A_{max} following the method below.

We first **convert A_{sat} to** Vc_{max} using 'one-point' method, equation 3 in (De Kauwe et al., 2016).

$$\hat{V}_{cmax} = A_{sat}\left(\frac{C_i + K_m}{C_i - \Gamma^*} - 0.015\right)$$

We used R package *Plantecophys* (Duursma, 2015) to do so using the following codes.

```
library(plantecophys)
ghana_data2 <- fitaci(data2[i, ],
                      varnames = list(ALEAF = "Asat", Tleaf = "Mean.Tleafasat",
                          Ci = "Mean.Ciasat", PPFD = "PARi", Rd = "DResp"),
                      fitTPU = FALSE, Tcorrect = F, Patm = 100,  PPFD = 2000,
                      fitmethod = "onepoint")
# Dresp is dark respiration reported by LICOR, PARi is light environment of
# the chamber at 2000 µmol m–2 s–1, Mean.Ciasat is leaf-internal CO2 found
```

```
# by LICOR, while leaf external CO2 was fixed to 400 ppm, Mean.Tleafasat is the
# leaf temperature reported by LICOR, chamber temperature was kept at 30 degree
#          so Mean.Tleafasat is around 30 degree for most measurements.
```

We then **convert A_{max} to** J_{max}, using 'Jmax limitation equation'.

However, there are two 'J_{max} limitation methods' that leads to two equations linking A_{max} and J_{max}. Well, if you ignore 'J_{max} limitation' then simply $A_{max} = J_{max} / 4$. (Stocker *et al.*, 2020) explains the two equations very well. More information could be found from these papers (Bernacchi, Pimentel and Long, 2003; H. Wang, Prentice, Keenan, *et al.*, 2017; Smith *et al.*, 2019).

In this paper, we used the first equation, which is equation 13 in (Stocker et al., 2020):

$$A_J = \varphi_0 \, I_{abs} \, m \, \underbrace{\frac{1}{\sqrt{1 + \left(\frac{4 \, \varphi_0 \, I_{abs}}{J_{max}}\right)^2}}}_{L}.$$

While there are also the second equation, which is equation F20 in (Stocker et al., 2020):

$$A_J = \left(\frac{m}{4}\right) \frac{\varphi_0 I_{abs} + J_{max} \pm \sqrt{(\varphi_0 I_{abs} + J_{max})^2 - 4\theta\varphi_0 I_{abs} J_{max}}}{2\theta}$$

R package '*rpmodel'* (we will use this later) do have both equations written in, but for an unknown reason, results given by the second equation (called Smith19 in the package) have unreasonably low J_{max}. It is more likely to be coding issue because the python version of 'rpmodel' reports reasonable results for both methods. The python version is called 'pyrealm' (https://pyrealm.readthedocs.io/en/latest/index.html) (https://pypi.org/project/pyrealm/). This is out of the scope of this paper, so results are not

included. Eventually we used R package 'rpmodel' with the first equation (named 'Wang17' in the package).

However, package '*Plantecophys*' used the second equation. To be consistent with *rpmodel*, we modified source codes of *Plantecophys* in function *photosyn.R*, by **replacing**

```
Jfun <- function(PPFD, alpha, Jmax, theta){
  (alpha*PPFD + Jmax -
     sqrt((alpha*PPFD + Jmax)^2 - 4*alpha*theta*PPFD*Jmax))/(2*theta)
}

inverseJfun <- function(PPFD, alpha, J, theta){
  J*(J*theta - alpha*PPFD)/(J - alpha*PPFD)
}
```

With

```
Jfun <- function(PPFD, alpha, Jmax, theta){
  alpha*PPFD/sqrt(1+(alpha*PPFD/Jmax)^2)
}

inverseJfun <- function(PPFD, alpha, J, theta){
  sqrt(1/(1/J^2 - 1/ (alpha*PPFD)^2 ))
}
```

Now, J_{max} could be obtained by

```
   ghana_data2 <- fitaci(data2[i, ],
                         varnames = list(ALEAF = "Amax", Tleaf = "Mean.Tleafamax",
                            Ci = "Mean.Ciamax", PPFD = "PARi", Rd = "DResp"),
                         fitTPU = FALSE, Tcorrect = F, Patm = 100, PPFD = 2000,
                         fitmethod = "onepoint")
# Dresp is dark respiration reported by LICOR, PARi is light environment of
# the chamber at 2000 µmol m–2 s–1, Mean.Ciasat is leaf-internal CO2 found
# by LICOR, while leaf external CO2 was fixed to 400 ppm, Mean.Tleafasat is the
# leaf temperature reported by LICOR, chamber temperature was kept at 30 degree
          # so Mean.Tleafasat is around 30 degree for most measurements.
```

Note that temperature correction was turned off in the above. The outputs Vc_{max} and Jmax are under measurement chamber temperature (around 30 degree). We used function 'ftemp_inst_vcmax' provided by *rpmodel* to standardise Vc_{max} and J_{max} from measurement temperature to mean annual air temperature of the site, using equation in (Stocker *et al.*, 2020). We tagged the above as Jmax_onepoint_tair and Vcmax_onepoint_tair.

Now, GPP, LUE, A_J and A_C could be calculated using Jmax_onepoint_tair and Vcmax_onepoint_tair.

First, A_C and A_J need to be calculated using:

$$A_C = V_{cmax}\, m_C$$

$$m_C = \frac{c_i - \Gamma^*}{c_i + K},$$

where c_i is given by $c_a \chi$.

$$A_J = \varphi_0\, I_{abs}\, m \frac{1}{\sqrt{1 + \left(\frac{4\,\varphi_0\, I_{abs}}{J_{max}}\right)^2}}$$

with

$$m = \frac{c_i - \Gamma^*}{c_i + 2\Gamma^*}.$$

Next, we should check whether $A_C = A_J$, following coordination hypothesis (H. Wang, Prentice, Davis, *et al.*, 2017) (Figure S2). Upon checking coordination, we calculate the per unit leaf surface area assimilation rate following A_J only because (1) we are comparing to other light use efficiency model (MODIS) (2) P-model is essentially a light use efficiency model and was presented using A_J equation (H. Wang, Prentice, Keenan, *et al.*, 2017; Stocker *et al.*, 2020)

The last step is to upscale per unit leaf surface area (*A*) to GPP using fAPAR. We could also calculate the traits-based LUE from A_J, using: LUE = A_J / Iabs.

Parameters involved above are available in '*rpmodel'* and explained in (Stocker *et al.*, 2020). The only difference is that we are now using the Jmax_onepoint_tair and Vcmax_onepoint_tair calculated above, instead of P-model prediction of optimality theory based Vc_{max} and J_{max}.

The above could be done using codes in '*rpmodel'* specifically:

```
jmax = Jmax_onepoint_tair / (10^6 /24/3600),
vcmax = Vcmax_onepoint_tair / (10^6 /24/3600), # mol C m-2  day-1
patm = calc_patm(elv),
co2 = 414,
kphio = (0.352+0.021*tc-tc^2 * 3.4/10^4)/8,
# kphio is from Peng et al New phytologist 2020
ca = co2_to_ca( co2, patm ),
## photorespiratory compensation point - Gamma-star (Pa)
gammastar = calc_gammastar( tc, patm ),
## Michaelis-Menten coef. (Pa)
kmm = calc_kmm( tc, patm ),   ##
## viscosity correction factor = viscosity( temp, press )/viscosity( 25 degC, 1013.25 Pa)
ns      = viscosity_h2o( tc, patm ),  # Pa s
ns25    = viscosity_h2o( kTo, kPo ),  # Pa s
ns_star = ns / ns25,  # (unitless)
xi  = sqrt( (beta * ( kmm + gammastar ) ) / ( 1.6 * ns_star ) ),
chi = gammastar / ca + ( 1.0 - gammastar / ca ) * xi / ( xi + sqrt(VPDmean) ),
ci = chi * ca,
gamma = gammastar / ca,
kappa = kmm / ca,
## use chi for calculating mj
mj = (chi - gamma) / (chi + 2 * gamma),
## mc
mc = (chi - gamma) / (chi + kappa),
## mj:mv
mjoc = (chi + kappa) / (chi + 2 * gamma),
a_c = vcmax * (ci - gammastar) / (ci + kmm),
fact_jmaxlim = 1/(sqrt(1+(4*kphio*ppfd_field /jmax)^2)),
a_j = kphio * ppfd_field  * (ci - gammastar)/(ci + 2 * gammastar) * fact_jmaxlim,
# unit is mol C /m2 /day
LUE = a_j * c_molmass / (ppfd_field /4.6) ,
# ppfd is in unit (mol /m2 / day), use 4.6 to convert to MJ/m2/day, now LUE is in gC/MJ
a_coordinated=(a_j+a_j)/2,
# follow A_j only after checking coordination hypothesis
        gpp_calculated = a_coordinated *FAPAR_field*  c_molmass / 10^6 * 10000 * 365
```

Experiment P-model_null, P-model_P and P-model_Pf

The R package 'rpmodel' can be used to predict values of ci/ca, V_{cmax} and J_{max} from climate variables. These values, combined with MODIS fAPAR (MOD15), were used to derive the P-model_P. Combined with field-measured fAPAR, they were used to derive P-model_Pf. Combined with MODIS fAPAR and ERA5 PPFD, they were used to provide P-model_0 (Table 1).

P-model_null, P-model_P and P-model_Pf share the same codes as shown below, just with different input variables of fAPAR and PPFD (Table 1).

```
library(rpmodel)
 rp_model_output<-rpmodel(
   tc=temp_result$tc,
   vpd=temp_result$VPDmean,
```

```
    co2=temp_result$co2,
    fapar=temp_result$FAPAR,
    ppfd=temp_result$ppfd ,
    patm = NA,
    elv=temp_result$elv,
    beta = 146,
    soilm = 1,
    meanalpha = 1,
    apar_soilm = 0,
    bpar_soilm = 0.733,
    c4 = FALSE,
    method_jmaxlim = "wang17", #Other options are "smith19" or 'none' "wang17",
    do_ftemp_kphio = TRUE,
    do_soilmstress = FALSE,
    returnvar = NULL,
    verbose = FALSE
  )
rp_model_output$gpp<-rp_model_output$gpp / 10^6 * 10000 * 365
        #from g C m-2 day-1 to MgC per ha yr-1
```

6.7.5 To reproduce Figure S1

Using Google Earth Engine, we retrieved MODIS GPP from the collection 'MODIS/006/MOD17A3HGF' for the period 20010101 to 20201231 (The gap filled and quality-controlled version of MOD17A2H); We drew a rectangular area of 0.5° x 0.5° (or 50 x 50 km) over Bobiri forest, where the study site BOB is located, and visualized the mean GPP of the area over the period (Figure S1).

6.7.6 To reproduce Figure 1 and Figure 3

(Codes in Zenodo deposit 2_Figure_four_timeseries_of_fapar)

For the period 20010101 to 20201231, we extracted MOD17A2H GPP of the 14 plots using their coordinates and calculated the mean GPP per site (not per plot). We also extracted MODIS fAPAR (MOD15A2H) of the 14 plots and averaged them per site. To remove cloud contaminated GPP and fAPAR, we selected only CLOUDSTATE=00 and =10. Since MODIS GPP and fAPAR share the same CLOUDSTATE, this ensures that the fAPAR used in P-model_PPFD is identical to that used in MODIS GPP (Table 1) (see Rationale).

To illustrate the spatial cover of fAPAR cloud contamination we used MODIS MOD15A2H at timestamp A2016249. Pixels contaminated by cloud were identified using 'cloudstate = 01' provided in band 'faparlaiQC' (Figure 1). To illustrate the seasonal variation of fAPAR and cloud status, we calculate monthly average from 20010101 to 20201231 for fapar and for the percentage of cloud contamination (cloudstate = 01) (Figure 4).

6.7.7 To reproduce Figure 2 and Figure S4

(Codes in Zenodo deposit 5.compare_to_trendy_flux_com)

MODIS GPP was obtained from MOD15A2H as explained above (See 5.4).

There is a flux tower at ANK (GH-Ank), but not at BOB or KOG. Therefore, we compared in-situ measured GPP at the three sites with FLUXCOM. For FLUXCOM, we chose the RS_METEO version instead of RS because the magnitude of GPP in RS_METEO does not involve uncertainty from MODIS fAPAR, which makes the comparison between FLUXCOM and MODIS GPP more independent. Note that the seasonal variation of GPP in RS_METEO version does involve uncertainty due to MODIS fAPAR, but this seasonal variation was not studied here. For TRENDY, we analysed the model outputs in version 9 under the S2, in which climate and CO_2 change while land use is kept constant. We extracted values of the grid cells where the three study sites stand, for output "gpp," "gpppft," and "landcoverfrac." The latter two together could determine a forest-only GPP (Figure S4). For both TRENDY and FLUXCOM, we extracted the grid cells where the forest plots fall, as an average from 2009 to 2019.

6.8 Supplementary figures

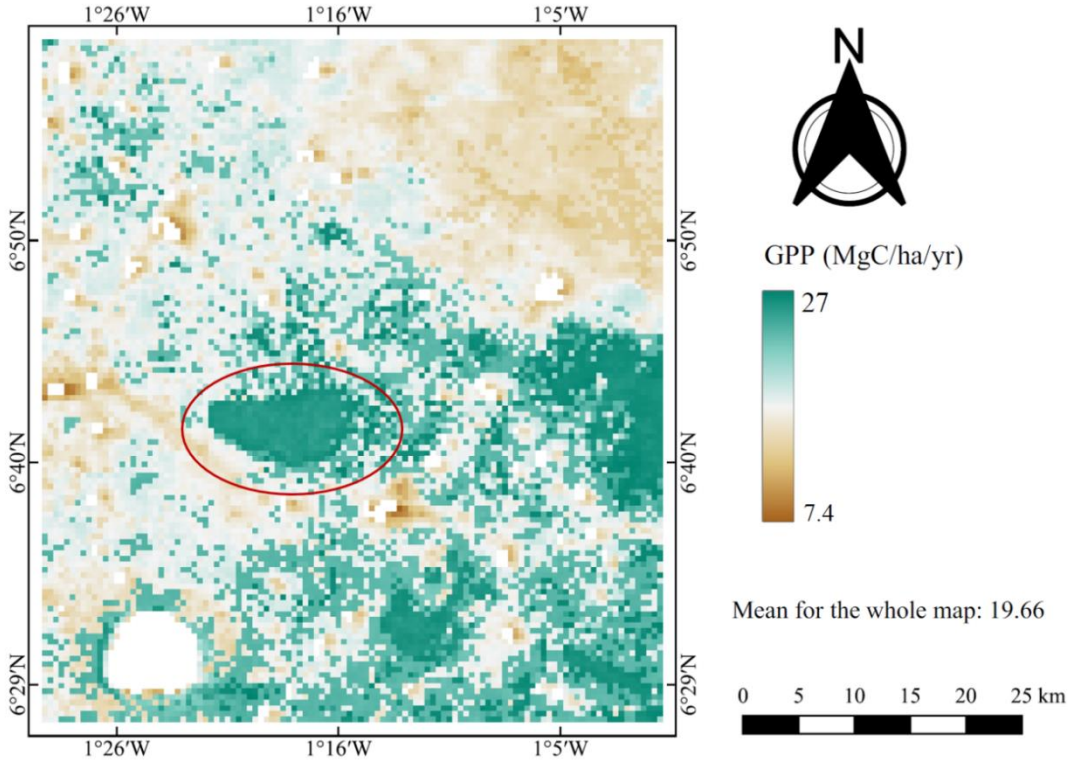
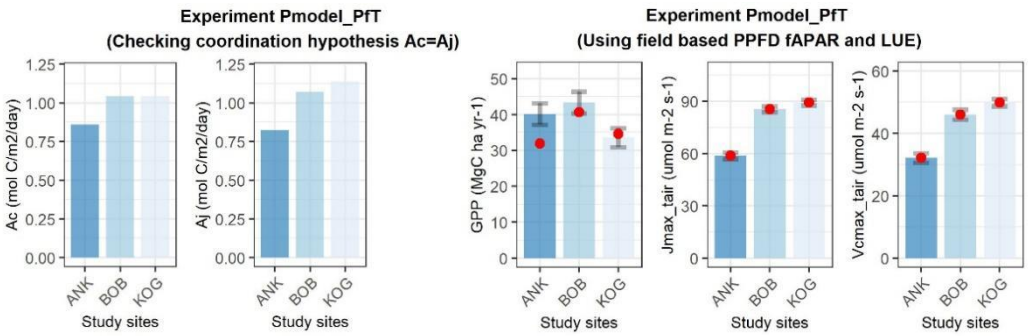


Figure S 1 MODIS gross primary productivity (GPP). The red circle highlight Bobiri (BOB) forest reserve, surrounded by farmland. Six one-hectare plots were established for GPP measurements in this forest reserve. The whole map area is roughly equal to a grid cell in TRENDY models, where the highest resolution is half-degree (or 50 x 50 km). We visualized the GPP of the area averaged over the period 20010101 to 20201231 using product MOD17A3HGF (500 m resolution), which has been cloud contamination filtered and gap filled. The figure shows that (1) West-African forests are very fragmented and the study site BOB is surrounded by farmland, which makes plant functional type recognition an important issue in modelling (see hypotheses for Objective 3 in main text). (2) MODIS GPP and TRENDY models are on different resolution. Study plots fall into different pixels of MODIS but into the same pixel of a carbon model.



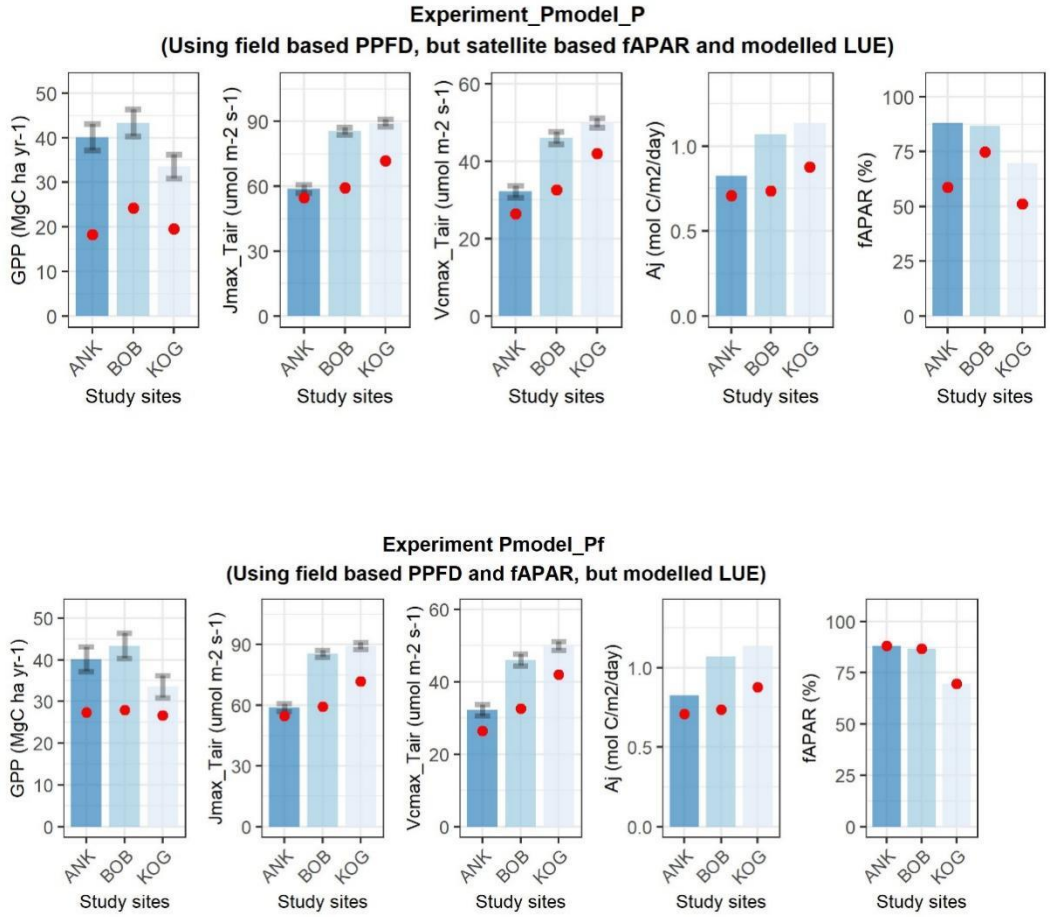


Figure S 2 Comparing in-situ gross primary productivity (GPP, MgC ha^{-1} $year^{-1}$) (Blue bar) to GPP of multiple experiments (red dots). Precipitation decreases from ANK to BOB, KOG. The figures also show data (blue bars) model (red dots) comparison for rubisco carboxylation capacity (Vc_{max}, umol CO_2 m^{-2} s^{-1}), and electron transport capacity (J_{max}, umol CO_2 m^{-2} s^{-1}), photosynthesis on the enzyme-limited (Ac) and electron transport-limited (A_j) rates, all under mean annual air temperature. Note that for experiments P-model_P and P-model_Pf, P-model predicts Vc_{max} and J_{max} with the assumption that $A_C = A_J$ (coordination hypothesis). Therefore, only A_J was displayed. For experiment P-model_PfT however, A_C and A_J are independently calculated and thus A_C is not identical to A_J. All variables were calculated under mean annual air temperature not standardized to 25 °C.

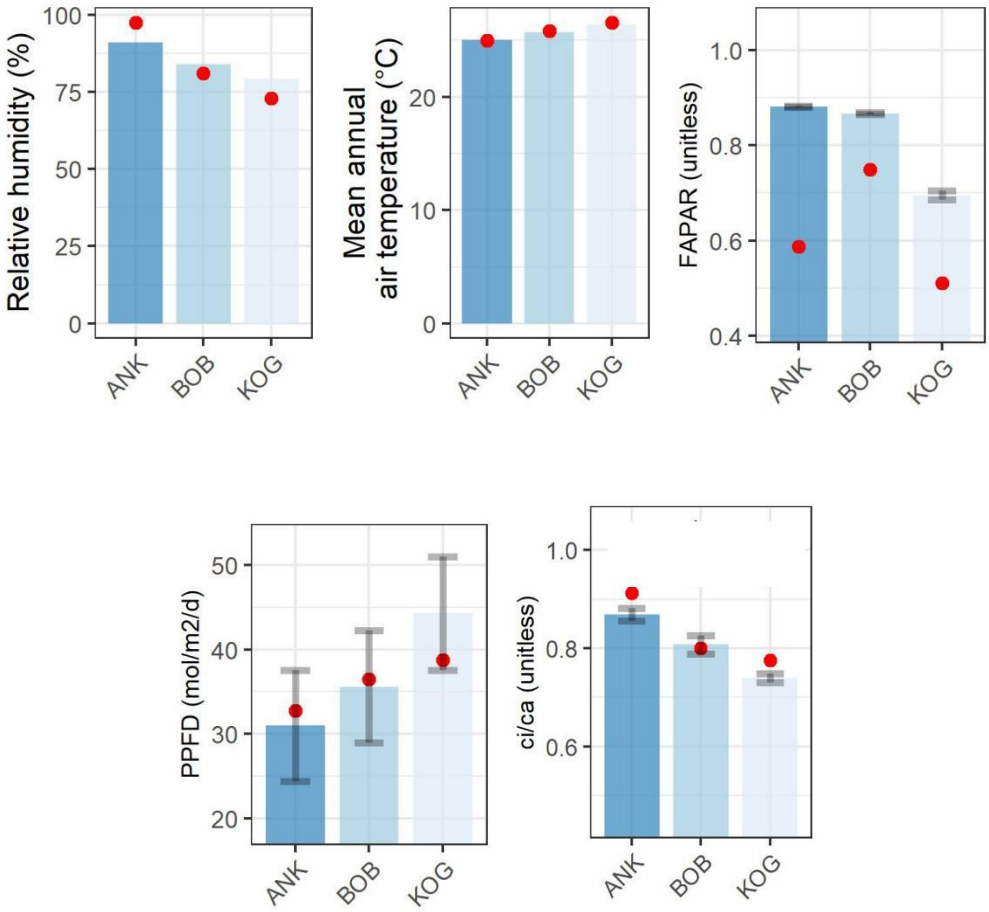


Figure S 3 Field measurements (blue bars) and model (or from global products, red dots) comparison for relative humidity, mean annual temperature, leaf internal to external CO_2 concentration (ci/ca, or c_i/c_a), fraction of absorbed photosynthetically active radiation (fAPAR) and photosynthetic photon flux density (PPFD). See Supplementary notes for source of data.

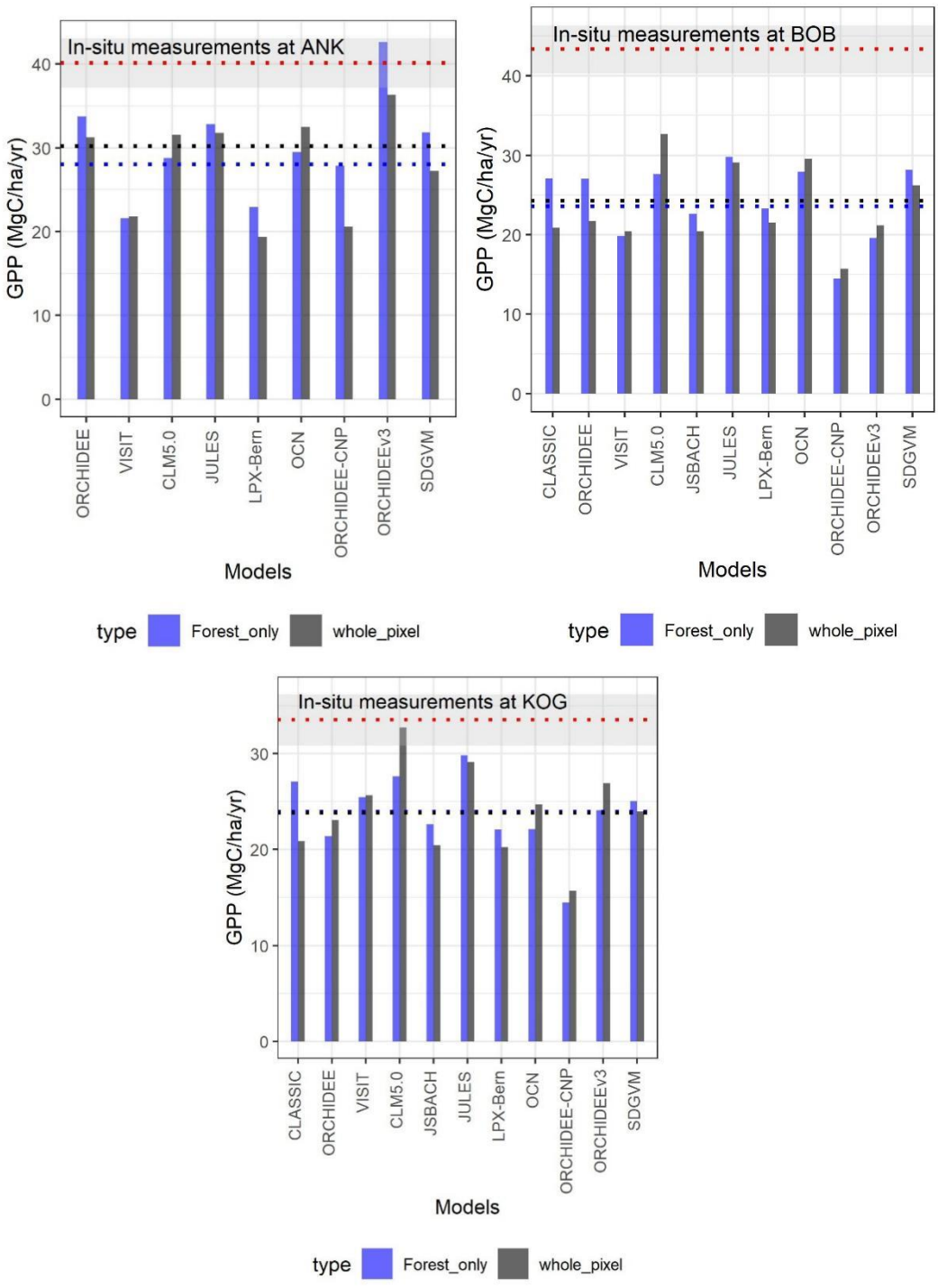


Figure S 4 Comparing Forest only gross primary productivity (GPP) (blue) to the GPP of the whole pixel (black), which is a mixture of agricultural land, forest and grass at the three study sites, with percentage vary considerably among models. The analysis is only possible for TRENDY models that reported GPP of each plant functional type. The red line and grey zone denote field measured GPP and its uncertainty.

6.9 References for Paper 3

Anav, A. *et al.* (2015) 'Spatiotemporal patterns of terrestrial gross primary production: A review', *Reviews of Geophysics*, 53(3). Available at: https://doi.org/10.1002/2015RG000483.

de Araújo, A.C. *et al.* (2010) 'The spatial variability of CO2 storage and the interpretation of eddy covariance fluxes in central Amazonia', *Agricultural and Forest Meteorology*, 150(2), pp. 226–237. Available at: https://doi.org/10.1016/ j.agrformet.2009.11.005.

Ardö, J. (2015) 'Comparison between remote sensing and a dynamic vegetation model for estimating terrestrial primary production of Africa', *Carbon Balance and Management*, 10(1). Available at: https://doi.org/10.1186/s13021-015-0018-5.

Babst, F. *et al.* (2021) 'Modeling Ambitions Outpace Observations of Forest Carbon Allocation', *Trends in Plant Science*, 26(3). Available at: https://doi.org/ 10.1016/j.tplants.2020.10.002.

Badgley, G. *et al.* (2019) 'Terrestrial gross primary production: Using NIRV to scale from site to globe', *Global Change Biology*, 25(11). Available at: https://doi.org/10.1111/gcb.14729.

Berg, S. *et al.* (2019) 'Ilastik: interactive machine learning for (bio) image analysis', *Nature methods*, 16(12), pp. 1226–1232.

Bernacchi, C., Pimentel, C. and Long, S.P. (2003) 'In vivo temperature response functions of parameters required to model RuBP-limited photosynthesis', *Plant, Cell & Environment*, 26(9), pp. 1419–1430.

Billesbach, D.P. *et al.* (2019) 'Effects of the Gill-Solent WindMaster-Pro "w-boost" firmware bug on eddy covariance fluxes and some simple recovery strategies', *Agricultural and Forest Meteorology*, 265, pp. 145–151. Available at: https://doi.org/10.1016/j.agrformet.2018.11.010.

Bonan, G.B. *et al.* (2011) 'Improving canopy processes in the Community Land Model version 4 (CLM4) using global flux fields empirically inferred from FLUXNET data', *Journal of Geophysical Research*, 116(G2). Available at: https://doi.org/10.1029/2010jg001593.

Buchanan, G.M. *et al.* (2021) 'The impact of tree loss on carbon management in West Africa', *Carbon Management*, 12(6), pp. 623–633.

Burton, C., Rifai, S. and Malhi, Y. (2018) 'Inter-comparison and assessment of gridded climate products over tropical forests during the 2015/2016 El Niño', *Philosophical Transactions of the Royal Society B: Biological Sciences*, 373(1760), p. 20170406. Available at: https://doi.org/10.1098/rstb.2017.0406.

Chen, J.M. *et al.* (2022) 'Global datasets of leaf photosynthetic capacity for ecological and earth system research', *Earth System Science Data*, 14(9), pp. 4077–4093. Available at: https://doi.org/10.5194/essd-14-4077-2022.

Chen, M. *et al.* (2017) 'Regional contribution to variability and trends of global gross primary productivity', *Environmental Research Letters*, 12(10), p. 105005.

Chen, Y. *et al.* (2021) 'Improved Global Maps of the Optimum Growth Temperature, Maximum Light Use Efficiency, and Gross Primary Production for Vegetation', *Journal of Geophysical Research: Biogeosciences*, 126(4), p. e2020JG005651. Available at: https://doi.org/10.1029/2020JG005651.

Ciais, P. *et al.* (2014) 'Carbon and other biogeochemical cycles', in *Climate change 2013: the physical science basis. Contribution of Working Group I to the Fifth Assessment Report of the Intergovernmental Panel on Climate Change*. Cambridge University Press, pp. 465–570.

Cornwell, W.K. *et al.* (2016) 'A global dataset of leaf delta 13C values', *Scientific*

Data [Preprint].

De Kauwe, M.G. *et al.* (2016) 'A test of the 'one-point method'for estimating maximum carboxylation capacity from field-measured, light-saturated photosynthesis', *New Phytologist*, 210(3), pp. 1130–1144.

Domingues, T.F. *et al.* (2010) 'Co-limitation of photosynthetic capacity by nitrogen and phosphorus in West Africa woodlands', *Plant, Cell & Environment*, 33(6), pp. 959–980. Available at: https://doi.org/10.1111/J.1365-3040.2010.02119.X.

Dong, N. *et al.* (2022) 'Rising CO2 and warming reduce global canopy demand for nitrogen', *New Phytologist*, 235(5), pp. 1692–1700.

Duursma, R.A. (2015) 'Plantecophys-an R package for analysing and modelling leaf gas exchange data', *PloS one*, 10(11), p. e0143346.

Farquhar, G.D., von Caemmerer, S. and Berry, J.A. (1980) 'A biochemical model of photosynthetic CO2 assimilation in leaves of C3 species', *Planta*, 149(1), pp. 78–90. Available at: https://doi.org/10.1007/BF00386231.

Fensholt, R. and Proud, S.R. (2012) 'Evaluation of Earth Observation based global long term vegetation trends - Comparing GIMMS and MODIS global NDVI time series', *Remote Sensing of Environment*, 119, pp. 131–147. Available at: https://doi.org/10.1016/j.rse.2011.12.015.

Frankenberg, C. *et al.* (2011) 'New global observations of the terrestrial carbon cycle from GOSAT: Patterns of plant fluorescence with gross primary productivity', *Geophysical Research Letters*, 38(17). Available at: https://doi.org/10. 1029/2011G L048738.

Franklin, O. *et al.* (2020) 'Organizing principles for vegetation dynamics', *Nature Plants*, 6(5), pp. 444–453. Available at: https://doi.org/10.1038/s41477-020-0655-x.

Friedlingstein, P. *et al.* (2020) 'Global Carbon Budget 2020', *Earth System Science Data*, 12(4). Available at: https://doi.org/10.5194/essd-12-3269-2020.

Friend, A. (2001) 'Modelling canopy CO2 fluxes: are 'big-leaf'simplifications justified?', *Global Ecology and Biogeography*, 10(6), pp. 603–619.

Fu, Z. *et al.* (2018) 'The surface-atmosphere exchange of carbon dioxide in tropical rainforests: Sensitivity to environmental drivers and flux measurement methodology', *Agricultural and Forest Meteorology*, 263, pp. 292–307. Available at: https://doi.org/10.1016/j.agrformet.2018.09.001.

Fuster, B. *et al.* (2020) 'Quality Assessment of PROBA-V LAI, fAPAR and fCOVER Collection 300 m Products of Copernicus Global Land Service', *Remote Sensing*, 12(6), p. 1017. Available at: https://doi.org/10.3390/rs12061017.

Grace, J. *et al.* (2001) 'Productivity of Tropical Rain Forests', in *Terrestrial Global Productivity*. Available at: https://doi.org/10.1016/b978-012505290-0/50018-1.

Gvozdevaite, A. *et al.* (2018) 'Leaf-level photosynthetic capacity dynamics in relation to soil and foliar nutrients along forest–savanna boundaries in Ghana and Brazil', *Tree Physiology*, 38(12), pp. 1912–1925. Available at: https://doi.org/10.1093/ treephys/tpy117.

Harrison, S.P. *et al.* (2021) 'Eco-evolutionary optimality as a means to improve vegetation and land-surface models', *New Phytologist*, 231(6), pp. 2125–2141. Available at: https://doi.org/10.1111/nph.17558.

Hayek, M.N. *et al.* (2018) 'A novel correction for biases in forest eddy covariance carbon balance', *Agricultural and Forest Meteorology*, 250–251, pp. 90–101. Available at: https://doi.org/10.1016/j.agrformet.2017.12.186.

Hickler, T. *et al.* (2008) 'CO2 fertilization in temperate FACE experiments not representative of boreal and tropical forests', *Global Change Biology*, 14(7). Available at: https://doi.org/10.1111/j.1365-2486.2008.01598.x.

Hilker, T. *et al.* (2008) 'The use of remote sensing in light use efficiency based models of gross primary production: A review of current status and future requirements',

Science of The Total Environment, 404(2–3), pp. 411–423. Available at: https://doi.org/10.1016/j. scitotenv.2007.11.007.

Jin, W. *et al.* (2016) 'Leaf development and demography explain photosynthetic seasonality in Amazon evergreen forests', *Science*, 351(6276), pp. 972–976. Available at: https://doi.org/10.1126/science.aad5068.

Joiner, J. *et al.* (2018) 'Estimation of terrestrial global gross primary production (GPP) with satellite data-driven models and eddy covariance flux data', *Remote Sensing*, 10(9), p. 1346.

Jung, M. *et al.* (2011) 'Global patterns of land-atmosphere fluxes of carbon dioxide, latent heat, and sensible heat derived from eddy covariance, satellite, and meteorological observations', *Journal of Geophysical Research: Biogeosciences*, 116(3). Available at: https://doi.org/10.1029/2010JG001566.

Keenan, T.F. and Niinemets, Ü. (2016) 'Global leaf trait estimates biased due to plasticity in the shade', *Nature Plants*, 3(1), pp. 1–6. Available at: https://doi.org/10.1038/ nplants.2016.201.

Liu, Y.Y. *et al.* (2015) 'Recent reversal in loss of global terrestrial biomass', *Nature Climate Change*, 5(5). Available at: https://doi.org/10.1038/nclimate2581.

Madansky, A. and Alexander, H. (2017) 'Weighted standard error and its impact on significance testing', *The Analytical Group, Inc* [Preprint].

Malhi, Y. *et al.* (2021) 'The Global Ecosystems Monitoring network: Monitoring ecosystem productivity and carbon cycling across the tropics', *Biological Conservation*, 253, p. 108889. Available at: https://doi.org/10.1016/J.BIOCON.2020.108889.

Moore, S. *et al.* (2018) 'Forest biomass, productivity and carbon cycling along a rainfall gradient in West Africa', *Global Change Biology*, 24(2), pp. e496–e510. Available at: https://doi.org/10.1111/gcb.13907.

Morel, A.C. *et al.* (2019) 'Carbon dynamics, net primary productivity and human-appropriated net primary productivity across a forest–cocoa farm landscape in West Africa', *Global Change Biology*, 25(8). Available at: https://doi.org/10.1111/gcb.14661.

Oliveras, I. *et al.* (2020) 'The Influence of Taxonomy and Environment on Leaf Trait Variation Along Tropical Abiotic Gradients', *Frontiers in Forests and Global Change*, 3, p. 18. Available at: https://doi.org/10.3389/FFGC.2020.00018/BIBTEX.

Pan, Y. *et al.* (2011) 'A large and persistent carbon sink in the world's forests', *Science*, 333(6045). Available at: https://doi.org/10.1126/science.1201609.

Pastorello, G. *et al.* (2020) 'The FLUXNET2015 dataset and the ONEFlux processing pipeline for eddy covariance data', *Scientific Data*, 7(1), p. 225. Available at: https://doi.org/10.1038/s41597-020-0534-3.

Peng, Y. *et al.* (2021) 'Global climate and nutrient controls of photosynthetic capacity', *Communications Biology 2021 4:1*, 4(1), pp. 1–9. Available at: https://doi. org/ 10. 1038/ s42003-021-01985-7.

Peng, Y., Bloomfield, K.J. and Prentice, I.C. (2020) 'A theory of plant function helps to explain leaf-trait and productivity responses to elevation', *New Phytologist*, 226(5), pp. 1274–1284. Available at: https://doi.org/10.1111/NPH.16447.

Prentice, I.C. *et al.* (2015) 'Reliable, robust and realistic: The three R's of next-generation land-surface modelling', *Atmospheric Chemistry and Physics*, 15(10), pp. 5987–6005. Available at: https://doi.org/10.5194/ACP-15-5987-2015.

Pugh, T.A.M. *et al.* (2018) 'A Large Committed Long-Term Sink of Carbon due to Vegetation Dynamics', *Earth's Future*, 6(10). Available at: https://doi.org/ 10.1029/2018EF000935.

Rödig, E. *et al.* (2018) 'The importance of forest structure for carbon fluxes of the Amazon rainforest', *Environmental Research Letters*, 13(5), p. 054013. Available at: https://doi.org/10.1088/1748-9326/aabc61.

Rogers, A. *et al.* (2017) 'A roadmap for improving the representation of photosynthesis in Earth system models', *New Phytologist*, 213(1), pp. 22–42. Available at: https://doi.org/10.1111/NPH.14283.

Running, S., Mu, Q. and Zhao, M. (2015) 'MOD17A2H MODIS/Terra Gross Primary Productivity 8-Day L4 Global 500m SIN Grid V006'. NASA EOSDIS Land Processes DAAC. Available at: https://doi.org/10.5067/MODIS/MOD17A2H.006.

Seiler, C. *et al.* (2022) 'Are terrestrial biosphere models fit for simulating the global land carbon sink?', *Journal of Advances in Modeling Earth Systems*, 14(5), p. e2021MS002946.

Smith, N.G. *et al.* (2019) 'Global photosynthetic capacity is optimized to the environment'. Available at: https://doi.org/10.1111/ele.13210.

Stocker, B.D. *et al.* (2020) 'P-model v1.0: An optimality-based light use efficiency model for simulating ecosystem gross primary production', *Geoscientific Model Development*, 13(3), pp. 1545–1581. Available at: https://doi.org/10.5194/GMD-13-1545-2020.

Sudmanns, M. *et al.* (2020) 'Assessing global Sentinel-2 coverage dynamics and data availability for operational Earth observation (EO) applications using the EO-Compass', *International Journal of Digital Earth*, 13(7), pp. 768–784. Available at: https://doi.org/10.1080/17538947.2019.1572799.

Sun, Y. *et al.* (2014) 'Impact of mesophyll diffusion on estimated global land CO2 fertilization', *Proceedings of the National Academy of Sciences*, 111(44), pp. 15774–15779. Available at: https://doi.org/10.1073/pnas.1418075111.

Tian, Z. *et al.* (2023) 'Fusion of multiple models for improving gross primary production estimation with eddy covariance data based on machine learning', *Journal of Geophysical Research: Biogeosciences*, p. e2022JG007122.

Tomlinson, K.W. *et al.* (2013) 'Leaf adaptations of evergreen and deciduous trees of semi-arid and humid savannas on three continents', *Journal of Ecology*, 101(2), pp. 430–440.

Wang, H., Prentice, I.C., Davis, T.W., *et al.* (2017) 'Photosynthetic responses to altitude: an explanation based on optimality principles', *New Phytologist*, 213(3), pp. 976–982. Available at: https://doi.org/10.1111/NPH.14332.

Wang, H., Prentice, I.C., Keenan, T.F., *et al.* (2017) 'Towards a universal model for carbon dioxide uptake by plants', *Nature Plants 2017 3:9*, 3(9), pp. 734–741. Available at: https://doi.org/10.1038/s41477-017-0006-8.

Wang, L. *et al.* (2017) 'Evaluation of the latest MODIS GPP products across multiple biomes using global eddy covariance flux data', *Remote Sensing*, 9(5). Available at: https://doi.org/10.3390/rs9050418.

Weiss, M. and Baret, F. (2017) 'CAN_EYE V6. 4.91 user manual'.

Wood, T.E., Cavaleri, M.A. and Reed, S.C. (2012) 'Tropical forest carbon balance in a warmer world: A critical review spanning microbial- to ecosystem-scale processes', *Biological Reviews*, 87(4). Available at: https://doi.org/10.1111/j.1469-185X.2012.00232.x.

Wullschleger, S.D. *et al.* (2014) 'Plant functional types in Earth system models: past experiences and future directions for application of dynamic vegetation models in high-latitude ecosystems', *Annals of Botany*, 114(1), pp. 1–16. Available at: https://doi.org/10.1093/aob/mcu077.

Xu, L. *et al.* (2015) 'Satellite observation of tropical forest seasonality: spatial patterns of carbon exchange in Amazonia', *Environmental Research Letters*, 10(8), p. 084005.

Yang, R. *et al.* (2022) 'Divergent historical GPP trends among state-of-the-art multi-model simulations and satellite-based products', *Earth System Dynamics*, 13(2). Available

at: https://doi.org/10.5194/esd-13-833-2022.

Zhang, Y. *et al.* (2020) 'Modeling the impacts of diffuse light fraction on photosynthesis in ORCHIDEE (v5453) land surface model', *Geoscientific Model Development*, 13(11), pp. 5401–5423. Available at: https://doi.org/10.5194/gmd-13-5401-2020.

Zhang, Y., Chen, J.M. and Miller, J.R. (2005) 'Determining digital hemispherical photograph exposure for leaf area index estimation', *Agricultural and Forest Meteorology*, 133(1–4), pp. 166–181.

Zhang, Y. and Ye, A. (2021) 'Would the obtainable gross primary productivity (GPP) products stand up? A critical assessment of 45 global GPP products', *Science of The Total Environment*, 783, p. 146965.

Zhao, M. *et al.* (2005) 'Improvements of the MODIS terrestrial gross and net primary production global data set', *Remote Sensing of Environment*, 95(2). Available at: https://doi.org/10.1016/j.rse.2004.12.011.

7 GENERAL DISCUSSION

The discussion first summarises the key points arising from the research conducted in this thesis. It then highlights limitations and points to future research priorities and directions. The thesis ends with a synthesis of key findings and draws some overall conclusions and insights.

7.1 Key findings and implications

7.1.1 Paper 1:

Hypothesis 1: Knowing that along a wet–dry gradient in West Africa there was evidence that NPP was higher than along equivalent gradients in Amazonia (Malhi et al., 2015; Moore et al., 2018), I hypothesised that there would be higher CUE in Africa (i.e., less autotrophic respiration and similar GPP to Amazonia)

I completed the forest carbon budget for the study plots and found generally higher autotrophic respiration, lower CUE and higher GPP in Africa. Previous studies on neotropical and Asian rainforests found that tropical forests had low CUE. The first African forest whole carbon budgets were revealed here, highlighting that tropical forests indeed have generally lower CUE. The hypothesis is rejected.

Hypothesis 2: Variations in both GPP and CUE contribute to explaining the spatial variation in NPP.

Both variations in GPP and CUE contribute to explaining the spatial variation in NPP. In both regions, GPP explains more. However, the variation in CUE is not trivial and needs to be taken into account in vegetation models.

Hypothesis 3: Knowing that GPP declines towards drier sites along aridity gradients in Amazonia, we hypothesised that GPP declines towards drier sites in West African forests.

However, I found that GPP peaked at the mid-aridity sites along the West African aridity gradient. Combining knowledge from Paper 2, the pattern is likely to arise from (1) declining LAI towards drier sites but (2) increasing photosynthesis rate and photosynthesis capacity per leaf area towards the drier sites. See 7.2.2 for more information about the mid-aridity site. The hypothesis is rejected.

Hypothesis 4: At the study site ANK, there are valley swampy forests and upland forests. At site BOB, forests vary from selectively logged 20 to 50 years ago to intact forest; at site KOG, forests transition from mesic savanna to dry forests. I hypothesised that there would be no difference in the carbon budget at any site, but that there would be a difference between sites.

I indeed found no significant differences within sites. The carbon flux partitioning (partition of Ra and NPP into organs) and the magnitude of NPP and GPP differed between sites but were not different within a site. Moreover, there was a large difference between Amazonia forests and West African forests. West African forests consistently allocate more GPP to leaf respiration and canopy NPP. The hypothesis is accepted.

7.1.2 Paper 2:

Question 1: Are photosynthesis rates higher under drier environments, and if so, why do plants growing in drier climates adopt such a photosynthetic strategy?

Yes. Plants grown in drier climates did appear to adopt such a photosynthetic strategy in response to (1) more light and (2) less leaf-internal CO_2. Specifically, high J_{max} (and higher A_J) resulted from acclimation to a brighter environment in drier sites. Less leaf-internal CO_2 is induced by less stomatal conductance (to reduce transpiration). Following the coordination hypothesis (stating that $A_J = A_c$), arid land-grown plants invest in high Vc_{max} (to deal with less ci) to boost A_C to the level of A_J .

Question 2: How is the higher net assimilate rate (photosynthesis) in drier vegetation reconciled with water transportation, given greater water stress in drier places?

Higher transpiration demands in dry sites, compared to wet sites, are met by higher xylem-specific hydraulic conductivity (higher efficiency in water delivery), less stomatal conductance, a lower leaf-to-wood ratio and higher deciduousness. Such a strategy, along with higher photosynthetic capacity, maximises plant per leaf area photosynthesis during periods when plants have adequate access to water (Tomlinson *et al.*, 2013). 'Greater water stress' refers to higher transpiration (water loss) and less precipitation but not necessarily less access to belowground water (see Limitations).

7.1.3 Paper 3:

Question 1: Is there consistency between the values of GPP estimated for these field sites and the in situ measured photosynthetic traits?

Yes, although a slight mismatch was found at the Ankasa site. This provides evidence that both the GEM carbon field measurements and the trait data collections are of adequate quality and that there is indeed unusually high productivity in the studied West African forest study sites.

Question 2: Can vegetation models (both P-model and Trendy) and other GPP products (FLUXCOM and MODIS) simulate the high productivity of West African forests? If not, what leads to the data-model discrepancy?

Models and GPP products underestimate the productivity of West African forests. The underestimation of fAPAR (mostly due to heavy cloudiness) and of light use efficiency (due to underestimated photosynthetic capacity) are the main causes of the data-model discrepancy.

7.2 General Discussions and Limitations

7.2.1 Uncertainty in the field-observed GPP

Although 'field observed' has often been more trusted by researchers over 'model estimated' GPP, there is a certain extent of uncertainty in the 'field observed' GPP.

There are mainly four sources of uncertainty, in my own opinion: (1) respiration; (2) leaf area index; (3) systematic error; and (4) the use of root-shoot ratio to estimate belowground biomass/NPP, and the use of the allometry equation to determine biomass could potentially involve large uncertainty, which has been extensively discussed (Réjou-Méchain *et al.*, 2017; Waring & Powers, 2017) and thus is not explained here.

For respiration, I upscaled leaf dark respiration measurements to the canopy level total respiration using the leaf area index (explained below) and temperature correction (Wang *et al.*, 2020; Mujawamariya *et al.*, 2021), which could have introduced large uncertainty. More factors should be considered but were not due to technical challenges; for example, inhibition of daytime respiration (Keenan *et al.*, 2019). To separate soil respiration into rhizosphere (fine roots) respiration and soil organic matter respiration, the GEM protocol uses 'partitioning experiments', which brings major uncertainty into the estimates of GPP, Ra and CUE (not NPP) (Riutta *et al.*, 2021).

It is very challenging to estimate the leaf area index in dense tropical forests. The key message in the first paper depends strongly on canopy respiration. We were therefore very meticulous about the calculation of canopy respiration as a product of leaf area index (LAI)

and leaf dark respiration. The third paper relies heavily on field-measured fAPAR. It is therefore crucial to minimise uncertainty in field-based LAI and fAPAR. LAI and fAPAR were derived from hemispherical photos (22,000 photos in total), which unfortunately do vary depending on derivation methods. To my knowledge, there is no published hemispherical photo processing protocol designed for tropical forests. I, therefore, tried many methods. Ideally, the leaf area index should (1) decrease towards drier sites and (2) decrease into the dry season, but we did not see such a decrease in the first attempt at leaf area index calculation. The problem lies in the faulty auto threshold for pixel classification in the Hemisfer software. According to the Hemisfer software manual, the problem could be solved by manual visualisation and tuning to ensure a correct threshold. Unfortunately, this was not possible for Ghana because there are too many photos (22000+) to go through manually. I then solved the issues by (1) using the machine learning-based software 'Ilastik' for leaf-sky pixel classification and (2) using CANEYE, which does well in considering the clumping effect, to analyse the classified pictures. The method still works well even though there are strong clumping effects, and photos were taken under varying weather conditions. I also tried other methods of LAI estimate but no satisfactory outcome. For example, LiDAR did not work well due to the super high (40 m+) and multilayer canopy with dense lianas. In addition, LAI derived from litterfall does not make sense due to complicated leaf phenology.

Finally, data digitisation, cleaning, quality control and meta-data archives have often been overlooked, but, in my opinion, they could be the major source of uncertainty. Many methods and codes have been generated to tackle this following applied practice over the past decade. More importantly, these should be recognised in the calculation of 'standard error' for the uncertainty of plot-scale GPP estimates, which should join both systematic error and random errors of each GPP component. I gathered suggestions on (and was taught) GEM data processing remotely by many senior researchers in the lab during the

pandemic. These efforts form the basis of the first paper. To benefit future researchers (also as a way of expressing my gratitude to former lab members), I compiled their code and hope to revise the GEM protocol by adding information on raw data cleaning, calculation, quality control, and uncertainty propagation.

Future researchers are encouraged to work on the above four sources of uncertainty, which will substantially improve the credibility of forest-inventory-based GPP estimates.

7.2.2 How could Bobiri forests be the most productive tropical forests, even under the challenge of aridity

To the author's knowledge, the GPP and NPP measured at plot BOB-02 (within site Bobiri) are the highest for intact forest records to date, saving that logged Malaysian forests have higher NPP reported (Riutta *et al.*, 2018). The explanation of Bobiri forest productivity (as in the Synthesis of thesis) was only briefly touched upon in the discussion of Paper 1 and Paper 3, but the comparison of traits between Bobiri and other tropical forests was not done. Future researchers could compare the plant functional traits of the Bobiri forest to those of pantropical and global histograms, which could provide a comprehensive explanation of Bobiri forest productivity from a physiological perspective.

Paper 2 explains that near drier tropical sites[3], plants appear to have a higher net assimilation rate (photosynthesis per leaf area) and higher photosynthetic capacity, but they have less stomatal conductance, a lower leaf area index (Figure 1 in Paper 2) and more deciduousness (less time for photosynthesis). As a result, the mid-aridity site is the most productive.

Paper 1 shows that along the West African aridity gradient, the mid-aridity site is more productive than the wettest site, which has similar productivity to the wet evergreen lowland Amazonia sites. The mid-aridity site is very productive because it has not only a

[3] See Paper 2 for hydraulic modelling and definition of aridity. In our study region, the dry site has high air dryness and low soil moisture, but no information is available on belowground water table.

low fAPAR (or LAI) but also very high light use efficiency [4](i.e., high photosynthetic capacity and high net assimilation rate), which together fixed a large amount of carbon. The large amount of carbon fixed is then predominantly allocated to leaves (Paper 1) to enable quick leaf replacement (i.e., approximately 5 months leaf lifespan) (Moore *et al.*, 2018), which allows semideciduous phenology. Phenology, in turn, reduces hydraulic pressure (allowing higher stomatal conductance), and younger leaves have higher photosynthetic capacity (Jin *et al.*, 2016). Paper 3 also shows that field-sampled photosynthetic traits are consistent with the measured high productivity of the studied forests.

The above explanation of Bobiri forest productivity did not consider environmental constraints. First, Paper 1 presents West African and Amazonia forests along aridity gradients (ranked by air dryness and precipitation), but West African forests might have ample belowground water access (depending on rooting depth) or more soil vegetation available water (depending on soil characteristics). Future researchers are encouraged to investigate belowground water table and plants rooting depth at these sites. Predawn and midday leaf water potential data (not included in Paper 2) can shed light on the plant's access to belowground water (Ding *et al.*, 2021). Second, rapid carbon cycling and leaf replacement require the support of nutrients, but I have not discussed the difference in soil nutrients between West African and Amazonia sites, although data were presented in Paper 1 Table S2. It is shown in Table S2 that Bobiri forests soil has substantially higher carbon exchange capacity than Amazonia forests soil. I surmise that it should link with Harmattan (West Africa trade wind) and Sahara dust deposition (Caton Harrison *et al.*, 2021) where further investigation is needed. Third, the special carbon strategy and phenology may also be a legacy of a historical climate drier than Holocene (See 7.2.3).

[4] The explanation follows light use efficiency model structure, where GPP = LUE * fAPAR * PPFD. This methods of GPP calculation is adopted

7.2.3 Is West African forest semievergreen or semideciduous?

In this thesis, West African forests are frequently referred to as "semideciduous" without providing further information, primarily due to the author's limited knowledge of West African phenology. Compared to lowland Amazonia forests (>12 months leaf lifespan), West African forests have shorter leaf longevity of approximately 5 months. However, except for the driest plots in Kogaye, these forests remain green throughout the year, and the leaf area index varies only between 4 and 5 (unpublished data). Note that wet evergreen Amazonia rainforests have leaf area index of around 5 (Malhi *et al.*, 2009). It is plausible that leaves are growing and dying at any time of the year, with a greater growth rate in the summer season.

In the literature, the term ‘semideciduous’ has been used in many field studies from Central and South America (Daubenmire, 1972; Morellato *et al.*, 2013) and Australia (Myers *et al.*, 1997) since the 1970s. However, there is no clear definition. Semideciduous forest was defined as ‘20–50% of tree species losing their leaves during alternating dry and wet periods’ (Lisi *et al.*, 2008) and semideciduous species is ‘a species in which canopy fell to below 50% of full canopy in each of the dry seasons’ (Williams *et al.*, 1997), while many studies use the term without prior definition (apologies, as the term is also used in my thesis without pre-definition). Apparently, both definitions do not cover West African forests.

If West African forests do have suitable temperatures and soil moisture to be considered evergreen, why are they green due to quickly replacing leaves? How does the phenology of West African forests differ from that of other tropical ‘semideciduous’ forests and from that of wet evergreen lowland Amazonia forests? Could this be linked to the monsoon climate with two rainy seasons, ample soil nutrient availability, or palaeoclimate dating back to approximately 32 ka BP when West Africa was believed to have been entirely savanna (Allen *et al.*, 2020).

Seasonal variation in the leaf area index, litterfall, dendrometer (seasonal stem growth), and leaf water potential will be required to reveal the phenology of these forests. Leaf longevity of leaves under both sun and shade will also be useful to investigate, as I also observed when I was in the field during the driest months that abscission is on the leaves under shade.

Confusingly, there is no 'semideciduous' biome in the models. Instead, since the first generation of models, there have been 'evergreen', 'raingreen' (phenology responses to soil moisture) to 'summer green' (phenology depends on temperature) phenology (Bondeau *et al.*, 1999; Allen *et al.*, 2020). Temperate deciduous forests could be well represented with 'summer green'. 'Raingreen' was frequently associated with 'Tropical deciduous forest biome' However, 'raingreen' may not correspond to semi-deciduous (Bonan *et al.*, 2003; Sitch *et al.*, 2003), and there is large intermodel disagreement over 'raingreen' areas (Bondeau *et al.*, 1999).

In models, the simulated biome 'Tropical Raingreen Forest' covers a land area as large as 'Tropical Evergreen Forest', especially on the African continent (Allen *et al.*, 2020). After revealing the driving environmental factors of West African phenology, we could then propose a model simulation approach that fits field observations.

7.2.4 whether the findings from Ghana can be applied to other African forests

It is highly possible that the findings in Paper 3 are applicable to other African forests (see discussion in paper 3). The trend of traits along aridity gradient revealed in Paper 2 should be applicable to other broadleaf forests as theoretically expected by Optimality theory. Although it is possible that traits measured at Ghanaian forests are applicable to other Upper Guinea Forests given similarity in common species (Hawthorne & Jongkind, 2006), plants functional traits should be rather different between Upper and Lower Guinea Forests (Aguirre-Gutiérrez *et al.*, 2021). I have already known that the productivity, carbon

allocation, and NPP partitioning are very contrasting between Upper and Lower Guinea forests (unpublished results). Moreover, findings from the studied forests would not represent other African ecosystems including swamp forest, highland forests, forests with abundant palms (Bocko *et al.*, 2023), mangrove (Feka & Ajonina, 2011) and sparse savanna.

Moreover, the thesis focused on spatial variation only, without time-series data presented. The spatial variation revealed how plants adapted to different growth environments in the past and highlighted the present diverse forests biogeography. I have been very cautious in making temporal inference from the findings in the thesis. There are ongoing debates on whether such 'Space for Time substation' should be applied in climate change ecology (Pickett, 1989; Blois *et al.*, 2013; Damgaard, 2019), but at least for West African forests specifically, the short term (several years) response to drought was found different to long term (two decades) response to aridity (Fauset *et al.*, 2012). Therefore, it is unlikely that the variation along the aridity gradient in this thesis could inform effect of climate change.

7.3 Concluding remark

The thesis presents the first full carbon budget of African forests and shows how these forests diverge from previously studied sites in Amazonia (paper 1), and also diverge from model predictions and satellite estimates (paper 3). The study sheds light on the unique characteristics of West African forests, including their distinct carbon budget and photosynthesis strategy (Paper 2). These forests exhibit higher productivity, lower carbon use efficiency, and greater allocation of GPP to leaves compared to other tropical forests. Notably, the thesis also reports the most productive (both NPP and GPP) intact forests measured to date – Bobiri forests in Ghana, West Africa.

The depth of the thesis lies in that it not only reports productivity but also explains the physiological 'why' behind high productivity (See 7.2.2) and reveals why it has been underestimated in the literature (Paper 3). However, fAPAR was underestimated due to heavy cloudiness in the region (Paper 3), and LUE was also underestimated, which may be associated with the scarcity of field measurements. Therefore, GPP was severely underestimated in many models.

Nonetheless, it is important to acknowledge that the study sites in Ghana may not fully represent the carbon budgets and photosynthesis strategies of all African tropical forests. By highlighting the uniqueness of West African forests, the study calls for further research into this poorly studied ecosystem (see Introduction). It is important to note that West African forests are highly fragmented and are still experiencing tree loss (Buchanan *et al.*, 2021), as exemplified by the most productive study site, Bobiri, which now only covers an area of 54 km^2. Urgent conservation action is needed to protect this biomass-rich (Cuni-Sanchez *et al.*, 2021), highly productive (this study) and biodiverse forest (Luiselli *et al.*, 2019).

7.4 Future research directions:

7.4.1 West African forest carbon budget before and after the El Niño drought event

(Bennett *et al.*, 2021) suggested that African forests are more resistant to drought than other tropical forests, which is likely linked to the long history of greater climatic variation in the African tropics compared to in Amazonia. However, the study was conducted using mortality rate and stem biomass only. It is not known how forest NPP and GPP respond to extreme drought. An extreme drought event occurred at the end of 2015. Paper 1 used data from all available years (2012 to 2016) without investigating the effect of extreme drought

due to data quality issues. Since semideciduous forests may be more resistant to drought events than evergreen forests, an investigation into the impact of drought on carbon cycling in the study region could yield valuable ecological insights.

7.4.2 How does GPP vary along tropical aridity gradients?

Paper 3 focused on the magnitude of GPP but not the variation in GPP along the aridity gradient. I decided to avoid discussing variation along the aridity gradient because there are only three sites that are insufficient to form a trend (see Method for study scales). It was hinted in Paper 1 and 3 that from wet to dry tropical sites, photosynthetic capacity and net assimilation rate per leaf area increase, but leaf area index and leaf internal CO_2 concentration decrease. As a result, GPP peaks at the mid-aridity site. Further research extending the West African aridity gradient into northern Ghana or incorporating data from other tropical aridity gradients will have a great potential to real how aridity drive spatial variation of tropical GPP.

Moreover, P-model (the optimality theory-based model) does estimate an increase in Vc_{max} and J_{max} towards drier sites, and the pattern arises from brighter light, more than from higher VPD. The relative importance of VPD and light in regulating photosynthesis traits along an aridity gradient could be tested by comparing leaves under sun to leaves under shade, which would deepen the investigation. P-model could be used to predict Vc_{max}, J_{max}, A_{sat} and A_{max} (a method was proposed in Paper 3 supplementary), but further investigation is needed to distinguish modelled sun and shade leaves.

7.4.3 Do West African forests have a higher land carbon sink than Amazonia?

As the first paper quantifies the whole carbon budget, the dataset also includes the land carbon sink (i.e., net ecosystem exchange) estimates. However, Paper 1 does not report or discuss the land carbon sink of forests because there is high uncertainty. At the moment, the land carbon sink is calculated as (Mills *et al.*, 2023):

land carbon sink, or net ecosystem exchange = NPP – soil respiration * percentage of heterotrophic,

where the percentage has dominating uncertainty. To avoid the percentage of heterotrophic respiration, future researchers could try to calculate land carbon sink = NPP – SOM decomposition respiration. Soil organic matter (SOM) decomposition respiration is a special measurement in the GEM protocol, using a long soil respiration collar without roots inside. Using such a special respiration collar may largely constraint uncertainty in net ecosystem exchange because it bypasses other highly uncertain measurements of respiration (e.g., leaf respiration). Another way forward would be to calculate the carbon sink in the stem, which depends only on 'census data' with high credibility. One could also compare net ecosystem exchange from Ankasa (West African site) flux towers to lowland Amazonia flux towers. In short, the four sets of data discussed above, if a future researcher could compile, have high potential to shed light on the West African forestland carbon sink in comparison to Amazonia.

7.4.4 Pantropical GPP data-model comparison

Paper 3 presents a method to calculate GPP from A_{sat} and A_{max} measurements (i.e., experiment P-model_PfL, details provided in the Methods section of Paper 3) using equations migrated from P-model. The study yielded insight into the data-model discrepancy of GPP of West African forests and revealed consistency between photosynthesis traits and GPP measurements. The success in Ghana hints that future researchers could attempt the method, again with a focus on the magnitude of GPP, but on more tropical sites. As mentioned in the discussion section of Paper 3, previous studies also reported a data-model discrepancy for multiple Amazon forest sites which open a large research gap.

7.4.5 Biomass-oriented carbon credits could miss the most productive forests in the tropics.

Net primary productivity (NPP) measures the amount of energy that a forest harness and become available to other creatures, and thus nourish biodiversity. Moreover, net ecosystem productivity (NEP) measures the amount of carbon that an ecosystem sequesters from the atmosphere, and thus decelerate global warming. However, despite the importance of NEP and NPP, carbon benefits or carbon credits currently considered in forest conservation plan mostly refer to biomass, instead of NEP nor NPP. (Fu *et al.*, 2018) showed that across many tropical flux towers, NEP is largest at lower GPP and lower biomass sites. I also found, among our study sites, biomass do not correlate with NPP (Figure 2 in Paper 1). Evidently, one could surmise that in both tropical flux tower networks and in GEM, there will be a negative (or lack of) correlation between biomass and NPP or NEE. If so, a warning siren will sound on biomass-oriented carbon credits as it will miss the forests that provide most ongoing carbon benefits.

7.4.6 Data-model comparison for tropical autotrophic respiration

Paper 2 mentioned CUE in the Introduction. However, current vegetation models do not have a parameter named 'CUE', but they first calculate GPP, then 'maintenance respiration' and 'growth respiration', whose sum is autotrophic respiration. Then, NPP was calculated as GPP – autotrophic respiration. However, there is not much field evidence supporting such a simulation where the GEM dataset could be used for data-model comparison.

7.4.7 The cocoa farms around Bobiri forest and in Kakum Ghana

I was very surprised when I found most models are simulating cocoa farms as being as productive as Bobiri forests (the most productive forests), because of the very high photosynthesis capacity of 'C3 Agricultural land' and 'C4 grassland' (Figure S4, Paper 3).

In fact, field studies have shown that cocoa farms can have even higher net primary productivity (NPP) than Bobiri and Kakum forests (Morel *et al.*, 2019), suggesting their potential for carbon offsetting if properly managed. The study showed large human-appropriate NPP (HANPP) because of (1) higher total NPP than adjacent forests and (2) large carbon flow belowground via cocoa fruit deposition. However, for cocoa farms to be carbon positive (i.e., carbon flowing from the atmosphere to the land), heterotrophic respiration needs to be smaller than NPP. Unfortunately, there are currently no measurements of net ecosystem exchange or respiration for cocoa farms, making it a potential area for future research.

8 REFERENCES FOR INTRODUCTION AND DISCUSSION

Abbas S, Wong MS, Wu J, Shahzad N, Muhammad Irteza S. **2020**. Approaches of Satellite Remote Sensing for the Assessment of Above-Ground Biomass across Tropical Forests: Pan-tropical to National Scales. *Remote Sensing* **12**: 3351.

Aguirre-Gutiérrez J, Rifai S, Shenkin A, Oliveras I, Bentley LP, Svátek M, Girardin CAJ, Both S, Riutta T, Berenguer E, *et al.* 2021. Pantropical modelling of canopy functional traits using Sentinel-2 remote sensing data. *Remote Sensing of Environment* **252**: 112122.

Allen JR, Forrest M, Hickler T, Singarayer JS, Valdes PJ, Huntley B. **2020**. Global vegetation patterns of the past 140,000 years. *Journal of Biogeography* **47**: 2073–2090.

Anav A, Friedlingstein P, Beer C, Ciais P, Harper A, Jones C, Murray-Tortarolo G, Papale D, Parazoo NC, Peylin P, *et al.* 2015. Spatiotemporal patterns of terrestrial gross primary production: A review. *Reviews of Geophysics* **53**.

Anderson-Teixeira KJ, Davies SJ, Bennett AC, Gonzalez-Akre EB, Muller-Landau HC, Joseph Wright S, Abu Salim K, Almeyda Zambrano AM, Alonso A, Baltzer JL. **2015**. CTFS-Forest GEO: a worldwide network monitoring forests in an era of global change. *Global change biology* **21**: 528–549.

Anderson-Teixeira KJ, Herrmann V, Morgan RB, Bond-Lamberty B, Cook-Patton SC, Ferson AE, Muller-Landau HC, Wang MMH. **2021**. Carbon cycling in mature and regrowth forests globally. *Environmental Research Letters* **16**.

Anderson-Teixeira KJ, Wang MMH, Mcgarvey JC, Lebauer DS. **2016**. Carbon dynamics of mature and regrowth tropical forests derived from a pantropical database (TropForC-db). *Global Change Biology* **22**: 1690–1709.

Appiah D, Osman B, Boafo J. **2014**. Land Use and Misuse; Human Appropriation of Land Ecosystems Services in Ghana. *International Journal of Ecosystem* **4**: 24–33.

Ardö J. **2015**. Comparison between remote sensing and a dynamic vegetation model for estimating terrestrial primary production of Africa. *Carbon Balance and Management* **10**.

Babst F, Friend AD, Karamihalaki M, Wei J, von Arx G, Papale D, Peters RL. **2021**. Modeling Ambitions Outpace Observations of Forest Carbon Allocation. *Trends in Plant Science* **26**.

Badgley G, Anderegg LDL, Berry JA, Field CB. **2019**. Terrestrial gross primary production: Using NIRV to scale from site to globe. *Global Change Biology* **25**.

Bahar NHA, Ishida FY, Weerasinghe LK, Guerrieri R, O'Sullivan OS, Bloomfield KJ, Asner GP, Martin RE, Lloyd J, Malhi Y, *et al.* 2017. Leaf-level photosynthetic capacity in lowland Amazonian and high-elevation Andean tropical moist forests of Peru. *New Phytologist* **214**: 1002–1018.

Bauman D, Fortunel C, Delhaye G, Malhi Y, Cernusak LA, Bentley LP, Rifai SW, Aguirre-Gutiérrez J, Menor IO, Phillips OL, *et al.* 2022. Tropical tree mortality has increased with rising atmospheric water stress. *Nature*.

Bennett AC, Dargie GC, Cuni-Sanchez A, Mukendi JT, Hubau W, Mukinzi JM, Phillips OL, Malhi Y, Sullivan MJP, Cooper DLM, *et al.* 2021. Resistance of African tropical forests to an extreme climate anomaly. *Proceedings of the National Academy of Sciences of the United States of America* **118**.

Blois JL, Williams JW, Fitzpatrick MC, Jackson ST, Ferrier S. **2013**. Space can substitute for time in predicting climate-change effects on biodiversity. *Proceedings of the National Academy of Sciences* **110**: 9374–9379.

Blundo C, Carilla J, Grau R, Malizia A, Malizia L, Osinaga-Acosta O, Bird M, Bradford M, Catchpole D, Ford A. **2021**. Taking the pulse of Earth's tropical forests using networks of highly distributed plots. *Biological Conservation* **260**: 108849.

Bocko YE, Panzou GJL, Dargie GC, Mampouya YEW, Mbemba M, Loumeto JJ, Lewis SL. **2023**. Allometric equation for Raphia laurentii De Wild, the commonest palm in the central Congo peatlands. *Plos one* **18**: e0273591.

Bonan GB, Lawrence PJ, Oleson KW, Levis S, Jung M, Reichstein M, Lawrence DM, Swenson SC. **2011**. Improving canopy processes in the Community Land Model version 4 (CLM4) using global flux fields empirically inferred from FLUXNET data. *Journal of Geophysical Research* **116**.

Bonan GB, Levis S, Sitch S, Vertenstein M, Oleson KW. **2003**. A dynamic global vegetation model for use with climate models: concepts and description of simulated vegetation dynamics. *Global Change Biology* **9**: 1543–1566.

Bondeau A, Kicklighter D, Kaduk J, Intercomparison TPOTPNM. **1999**. Comparing global models of terrestrial net primary productivity (NPP): importance of vegetation structure on seasonal NPP estimates. *Global Change Biology* **5**: 35–45.

Bousquet P, Peylin P, Ciais P, Le Quere C, Friedlingstein P, Tans PP. **2000**. Regional changes in carbon dioxide fluxes of land and oceans since 1980. *Science* **290**.

Bouvet A, Mermoz S, Le Toan T, Villard L, Mathieu R, Naidoo L, Asner GP. **2018**. An above-ground biomass map of African savannahs and woodlands at 25 m resolution derived from ALOS PALSAR. *Remote sensing of environment* **206**: 156–173.

Brodribb TJ. **2009**. Xylem hydraulic physiology: the functional backbone of terrestrial plant productivity. *Plant Science* **177**: 245–251.

Buchanan GM, Field RH, Bradbury RB, Luraschi B, Vickery JA. **2021**. The impact of tree loss on carbon management in West Africa. *Carbon Management* **12**: 623–633.

Cai W, Prentice IC. **2020**. Recent trends in gross primary production and their drivers: analysis and modelling at flux-site and global scales. *Environmental Research Letters* **15**: 124050.

Canadell JG, Monteiro PMS, Costa MH, Cunha LC da, Cox PM, Eliseev AV, Henson S, Ishii M, Jaccard S, Koven C, *et al.* 2021. Global carbon and other biogeochemical cycles and feedbacks. In: Climate Change 2021: The Physical Science Basis. Contribution of Working Group I to the Sixth Assessment Report of the Intergovernmental Panel on Climate Change.

Caton Harrison T, Washington R, Engelstaedter S, Jones RG, Savage NH. **2021**. Influence of Orography Upon Summertime Low-Level Jet Dust Emission in the Central and Western Sahara. *Journal of Geophysical Research: Atmospheres* **126**.

Chiti T, Certini G, Grieco E, Valentini R. **2010**. The role of soil in storing carbon in tropical rainforests: The case of Ankasa Park, Ghana. *Plant and Soil* **331**: 453–461.

Ciais P, Sabine C, Bala G, Bopp L, Brovkin V, Canadell J, Chhabra A, DeFries R, Galloway J, Heimann M. **2014**. Carbon and other biogeochemical cycles. In: Climate change 2013: the physical science basis. Contribution of Working Group I to the Fifth Assessment Report of the Intergovernmental Panel on Climate Change. Cambridge University Press, 465–570.

Cleveland CC, Taylor P, Chadwick KD, Dahlin K, Doughty CE, Malhi Y, Smith WK, Sullivan BW, Wieder WR, Townsend AR. **2015**. A comparison of plot-based satellite and Earth system model estimates of tropical forest net primary production. *Global Biogeochemical Cycles* **29**: 626–644.

Collalti A, Ibrom A, Stockmarr A, Cescatti A, Alkama R, Fernández-Martínez M, Matteucci G, Sitch S, Friedlingstein P, Ciais P, *et al.* 2020. Forest production efficiency increases with growth temperature. *Nature Communications* **11**.

Corlett RT. **2016**. The impacts of droughts in tropical forests. *Trends in plant science* **21**: 584–593.

Cox PM, Betts RA, Jones CD, Spall SA, Totterdell IJ. **2000**. Acceleration of global warming due to carbon-cycle feedbacks in a coupled climate model. *Nature* **408**.

Cox PM, Pearson D, Booth BB, Friedlingstein P, Huntingford C, Jones CD, Luke CM. **2013**. Sensitivity of tropical carbon to climate change constrained by carbon dioxide variability. *Nature* **494**.

Cuni-Sanchez A, Sullivan MJ, Platts PJ, Lewis SL, Marchant R, Imani G, Hubau W, Abiem I, Adhikari H, Albrecht T. **2021**. High aboveground carbon stock of African tropical montane forests. *Nature* **596**: 536–542.

Damgaard C. **2019**. A critique of the space-for-time substitution practice in community ecology. *Trends in ecology & evolution* **34**: 416–421.

Daubenmire R. **1972**. Phenology and other characteristics of tropical semi-deciduous forest in north-western Costa Rica. *The Journal of Ecology*: 147–170.

Deans RM, Brodribb TJ, Busch FA, Farquhar GD. **2020**. Optimization can provide the fundamental link between leaf photosynthesis, gas exchange and water relations. *Nature Plants* **6**: 1116–1125.

Ding Y, Nie Y, Chen H, Wang K, Querejeta JI. **2021**. Water uptake depth is coordinated with leaf water potential, water-use efficiency and drought vulnerability in karst vegetation. *New Phytologist* **229**: 1339–1353.

Domingues TF, Meir P, Feldpausch TR, Saiz G, Veenendaal EM, Schrodt F, Bird M, Djagbletey G, Hien F, Compaore H, *et al.* 2010. Co-limitation of photosynthetic capacity by nitrogen and phosphorus in West Africa woodlands. *Plant, Cell & Environment* **33**: 959–980.

Dong N, Wright IJ, Chen JM, Luo X, Wang H, Keenan TF, Smith NG, Prentice IC. **2022**. Rising CO2 and warming reduce global canopy demand for nitrogen. *New Phytologist* **235**: 1692–1700.

Doughty R, Kurosu TP, Parazoo N, Köhler P, Wang Y, Sun Y, Frankenberg C. **2022**. Global GOSAT, OCO-2, and OCO-3 solar-induced chlorophyll fluorescence datasets. *Earth System Science Data* **14**: 1513–1529.

Enquist BJ, Bentley LP, Shenkin A, Maitner B, Savage V, Michaletz S, Blonder B, Buzzard V, Espinoza TEB, Farfan-Rios W, *et al.* 2017. Assessing trait-based scaling theory in tropical forests spanning a broad temperature gradient. *Global Ecology and Biogeography* **26**: 1357–1373.

Farquhar GD, von Caemmerer S, Berry JA. **1980**. A biochemical model of photosynthetic CO2 assimilation in leaves of C3 species. *Planta* **149**: 78–90.

Fattore F, Bertolini T, Materia S, Gualdi S, Thongo M'Bou A, Nicolini G, Valentini R, De Grandcourt A, Tedesco D, Castaldi S. **2014**. Seasonal trends of dry and bulk concentration of nitrogen compounds over a rain forest in Ghana. *Biogeosciences* **11**.

Fauset S, Baker TR, Lewis SL, Feldpausch TR, Affum-Baffoe K, Foli EG, Hamer KC, Swaine MD. **2012**. Drought-induced shifts in the floristic and functional composition of tropical forests in Ghana. *Ecology letters* **15**: 1120–1129.

Feka NZ, Ajonina GN. **2011**. Drivers causing decline of mangrove in West-Central Africa: a review. *International Journal of Biodiversity Science, Ecosystem Services & Management* **7**: 217–230.

Fensholt R, Proud SR. **2012**. Evaluation of Earth Observation based global long term vegetation trends - Comparing GIMMS and MODIS global NDVI time series. *Remote Sensing of Environment* **119**: 131–147.

Flack-Prain S, Meir P, Malhi Y, Smallman TL, Williams M. **2019**. Leaf Area Index Changes Explain GPP Variation across an Amazon Drought Stress Gradient. *Biogeosciences Discussions*.

Forkuor G, Zoungrana J-BB, Dimobe K, Ouattara B, Vadrevu KP, Tondoh JE. **2020**. Above-ground biomass mapping in West African dryland forest using Sentinel-1 and 2 datasets-A case study. *Remote Sensing of Environment* **236**: 111496.

Frankenberg C, Fisher JB, Worden J, Badgley G, Saatchi SS, Lee JE, Toon GC, Butz A, Jung M, Kuze A, *et al.* 2011. New global observations of the terrestrial carbon cycle from GOSAT: Patterns of plant fluorescence with gross primary productivity. *Geophysical Research Letters* **38**.

Franklin O, Harrison SP, Dewar R, Farrior CE, Brännström Å, Dieckmann U, Pietsch S, Falster D, Cramer W, Loreau M, *et al.* 2020. Organizing principles for vegetation dynamics. *Nature Plants* **6**: 444–453.

Friedlingstein P, Jones MW, O'Sullivan M, Andrew RM, Hauck J, Peters GP, Peters W, Pongratz J, Sitch S, Le Quéré C, *et al.* 2019. Global carbon budget 2019. *Earth System Science Data* **11**.

Friedlingstein P, O'Sullivan M, Jones MW, Andrew RM, Hauck J, Olsen A, Peters GP, Peters W, Pongratz J, Sitch S, *et al.* 2020. Global Carbon Budget 2020. *Earth System Science Data* **12**.

Fu Z, Gerken T, Bromley G, Araújo A, Bonal D, Burban B, Ficklin D, Fuentes JD, Goulden M, Hirano T, *et al.* 2018. The surface-atmosphere exchange of carbon dioxide in tropical rainforests: Sensitivity to environmental drivers and flux measurement methodology. *Agricultural and Forest Meteorology* **263**: 292–307.

Fuster B, Sánchez-Zapero J, Camacho F, García-Santos V, Verger A, Lacaze R, Weiss M, Baret F, Smets B. **2020**. Quality Assessment of PROBA-V LAI, fAPAR and fCOVER Collection 300 m Products of Copernicus Global Land Service. *Remote Sensing* **12**: 1017.

Fyllas NM, Bentley LP, Shenkin A, Asner GP, Atkin OK, Díaz S, Enquist BJ, Farfan-Rios W, Gloor E, Guerrieri R, *et al.* 2017. Solar radiation and functional traits explain the decline of forest primary productivity along a tropical elevation gradient. *Ecology Letters* **20**: 730–740.

Gillman LN, Wright SD, Cusens J, Mcbride PD, Malhi Y, Whittaker RJ. **2015**. Latitude, productivity and species richness. *Global Ecology and Biogeography* **24**: 107–117.

Goetz SJ, Baccini A, Laporte NT, Johns T, Walker W, Kellndorfer J, Houghton RA, Sun M. **2009**. Mapping and monitoring carbon stocks with satellite observations: a comparison of methods. *Carbon balance and management* **4**: 1–7.

Grace J, Malhi Y, Meir P, Higuchi N. **2001**. Productivity of Tropical Rain Forests. In: Terrestrial Global Productivity.

Green JK, Berry J, Ciais P, Zhang Y, Gentine P. **2020**. Amazon rainforest photosynthesis increases in response to atmospheric dryness. *Science Advances* **6**.

Grossiord C, Buckley TN, Cernusak LA, Novick KA, Poulter B, Siegwolf RTW, Sperry JS, McDowell NG. **2020**. Plant responses to rising vapor pressure deficit. *New Phytologist* **226**: 1550–1566.

Gvozdevaite A. **2018**. The role of economic, venation and morphological leaf traits in plant and ecosystem function along forest-savanna gradients in the tropics.

Gvozdevaite A, Oliveras I, Domingues TF, Peprah T, Boakye M, Afriyie L, da Silva Peixoto K, de Farias J, Almeida de Oliveira E, Almeida Farias CC, *et al.* 2018. Leaf-level photosynthetic capacity dynamics in relation to soil and foliar nutrients along forest–savanna boundaries in Ghana and Brazil. *Tree Physiology* **38**: 1912–1925.

Gyamfi-Ampadu E, Gebreslasie M. **2021**. Two Decades Progress on the Application of Remote Sensing for Monitoring Tropical and Sub-Tropical Natural Forests: A Review. *Forests* **12**: 739.

Hardy OJ, Born C, Budde K, Daïnou K, Dauby G, Duminil J, Ewédjé E-EBK, Gomez C, Heuertz M, Koffi GK, *et al.* 2013. Comparative phylogeography of African rain forest trees: A review of genetic signatures of vegetation history in the Guineo-Congolian region. *Comptes Rendus Geoscience* **345**: 284–296.

Harrison SP, Cramer W, Franklin O, Prentice IC, Wang H, Brännström Å, de Boer H, Dieckmann U, Joshi J, Keenan TF, *et al.* 2021. Eco-evolutionary optimality as a means to improve vegetation and land-surface models. *New Phytologist* **231**: 2125–2141.

Hawthorne WD, Jongkind CC. **2006**. *Woody plants of Western African forests, A guide to the forest trees, shrubs and lianes from Senegal to Ghana*. Royal Botanic Gardens, Kew.

Hickler T, Smith B, Prentice IC, Mjöfors K, Miller P, Arneth A, Sykes MT. **2008**. CO2 fertilization in temperate FACE experiments not representative of boreal and tropical forests. *Global Change Biology* **14**.

Hubau W, Lewis SL, Phillips OL, Affum-Baffoe K, Beeckman H, Cuní-Sanchez A, Daniels AK, Ewango CEN, Fauset S, Mukinzi JM. **2020**. Asynchronous carbon sink saturation in African and Amazonian tropical forests. *Nature* **579**: 80–87.

Jiang C, Ryu Y, Wang H, Keenan TF. **2020**. An optimality-based model explains seasonal variation in C3 plant photosynthetic capacity. *Global Change Biology* **26**: 6493–6510.

Jin W, P. AL, P. LA, Natalia R-C, Matthew H, T. WK, Kaiyu G, C. SS, Bradley C, Neill P, *et al.* 2016. Leaf development and demography explain photosynthetic seasonality in Amazon evergreen forests. *Science* **351**: 972–976.

Joshi J, Stocker BD, Hofhansl F, Zhou S, Dieckmann U, Prentice IC. 2022. Towards a unified theory of plant photosynthesis and hydraulics. *Nature Plants* **8**: 1304–1316.

Jung M, Koirala S, Weber U, Ichii K, Gans F, Camps-Valls G, Papale D, Schwalm C, Tramontana G, Reichstein M. 2019. The FLUXCOM ensemble of global land-atmosphere energy fluxes. *Scientific Data* **6**: 74.

Jung M, Reichstein M, Margolis HA, Cescatti A, Richardson AD, Arain MA, Arneth A, Bernhofer C, Bonal D, Chen J, *et al.* 2011. Global patterns of land-atmosphere fluxes of carbon dioxide, latent heat, and sensible heat derived from eddy covariance, satellite, and meteorological observations. *Journal of Geophysical Research: Biogeosciences* **116**.

Kattge J, Bönisch G, Díaz S, Lavorel S, Prentice IC, Leadley P, Tautenhahn S, Werner GD, Aakala T, Abedi M. 2020. TRY plant trait database–enhanced coverage and open access. *Global change biology* **26**: 119–188.

Keenan TF, Migliavacca M, Papale D, Baldocchi D, Reichstein M, Torn M, Wutzler T. 2019. Widespread inhibition of daytime ecosystem respiration. *Nature Ecology and Evolution* **3**: 407–415.

Koch B. 2010. Status and future of laser scanning, synthetic aperture radar and hyperspectral remote sensing data for forest biomass assessment. *ISPRS Journal of Photogrammetry and Remote sensing* **65**: 581–590.

Laurin GV, Chen Q, Lindsell JA, Coomes DA, Del Frate F, Guerriero L, Pirotti F, Valentini R. 2014. Above ground biomass estimation in an African tropical forest with lidar and hyperspectral data. *ISPRS Journal of Photogrammetry and Remote Sensing* **89**: 49–58.

Lisi CS, Fo MT, Botosso PC, Roig FA, Maria VR, Ferreira-Fedele L, Voigt AR. 2008. Tree-ring formation, radial increment periodicity, and phenology of tree species from a seasonal semi-deciduous forest in southeast Brazil. *Iawa Journal* **29**: 189–207.

Liu Y, Chen JM, He L, Wang R, Smith NG, Keenan TF, Rogers C, Li W, Leng J. 2023. Global photosynthetic capacity of C3 biomes retrieved from solar-induced chlorophyll fluorescence and leaf chlorophyll content. *Remote Sensing of Environment* **287**: 113457.

Liu YY, Van Dijk AIJM, De Jeu RAM, Canadell JG, McCabe MF, Evans JP, Wang G. **2015**. Recent reversal in loss of global terrestrial biomass. *Nature Climate Change* **5**.

Longdoz B, Granier A, Loustau D, Bakker M, Delzon S, Kowalski AS, Rambal S, Dufrene E, Bonal D, Nouvellon Y. **2010**. Environmental control of carbon fluxes in forest ecosystems in France: a comparison of temperate, Mediterranean and tropical forests. *Loustau, D., Éditions Quae, Versailles*: 27–53.

Luiselli L, Dendi D, Eniang EA, Fakae BB, Akani GC, Fa JE. **2019**. State of knowledge of research in the Guinean forests of West Africa region. *Acta Oecologica* **94**: 3–11.

Luiselli L, Fa JE. **2019**. Ecology and conservation of West African forests: An introduction. *Acta Oecologica* **94**: 1–2.

Mahecha MD, Reichstein M, Carvalhais N, Lasslop G, Lange H, Seneviratne SI, Vargas R, Ammann C, Arain MA, Cescatti A. **2010**. Global convergence in the temperature sensitivity of respiration at ecosystem level. *Science* **329**: 838–840.

Malhi Y, Adu-Bredu S, Asare RA, Lewis SL, Mayaux P. **2013**. African rainforests: Past, present and future. *Philosophical Transactions of the Royal Society B: Biological Sciences* **368**.

Malhi Y, Aragão LEOC, Metcalfe DB, Paiva R, Quesada CA, Almeida S, Anderson L, Brando P, Chambers JQ, da Costa ACL, *et al.* 2009. Comprehensive assessment of carbon productivity, allocation and storage in three Amazonian forests. *Global Change Biology* **15**: 1255–1274.

Malhi Y, Doughty C, Galbraith D. **2011**. The allocation of ecosystem net primary productivity in tropical forests. *Philosophical Transactions of the Royal Society B: Biological Sciences* **366**: 3225–3245.

Malhi Y, Doughty CE, Goldsmith GR, Metcalfe DB, Girardin CAJ, Marthews TR, del Aguila-Pasquel J, Aragão LEOC, Araujo-Murakami A, Brando P, *et al.* 2015. The linkages between photosynthesis, productivity, growth and biomass in lowland Amazonian forests. *Global Change Biology* **21**.

Malhi Y, Girardin C, Metcalfe DB, Doughty CE, Aragão LEOC, Rifai SW, Oliveras I, Shenkin A, Aguirre-Gutiérrez J, Dahlsjö CAL, *et al.* 2021. The Global Ecosystems Monitoring network: Monitoring ecosystem productivity and carbon cycling across the tropics. *Biological Conservation* **253**: 108889.

Malhi Y, Roberts JT, Betts RA, Killeen TJ, Li W, Nobre CA. **2008**. Climate change, deforestation, and the fate of the Amazon. *Science* **319**.

Malhi Y, Rowland L, Aragão LEOC, Fisher RA. **2018**. New insights into the variability of the tropical land carbon cycle from the El Niño of 2015/2016. *Philosophical Transactions of the Royal Society B: Biological Sciences* **373**.

Mencuccini M, Manzoni S, Christoffersen B. **2019**. Modelling water fluxes in plants: from tissues to biosphere. *New Phytologist* **222**: 1207–1222.

Mengoli G, Agustí-Panareda A, Boussetta S, Harrison SP, Trotta C, Prentice IC. **2022**. Ecosystem Photosynthesis in Land-Surface Models: A First-Principles Approach Incorporating Acclimation. *Journal of Advances in Modeling Earth Systems* **14**: e2021MS002767.

Menon S, Denman KL, Brasseur G, Chidthaisong A, Ciais P, Cox PM, Dickinson RE, Hauglustaine D, Heinze C, Holland E. **2007**. *Couplings between changes in the climate system and biogeochemistry*. Lawrence Berkeley National Lab.(LBNL), Berkeley, CA (United States).

Merbold L, Ardö J, Arneth A, Scholes RJ, Nouvellon Y, De Grandcourt A, Archibald S, Bonnefond JM, Boulain N, Brueggemann N, *et al.* 2009. Precipitation as driver of carbon fluxes in 11 African ecosystems. *Biogeosciences* **6**.

Mills MB, Malhi Y, Ewers RM, Kho LK, Teh YA, Both S, Burslem DF, Majalap N, Nilus R, Huaraca Huasco W. **2023**. Tropical forests post-logging are a persistent net carbon source to the atmosphere. *Proceedings of the National Academy of Sciences* **120**: e2214462120.

Moore S, Adu-Bredu S, Duah-Gyamfi A, Addo-Danso SD, Ibrahim F, Mbou AT, de Grandcourt A, Valentini R, Nicolini G, Djagbletey G, *et al.* 2018. Forest biomass, productivity and carbon cycling along a rainfall gradient in West Africa. *Global Change Biology* **24**: e496–e510.

Morel AC, Adu Sasu M, Adu-Bredu S, Quaye M, Moore C, Ashley Asare R, Mason J, Hirons M, McDermott CL, Robinson EJZ, *et al.* 2019. Carbon dynamics, net primary productivity and human-appropriated net primary productivity across a forest–cocoa farm landscape in West Africa. *Global Change Biology* **25**.

Morellato LPC, Camargo MGG, Gressler E. **2013**. A review of plant phenology in South and Central America. *Phenology: an integrative environmental science*: 91–113.

Mujawamariya M, Wittemann M, Manishimwe A, Ntirugulirwa B, Zibera E, Nsabimana D, Wallin G, Uddling J, Dusenge ME. **2021**. Complete or overcompensatory thermal acclimation of leaf dark respiration in African tropical trees. *New Phytologist* **229**: 2548–2561.

Myers BA, Duff G, Eamus D, Fordyce I, O'Grady A, Williams R. **1997**. Seasonal variation in water relations of trees of differing leaf phenology in a wet–dry tropical savanna near Darwin, northern Australia. *Australian Journal of Botany* **45**: 225–240.

Oliveras I, Bentley L, Fyllas NM, Gvozdevaite A, Shenkin AF, Peprah T, Morandi P, Peixoto KS, Boakye M, Adu-Bredu S, *et al.* 2020. The Influence of Taxonomy and Environment on Leaf Trait Variation Along Tropical Abiotic Gradients. *Frontiers in Forests and Global Change* **3**: 18.

Pan Y, Birdsey RA, Fang J, Houghton R, Kauppi PE, Kurz WA, Phillips OL, Shvidenko A, Lewis SL, Canadell JG, *et al.* 2011. A large and persistent carbon sink in the world's forests. *Science* **333**.

Parazoo NC, Bowman K, Fisher JB, Frankenberg C, Jones DBA, Cescatti A, Pérez-Priego Ó, Wohlfahrt G, Montagnani L. **2014**. Terrestrial gross primary production inferred from satellite fluorescence and vegetation models. *Global Change Biology* **20**.

Pastorello G, Trotta C, Canfora E, Chu H, Christianson D, Cheah Y-W, Poindexter C, Chen J, Elbashandy A, Humphrey M, *et al.* 2020. The FLUXNET2015 dataset and the ONEFlux processing pipeline for eddy covariance data. *Scientific Data* **7**: 225.

Patenaude G, Milne R, Dawson TP. **2005**. Synthesis of remote sensing approaches for forest carbon estimation: reporting to the Kyoto Protocol. *Environmental Science & Policy* **8**: 161–178.

Peng Y, Bloomfield KJ, Cernusak LA, Domingues TF, Colin Prentice I. **2021**. Global climate and nutrient controls of photosynthetic capacity. *Communications Biology 2021 4:1* **4**: 1–9.

Peng Y, Bloomfield KJ, Prentice IC. **2020**. A theory of plant function helps to explain leaf-trait and productivity responses to elevation. *New Phytologist* **226**: 1274–1284.

Piao S, Fang J, Ciais P, Peylin P, Huang Y, Sitch S, Wang T. **2009**. The carbon balance of terrestrial ecosystems in China. *Nature* **458**.

Pickett ST. **1989**. Space-for-time substitution as an alternative to long-term studies. In: Long-term studies in ecology: approaches and alternatives. Springer, 110–135.

Prentice IC, Dong N, Gleason SM, Maire V, Wright IJ. **2014**. Balancing the costs of carbon gain and water transport: testing a new theoretical framework for plant functional ecology. *Ecology Letters* **17**: 82–91.

Prince A, Smolensky P. **2004**. *Optimality Theory: Constraint interaction in generative grammar*. John Wiley & Sons.

Pugh TAM, Jones CD, Huntingford C, Burton C, Arneth A, Brovkin V, Ciais P, Lomas M, Robertson E, Piao SL, *et al.* 2018. A Large Committed Long-Term Sink of Carbon due to Vegetation Dynamics. *Earth's Future* **6**.

Réjou-Méchain M, Tanguy A, Piponiot C, Chave J, Hérault B. **2017**. biomass: an r package for estimating above-ground biomass and its uncertainty in tropical forests. *Methods in Ecology and Evolution* **8**: 1163–1167.

Riutta T, Kho LK, Teh YA, Ewers R, Majalap N, Malhi Y. **2021**. Major and persistent shifts in below-ground carbon dynamics and soil respiration following logging in tropical forests. *Global Change Biology* **27**: 2225–2240.

Riutta T, Malhi Y, Kho LK, Marthews TR, Huaraca Huasco W, Khoo MS, Tan S, Turner E, Reynolds G, Both S, *et al.* 2018. Logging disturbance shifts net primary productivity and its allocation in Bornean tropical forests. *Global Change Biology* **24**.

Rogers A, Medlyn BE, Dukes JS, Bonan G, von Caemmerer S, Dietze MC, Kattge J, Leakey ADB, Mercado LM, Niinemets Ü, *et al.* 2017. A roadmap for improving the representation of photosynthesis in Earth system models. *New Phytologist* **213**: 22–42.

Running S, Mu Q, Zhao M. **2015**. MOD17A2H MODIS/Terra Gross Primary Productivity 8-Day L4 Global 500m SIN Grid V006.

Schimel D, Stephens BB, Fisher JB. **2015**. Effect of increasing CO2 on the terrestrial carbon cycle. *Proceedings of the National Academy of Sciences* **112**: 436–441.

Sitch S, Smith B, Prentice IC, Arneth A, Bondeau A, Cramer W, Kaplan JO, Levis S, Lucht W, Sykes MT. **2003**. Evaluation of ecosystem dynamics, plant geography and terrestrial carbon cycling in the LPJ dynamic global vegetation model. *Global change biology* **9**: 161–185.

Smith NG, Keenan TF, Prentice IC, Wang H, Wright IJ, Niinemets U, Crous KY, Domingues TF, Guerrieri R, Ishida FY, *et al.* 2019. Global photosynthetic capacity is optimized to the environment.

Stocker BD, Wang H, Smith NG, Harrison SP, Keenan TF, Sandoval D, Davis T, Prentice IC. **2020**. P-model v1.0: An optimality-based light use efficiency model for simulating ecosystem gross primary production. *Geoscientific Model Development* **13**: 1545–1581.

Sudmanns M, Tiede D, Augustin H, Lang S. **2020**. Assessing global Sentinel-2 coverage dynamics and data availability for operational Earth observation (EO) applications using the EO-Compass. *International Journal of Digital Earth* **13**: 768–784.

Timothy D, Onisimo M, Riyad I. **2016**. Quantifying aboveground biomass in African environments: A review of the trade-offs between sensor estimation accuracy and costs. *Tropical Ecology* **57**: 393–405.

Tomlinson KW, Poorter L, Sterck FJ, Borghetti F, Ward D, de Bie S, van Langevelde F. **2013**. Leaf adaptations of evergreen and deciduous trees of semi-arid and humid savannas on three continents. *Journal of Ecology* **101**: 430–440.

Tramontana G, Jung M, Schwalm CR, Ichii K, Camps-Valls G, Ráduly B, Reichstein M, Arain MA, Cescatti A, Kiely G, *et al.* 2016. Predicting carbon dioxide and energy fluxes across global FLUXNET sites with regression algorithms. *Biogeosciences* **13**.

Tucker C, Brandt M, Hiernaux P, Kariryaa A, Rasmussen K, Small J, Igel C, Reiner F, Melocik K, Meyer J, *et al.* 2023. Sub-continental-scale carbon stocks of individual trees in African drylands. *Nature* **615**: 80–86.

Wang H, Atkin OK, Keenan TF, Smith NG, Wright IJ, Bloomfield KJ, Kattge J, Reich PB, Prentice IC. **2020**. Acclimation of leaf respiration consistent with optimal photosynthetic capacity. *Global Change Biology* **26**: 2573–2583.

Wang H, Prentice IC, Davis TW, Keenan TF, Wright IJ, Peng C. **2017a**. Photosynthetic responses to altitude: an explanation based on optimality principles. *New Phytologist* **213**: 976–982.

Wang H, Prentice IC, Keenan TF, Davis TW, Wright IJ, Cornwell WK, Evans BJ, Peng C. **2017b**. Towards a universal model for carbon dioxide uptake by plants. *Nature Plants 2017 3:9* **3**: 734–741.

Waring BG, Powers JS. **2017**. Overlooking what is underground: Root:shoot ratios and coarse root allometric equations for tropical forests. *Forest Ecology and Management* **385**: 10–15.

White F. **1983**. *The vegetation of Africa.*

Williams RJ, Myers BA, Muller W, Duff GA, Eamus D. **1997**. Leaf phenology of woody species in a north Australian tropical savanna. *Ecology* **78**: 2542–2558.

Wood TE, Cavaleri MA, Reed SC. **2012**. Tropical forest carbon balance in a warmer world: A critical review spanning microbial- to ecosystem-scale processes. *Biological Reviews* **87**.

Wright IJ, Reich PB, Cornelissen JHC, Falster DS, Groom PK, Hikosaka K, Lee W, Lusk CH, Niinemets Ü, Oleksyn J. **2005**. Modulation of leaf economic traits and trait relationships by climate. *Global Ecology and Biogeography* **14**: 411–421.

Xu M, Shang H. **2016**. Contribution of soil respiration to the global carbon equation. *Journal of plant physiology* **203**: 16–28.

Xu H, Wang H, Prentice IC, Harrison SP, Wright IJ. **2021**. Coordination of plant hydraulic and photosynthetic traits: confronting optimality theory with field measurements. *New Phytologist* **232**: 1286–1296.

Yang R, Wang J, Zeng N, Sitch S, Tang W, McGrath MJ, Cai Q, Liu D, Lombardozzi D, Tian H, *et al.* 2022. Divergent historical GPP trends among state-of-the-art multi-model simulations and satellite-based products. *Earth System Dynamics* **13**.

Zhang Y, Song C, Sun G, Band LE, Noormets A, Zhang Q. **2015**. Understanding moisture stress on light use efficiency across terrestrial ecosystems based on global flux and remote-sensing data. *Journal of Geophysical Research: Biogeosciences* **120**: 2053–2066.

Zhao M, Heinsch FA, Nemani RR, Running SW. **2005**. Improvements of the MODIS terrestrial gross and net primary production global data set. *Remote Sensing of Environment* **95**.

Zhao M, Running SW. **2010**. Drought-Induced Reduction in GlobalTerrestrial Net Primary Productionfrom 2000 Through 2009. *Science* **329**: 940–943.

Zuidema PA, Babst F, Groenendijk P, Trouet V, Abiyu A, Acuña-Soto R, Adenesky-Filho E, Alfaro-Sánchez R, Aragão JRV, Assis-Pereira G, *et al.* 2022. Tropical tree growth driven by dry-season climate variability. *Nature Geoscience* **15**.